ROYAUME DU MAROC
Université Mohammed V - RABAT -
جامعة محمد الخامس – الرباط –
Faculté des sciences
كلية العلوم

CENTRE D'ETUDES DOCTORALES - SCIENCES ET TECHNOLOGIES

N° d'ordre : 3111

THESE

En vue de l'obtention du : ***DOCTORAT***

Centre de recherche : Eau, Ressources Naturelles, Environnement et Développement durable (CERN2D)
Structure de Recherche : laboratoire de Spectroscopie, Modélisation Moléculaire, Matériaux, Nanomatériaux, Eau et Environnement (LS3MN2E)
Discipline : Chimie
Spécialité : Chimie-physique

Présentée et soutenue le : *(23/06/2018)* ***par :***

Salma BOUGARRANI

Development of Ca_xMnO_y/TiO_2 Composites for efficient Photo-degradation of organic pollutants from water using Advanced Oxidation Processes

JURY

Mohammed FEKHAOUI, PES, Institut Scientifique de Rabat	*Président*
Mohammed El AZZOUZI, PES, Faculté des Sciences de Rabat	*Directeur de Thèse*
Abderrahim El HOURCH, PES, Faculté des Sciences de Rabat	*Co- Directeur de Thèse*
Abdelmalek DAHCHOUR, PES, l'Institut Agronomique Hassan II de Rabat	*Rapporteur*
Najem HASSANAIN, PES, Faculté des Sciences de Rabat	*Rapporteur*
Mohamed SARAKHA, PES, Université Clermont-Ferrand –France	*Examinateur*
Roger GLASER, PES, Université Leipzig-Allemagne	*Examinateur*
Kamal El HAJI, PES, Directeur d'ISHEDD-Rabat	*Invité*

Année Universitaire : 2018-2019

✉ Faculté des Sciences, avenue Ibn Battouta, BP. 1014 RP, Rabat –Maroc
☎ 00212(0) 37 77 18 76 🖷 00212(0) 5 37 77 42 61 ; http://www.fsr.um5.ac.ma

Acknowledgement

Before I started my PhD in Chemistry, I decided to take a gap year to go improve my Chinese proficiency in Beijing China from a beginner to an intermediate level. I got a Confucius Institute scholarship and off I went to the Far East to have a better understanding of this country and its culture. I loved it, I learned so much about the language, the food and the culture but I was in shock as I discovered a city with one of the highest pollution rate in the world. Though I had always been interested in Sustainable Chemistry academically, with this experience my scholarly interests collided abruptly with my personal life. I thought to myself there must be something I could do to contribute to the global effort of depollution.
During a summer school in Germany, we were asked:" why do a thesis? And above all, why especially this thesis? So, chance or coincidence? Is my subconscious a determining factor in this thesis choice that I thought I was conscious and thoughtful? I'm not sure about it, the only thing that I really believe is this research would not have been possible without the scientific and personal support of many people. It is obvious that the first page of this manuscript is dedicated to them.

Over the course of conducting this research, I was extremely fortunate to have been surrounded by many great people who have challenged me and provided opportunities to learn and grow.
Firstly, I much appreciated the most valuable support, advice and comments from my principal supervisor, Professor Mohammed El Azzouzi from the Faculty of Sciences Rabat. I would like to express my gratitude to him for giving me the possibility to learn more by having responsibilities beyond my PhD thesis and for his invaluable and warm assistance and endless support during this long doctoral experience.
I would also like to thank my supervisor Adjunct Professor Abderrahim El Hourch for introducing me to the interesting world of research and for advising me along the way.
I warmly thank Professor Roger Gläser, from Leipzig University, who gave me the opportunity to work in his research group in Institute of Chemical Technology Leipzig. His guidance during these period has been extremely valuable. Thank you for your insight and feedback throughout this process, your wisdom, support and optimism have made this difficult endeavor possible.
Next, I would like to extend my thanks to Professor John Anthony Byrne from Ulster University in UK for hosting me at Nanotechnology and Integrated Bioengineering Centre. His patience and understanding taught me a lot and gave me the opportunity to get through and finish my commitments for my Ph.D. program.
I am very grateful to Professor Moisés Canle López from Faculty of Sciences & CICA Coruña, Spain for helping me in the revision of the main manuscripts and data fitting.

I acknowledge Professor Abdul Chaudhary from Brunel University UK for his availability, his help and encouragement.
I am also grateful to Professor Sema Erdemoğlun from Inonu University, Malatya, Turkey; my Turkish exchange was a valuable experience in terms of both professional and personal development.
I would like to express my sincere thanks to the supervisory committee members, Pr. Mohammed FEKHAOUI, from scientific institute of Rabat.
Official reviewers of this thesis, Professor Abdelmalek DAHCHOUR from Institute Hassan II (IAV) Rabat, I express my sincere thanks for the honor you give me in agreeing to judge this thesis.
Professor Najem Hassanain from the Faculty of Sciences Rabat is greatly appreciated for his efforts, valuable insight and comments on this thesis.
Professor Mohamed Sarakha from Clermont Ferrand University France, it was during my defense that I had the pleasure to discover an eminent scientist. I would like to thank you for your comments, recommendations and relevant questions.
Professor Kamal El HAJI from ISHEDD- Rabat (Institute of high studies in Sustainable Development) for valuable advice and insights on my studies. I express my sincere thanks for the honor you give me in agreeing to judge this thesis.
Secondly, many thanks are due to co-authors and colleagues, karl Striegler, Preetam Sharma, Robert Arndt, Hatice Çağlar Yılmaz, Emrah Akgeyik, Lahbib Latrach. To my friends in Rabat and Fes who were always sources of joy and moral support, I would never forget the positive energy and true friendship that I've had with Yasmine, Nouha, Imane, Laila, salma, Asmae, Soukaina.

Finally, my whole heartfelt gratitude to my family. Words cannot express how grateful I am to them: my lovely Mother for her unconditional love and motivation, dear Father for all his constant support and encouragement, my brothers and friends Younes & Youssef for their support, love and encouragement. All the people who supported loved and encouraged me and told me that everything is possible as long as you decide so. I'm very proud and fortunate to have them as my family.
Thank you! Without your love and support, I don't think I can persist to the end of my PhD track.

Funding: Research needs money! National Center for Scientific and Technical Research Morocco, for CNRST Excellence scholarship, Chinese government scholarship, Tubitak-CNRST funding, DAAD scholarship and British Council funding are acknowledged for financial support. Thank you for all the scholarship I received to spend a decent and cheerful life.

Dedication

This thesis and all of my academic achievements are dedicated to:

My beloved mother,

Whose example will forever inspire my human experience,

My beloved father

For his endless support, inspiration and sacrifices

In my heart, you will always stay

My brothers and friends Younes & Youssef

For their support, love and encouragement

For my beloved fiance Aziz

For his love, patience and gentleness

All the people who supported loved and encouraged me and told me that everything is possible as long as you decide so.

I am very proud and fortunate to have them as my family.

Thank you! Without your love and support, I don't think I can persist to the end of my PhD track.

Through this thesis the expression of my deep love.

Abstract

Water contamination is a global problem and the growing utilization of limited water resources creates a need for efficient treatment methods. Water treatment using photocatalysis has gained extensive attention in recent years. Photocatalysis is promising technology from green chemistry point of view. Within this thesis new heterostructures of TiO_2 (Hombikat UV100) with layered manganese dioxide (birnessite) was investigated to improve the photocatalytic efficiency under UV-Vis irradiation. Ca_xMnO_y was prepared by a precipitation method and then mixed with TiO_2 by mechanical grinding following by annealing at 500°C to obtain Ca_xMnO_y-TiO_2. Photocatalytic activity of prepared samples in aqueous environment was tested using model compounds such as methylene blue, phenol and imazapyr herbicide. Ca_xMnO_y layers are proposed to be encapsulating the TiO_2 particles and the highest degradation rate of imazapyr was observed when 5% of Ca_xMnO_y was used in the synthesis of the composite.

The structure and properties of the intermediate products were examined and excellent mineralization was observed in the case of Ca_xMnO_y-TiO_2 as compared to TiO_2 system (UV100 and Degussa P25), plausible mineralization pathways for imazapyr was proposed based on the identified intermediates. Ca_xMnO_y contributed to the enhanced photocatalytic activity of Ca_xMnO_y-TiO_2 in three ways: extending the light absorbance into the visible range due the reduction of the band gap from 3.18 eV to 2.89 eV for pure TiO_2 and Ca_xMnO_y-TiO_2 composite respectively, possibly improving charge transfer and lowering recombination of charge carriers, and finally by altering intermediate adsorption and degradation due to the greater adsorption of polar species on the surface of the Ca_xMnO_y, and thus promote their photocatalytic decomposition.

In addition, a comparative study on the degradation of imazapyr in aqueous solution by ozonation, photocatalysis and photocatalytic ozonation in the presence of Ca_xMnO_y-TiO_2 composite have been investigated in this research. Effects of operational parameters on imazapyr removal efficiency including Ca_xMnO_y-TiO_2 dosing, initial herbicide concentration and pH were also studied. Photocatalytic ozonation process in the presence Ca_xMnO_y-TiO_2 leads to a ca. 2-fold rate enhancement for imazapyr and a ca.4.3-fold for intermediate products , while compared to photocatalytic ozonation in the presence of commercial TiO_2 (Hombikat UV100).

Particular emphasis was also given to the effect of humic acids extracted from Chaouia soil in Morocco, on the reaction kinetics and mechanisms of imazapyr degradation. Obtained results clearly demonstrate that at high concentration, humic acids exhibit a screening effect on the photochemical degradation of imazapyr, but also acts as hydroxyl radical scavengers, which

induced a decrease of imazapyr degradation. These findings provide further insights into the assessment of pesticides elimination in natural waters where HA exists ubiquitously.

Keywords: AOPs, birnessite, CaxMnOy-TiO_2 composite, degradation pathway, Imazapyr, Ozonation, Photocatalysis, POPs, surface modification, water treatment

Résumé

La dégradation de l'environnement et la pénurie d'eau salubre sont des obstacles majeurs au développement durable. Les progrès socioéconomiques ne sont pas viables sans air propre, sans eau potable, sans sols fertiles pour la production végétale et animale, ni sans environnement propre et stable propice au travail et à la vie.

L'eau est une ressource socio-économique vitale limitée. Elle fait l'objet d'une demande croissante à des fins domestiques et industrielles, ce qui menace la pérennité des eaux souterraines et a des conséquences pour l'agriculture, la foresterie, l'industrie et les réserves d'eau potable. Il est essentiel que les ressources en eau soient gérées de manière stratégique et durable, d'où le besoin de développer des méthodes de traitement efficaces. Le traitement des eaux par photocatalyse a fait l'objet d'une attention particulière ces dernières années. La photocatalyse est une technologie prometteuse du point de vue de la chimie verte.

Le mémoire de thèse intitulé « **Development of Ca_xMnO_y/TiO_2 Composites for efficient Photo-degradation of organic pollutants from water using Advanced Oxidation Processes**» porte sur l'étude de la photodégradation des polluants organiques persistants, en utilisant des nouveaux composites à base d'oxyde de manganèse et d'oxyde de titanium Ca_xMnO_y/TiO_2. Ce travail s'inscrit dans un thème de recherche pratique et fondamentale et dont le besoin du pays est immédiat afin de traiter les eaux polluées. Afin de répondre à cette problématique, nous nous intéressons d'abord à la synthèse et au développement de photo-catalyseurs actifs sous la lumière solaire mais aussi à la cinétique et au devenir photochimique des polluants sélectionnés.

Dans le premier chapitre, nous avons présenté une analyse bibliographique sur les procédés d'oxydation avancés et leurs applications dans le traitement des eaux, tout en mettant en avant les caractéristiques de ces semi-conducteurs et plus particulièrement le dioxyde de titanium et l'intérêt du couplage avec d'autres photo-catalyseurs pour une application en présence de la lumière solaire. La problématique a été bien élucidée ainsi que le besoin immédiat du pays à adopter des technologies vertes afin de traiter les eaux polluées.

Le deuxième chapitre retrace les résultats de synthèses des nouveaux composites à base d'oxyde de manganèse et d'oxyde de titanium. L'ensemble des techniques de caractérisation utilisées et permettant de déterminer les propriétés structurales, morphologiques et optiques et les surfaces spécifiques des composites ont été décrites. Le composite 5% Ca_xMnO_y-TiO_2 synthétisé par précipitation suivi d'un broyage mécanique avec l'oxyde de titanium commerciale (Hombikat UV) a relevé une haute performance sur la dégradation du bleu de méthylène, du phénol ainsi que de l'Imazapyr sous irradiation par la lumière visible.

Dans un troisième chapitre, nous proposons une approche spectroscopique pour évaluation des produits intermédiaires générés au cours de la photo dégradation de l'herbicide imazapyr. En présence de 5% Ca_xMnO_y-TiO_2, nous avons pu conclure que la concentration des intermédiaires augmentent continuellement en fonction du temps pour atteindre un maximum après 180 min d'irradiation et commencer à diminuer dans les heures qui suivent, tandis que les produits intermédiaires augmentent continuellement avec le temps en présence de TiO_2. Ce résultat indique que la structure et la propriété des produits intermédiaires générés dans les deux systèmes sont différentes et que la haute performance du système Ca_xMnO_y-TiO_2 est attribuée à la modification de la surface, rendue plus sélective dans l'adsorption des réactifs organiques polarisés et ainsi favorise leurs photo dégradation. Finalement, la structure et les propriétés des produits intermédiaires ont été examinées et un mécanisme photocatalytique a été discuté en détail.

La minéralisation de l'imazapyr et du phénol par le composite Ca_xMnO_y-TiO_2 a été élucidé en solution aqueuse, il a été démontré que le taux de minéralisation en présence du composite Ca_xMnO_y-TiO_2 est 5 fois plus élevé que le TiO_2 UV100 non modifié sous la lumière visible.

Le dépôt d'oxyde de manganèse principalement à la surface du dioxyde de titanium a permis de modifier les propriétés optique du TiO_2, cette modification a déplacé le domaine d'absorption de la lumière UV vers le début de la lumière visible.

L'amélioration de l'activité photo-catalytique a été attribuée au rétrécissement de la bande interdite ainsi qu'à la réduction de la recombinaison électron-trou, produisant ainsi une séparation de charge efficace et un transfert entre les matériaux.

Le quatrième chapitre rapporte d'une manière détaillée une étude comparative sur la dégradation de l'imazapyr en solution aqueuse par l'ozonation, la photocatalyse et par l'ozonation photocatalytique en présence du composite Ca_xMnO_y-TiO_2. Les résultats de cette recherche montrent que l'ozonation photocatalytique est très efficace pour le traitement des polluants persistants.

Les résultats du cinquième chapitre constituent une suite logique du 4 ^{ème} chapitre qui met en jeu l'effet du pH, de la concentration initiale des polluants ainsi que de la dose du catalyseur afin d'obtenir les cinétiques de dégradation les plus rapides.

Enfin, ce mémoire se termine par un sixième chapitre qui traite l'influence des acides humiques extraits du sol de la Chaouia sur la dégradation des métaux de transition ainsi que sur l'herbicide Imazapyr. Les résultats montrent clairement que les acides humiques d'une concentration élevée ralentissent la réaction de la photo dégradation des polluants pointés.

En définitive, ce travail s’insère bien dans le contexte de développement de stratégies pour les mesures de protection de l'environnement au Maroc, et en particulier la protection des ressources en eau.

Mots-clés : POA (Procédés d’oxydation avancée), birnessite, Ca_xMnO_y-TiO_2 composite, photodégradation, Imazapyr, Ozonation, Photocatalyse, POPs (Polluants Organiques Persistants), modification de surface, traitement des eaux

ملخص

يشكل التدهور البيئي ونذرة المياه النظيفة عقبات رئيسية أمام التنمية المستدامة. كما أن التقدم الاجتماعي والاقتصادي غير مستدام بدون هواء نظيف وبدون مياه شرب وبدون بيئة نظيفة ومستقرة مواتية للعمل والحياة. إن المياه مورد اجتماعي واقتصادي حيوي محدود. فهناك طلب متزايد عليه للأغراض المنزلية والصناعية، مما يهدد استدامة المياه الجوفية، ولهذا عواقب على الزراعة والغابات والصناعة وإمدادات مياه الشرب. لهذا من الضروري إدارة الموارد المائية بطريقة استراتيجية ومستدامة، مما يفرض الحاجة إلى تطوير أساليب معالجة فعالة. ولقد شكلت معالجة المياه عن طريق التحفيز الضوئي (Photocatalysis) موضع اهتمام خاص في السنوات الأخيرة، إنها تكنولوجيا واعدة من وجهة نظر الكيمياء الخضراء.

هذه الأطروحة بعنوان " Ca_xMnO_y / TiO_2 مركب متطور ناجع في التحليل الضوئي لملوثات المياه العضوية باستخدام عمليات الأكسدة المتقدمة". هي دراسة الملوثات العضوية الثابتة، وذلك باستخدام مركبات جديدة مكونة من أكسيد المنغنيز وأكسيد التيتانيوم Ca_xMnO_y / TiO_2. هذا العمل يندرج في إطار البحث التطبيقي والأساسي كما يشكل حاجة فورية للبلاد.

لمعالجة هذه الإشكالية، نركز أولا على تخليق وتطوير المحفزات الضوئية الناشطة تحت ضوء الشمس ولكن أيضا على صيروة الملوثات المختارة.

في الفصل الأول، قدمنا الأدبيات المتعلقة بعمليات الأكسدة المتقدمة وتطبيقاتها في مجال معالجة المياه، مع تسليط الضوء على خصائص أشباه الموصلات وخاصة ثاني أكسيد التيتانيوم أهمية اقترانه مع غيره من المحفزات الضوئية في وجود ضوء الشمس. لقد تم دراسة المشكلة جيداً تلبية لحاجة البلاد الفورية إلى تقنيات خضراء لمعالجة المياه الملوثة.

الفصل الثاني يعيد تحديد نتائج توليفات المركبات الجديدة على أساس أكسيد المنغنيز وأكسيد التيتانيوم، حيث تم وصف جميع تقنيات التوصيف المستخدمة لتحديد الخصائص التركيبية والمورفولوجية والبصرية والمساحات السطحية للمركبات. إن مركب 5٪ Ca_xMnO_y / TiO_2 الناجم من تقنية الترسيب متبوعة بالطحن الميكانيكي مع أكسيد التيتانيوم التجاري (Hombikat UV) برهن على كفاءة عالية في تحليل الميثيلين الأزرق والفينول والإيمازابير تح إضاءة أشعة الشمس المرئية.

في الفصل الثالث، نقترح مقاربة سبيكتروسكوبية لتقييم المركبات الوسيطة المتولدة أثناء التحليل الضوئي لمبيد الأعشاب imazapyr. في ظل وجود 5٪ Ca_xMnO_y / TiO_2، استنتجنا أن تركيز المركبات الوسيطة تزيد باستمرار مع مرور الوقت لتصل حدها الأقصى بعد 180 دقيقة من الإشعاع، وتبدأ في الانخفاض في الساعات الموالية، في حين أن زيادة المركبات الوسيطة باستمرار مع مرور الوقت في وجود TiO_2. تشير هذه النتيجة إلى أن بنية وخصائص المركبات الوسيطة التي تشكلت في النظامين هي مختلفة، وأن ارتفاع أداء

نظام Ca_xMnO_y / TiO_2 يعود إلى تغيير السطح الذي صار أكثر قدرة على انتقاء المواد العضوية المستقطبة الملوِثة التي يمصها، وهكذا يسهل عملية التحليل الضوئي. وفي النهاية، تم فحص بنية وخصائص المركبات الوسيطة وتمت مناقشة آلية للتحفيز الضوئي بالتفصيل.

تحليل إيمازبير والفينول بواسطة مركب Ca_xMnO_y / TiO_2 تبين في محلول مائي، وقد تمت البرهنة على أن معدل التحليل بوجود مركب Ca_xMnO_y / TiO_2 هو 5 مرات أعلى من TiO_2 UV100 غير المعدل تحت أشعة الشمس المرئية.

ترسب أكسيد المنغنيز بشكل رئيسي على سطح ثاني أكسيد التيتانيوم أدى إلى تعديل الخصائص البصرية ل TiO_2، هذا التعديل نقل مجال الامتصاص من مجال الأشعة البنفسجية إلى مجال بداية الضوء المرئي. ويعزى نشاط التحفيز الضوئي إلى تقلص النطاق الممنوع، وكذا إلى تقليص إعادة تركيب الإلكترون الثقب، وبالتالي إنتاج فصل فعال بين الشحنات ونقلا بين المعادن.

يقدم الفصل الرابع تقريرا مفصلا لدراسة مقارنة لتحلل إيمازبير في محلول مائي بفعل الأوزنة والأوزنة التحليلية الضوئية بوجود مركب Ca_xMnO_y / TiO_2. تظهر نتائج هذا البحث أن الأوزنة التحليلية الضوئية فعالة جدا في معالجة الملوثات الثابتة.

نتائج الفصل الخامس هي استمرار منطقي للفصل الرابع الذي ينطوي على تأثير الرقم الهيدروجيني والتركيز الأولي للملوثات وجرعة المحفز من أجل الحصول على أسرع تحلل.

وأخيرًا، تختتم هذه الرسالة بفصل سادس يتناول تأثير الأحماض الدبالية، المستخلصة من تربة منطقة الشاوية بالمغرب، على تحلل المعادن الانتقالية وعلى مبيد الأعشاب إيمازابير. النتائج تظهر بوضوح أن الأحماض الدبالية ذات التركيز العالي تبطئ رد فعل التحلل الضوئي للملوثات المعنية.

في نهاية المطاف، ينخرط هذا العمل بشكل جيد في سياق تطوير تدابير حماية البيئة في المغرب، وعلى وجه الخصوص حماية الموارد المائية.

List of publications

This thesis is based on the following papers, which are referred throughout the text by their Roman numerals:

I. **S. Bougarrani**, K. Skadell, R. Arndt, M. El Azzouzi, and R. Gläser, "Novel Ca_xMnO_y/TiO_2 composites for efficient photocatalytic degradation of methylene blue and the herbicide imazapyr in aqueous solution under visible light irradiation," Journal of environmental chemical engineering, vol. 6, no. 2, pp. 1934–1942, 2018.

II. **S. Bougarrani**, P. K. Sharma, J. W. J. Hamilton, A. Singh, M. Canle, M. El Azzouzi, A. Byrne. Photocatalytic degradation of imazapyr using Ca_xMnO_y-TiO_2 heterostructures under UV and visible irradiation: evaluation of main intermediates, Applied Catalysis B*:* Environmental, submitted.

III. **S. Bougarrani**, L. Latrach , L. El Azzouzi, A. Bouziani, S. Chhaiba, A. J. Chaudhary, M. El Azzouzi, Aqueous Imazapyr Degradation by Ozonation, Photocatalysis, and Photocatalyzed ozonation by CaxMnOy-TiO_2 Composite, Environmental Chemistry, accepted

IV. **S. Bougarrani**, L. El Azzouzi, S. Akel, L. Latrach, A. Bouziani, M. El Azzouzi, Factors Influencing Imazapyr Herbicide Removal from Wastewater Using Photocatalytic Ozonation Acta Chim. Slov. 2018, 65, –DOI: 10.17344/acsi.2018.4297,

V. **S. Bougarrani**, L. El azzouzi, A. Bouziani , S. Akel, L. Latrach , Z. Baicha, M. El azzouzi. The influence of humic acids extracted from Chaouia soil on the behavior of transition metal ions and pesticides, Mor. J. Chem. 5 N°3 (2017) 446-452

Author's contribution

Salma Bougarrani is the principal author and investigator and also the corresponding author of all the cited papers I, II, III, IV, V.

Paper not included in this thesis:

VI. H. Çağlar Yılmaz, E. Akgeyik, **S. BOUGARRANI**, M. El Azzouzi, S. Erdemoğlu. Photocatalytic degradation of amoxicillin by reflux synthesized Co doped TiO_2 and monitoring of degradation products by LC–MS/MS. Environmental Pollution. 2018

Participation in Conferences

I. **S. Bougarrani**, L. Latrach, M. El Azzouzi. Factors Influencing Imazapyr Herbicide Removal from Wastewater Using Photocatalytic Ozonation. *6th International Conference on Environmental Management, Planning and Economics (CEMEPE) and Sector conference, Greece, 2017*

II. **S. Bougarrani**, M. El azzouzi, K. Skadell, R. Arndt,R. Gläser, Efficient photocatalytic degradation imazapyr herbicide in aqueous solution under visible light irradiation. *Maghreb Scientific Days, Reuse of treated wastewater in the Maghreb countries, Hammamat, Tunis,2017*

III. **S. Bougarrani**, L. El azzouzi, A. Bouziani, S. Akel, L. Latrach, Z. Baicha, M. El azzouzi. The influence of humic acids extracted from Chaouia soil on the behavior of transition metal ions and pesticides. *28thInternational Conference on Photochemistry ICP Strasbourg, France 2017*

IV. **S. Bougarrani**, M. El azzouzi, R. Gläser, Development of new visible light driven based on birnessite and titanium dioxide materials. *2nd Summer School on Sustainable Chemistry for Sustainable Development Leuphana University of Luneburg, Germany, Sept 2016*

V. **S. Bougarrani**, M. El azzouzi and L. Hasnaoui. The Use of Ozone Process in Drinking Water Treatment; Investigation of the influence of Operational Parameters. *International conference of water energy and climate change (WECC) Marrakech, Morocco, 2016*

Table of Contents

List of Tables

List of Figures and Illustrations

List of Symbols, Abbreviations and Nomenclature

Symbol Definition
λmax Wavelength of maximum absorbance, *nm*
λ Wavelength, *nm*
t Time, *min*
M+ Metal ion
M Molar mass [g/mol]
m Mass [g]
kapp Apparent pseudo-first order rate constant [1/h] or [1/min]
k Rate constant, *min-1*
hv Irradiation energy in photocatalysis
h+ Photogenerated hole
E° Oxidation-reduction (redox) potential
e- Electron
C_0 Initial concentration of substrate, *mg L-1*
C Concentration of substrate, *mg L-1*
at% Atomic percent
•OH hydroxyl radicals
% I Intensity of luminescence (%)

Abbreviations and Nomenclature

AOPs Advanced Oxidation Processes
AOX absorbable organic halogens
APCI Atmospheric Pressure Chemical Ionization
BET Brunauer, Emmett, and Teller theory of gas adsorption
BJH Barrett-Joyner-Halenda analysis
CAS Chemical Abstract Service
CB Conduction band
COD Chemical Oxygen Demand
CO_2 Carbon Dioxide
DRS Diffuse Reflectance Spectra
ECs Emerging Contaminants
EDCs Endocrine Disrupting Chemicals
EDX energy dispersive X-ray spectroscopy
Eg Band gap energy
EPA Environmental Protection Agency
EPR electron paramagnetic resonance
ESI Electrospray Ionization
EU European Union
EV Electron Volt
FTIR Fourier transform Infrared spectroscopy
FA Fulvic acid
h^+ Hole
H_2O_2 Hydrogen peroxide
HA Humic Acids
herb Herbicide
HPLC High Performance Liquid Chromatography
ICP-OES Elemental analysis via inductively coupled plasma optical emission spectroscopy

IMAZ Imazapyr
KBr Potassium bromide
KCl Potassium chloride
LC Liquid chromatography
MB methylene blue
MS Mass Spectrometry
NPs nanoparticles
O_3 Ozone
Ozone–Granulated Activated Carbon systems (O_3/GAC)
pH potential Hydrogen
PL photoluminescence
POPs Persistent Organic Pollutants
PXRD Powder X-ray diffraction
SC Semiconductor
SEM Scan electron microscopy
TEM transmission electron microscopy
The Food & Agriculture Organization (FAO)
TiO_2 Titanium dioxide
TOC Total Organic Carbon
TRB Tribenuron-methyl
USEPA United States Environmental Protection Agency
UV ultraviolet
UV-vis DRS ultraviolet-visible light diffuse reflectance spectroscopy
UV-Vis Ultraviolet – Visible
VB valence band
World Health Organization (WHO),
XPS X-ray photoelectron spectroscopy
XRD X-ray diffraction

Chapter 1: Introduction and literature review

1.1. Background

Even though water covers more than 70% of the Earth's surface, only 3% of it is fresh. A large percentage of this freshwater is either in the form of ice-caps or glaciers, in remote areas or impossible to exploit due to seasonal variations [1].

Nowadays worldwide, access to safe water of about 3.5 billion people are not fulfilled, nearly 2.5 billion people do not have admittance to improved sanitation and around 768 million people do not have admittance to improved source of water, furthermore, water contamination and lack of sanitation and hygiene cause approximately 1.7 million deaths every year [2]. According to some estimation, through 2050 more than 40% of global population will live in conditions of severe water stress [3]. The population growth, economic development and urban expansion will increase demand of freshwater in the future, which in turn will affect water-intensive industries [4].

The United Nations has completed recently a report that calls for a radical rethink of policies to manage fresh drinking water. It has been mentioned that freshwater is not being used sustainably, and water management is fragmented, concluding that the future of the humanity is increasingly uncertain and risks are set to deepen [5]. Efficient management of water resources is therefore of vital importance, especially in areas that are heavily urbanized or industrialized.

The presence of numerous organic compounds (emerging contaminants (EC), and endocrine disrupting compounds (EDCs)) has been demonstrated in thousands of publications (www.scopus.com) in recent years, giving rise to increasing worries [6] . Sources of organic pollutants in the environment are diverse and can be classified either as point sources (municipal wastewater treatment plants, industrial installations, hospitals, livestock farms) or as diffuse (non-point) sources, such as pesticide runoff from agricultural lands or unprotected landfill leachates [7].

The EPA (Environmental Protection Agency, 2010) has summarized the influent-to-effluent removals in conventional wastewater treatment plants for some classes of ECs, typically plasticizers and flame retardants. Between 2003 and 2008, 246 compounds were screened using 88 references and a database with removal efficiencies was compiled [5].

Table 1.1. Sources of major emerging contaminants in the aquatic environment

Category	***Important subclasses***	***Major sources***	
		Distinct	*Nonexclusive*
Pharmaceuticals	NSAIDs[a], lipid regulator, anticonvulsants, antibiotics, *β*-blockers and stimulants	□ Domestic wastewater (from excretion) □ Hospital effluents □ Run-off from CAFOs[b] and aquaculture	Sources that are not exclusive to individual categories include: □ Industrial wastewater (from product manufacturing discharges) □ Landfill leachate (from improper disposal of used, defective or expired items)
Personal care products	Fragrances, disinfectants, UV filters, and insect repellents	□ Domestic wastewater (from bathing, shaving, spraying, swimming and etc.)	
Steroid hormones	Estrogens	□ Domestic wastewater (from excretion) □ Run-off from CAFOs and aquaculture	
Surfactants	Non-ionic surfactants	□ Domestic wastewater (from bathing, laundry, dishwashing and etc.) □ Industrial wastewater (from industrial cleaning discharges)	
Industrial chemicals	Plasticizers, fire retardants	□ Domestic wastewater (by leaching out of the material)	
Pesticides	Organochlorine insecticides, organophosphorus insecticides, herbicides and fungicides	□ Domestic wastewater (from improper cleaning, run-off from gardens, lawns and roadways and etc.) □ Agricultural runoff	

[a] NSAIDs: non-steroidal anti-inflammatory drugs; [b] CAFOs: concentrated animal feeding operations.

More than 139 million organic and inorganic substances documented have been also registered in CAS (Chemical Abstract Service) in 2018, but only 348000 are regulated somewhere in the world [8].

Table 1.1 summarizes the source categories of some major emerging contaminants in aquatic ecosystem. This study concluded that most of the emerging contaminants and their bioactive

metabolites are continually being introduced to the aquatic environment as complex mixtures via a number of routes but primarily through both untreated and inadequately treated sewage. Thus, most of them pass through the treatment plant and enter the aquatic environment, leading to potential adverse effects on the ecology.

The potential risks to human health and the overall environment are not understood in their entirety, but at least some harmful effects have already been clearly demonstrated. They can cause adverse health effects on humans and other living species [9].

Advanced oxidation processes (AOPs) are promising techniques, which can be used as alternative processes or polishing step in wastewater treatment [10]. Nowadays, AOPs are under extensive interest of many researchers mainly due to non-selectivity regarding the contaminant oxidation, possibility of complete mineralization of pollutants, and lack of solid waste formation during majority of AOPs [11]. Photocatalysis as one of AOPs has gained an extensive attention in last decades for water treatment.

Among AOPs, heterogeneous photocatalysis using TiO_2 has been widely investigated for the degradation of POPs in water [12]. The key advantage of AOPs is the complete mineralization of organic carbon into CO_2 and H_2O, whilst photocatalytic AOPs systems offer further advantages of low cost due to the use of catalytic materials, no consumable chemicals and the potential use of sunlight. The main drawback to this technique is again the energy consumption required for the UV lamps, but solar photocatalysis poses an alternative to this. However solar photocatalysis is not viable in every country due to local weather conditions. Therefore, under solar irradiation, in which content of UV light is about 3 – 6% (based on energy and not on photon number) [13], the photocatalytic activity of TiO_2 significantly decreases. Poor selectivity of TiO_2 photocatalysis in the degradation of low-level of POPs in polluted waters in the presence of other higher-level POPs is another disadvantage of heterogeneous photocatalysis treatment [14]. The fine particle size of the TiO_2 particles, together with the large surface area-to-volume ratio and surface energy creates strong tendency for such catalyst particles to agglomerate during the operation. Such particle agglomeration is highly detrimental in view of particle size preservation, surface area, reduction and reusable lifespan [15]. To overcome these limitations, doping TiO_2 with metals and non-metallic elements is a promising approach which not only extends the TiO_2 response to the visible region but also helps to decrease the recombination of charge carriers thus enhancing the interfacial charge transfer rate. Modification of titanium dioxide with noble metals or its combination with another oxide is an efficient approach to improve photocatalytic performance of titanium dioxide [16,17].

In spite of numerous studies conducted in the field of advanced materials for photocatalysis, many questions are still open and effect of some parameters on photocatalytic activity is underestimated or even neglected in many works. Hence, further investigations are needed in order to find out ways to improve photocatalytic activity of TiO_2 and study effect of different parameters on its performance.

1.2. State of the art: Water treatment in Morocco

Morocco is predicted to have a water deficit by 2020. The Souss-Massa region in Southern Morocco, for instance, is already under significant water stress. The main industries in Morocco are food, tobacco, chemicals, mechanical, metal, electronics, construction materials, leather, and textiles. Industrial activity is concentrated in the north west of the country. Forty-nine percentage of industries are located in Casablanca. The majority of domestic and industrial wastewater of the urban and rural centers is discharged into the natural environment, without preliminary treatment. Rivers receive directly approximately 30% of total water pollution and 27% is absorbed by soil and groundwater. Industrial effluents convey heavy organic and toxic pollution. 98% is poured into the sea (944.7 million of m^3) and the remainder into the water network or directly onto the ground. The basic water law in Morocco is no. 10-95, which introduces the legislative, economic and organizational instruments necessary for the institution of a decentralized and participative water resource management and use program. One of the most important components of Law 10-95 is the creation of a water pollution tax based on the "user-pays" — "polluter pays" principle, and quality protection.

The Moroccan Department of the Environment has also developed an incentive financial instrument to avoid industrial pollution under its FODEP Foundation for Democratic Peocess program. The purposes of this program are to (I) ensure respect for the environment, (2) save natural resources, and (3) reduce water and air pollution and solid waste. This program, financed by the German Government, has a total budget of 240 million Dirhams (MDH) (about 22 million Euros). Pollution targeted is from small and medium-sized industry. This program provides financial support to downstream production wastewater, solid waste and air pollution treatment projects and integrated production projects aimed at reducing water pollution, solid waste or air pollution from the start, as well as saving resources (water, energy. etc.) by using non-polluting technologies.

Up to time of writing, this program had funded 95 projects for a total amount of 44 million Euros

of which 57 million are related to wastewater treatment. An example is the 155-thousand-Euros wastewater treatment station installed in a poultry slaughterhouse in Settat. Being aware of the important threat that such diverse industrial wastewater means to Morocco's natural water resources, several innovative studies related to the development of new treatment technologies have been performed by Moroccan researchers, sometimes in collaboration with foreign institutions. Many of these studies deal with treatment of textile industry effluents mostly by photocatalytic processes or electrocoagulation. For instance, evaluation of the efficiency of photocatalytic treatment of the model textile industry water pollutant Acid Red 88 dye, using Silica gel-supported titanium dioxide photocatalysts made by sintering TiO_2/SiO_2 mixtures with varied TiO_2 contents, calcination temperatures and times. Furthermore, the photocatalytic degradation of the textile dye Basic Red 18 was evaluated for two different types of TiO_2, Degussa P25 (80% anatase) and Framitalia (100% anatase). Results were compared with the efficiency of decolonization using an H_2O_2/UV system. Finally, a marine mussel test was used to evaluate the efficiency of photocatalytic oxidation with TiO_2 for eliminating eco-toxicity. Moroccan researchers have also studied the feasibility of electrocoagulation for treating textile wastewater to determine the optimal operating conditions and find out which iron hydroxide, formed during electrolysis, is responsible for the electrocoagulation process. The removal of coloring compounds from a textile effluent was evaluated by preparing the inorganic coagulants from electrolysis of NaOH, NaCI, and NaOH + NaCl solutions, using sacrificial aluminum electrodes operated at an electrical potential of 12 V. Other researchers have focused, not on the development of a specific industrial wastewater treatment technology, but on assessment of poor water quality based on physicochemical and ecotoxicological analyses [31]. The studied area, located in the north of Morocco included the River Sbou and its tributary the Fez River. The Mehrez Stream which discharges huge amounts of untreated municipal and industrial wastewater into the Fez River, is also included. The sample period was from May 10 to 25, 2012. The major quality problems are low dissolved oxygen, high turbidity organic flatter and ammonia content, severe chromium and copper pollution and high acute and chronic toxicity. This results in the loss of the aquatic life which still flourishes in the Fez River upstream from the Fez Medina. Well water in the region of Fez has moderately poor quality with nitrate and metal enrichments. Use of water from rivers or from untreated wells for drinking or for agriculture may place the health of the population at risk on human health and the environment and promoting the use of integrated pest management and of alternative approaches or techniques such as non-chemical alternatives to pesticides.

1.3. Thesis objectives

The primary focus of this thesis work is to develop a novel photocatalyst systems and to assess the potential of different AOPs for the degradation of organic pollutants from wastewater. New findings of this PhD thesis will be put into context. Finally, there is a conclusion on the work, and perspectives are brought forth on future research needs in the present area.
Research has focused on the following research and development stage which comprised of:

1. Synthesize and explore the optimal synthesis conditions for layered manganese oxide (birnessite) Ca_xMnO_y with adjusting the synthetic parameters including the molar ratio of calcium and manganese oxides type and ratio.

2. Synthesize the new heterostructures of TiO_2 (Hombikat UV100) with layered manganese oxide (birnessite) with adjusting the synthetic parameters including the molar ration of Ca_xMnO_y to TiO_2, and calcination temperature.

3. Characterize the synthesized composites using Ultraviolet-Visible absorption spectroscopy (UV-Vis), Scanning Electron Microscopy (SEM-EDX), Transmission Electron Microscopy (TEM), X-Ray Diffraction (XRD), surface areas (BET), X-ray photoelectron spectra (XPS), Photoluminescence spectra (PL), Nitrogen sorption and Elemental analysis via inductively coupled plasma optical emission spectroscopy (ICP-OES)
4. Undertake the photodegradation studies in the presence of the synthesised composites under visible & UV light to investigate the photocatalytic degradation of methylene blue, phenol as a model compound and imazapyr herbicide as a real pollutant.
5. Conduct adsorption studies, including baseline studies of selected pollutants adsorption, onto the Ca_xMnO_y-TiO_2 composites.
6. Evaluate pollutants concentration as a function of time with UV-Vis spectroscopy, high pressure liquid chromatography (HPLC) and MS-ESI.
7. Evaluate mineralization and oxidation of organic contaminants with total organic carbon (TOC).

8. Study the environmental fate of the products of photochemical degradation and evaluation of main intermediate products of imazapyr degradation.
9. Evaluate kinetics and compare performance of the synthesised composites with commercial standard TiO_2 powder (UV-100; P-25) when applied to the photocatalytic degradation of the aqueous solutions of selected pollutants (methylene blue, phenol and imazapyr).
10. Study the effect of the operating parameters such as catalyst concentration, initial pollutants concentration, pH, the wavelength of light on the photocatalytic degradation of selected pollutant.
11. Investigate the degradation rate of imazapyr using a variety of advanced oxidation processes (photolysis, photocatalysis, ozone, photocatalytic ozonation) in the presence of Ca_xMnO_y-TiO_2 composites and compare their performance to the commercially available TiO_2 (UV-100 and P-25).
12. Investigate and quantify the effects of inorganics and organics present in wastewater as scavengers limiting degradation efficiency of imazapyr.

1.4. Thesis Overview

This PhD thesis consists of five submitted manuscripts and two other manuscripts in preparation. Furthermore, it includes a background discussion of the most relevant literature regarding AOPs and photocatalysis particularly, and a general background to POPs chemistry.

This dissertation is divided into seven chapters:

Chapter 1 is a general introduction to the subject of remediation and chemical oxidation of water pollutants. It explains the background information needed to understand the chemistry behind AOP and photocatalysis particularly, with modified titanium dioxide as the subject of interest. The properties of catalyst in terms of its ability to degrade organic molecules are discussed. The basis of this first chapter is to provide a general background to POPs chemistry, a more detailed introduction will then be given at the beginning of each individual chapter, concerning the purpose of the research that has been conducted there.

Chapter 2 reports the synthesis of Ca_xMnO_y-TiO_2 composites with different manganese oxide birnessite fractions (1 to 50wt.-%) for efficient photocatalytic degradation of methylene blue and the herbicide imazapyr in aqueous solution under visible light irradiation, the results suggested that a correlation exists between the calcium manganese oxide content, oxidation state and the changes in the UV–Vis absorption properties. The composite with 5 % Ca0.1MnOy/TiO_2 possessed the highest photocatalytic performance among all the as-obtained catalysts, the enhanced photocatalytic activity was attributed to the reduction of the band gap from 3.18 eV to 2.89 eV for pure TiO_2 and 5 % Ca0.1MnOy/TiO_2 composite respectively.

Chapter 3 describes the photocatalytic removal of imazapyr from aqueous solution by Ca_xMnO_y-TiO_2 composite and the evaluation of main intermediate products. Modification of existing photocatalyst with (birnessite) to improve degradation activity towards model pollutants was investigated. Highly efficient new visible light driven Ca_xMnO_y-TiO_2 composite was successfully synthesized based on the precipitation of manganese oxide and mixing with commercial titanium dioxide TiO_2, by mechanical grinding, followed by annealing. Ca_xMnO_y-TiO_2 composite was assessed for the photocatalytic degradation of phenol and imazapyr herbicide, as model pollutants. Ca_xMnO_y-TiO_2 materials have recently been implicated for increased degradation efficiency and possible visible light absorption capabilities. This work uses kinetic and product formation data to compare Ca_xMnO_y-TiO_2 catalyst to pure titanium dioxide catalysts.

In this submitted manuscript, the Ca_xMnO_y-TiO_2 composite showed a much higher degradation rate (10.6 μM h^{-1}) than the unmodified TiO_2 UV100 (7.4 mM h^{-1}) for imazapyr degradation under UV-Vis irradiation. Comparison of the mineralization rate are 4.07 μM h^{-1} and 1.21 μM h^{-1} (0.679 ppm h^{-1} and 0.195 ppm h^{-1}) for Ca_xMnO_y-TiO_2 and TiO_2 composite respectively. The photodegradation process of imazapyr was examined in additional detail by considering intermediate species. In the Ca_xMnO_y-TiO_2 system, the concentration of intermediate products were continuously increased with prolonging irradiation time to achieve a maximum at 180 min of irradiation before a decreases of more than half in next hours. Whereas intermediate products were continuously increased with prolonging irradiation time and are maintain not decomposed, in the case of the TiO_2 system. This result suggested the enhanced photoactivity of the modified sample for intermediate products could more easily adsorb polarized organic reactants and thus promote their photocatalytic decomposition. On the basis of the experimental results, a photocatalytic mechanism was discussed in detail.

Chapter 4 entails the study of aqueous imazapyr degradation by ozonation, photocatalysis, and photocatalyzed ozonation by Ca_xMnO_y-TiO_2 Composite. The kinetics of the photocatalytic degradation of imazapyr were analyzed taking into account the effect of the pH, the Ca_xMnO_y-TiO_2 mass concentration as well as imazapyr concentration. The results of this study show that imazapyr removal followed a first-order kinetic model with a rate constant of 0.547 min^{-1} and 0.425 min^{-1} for photocatalytic ozonation and heterogeneous photocatalysis respectively, while second-order kinetic for ozonation process with a rate constant of 0.053 $mol.L^{-1}.min^{-1}$ at pH 7. Complete degradation of imazapyr was achieved within 10 min using photocatalytic ozonation for 5µM of imazapyr in the presence of 100 $mg.L^{-1}$ of Ca_xMnO_y-TiO_2 composite at pH 7. The high constant rate exhibited by Ca_xMnO_y-TiO_2 in the presence of ozone may be explained considering the high hydroxyl surface population of this sample supported by the fact that the deposition of the porous manganese oxide mainly on the surface of titanium dioxide that can easily accommodate the hydroxyl groups. Furthermore, it was also considered that the dissolved ozone was easy to accept electrons generated on the surface of Ca_xMnO_y-TiO_2 so that the recombination of the positive hole and negative electron pairs was hindered, ultimately a large number of radicals formed.

Chapter 5 explores the factors influencing imazapyr herbicide removal from wastewater using photocatalytic ozonation in the presence of commercial UV 100, this study investigates the degradation of imazapyr herbicide from wastewater by photocatalytic ozonation using TiO_2 as a semiconductor. Effects of operational parameters on imazapyr removal efficiency including TiO_2 dosing, initial herbicide concentration and pH were also studied. Obtained results showed that more than 90% of removal efficiency representing the disappearance of Imazapyr was maintained until 7 µM, further increase of Imazapyr concentration leads to decrease in removal efficiency, the optimal TiO_2 loading where Imazapyr degradation reached the maximum removal rate of 93.0 % is (200 mg/L). Otherwise, the degradation of Imazapyr followed the first-order kinetics and complete degradation was achieved within 20 min using photocatalytic ozonation for 5µM of Imazapyr at pH 7. Photocatalytic rate constant of maximum removal of Imazapyr by photocatalytic ozonation process was 0.247 min^{-1}.

Chapter 6 investigates the influence of humic acids extracted from Chaouia soil on the behavior of transition metal ions and imazapyr herbicide, in this work, it was concluded that humic acids (HAs) have a variety of functional groups, which allow them to complex with metal ions and pesticides. Furthermore, these interactions can not only alter the environmental behavior, but also influence the removal and transportation of those pollutants. The effect of the presence of

HA on photolysis of Tribenuron-methyl (TRB) and Imazapyr (IMAZ) herbicides in water was studied by irradiation of different mixtures of HA/herbicide (0.5:1 and 1:1 by volume). The kinetic rate constant k of TRB and IMAZ decreases from 0.0029 h^{-1} to 0.0012 h^{-1} and from 0.242 h^{-1} to 0.014 h^{-1} in 0.5/1 HA/herb and 1/1 HA/herb respectively. The obtained results clearly demonstrate that HA substances exhibit a screening effect on the photochemical degradation of the two herbicides. The protective effect of HAs on the TRB and IMAZ degradation could be explained with an inclusion and/or adsorption of the herbicide molecules in the humic matrix.

Chapter 7 presents the major conclusions drawn from this dissertation. Recommendations for potential future research are also addressed in this chapter.

1.5. Treatment of wastewater containing organic matter

The total amount of wastewater (sewage, industrial and agricultural) globally discharged to water bodies is tens of millions of cubic meters per day [18]. According to some estimation, about 80-90 % of all wastewater in developing countries is not treated [19]. For instance, an estimated treatment capacity for sewage generated in major cities in India is only about 30 % [4]. Whereas in EU about 82 % of all generated urban wastewaters have received secondary treatment in 2009-2010 [20].

Amount of industrial wastewater varies significantly from country to country. It should be noted that in general almost all water utilized for industrial purposes ends up as wastewater. In developing countries quantities of wastewater generated by the same type of industry are generally higher [5,21].

1.5.1. Conventional Methods of Wastewater Treatment

Conventional wastewater treatment generally classified as 1) preliminary treatment 2) primary treatment 3) secondary treatment 4) Tertiary treatment or advanced treatment.

In **preliminary treatment**, impurities such as coarse solids, grit are removed. The objective is to protect the downstream equipment and to enhance the efficiency of the subsequent stages.

Primary treatment removes settable solids by sedimentation and floating materials such as oil and grease by techniques such as froth flotation.

Sedimentation removes a good percentage of organic and inorganic pollutants which can contribute a high reduction in COD. Some amount of heavy metals, organic nitrogen and phosphorous are also removed in this operation.

The effluent from primary treatment containing colloidal particles and dissolved compounds are given to the secondary treatment system for further treatment.

Secondary treatment generally employs aerobic biological treatment techniques. The objective of the treatment is to remove the colloidal and dissolved organic matter present in the effluent to an acceptable limit. Different methods and techniques are employed for biological treatment of waste water. It differs either in the way oxygen is supplied or in the way biological growth is maintained in the system. These techniques have a removal efficiency of 70-90% BOD (Biochemical Oxygen Demand). Despite applied treatment, wastewater effluent is characterized by high concentration of organic materials, high absorbable organic halogens (AOX), suspended solids, metal ions, tannins, lignin and derivatives, fatty acids, etc [18].and this system may fail if contains non-biodegradable compounds.

The non-biodegradable compounds are generally removed in the advanced treatment systems. But if these compounds have the ability to kill the microorganisms (phytotoxic), biological treatment systems will miserably fail. Hence, additional treatment should be applied in order to reach discharging limits and/or recommendations and minimize and/or prevent negative effect to the environment.

In **tertiary/Advanced treatment** systems removal of specific compounds are targeted. It generally includes chemical oxidation, reverse osmosis, ion exchange, microfiltration, nanofiltration etc. In some cases these techniques are used in combination with primary and secondary treatment (eg: chemical addition in primary and secondary treatment.

1.5.2. Advanced Oxidation Processes (AOPs) - An Overview

At the beginning of the 21st century, the world was facing a global water crisis, both in quality as in quantity, caused by population growth, rapid industrialization and poor management in the use of water. Throughout the century, the increase was added to these parameters uncontrolled use of water in different sectors such as agriculture, domestic and industrial, that resulted in a growing pollution of the waters associated with the serious shortage problem of water. The use of non-regulated substances such as drugs, detergents, products for use personnel, surfactants, pesticides, flame retardants and additives, at low levels concentration, contribute to water pollution along with other pollutants such as the metals. Among these pollutants are the so-called pollutants emerging economies (CEs) [6,22], whose main characteristic is that they are not biodegradable by conventional treatments carried out in wastewater treatment plants.

In this context, Advanced Oxidation Processes (AOP) have been described as methods effective for the elimination of a large number of persistent pollutants. However, AOPs have the disadvantage of being relatively expensive since they require consumption elevated reagents and energy, which has somewhat limited large-scale application. However, with the advent of higher efficiency UV lamps, visible light catalysts, and improved reactor design, with the help of computational fluid dynamics and energy modeling, both UV and solar-based photocatalysis have great potential for large-scale application. In this way R & D (Research and Development) in this field is increasingly focused on those processes that can be carried out with sunlight.

Advanced oxidation processes AOPs are recommended when the wastewater contains recalcitrant organic compounds of low biodegradability and/or high chemical stability, such as pesticides and pharmaceuticals in water and wastewater. The purpose of these methods is to degrade these contaminants, converting them to carbon dioxide, water and inorganic ions, or to other innocuous products. In general, the AOPs when applied in a right place, give a good opportunity to reduce the contaminants' concentration from several hundred ppm to less than 5 ppb. That is why they are called the water treatment processes of the 21st century[23].

In some cases, the non-biodegradable initial compounds are converted to biodegradable compounds in which a combination of AOP and biological treatment can be used. The latter approach can be used as a pre-treatment method for wastewaters prior to biological treatments.

Advanced oxidation processes can provide a complete solution to the problem of wastewater pollutants, compared to most other methods that can leave the problem at a preliminary stage such as a phase separation where the problem of disposal still exists. Operational costs are reduced due to the lack of secondary waste stream that would be present if other processes, such as adsorption, ion exchange and stripping, were utilized [1,24].

Conventional AOPs can be divided on homogeneous and heterogeneous based on reactive phase. Among homogeneous conventional AOPs Fenton based process (Fenton, Fenton like, Sono-Fenton, Photo-Fenton, Electro-Fenton, Sono-electro-Fenton, Photo-electro-Fenton, Sono-photo-Fenton) and O_3 based processes (O_3, O_3 + UV) and H_2O_2 based processes (H_2O_2 + UV) and their combination can be emphasized. Photocatalysis, catalytic wet peroxide oxidation, catalytic ozonation, etc. are heterogeneous conventional AOPs. Depending on the way of hydroxyl radical generation chemical, electro-, sono- and photo-chemical AOPs can be distinguished. However, there are also alternative AOPs such as supercritical water oxidation, pulsed electron beam, γ-ray irradiation and microwaves [7, 21].

Although different AOPs have different degradation mechanisms, the reaction chemistries are similar, involving generation of highly reactive oxidation species such as hydroxyl radicals,

positive holes in semiconductors, and reactive oxygen species (ROS); TiO_2 surface-hole being the most oxidizing. One of the main elements of most AOPs is the production of free or surface hydroxyl radicals (•OH). Hydroxyl radicals have an oxidation potential of + 2.8 eV next only to fluorine in the list of known oxidants (Table 1.2.). These •OH radicals are produced by different processes with various oxidants such as hydrogen peroxide and/or ozone. Hydroxyl radical oxidation reaction mechanisms can be classified into three categories: hydrogen abstraction, electrophilic addition and electron transfer.

Table 1.2 Oxidation power of oxidation species

Oxidation species	Redox potential (eV)
Flourine	3.03
Hydroxyl radical	2.80
Ozone	2.07
Hydrogen peroxide	1.78
Permanganate	1.69
Chlorine dioxide	1.56
Chlorine	1.36
Oxygen	1.23

(Source: Zhou H and Smith D.W., 2002)

1.6. Recent review on Advanced Oxidation Processes (AOPs) involved in this research

1.6.1. Ozonation

Ozonation can be used for the degradation of organic pollutants in water. Ozone is a powerful oxidant (Electrochemical oxidation potential of 2.07V) which is generally produced by an electric discharge method in presence of air or oxygen. The degradation of pollutants in water using ozonation occurs through two mechanisms. One way is the direct reaction between the ozone and the dissolved compounds which is a highly selective process with low reaction rates and the other is the reaction between the generated radicals produced in the ozone decomposition and the dissolved compounds [25].

The first step of this process is the decomposition of ozone by hydroxide ions (Eq. 5.1). The formed hydroperoxyl radical is in an equilibrium state (Eq. 5.2). The superoxide anion radical and ozone then react to form ozonide anion radical (Eq. 5.3 & Eq. 5.4), which then immediately decomposes into oxygen and a hydroxyl radical (Eq. 5.5)[9,26]. Overall, three ozone molecules theorecally produce two hydroxyl radicals as shown in Eq. (5.6).

$O_3 + OH^- \rightarrow O_2^{\bullet} + HO_2^{\bullet}$ **(**Eq. **5.1)**

$HO_2^{\bullet} \leftrightarrow O_2^{\bullet -} + H^+$ **(**Eq. **5.2)**

$O_3 + O_2^{\bullet -} \rightarrow O_3^{\bullet -} + O^2$ **(**Eq. **5.3)**

$O_3^{\bullet -} + H^+ \leftrightarrow HO_3^{\bullet}$ **(**Eq. **5.4)**

$HO_3^{\bullet} \rightarrow {}^{\bullet}OH + O_2$ **(**Eq. **5.5)**

Overall:

$3O_3 + OH^- + H^+ \rightarrow 2OH^{\bullet} + 4O_2$ **(**Eq. **5.6)**

A major limitation of ozonation is the formation of potentially harmful by-products reacting with background compounds in water, one of which, bromate, is regulated and considered as a possible human carcinogen [21].

It is then important to optimize both the disinfection and oxidation processes of ozonation to minimize toxic by-product formation.

1.6.2. Ozone + catalyst (O_3/CAT)

Another opportunity to accelerate ozonation reactions is to use heterogeneous or homogeneous catalysts. Several metal oxides and metal ions (Fe_2O_3, Al_2O_3–Me, MnO_2, Ru/CeO_2, TiO_2–Me, Fe^2+, Fe^3+, Mn^2+, etc.) have been studied and sometimes a significant acceleration in the decomposition of the target compound has been achieved, although the reaction mechanism in most cases remained unclear.

Ajmal et al. [27] studied advanced oxidation of chlorobenzenes in wastewater as well as in model solutions using iron and manganese ions as heterogeneous catalysts. They concluded that the reduction of total organic carbon (TOC) and chemical oxygen demand (COD) from wastewater was more efficient with the ozone/catalyst system than oxidation with ozone at high pH values. The O_3/Mn(II) and O_3/Fe(II) systems were more effective in the removal of organochloride compounds than the O_3/Fe(III) and O_3/high pH systems. The study of Karpel Vel Leitner et al.

[28] concerned the catalytic ozonation of one model compound – succinic acid, which is barely oxidized by ozone alone. Catalytic ozonation process using Al_2O_3, TiO_2 in its anatase form, and clay as the support for metal catalysts was also studied. Salicylic acid was chosen as a model compound. In contrast to unassisted ozonation, TOC measurements showed complete removal of organics in catalytic ozonation.

Ozone–Granulated Activated Carbon systems (O_3/GAC) make a special case of catalytic ozonation. Quite well-known is the combined system O_3/GAC for biorefractory compounds (for example, pesticides) destruction where the GAC's bed life is prolonged due to the ozonated water [29]. Using the GAC as a catalyst for free radicals formation in ozonated water is much less studied and some results are quite contradictory.

1.6.3. Ozone–UV radiation (O_3/UV) Process

Hydroxyl radicals can be produced by using UV light to the ozonated water. In this process, a high synergistic effect between ozone and the UV radiation is observed. Photolysis of ozone generates hydrogen peroxide and thus O_3/UV involves all of the organic destruction mechanisms present in H_2O_2/O_3 and H_2O_2/UV processes. Ozone readily absorbs UV radiation at 254 nm wavelength (the extinction coefficient ε254 nm = 3300 M^{-1} cm^{-1}), which decomposes into O_2 and the oxygen atom O (1D) (excited state) as shown in Eq. 5.7. O (1D) is highly reactive and rapidly reacts with the water molecule to produce H_2O_2 as an intermediate, which then decomposes to $^{\bullet}OH$.

$$O_3 + h\nu \rightarrow O_2 + O\ (^1D) \qquad \text{(Eq. } \mathbf{5.7}\text{)}$$

$$O\ (^1D) + H_2O \rightarrow H_2O_2 \rightarrow 2\ ^{\bullet}OH \qquad \text{(Eq. } \mathbf{5.8}\text{)}$$

The generation of H_2O_2 in this method is much less efficient than the electrochemical method used in the industry. Hence the O_3/UV process would be expected to be more expensive than O_3/ H_2O_2 process[29].

Although photochemical cleavage of H_2O_2 is conceptionally the simplest method for the production of hydroxyl radicals, the exceptionally low molecular absorptivity of H_2O_2 at 254 nm (ε254nm = 18.6 M^{-1} cm^{-1}) limits the $^{\bullet}OH$ yield in the solution.

Table 1.3 shows that photolysis of ozone yields more radicals than the UV/ H_2O_2 process. The absorptivity of H_2O_2 can be increased by using UV lamps with output at lower wavelengths. In practice, the power requirement for UV lamps in the process of ozone photolysis is in *watts* range versus *kilowatts* for hydrogen peroxide photolysis.

Table 1.3 Formation of $^{\bullet}OH$ from photolysis of ozone and H_2O_2

Oxidant	ε 254 nm, M^{-1} cm^{-1}	Stoichiometry	$^{\bullet}OH$ formed per incident photon
H_2O_2	20	$H_2O_2 \rightarrow 2^{\bullet}OH$	0.09
O_3	3300	$3O_3 \rightarrow 2^{\bullet}OH$	2.00

If water solutions contain organic compounds strongly absorbing UV light, then UV radiation usually does not give any additional effect to ozone because of the screening of ozone from the UV by optically active compounds such as phenol, 5-methylresorcinol, xylenols, etc[26]. Although phenolic compounds (phenol, *p*-cresol, 2,3-xylenol, 3,4-xylenol) are easily oxidizable by ozone, complete mineralization to CO_2 and H_2O is uncommon.

1.6.4. Heterogeneous Photocatalysis

Unlike the previously mentioned AOP methods, photocatalysis up to this point has seen limited full-scale application either in drinking or wastewater treatment, but has garnered a significant amount of research interest in academia over the last three decades. The one major advantage of this process is the potential to use natural sunlight. Combined with a highly active catalyst, this technology could be applied worldwide not only for water treatment, but for hydrogen production, self-cleaning coatings, and many other uses.

This explains the fact that even though it has the least industrial application to date compared to ozonation and UV/H_2O_2, it has received the majority of the academic research, with >1000 papers published per year over the last decade, mostly with P25 TiO_2, an inexpensive and non-toxic photocatalyst.

Photocatalysis using a semiconductor have also earned an important place among the AOPs because of the absence of residuals after the treatment, the stability of the catalyst, and the possible use of solar light as light source. Photocatalytic semiconductors, such as TiO_2, ZnO and SnO_2, have attracted more and more attention for their potentials in photodegradation of harmful contents. Notably zinc oxide and titanium dioxide has played a much larger role compared to

other semiconductor photocatalysts due to its cost effectiveness, inert nature and photostability. TiO_2 has received much attention because of its strong oxidizing power of its holes, high photo-stability, low costs and long-term-stability against photo and chemical corrosion. TiO_2 is a naturally occurring mineral that commonly exists in three crystal forms: rutile, anatase and brookite. Anatase TiO_2 is transformed into rutile TiO_2 at temperatures above 900 K. TiO_2 is insoluble in water and in dilute acids but dissolves slowly in hot sulfuric acid. It has a high surface activity and good corrosion stability [6].

In the absence of light, the valence band (highest occupied molecular orbitals) is fully occupied by electrons whereas the conduction band (lowest unoccupied molecular orbitals) is unoccupied by electrons. The energy difference between the conduction and the valence bands is called the band gap (Ebg).

In semiconductors, electron transitions between the valence band and the conduction band can be affected by visible and UV light with photon energy equivalent to or higher than the band gap energy[23]. If a photon with energy greater than or equal to the band gap energy is absorbed, an electron is promoted from the valence band to the empty conduction band of the semiconductor particle creating an electron deficiency in the valence band called a valence band hole (hvb^+) which may be a strong oxidant. The conduction band electron (ecb^-) can either recombine with the valence band hole and produce heat or they can make their separate ways to the surface of the semiconductor particle where they have the possibility of reacting with surface absorbed species.

Photogenerated charge carriers (both ecb^- and hvb^+) that are able to make their way to the surface of the semiconductor particle, can react directly or indirectly with absorbed species. At the interface of the semiconductor and the solution medium, an adsorbed electron acceptor substrate (A_{ads}) is reduced by the transfer of a conduction band electron to the lowest unoccupied molecular orbital of the acceptor molecule, while an adsorbed electron donor substrate (D_{ads}) is oxidized by the transfer of a donor electron from the highest occupied molecular orbital to the valence band hole of the semiconductor particle. If oxygen is present in the water, it can capture the electron in the conduction band to form the superoxide radical ion while the valence band hole can react with surface-bound water molecule or hydroxide ion to produce hydroxyl radicals. Therefore, irradiation of a semiconductor particle initiates redox chemistry at the surface [19]. Hence, photogenerated electrons that make their way to the surface of the semiconductor can reduce the absorbed oxygen to water and photogenerated holes or produced hydroxyl radicals may oxidize any adsorbed contaminants to CO_2.

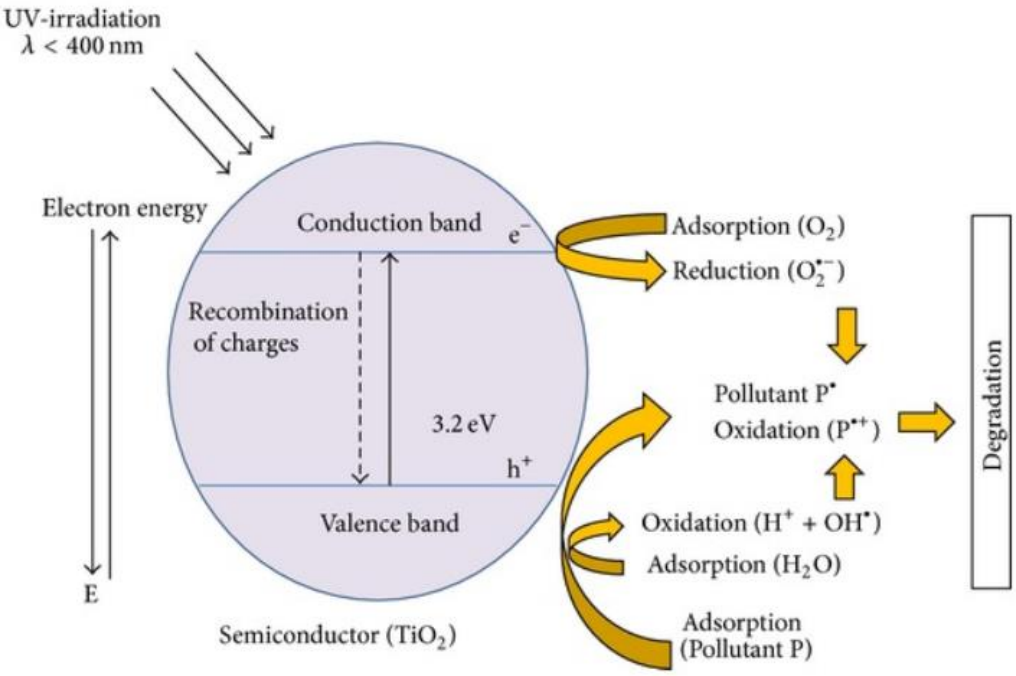

Figure 1.1. Photocatalysis mechanism.

Photocatalytic process in water can be divided on five steps:

1. Transfer of reactants in water to the surface of photocatalysts
2. Adsorption of reactants on the surface
3. Photonic activation of surface of photocatalyst and reaction in the adsorbed phase
4. Desorption of reaction products
5. Elimination of reaction products from the interface region.

The following general mechanism has been proposed for heterogeneous photocatalysis on TiO_2.

$TiO_2 + h\upsilon\ (\lambda < 380\ nm) \rightarrow\ \ h_{vb}^{+} + e_{cb}^{-}$ (Eq. **5.9)**

$h_{vb}^{+} + e_{cb}^{-} \rightarrow heat$ (Eq. **5.10)**

$h_{vb}^{+} + H_2O \rightarrow HO\bullet + H^{+}$ (Eq. **5.11)**

$h_{vb}^{+} + OH^{-} \rightarrow HO\bullet$ (Eq. **5.12)**

$e_{cb}^{-} + O_2 \rightarrow O_2\bullet^{-}$ (Eq. **5.13)**

$O_2\bullet^{-} + H^{+} \rightarrow HO_2\bullet$ (Eq. **5.14)**

$HO_2\bullet + HO_2\bullet \rightarrow H_2O_2 + O_2$ (Eq. **5.15)**

$H_2O_2 + e^- \rightarrow HO\bullet + OH^-$ (Eq**. 5.16)**

$O_2\bullet^- + H_2O_2 \rightarrow HO\bullet + OH^- + O_2$ (Eq**. 5.17)**

$H_2O_2 + h\upsilon \rightarrow 2\ HO\bullet$ (Eq. **5.18)**

Nevertheless, TiO_2 can be only activated near visible UV, which constitutes only about 3-5 % of the incoming solar energy on the Earth's surface. Because the application of TiO_2 in water and air purification is restricted as its intrinsic wide band gap (3.2 eV) requires high energy excitation such as UV light, which only composes 3-5% of solar irradiation. Thus, the major portion of solar energy (visible light) could not be used for photocatalytic reaction. Besides, high recombination rate of photo excited carriers is another limitation for the applicable fields of TiO_2. Due to the short life of photo excited carriers, only a small part of electrons and vacancies can move to its surface, which lead to further reduction of photocatalytic efficiency.

Numerous attempts to design photocatalytic materials with activity higher than that of TiO_2 were made recently. Modification of TiO_2 can lead to desired photocatalytic activity under visible light. One of the most efficient photocatalysts active under visible light is doping TiO_2 with noble metal, metals ions, transitions metals ions such as Mg, Mn, Co, etc.[30], to induce extensions of the absorption spectrum into the visible light spectrum (400 nm- 800 nm), where the day light source could be utilized effectively. Doping TiO_2 with transition metal ions offers a way to trap the charge carrier thus improving the efficiency of the catalyst.

However, these dopant metals have to be used in small quantity to avoid recombination of photogenerated electrons and holes, which is bolstered by the large amount of these dopant species. But the low content of metal doping leads to only small shift in the absorption edge of TiO_2 towards visible region. Generally, metals dopant such as V, Cr, and Mn form energy levels below the conduction band edge[31].

The formation of semiconductor composites comprising multicomponent or multiphase hetero-junctions is another effective strategy to design highly active photocatalyst systems. Wan et al.[32] suggested that efficient photocatalyst can be designed by combination of n-type semiconductor with hole-accepting semiconductor with relatively high structure openness degree.

One popular strategy is the decoration of photocatalytic materials with metal or metal oxide nanoparticles. In fact, the Fermi energy of the metal oxide nanoparticle is usually lower than that

of the semiconductor; facilitating electron transfer from the semiconductor to the metal oxide via the Schottky-contact [30,33].

1.6.5. Photocatalytic Ozonation

A combination of photocatalysis together with ozone, which is a strong oxidizer, is reasonable for the treatment of difficult to degrade organic compounds since the organic compounds are then expected to decompose more quickly and thoroughly in the presence of ozone, to carbon dioxide, water, or inorganic ions.

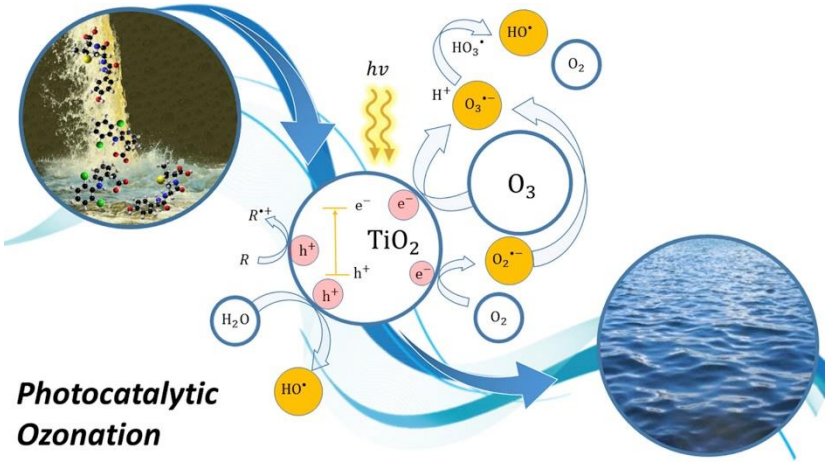

Figure 1.2. Photocatalytic ozonation mechanism

Source: Nuno F.F.Moreira et al (2015)

Sanchez et al. [26] combined these two methods for the removal of aniline from water and found that the decomposition rate of aniline is larger than when individually treated by either of the two methods, which indicates the presence of a synergistic effect of photocatalysis and ozonation. Photocatalytic oxidation and ozonation appear to be the most promising pre-treatment technologies compared with other advanced oxidation processes (AOPs) as shown by the large amount of information available in the literature. The principal mechanism of AOPs function is the generation of highly reactive free radicals. Consequently, a combination of two or more AOPs enhances free radical generation, which eventually leads to higher oxidation rates.

Principally, photocatalytic reactions commence by photoexciting the surface of photocatalyst with UV-Vis radiation, which can provide the appropriate band gap energy to generate photoactivated electron-hole pairs (Eq. **5.19)**. In parallel, ozone molecules can adsorb on the surface of the photocatalyst via three different interactions: physical adsorption, formation of weak hydrogen bonds with surface hydroxyl groups, and molecular or dissociative adsorption

into Lewis acid sites, each interaction resulting in the production of active oxygen radicals ($^{\bullet}O$) (Eq. **5.20)**. Furthermore, by employing wavelengths shorter than 300 nm, molecules of ozone and hydrogen peroxide would also absorb these wavelengths, producing active oxidising reagents (Eq. **5.21)** and (Eq. **5.22)** [34]. The photogenerated electrons on the photocatalyst surface (Eq. **5.19)** react with adsorbed oxygen and ozone molecules as electron acceptors (Eq. **5.23)** and (Eq. **5.24)** [35], and these reactions are important to decreasing the recombination rate of electron-hole pairs. The recombination of electrons and holes negatively affects reduction and oxidation reactions on the photocatalyst surface, quantitatively decreasing the effective interactions and consequently reducing the performance of this technology. The electron affinity of ozone (ca. 2.1 eV) is higher than that of oxygen (ca. 0.44 eV), which can promote photocatalytic reactions in the presence of ozone 6 (photocatalytic ozonation) more positively than in the presence of oxygen (simple photocatalysis). The hydrogen peroxide molecules that are generated can also react with photoexcited electrons on the photocatalyst surface, forming hydroxyl radicals (Eq. **5.25)**. The photogenerated holes (Eq. **5.19)** are assumed to directly attack the pollutant molecules adsorbed on the photocatalyst surface (Eq. **5.26)**, or to react with water molecules (acid conditions) or more efficiently with hydroxide anions (alkaline conditions), to produce hydroxyl radicals (Eq. **5.28)** which oxidise the pollutant molecules. Other oxidative species such as oxygen atom radicals ($^{\bullet}O$) and superoxide and ozonide radical anions ($^{\bullet}O_2^-$ and $^{\bullet}O_3^-$) are presumed to be generated as reactive intermediates in the photocatalytic ozonation medium, and could potentially oxidise the contaminants directly or reform to produce hydroxyl radicals via different chain reactions. Hydroxyl radicals produced in the aforementioned processes attack target pollutant molecules and decompose them non-selectively to less harmful substances (Eq. **5.26)**. Three possible mechanisms are assumed for the decomposition of pollutants by hydroxyl radicals: electron transfer, radical addition and hydrogen abstraction.

Initial reactions in the presence of photocatalyst, ozone and illumination:

$$\text{Photocatalyst} + h\nu \rightarrow \text{Photocatalyst} + e^- + h^+ \quad \text{(Eq. 5.19)}$$

$$O_3 + \text{Photocatalyst (active surface sites)} \rightarrow {}^{\bullet}O + O_2 \quad \text{(Eq. 5.20)}$$

$$O_3 + h\nu \rightarrow {}^{\bullet}O + O_2 \quad \text{(Eq. 5.21)}$$

$$H_2O_2 + h\nu \rightarrow 2\ OH^{\bullet} \quad \text{(Eq. 5.22)}$$

Possible reactions of photogenerated electrons (e^-) on the surface of photocatalyst:

$$O_2\,(ads) + e^- \rightarrow {}^{\bullet}O_2^- \quad \text{(Eq. 5.23)}$$

O_3 (ads) + e^- → $\bullet O_3^-$ (Eq. **5.24)**

H_2O_2 (ads) + e^- → $OH^\bullet$ + OH^- (Eq. **5.25)**

Possible reactions of photogenerated holes (h^+) on the surface of photocatalyst:

Pollutant $_{(ads)}$ + h^+ → [Pollutant]$^+$ (ads) → multistep CO_X, NO_X, SO_X, etc. (Eq. **5.26)**

$H_2O_{(ads)}$ + h^+ → OH• + H^+ (pH < 7) or $OH^-_{(ads)}$ + h^+ → $OH^\bullet$ (pH > 7) (Eq. **5.27)**

1.7. Major sources of wastewater

The main sources of emerging contaminants are municipal wastewater, hospital effluents, chemical manufacturing plants where any of the classes of ECs are manufactured or used, leakages and leachates from landfills, storm water runoffs and wastewater from livestock and agriculture [36]. A graphical description of the water cycle related to ECs is provided in Figure 1.3.

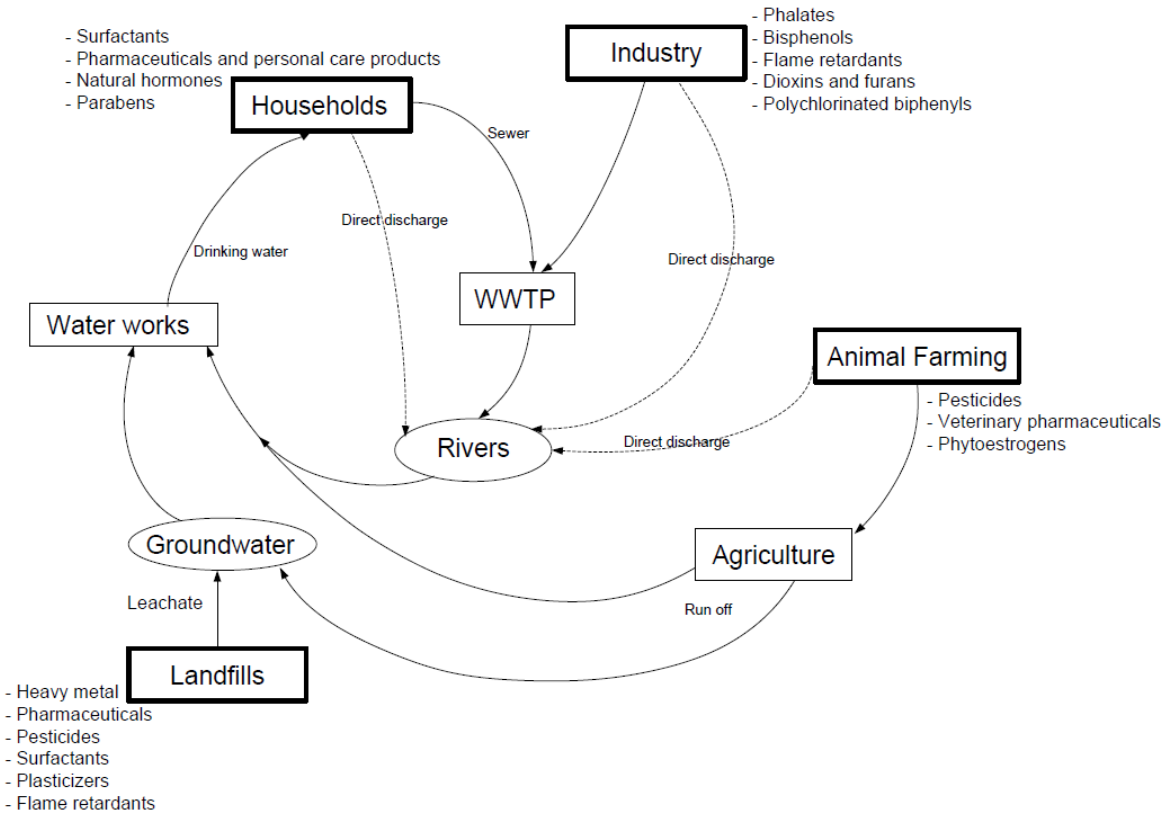

Figure.1.3 Water cycle of potential fate and transport of ECs (adapted from Petrovic, et al.2003)

Typically, the concentration of these emerging contaminants in treated wastewater, surface water and groundwater are in the range of 0.1 – 20 μg/L[37]. A study on concentrations of ECs in treated wastewater effluents, reported a range of 1.0 ng/L to 1.0 μg/L[38].

Concentrations of emerging contaminants can vary depending on the type of pollutant, the water source and the geographical location.

Municipal wastewater is a complex mixture of water with organic and inorganic compounds discharged from residences, offices, commercial facilities and institutions. More than 99% of the organic matter present in municipal wastewater consists of proteins and carbohydrates that originate from excreta, urine, food wastes and used water from bathing, washing and laundering. Since municipal wastewater contains human waste, a large number of micro-organisms are also present including pathogenic contaminants. Some of the waterborne bacterial diseases present in sewage include cholera, typhoid and tuberculosis [37].

Industrial wastewater effluents are produced by activities associated with raw material and food processing, manufacturing, paper production, petrochemical refining and the like. The main difference between municipal wastewater and industrial wastewater is the variable nature of industrial wastewater. The quality of municipal wastewater is similar irrespective of jurisdiction. However, this is not the case for industrial wastewater where the quality of wastewater from one industry has no correlation with that of another industry.

Each industry's wastewater is unique and comprised of chemicals used in their different processes. For example, metal processing industries release cadmium, chromium, iron, lead, nickel, titanium and zinc; textile industries discharge inks and dyes; the pulp and paper industry dispose a huge amount of chlorine-based substances along with suspended solids and organics; petrochemical industries release phenols and mineral oils.

1.7.1. Selection of model and real pollutant in this research

The selection of appropriate and representative pollutants was a crucial aspect of preparation for this research work. The criteria used in selection of the three representative molecules were:

- ✓ Belonging to different classes and different characteristic and type of effluent.
- ✓ Molecules that have high potential risk with a persistence in the environment or in relation to biological treatment, and
- ✓ Molecules likely to be found in high concentration (high production volume chemicals) for which analytical tools are available or accessible.

- **Methylene blue dye**

A large amount of industrial dyes are lost in the dying process. In the textile industry, this loss can be 4% of the dye used. If released directly into the aqueous environment, this can cause an aesthetic effect by changing the visible colour of the water. These dyes are highly stable and are not completely removed in conventional wastewater treatment processes [39].

The dyes and their by-products formed from the transformation during treatment and in the receiving body, can have a toxic effect on organisms in the environment. For photocatalytic research, dyes are one of the most common model compounds tested not only because they represent a persistent water pollutant, but when dissolved in water the bleaching of the dye during the reaction provides a quick and simple qualitative response [40]. As well dyes have characteristic absorption properties in the UV/visible spectrum, allowing UV-spectrophotometers to be used to determine kinetic data. Methylene blue (MB) is a cationic dye. In terms of use as a model compound: kinetic data in terms of parameters, photocatalytic degradation mechanisms with intermediate analysis, and tests on reactor configurations provide a framework for catalytic evaluation [41]. MB also has a high extinction coefficient in the visible range, allowing for lower concentrations to be used in the reaction. MB is relatively transparent to UV radiation which is used by the TiO_2 catalyst.

In recent study, feasibility of methylene blue (MB) as a test molecule for photocatalytic reactions was examined. Results suggests that methylene blue is inappropriate probe molecule for photocatalytic reactions since photosensitization may occur, which is difficult to distinguish from photocatalysis [42].

Photosensitization initiated by photoexcitation of MB adsorbed on the surface of photocatalyst, after which photoexcited electron in MB molecule is injected into solid material leading to decomposition of MB. Thus, in described case reaction is not photocatalytic. Therefore, organic dyes are recommended to be used as model pollutant just for primary tests and to be compared with other persistent compounds for testing photocatalytic activity, especially in visible light. As it was suggested by too many groups, measurements of action spectra can be an appropriate tool for confirmation of photocatalytic activity in visible light [43].

- **Phenolic compounds**

Phenolic compounds exist in water bodies due to the discharge of polluted wastewater from industrial, agricultural and domestic activities into water bodies. They also occur as a result of natural phenomena. These compounds are known to be toxic and inflict both severe and long-lasting effects on both humans and animals. They act as carcinogens and cause damage to the

red blood cells and the liver, even at low concentrations [44]. Interaction of these compounds with microorganisms, inorganic and other organic compounds in water can produce substituted compounds or other moieties, which may be as toxic as the original phenolic compounds.
Phenolic compounds have been enlisted by the United States Environmental Protection Agency (USEPA) and the European Union (EU) as pollutants of priority concern [31]. This enlistment is due to the fact that these chemicals are noted to be toxic and have severe short- and long-term effects on humans and animals. The occurrence of phenolic compounds in the aquatic environment is therefore not only objectionable and undesirable but also poses a danger as far as human health and wildlife are concerned [45].

- **Imazapyr herbicide**

The use of chemical pesticides in agriculture has resulted in widespread contamination of the environment on global scale. Congress charged the U.S. Environmental Protection Agency (EPA) to monitor water supplies to assess the degree of contamination by these chemicals [42]. Pesticide and nutrient use worldwide is expected to increase as nations try to maximize food production and assure food security by growing more food in country.
Many countries around the Mediterranean region and especially the Maghreb (Morocco) are facing problems of pollution of surface and groundwater's. In agricultural areas many active compounds (pesticides, fertilizers….) are often spread in uncontrolled amounts in the fields sometimes in high concentrations.
The so-called "second generation" of pesticides was developed in the period between 1945 and 1970. It started with the production of organophosphorous insecticides, carbamates and ureas (1940-1945s), followed by triazines and fungicides (benzimidazoles, pyrimidines, triazoles and imidazoles). Some pesticides of these groups are still used nowadays [46].

The imidazolinone molecules, introduced by American Cyanamid Company and manufacture by BASF, are one of the most active classes of herbicides. This family is currently in use in Moroccan agriculture as well as in other European countries (such as Italy) for weed control in cereals and sugar beet. Generally, imidazolinones consist of three essential part:

1. 1. A pyridine ring,
2. 2. An imidazole cycle,
3. 3. And an acid group linked to the pyridine ring.

It is a herbicide class consisting of five products, the structures of which are shown in Table 1.5.

Table 1.2 Chemical Formulas of the Imidazolinone Family

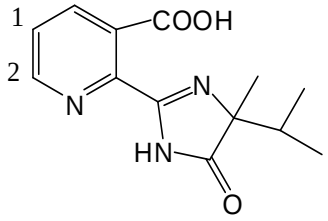

Substituants		
1	2	**Herbicide name**
-H	-H	**Imazapyr**
-CH_3	-H	**Imazapic**
-CH_2CH_3	-H	**Imazethapyr**
-CH_2OCH_3	-H	**Imazamox**
1+2		
-C_6H_6		**Imazaquin**

Imazapyr [2-(4-Methyl-5-oxo-4-propan-2-yl-1H-imidazol-2-yl) pyridine-3-carboxylic acid]**,** developed by American Cyanamid Company is a broad-spectrum poste emergence herbicide with longer residual activity[47]. Imazapyr belongs to the imidazolinone family of herbicides that become extensively used in a wide range of cropping systems in Morocco [48], they act in controlling plant growth by preventing the synthesis of branched-chain amino acids. It can also control annual and perennial grasses, sedges, broadleaf weeds, shrubs and deciduous trees.

Because they are weak acids herbicides, environmental pH will determine their chemical structure, which in turn, determines their environmental behaviour. Below pH 5, the adsorption capacity of imazapyr increases, and limits their movement in soil. Above pH 5, greater concentrations of imazapyr become negatively charged, fail to bind tightly with soils, and remain mobile in the environment [49]. However, they are considered priority pollutants in soil and water. Besides molecular structure, various soil constituents and properties, such as organic matter, clay content, and cation exchange capacity (CEC) affect the persistence of imazapyr in soil and its adsorption magnitude at low pH.

This class which are highly soluble in water, leach into deeper soil layers or ground water or show drift/run off into rivers and lakes, especially under unintended or negligent application. Concentrations in surface or ground water may exceed the legal limits (0.1 micrograms/L).

Imazapyr present an important interest owing to its utilization in the agriculture of beets and cereals control in Tadla region and owes its importance in Morocco to its success in controlling the perennial weed Solanum Elaeagnifolium Cav., which infests the Tadla area.

The Moroccan group has studied the behavior of imazapyr herbicides in water and soils [17]. The studies in soils revealed that these pesticides weakly interact with soil constituents and it could contaminate surface and groundwater supplies. Preliminary studies in water revealed that these molecules degraded moderately by photolysis and could have harmful effects on target and non-target organisms, and to enter surface and ground water.

Persistence and mobility of imazapyr has been studied in two Moroccan soils from the Rabat area, with differing organic matter content (red and organic soils), under laboratory conditions at 75% of their field capacities and 25–28 °C. Residue analysis was performed on the basis of a bioassay test using lentil (*Lens culinaris* Medic.) as indicator species. The residual activity of imazapyr accounted for 69%, 25%, 50% and 62%, 46%, 66% of the initial activity for the red and organic soils at 1, 5 and 10 mgL^{-1} respectively. The half-lives varied between 25 and 58 days for the red soil and 55 and 58 days for the organic soil. In the organic soil, imazapyr was highly mobile under the irrigation regime applied. Most of the activity was found in the first 3×75 mL of the effluents. A following biotest with the leached soil showed low remaining residual activity[17,50].

To better understand the behavior and mobility of imazapyr in the Moroccan environment, it is essential to consider its adsorption capacity which represents the most efficient and promising process determining the fate of herbicides in the environment. A breadth of knowledge on the sorption of herbicides in a variety of terrestrial soils exists, but information on imazapyr in soils and water of Morocco is lacking, and little informations are available concerning the photodegradation of imazapyr in water.

1.8. Regulations and Policy on the control of Pesticides Water Framework Directive

Regulators work on the basis of identifying hazardous pesticides and either banning or restricting their use. For example the department of Agriculture Food and Marine published a report on the sustainable use of pesticides (D.A.F.M. 2013). The plan defines a national strategy to achieve a sustainable use of pesticides and sets down objectives, quantifiable measures and timeframes to reduce the risks associated with the use of pesticides. This is a requirement under Directive

2009/128/EC (EC. 2009) of the European Parliament establishing a framework for Community action to achieve the sustainable use of pesticides.

However, as long as pesticides continued to be used in agriculture, a certain proportion will reach natural water systems, i.e., via surface runoff during strong rainfall events (Schulz 2004) and therefore developing methods for their removal from water supplies continues to be of importance.

The Stockholm convention on persistent organic pollutants (POPs) forms a framework, based on the precautionary principle, which aims to guarantee the safe elimination of those substances, which are harmful to human health and the environment, as well as reductions in their production and use (EC. 2004b). Persistent organic pollutants are defined by the convention as "*chemical substances that possess certain toxic properties and, unlike other pollutants, resist degradation*". POPs are particularly harmful for human health and the environment (EC. 2004b). The convention covers 18 priority POPs of which 12 are pesticides. (UN Economic and Social Council 2009).

There are a number of other pieces of EU legislation that relate to pesticides. Regulation 283/2013 (EC. 2013) sets out the data requirements for active substances that need to be submitted to the EU before placing them on the market. The data is mainly environmental and safety data. There is also a regulation on the marketing of pesticides (Regulation 1107/2009), which lays out the information that needs to be in place before a pesticide is released into the market. The EU is also trying to promote the sustainable use of pesticides by introducing Directive 2009/128/EC establishing community action to achieve the sustainable use of pesticides (EC. 2009), which aims at reducing the risks and impacts of pesticide use.

The evaluation, marketing and use of pesticides (herbicides, insecticides, fungicides, etc.) for plant protection within the European Union (EU) were first regulated under the Council Directive 91/414/EEC [14]. The Directive aimed to harmonize the approval of agricultural pesticides within the EU members and also to reevaluate the use of the 834 pesticides existing in the EEC at that time. This Directive lays out a comprehensive risk assessment and authorization procedure for active substances, and for products containing these substances. Each active substance has to be proven safe in terms of human health, including residues in the food chain, animal health and the environment, in particular related to groundwater and non-target organisms (such as birds, mammals, earthworms, bees), in order to be allowed to be marketed. Additionally, it is also stated that it is the responsibility of industry to provide the data showing that a substance can be used safely with respect to human health and the environment.

The Directive 91/414/EEC has been the subject of successive revisions being replaced by European Commission Directive EC 1107/2009. This Regulation aims, amongst other things, to ensure a high level of human, animal and environmental protection as well as to provide clearer rules to make the approval process for pesticides more efficient. In 1999 a new Directive was established (1999/45/CE) [15], which starts to include the agricultural pesticides in the legislation of dangerous substances, establishing as mandatory its reference in the labels and the safety data sheets.

The problems associate with water pollution and quality within the European Members prompted the establishment of the EU Water Directive Framework (WDF) in 2002 [16]. This WDF defined a new legislative approach to manage and to protect water by the coordination of different EU policies based on geographical and hydrological formation (river basins). WDF takes account all the aspects of water use and consumption. The goal is that all European waters have to achieve "good ecological and chemical status" to protect human health, water supply, natural ecosystems and biodiversity. This Directive has been updated by a more recent one [17]. The limits and guideline values for pesticides in drinking water have been issued by the World Health Organization (WHO), EU and many countries.

The EU has set standards for drinking water at a maximum permissible concentration (MCL) for any particular pesticide of 0.1 and 0.5 μg L^{-1} for the sum of all pesticides [18], including their degradation products (Directive 98/83/EC of the council).

The EU seeks to reduce the overall impact of pesticides on health and on environment, and regulate their actual usage. Consequently, in 2006 the European Commission proposed a strategy to improve the way pesticides are used across the EU.

This strategy aims to encourage low-input or pesticide-free cultivation, in particular through raising user awareness, promoting the use of codes of good practice and making financial means available for applied research and training. The potential for pesticide contamination of water resources can be reduced considerably through the use of carefully designed pesticide management practices, increasing awareness of farmers with regard to the handling and application of pesticides, guided by the following goals: i) the prevention of pest infestations, ii) the use of pesticides only when necessary, iii) the inclusion of environmental considerations in selection and application of pesticides, and iv) the use of management practices which reduce pesticide loss.

Knowledge on pesticide behavior under environmental conditions is essential to have a more accurate understanding of the hazard that these compounds may or may not possess and also to discover routes to remove them from water resources.

References

[1] M. Kermani *et al.*, "Heterogeneous catalytic ozonation by Nano-MgO is better than sole ozonation for metronidazole degradation, toxicity reduction, and biodegradability improvement," *Desalin. Water Treat.*, vol. 57, no. 35, pp. 16435–16444, 2016.

[2] T. O. Anode, H. Layered, D. Hydroxide, and M. C. Cathode, "Thèse – Tesi di Dottorato – PhD thesis Soliu Oladejo GANIYU Electrochemical Advanced Oxidation Processes for Removal of Organic pollutants from Water : Performance Studies for Sub-stoichiometric Titanium Oxide Anode and Hierarchical Layered Double Hydroxi," 2016.

[3] Unesco and T. United, "Water in a Changing World," *World Water*, vol. 11, no. 4, p. 349, 2009.

[4] L. Guppy and K. Anderson, "Global Water Crisis: the Facts," 2017.

[5] Bristol Water, "Water Quality Report," 2008.

[6] A. R. Ribeiro, O. C. Nunes, M. F. R. Pereira, and A. M. T. Silva, "An overview on the advanced oxidation processes applied for the treatment of water pollutants de fi ned in the recently launched Directive 2013 / 39 / EU," *Environ. Int.*, vol. 75, pp. 33–51, 2015.

[7] P. Stepnowski and A. Zaleska, "Comparison of different advanced oxidation processes for the degradation of room temperature ionic liquids," vol. 170, pp. 45–50, 2005.

[8] M. T. Bogert, "Chemical Abstracts," *Science (80-.).*, vol. 25, no. 641, pp. 579–580, 1907.

[9] M. Pirilä, *Adsorption and Photocatalysis in Water Treatment*. 2015.

[10] A. O. Ibhadon and P. Fitzpatrick, "Heterogeneous Photocatalysis: Recent Advances and Applications," *Catalysts*, vol. 3, pp. 189–218, 2013.

[11] I. K. Konstantinou and T. a. Albanis, "Photocatalytic transformation of pesticides in aqueous titanium dioxide suspensions using artificial and solar light: Intermediates and degradation pathways," *Appl. Catal. B Environ.*, vol. 42, no. 4, pp. 319–335, 2003.

[12] E. Topkaya, M. Konyar, H. C. Yatmaz, and K. Öztürk, "Pure ZnO and composite ZnO/TiO2catalyst plates: A comparative study for the degradation of azo dye, pesticide and antibiotic in aqueous solutions," *J. Colloid Interface Sci.*, vol. 430, pp. 6–11, 2014.

[13] M. Kralova, P. Dzik, M. Vesely, and J. Cihlar, "Preparation and characterization of doped titanium dioxide printed layers," *Catal. Today*, vol. 230, pp. 188–196, 2014.

[14] M. Saif and M. S. A. Abdel-Mottaleb, "Titanium dioxide nanomaterial doped with trivalent lanthanide ions of Tb, Eu and Sm: Preparation, characterization and potential applications," *Inorganica Chim. Acta*, vol. 360, no. 9, pp. 2863–2874, 2007.

[15] M. S. Hamdy *et al.*, "Parameters controlling the photocatalytic performance of ZnO/Hombikat TiO 2 composites," *J. Photochem. Photobiol. A Chem.*, vol. 228, no. 1, pp. 1–7, 2012.

[16] X.-J. Wen, C.-G. Niu, L. Zhang, and G.-M. Zeng, "Novel p–n heterojunction BiOI/CeO $_2$ photocatalyst for wider spectrum visible-light photocatalytic degradation of refractory pollutants," *Dalt. Trans.*, vol. 46, no. 15, pp. 4982–4993, 2017.

[17] P. Pizarro, C. Guillard, N. Perol, and J. M. Herrmann, "Photocatalytic degradation of imazapyr in water: Comparison of activities of different supported and unsupported TiO2-based catalysts," *Catal. Today*, vol. 101, no. 3–4 SPEC. ISS., pp. 211–218, 2005.

[18] S. Chiron, A. Fernandez-Alba, A. Rodriguez, and E. Garcia-Calvo, "Pesticide chemical oxidation: State-of-the-art," *Water Research*, vol. 34, no. 2. pp. 366–377, 2000.

[19] X. Bai, R. Zong, C. Li, D. Liu, Y. Liu, and Y. Zhu, "Enhancement of visible photocatalytic activity via Ag@C3N4core-shell plasmonic composite," *Appl. Catal. B Environ.*, vol. 147, pp. 82–91, 2014.

[20] T. Economist, "WaterStatistics," no. 505.

[21] S. Contreras, E. Pascual, S. Esplugas, J. Gim, and M. Rodrı, "Comparison of different

advanced oxidation processes for phenol degradation," *Water Res.*, vol. 36, pp. 1034–1042, 2002.
[22] S. Bougarrani, L. El Azzouzi, S. Akel, L. Latrach, A. Bouziani, and M. El Azzouzi, "Factors influencing Imazapyr herbicide removal from wastewater using photocatalytic ozonation," *Acta Chim.Slov.*, vol. 65, 2018.
[23] N. Riaz *et al.*, "Preparation, characterization and application of Cu–Ni/TiO 2 in Orange II photodegradation under visible light: effect of different reaction parameters and optimization," *RSC Adv.*, vol. 6, no. 60, pp. 55650–55665, 2016.
[24] J. Wang and F. E. Osterloh, "Limiting factors for photochemical charge separation in BiVO4/Co3O4, a highly active photocatalyst for water oxidation in sunlight," *J. Mater. Chem. A*, vol. 2, pp. 9405–9411, 2014.
[25] M. Bourgin *et al.*, "Effect of operational and water quality parameters on conventional ozonation and the advanced oxidation process O3/H2O2: Kinetics of micropollutant abatement, transformation product and bromate formation in a surface water," *Water Res.*, vol. 122, pp. 234–245, 2017.
[26] L. Sánchez, J. Peral, and X. Domènech, "Aniline degradation by combined photocatalysis and ozonation," *Appl. Catal. B Environ.*, vol. 19, no. 1, pp. 59–65, 1998.
[27] A. Ajmal, I. Majeed, and N. Malik, "Principles and mechanisms of photocatalytic dye degradation on TiO2 based photocatalysts : a," *R. Soc. Chem. Adv.*, vol. 4, pp. 37003–37026, 2014.
[28] J. Villaseñor *et al.*, "Catalytic ozonation: a promising advanced oxidation technology for water treatment," *Catal. Today*, vol. 53, no. 3, pp. 51–59, 2017.
[29] J. Wang *et al.*, "USE OF SELECTED ADVANCED OXIDATION PROCESSES (AOPs) FOR WASTEWATER TREATMENT – A MINI REVIEW," vol. 1, no. 3, pp. 1034–1042, 2015.
[30] S. Bougarrani, K. Skadell, R. Arndt, M. El Azzouzi, and R. Gläser, "Novel Cax MnOy /TiO2 Composites for Efficient Photocatalytic Degradation of Methylene Blue and the Herbicide Imazapyr in Aqueous Solution under Visible Light Irradiation," *J. Environ. Chem. Eng.*, 2018.
[31] W. W. Anku, M. A. Mamo, and P. P. Govender, "Phenolic Compounds in Water: Sources, Reactivity, Toxicity and Treatment Methods," *Phenolic Compd. - Nat. Sources, Importance Appl.*, 2017.
[32] N. Wang, L. Zhu, D. Wang, M. Wang, Z. Lin, and H. Tang, "Sono-assisted preparation of highly-efficient peroxidase-like Fe3O4magnetic nanoparticles for catalytic removal of organic pollutants with H2O2," *Ultrason. Sonochem.*, vol. 17, no. 3, pp. 526–533, 2010.
[33] Khan; M.M.; Ansari; S.A.; Amal; M.I.; Lee; J. and Cho; M.H., "Highly visible light active Ag@ TiO 2 nanocomposites synthesized using an electrochemically active biofilm: a novel biogenic approach," *Nanoscale*, vol. 10, no. 5, pp. 4427–4435, 2013.
[34] E. Mugunthan, M. B. Saidutta, and P. E. Jagadeeshbabu, "Photocatalytic degradation of diclofenac using TiO<inf>2</inf>–SnO<inf>2</inf>mixed oxide catalysts," *Environ. Technol. (United Kingdom)*, vol. 3330, no. November, 2017.
[35] M. A., E. R., and C. A., "Advanced Oxidation Processes (AOPs) for Removal of Pesticides from Aqueous Media," *Pestic. - Formul. Eff. Fate*, 2011.
[36] C. G. Aba-Guevara, I. E. Medina-Ramírez, A. Hernández-Ramírez, J. Jáuregui-Rincón, J. A. Lozano-Álvarez, and J. L. Rodríguez-López, "Comparison of two synthesis methods on the preparation of Fe, N-Co-doped TiO2materials for degradation of pharmaceutical compounds under visible light," *Ceram. Int.*, vol. 43, no. 6, pp. 5068–5079, 2017.
[37] T. D. Reynolds and P. Richards, "Unit Operations and Processes in Environmental Engineering, Second Edition," p. 816, 1995.
[38] R. L. Droste, "Theory and Practice of Water and Wastewater Treatment ," 1996.

[39] J. W. J. Hamilton *et al.*, "Evaluating the Mechanism of Visible Light Activity for N,F-TiO 2 Using Photoelectrochemistry," *J. Phys. Chem. C*, vol. 118, no. 23, pp. 12206–12215, 2014.
[40] S. Kalathil, M. M. Khan, S. A. Ansari, J. Lee, and M. H. Cho, "Band gap narrowing of titanium dioxide (TiO2) nanocrystals by electrochemically active biofilms and their visible light activity," *Nanoscale*, vol. 5, no. 14, p. 6323, 2013.
[41] S. Rehman, R. Ullah, A. M. Butt, and N. D. Gohar, "Strategies of making TiO2and ZnO visible light active," *J. Hazard. Mater.*, vol. 170, no. 2–3, pp. 560–569, 2009.
[42] M. M. Haque, D. Bahnemann, and M. Muneer, "Photocatalytic Degradation of Organic Pollutants : Mechanisms and Kinetics," *Org. Pollut. Ten Years After Stock. Conv. – Environ. Anal. Updat.*, vol. 3, pp. 294–326, 2012.
[43] R. L. Narayana, M. Matheswaran, A. Abd, and P. Saravanan, "Photocatalytic decolourization of basic green dye by pure and Fe , Co doped TiO 2 under daylight illumination," *DES*, vol. 269, no. 1–3, pp. 249–253, 2011.
[44] L. Zhang, L. Zhang, W. Zhang, and Y. Zhang, "Analysis of phenols by high-performance liquid chromatography with pre-column derivatization by 2-(9-carbazole)-ethyl-chloroformate," *Anal. Chim. Acta*, vol. 543, no. 1–2, pp. 52–57, 2005.
[45] I. Levchuk, *Titanium Dioxide Based Nanomaterials for Photocatalytic Water Treatment*. 2016.
[46] M. Carrier *et al.*, "Kinetics and reactional pathway of Imazapyr photocatalytic degradation Influence of pH and metallic ions," *Appl. Catal. B Environ.*, vol. 65, no. 1–2, pp. 11–20, 2006.
[47] A. Santoro, M. Mansour, M. Tropea, A. Scopa, and S. A. Bufo, "Residue analysis of imazapyr and chlozolinate in water using sunlight," *Bull. Environ. Contam. Toxicol.*, vol. 63, no. 1, pp. 33–38, 1999.
[48] A. A. Ismail *et al.*, "Photocatalytic degradation of imazapyr using mesoporous Al2O3-TiO2nanocomposites," *Sep. Purif. Technol.*, vol. 145, pp. 147–153, 2015.
[49] M. El Azzouzi, A. Dahchour, A. Bouhaouss, and M. Ferhat, "Study on the behaviour of imazapyr in two Moroccan soils," *Weed Res.*, vol. 38, no. 3, pp. 217–220, 1998.
[50] W. Xuedong, W. Huili, and F. Defang, "Biodegradation of imazapyr by free cells of Pseudomonas fluorescene biotype II and Bacillus cereus isolated from soil," *Bull. Environ. Contam. Toxicol.*, vol. 74, no. 2, pp. 350–355, 2005.

Chapter 2: Novel Ca_xMnO_y/TiO_2 Composites for Efficient Photocatalytic Degradation of Methylene Blue and the Herbicide Imazapyr in Aqueous Solution under Visible Light Irradiation

Salma Bougarrani[a*], Karl Skadell[b], Robert Arndt[b], Mohammed El Azzouzi [a], Roger Gläser[b]

[a] Laboratory of Spectroscopy, Molecular Modeling, Materials, Nanomaterials, Water and Environment (LS3MN2E), center: CERN2DFaculty of Sciences, University Med V , Avenue Ibn Battouta, BP 1014, Agdal, Rabat, Morocco

[b] Institute of Chemical Technology, Universität Leipzig, Linnéstr. 3, 04103 Leipzig, Germany

Correspondence:

Salma Bougarrani, Laboratory of Spectroscopy, Molecular Modeling, Materials, Nanomaterials, Water and Environment, Med V University, BP 1014, Agdal, Rabat, Morocco
Tel: +212660425050; Fax: +212 537 774 261
E-mail:salma.bougarrani@gmail.com

Graphical abstract

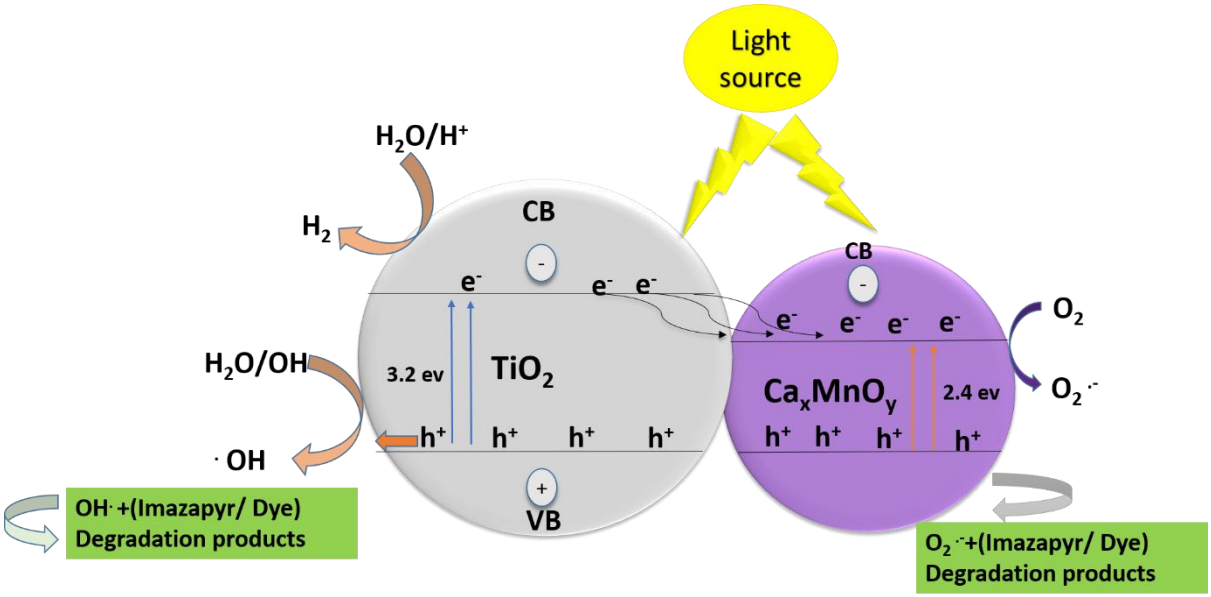

Mechanism of the enhancement in photocatalytic activity in Ca_xMnO_y–TiO_2 composites

Highlights

- Novel Ca_xMnO_y/TiO_2 and $MnOy/TiO_2$ composites were performed and investigated.
- The UV-vis light photodegradation of Methylene blue and Imazapyr herbicide depends on the calcium manganese oxide content, oxidation state and absorption properties
- Improvement of the photocatalytic activity of 5 % $Ca0.1MnOy/TiO_2$ composite attributed to the reduction of the band gap from 3.18 eV to 2.89 eV.
- Deposition of manganese oxide mainly on the surface of titanium dioxide leads to an efficient inhibition of electron-holes recombination rates.

Abstract

Ca_xMnO_y-TiO_2 composites with different manganese oxide birnessite fractions (1 to 50wt.-%) have been synthesized based on the precipitation of birnessite and mixing with commercial titanium dioxide TiO_2 by mechanical grinding. The Ca_xMnO_y-TiO_2 composites exhibited high photoactivity for the decomposition of imazapyr herbicide and methylene blue under UV-vis illumination. The results suggested that a correlation exists between the calcium manganese oxide content, oxidation state and the changes in the UV–vis absorption properties. The composit with 5 % Ca0.1MnOy/TiO_2 possessed the highest photocatalytic performance among all the as-obtained catalysts, the enhanced photocatalytic activity was attributed to the reduction of the band gap from 3.18 eV to 2.89 eV for pure TiO_2 and 5 % Ca0.1MnOy/TiO_2 composite respectively. In addition, an efficient inhibition of electron-holes recombination rates due to the deposition of manganese oxide mainly on the surface of titanium dioxide producing an efficient charge separation, and transfer between the materials. Furthermore, the photocatalytic rate constant was found to increase from 0.124 min^{-1} to 0.542 min^{-1} and from 0.155min^{-1} to 0.425 min^{-1} for methylene blue dye and imazapyr, in the presence of commercial titanium dioxide TiO_2 and 5 % $Ca_{0.1}MnO_y/TiO_2$ composite, respectively.

Keywords

Titanium dioxide, Birnessite, photo catalysis, imazapyr, Methylene blue

2.1. Introduction

The increase of the industrial and agricultural activities has become a serious problem that leads to an increasing contamination of air, water and soil [1, 2]. Undoubtedly, contamination of water supplies and resources due to the presence of dyes and pesticides has become a threatening menace in the recent days [3, 6]. Among the vast majority of procedures suggested to water and wastewater treatment, advanced oxidation processes (AOPs) has the unique position between other options [4,5] Among those, heterogeneous photocatalysis with UV-irradiated TiO_2 is gaining an increased attention as a promising technique for complete oxidative mineralization of pollutants without requiring secondary treatment of concentrated wastes[7].

Furthermore, TiO_2 has received much attention because of its strong oxidizing power of its holes, high photo-stability, low costs and long-term-stability against photo and chemical corrosion. [6, 7]. The main disadvantage of TiO_2 is its large band gap (3.2 eV) [8], TiO_2 is only sensitive to the UV part of the solar spectrum (<400 nm). As a result, only 5-8% of sunlight photons have the required energy [9, 3]. Many studies were targeted towards improving the photocatalytic efficiency by exploiting the broader part of the solar spectrum. The formation of semiconductor composites [10] comprising multicomponent or multiphase hetero-junctions to inhibit charge carrier recombination in heterogeneous photocatalysis is a very effective strategy to design highly active photocatalysts [11, 12]. One common strategy is coupling photocatalytic materials with another metal or metal oxide nanoparticle [13]. In fact, the Fermi energy of the metal oxide nanoparticle is usually lower than that of the semiconductor; [14] facilitating electron transfer from the semiconductor to the metal oxide via the Schottky-contact [10, 15].

As earth abundant and environmentally friendly materials, birnessites one of the most common types of manganese oxide, have been widely investigated owing to their important application in electrochemical capacitors [11,16], oxygen generation from water[17], the catalytic oxidation of organic dyes [18], and MnO_2-based gas sensors [19].
An exceptionally important n-type visible-light manganese oxide material with a narrow band gap of 2.20–2.63 eV, has attracted much attention in the field of photocatalysis due to its excellent electron transport properties [20], contrasting content of layer vacancies, Mn(III), and accordingly have different sorption and oxidation abilities [14, 27]. Recently, Zou and coworkers [30, 51] reported efficient catalytic activity for degradation of methylene blue under visible light radiation by MnO_2/TiO_2nanocomposite [28, 30]. Recently, synthetic manganese–calcium oxides were found to be active catalysts of water oxidation but at the atomic level their structure has remained

elusive [21]. The Ca^{2+} ion necessarily affects the charge balance, thus, the oxidation potentials of the calcium manganese oxides [19, 32]. Cortes et al. [38-39] have demonstrated that birnessite structures with Sr, Ca, B, and Al have potential for usage in water-splitting, and anhydrous Ca-Birnessite is predicted to have a suitable direct band gap for light capturing.

In view of the above, many studies have reported the catalytic oxidation of benzene over manganese oxides with ozone; other studies have shown the efficient degradation of organic dyes using Mn-doped TiO_2 as a visible light photocatalyst [22, 31]. On the other hand, manganese dioxide nanocrystals have been used for the photocatalytic degradation of rhodamine B, Congo red and methylene blue [31, 42]. However, there are only few reports on the degradation of pesticides from waste water on these catalysts [50].

Above all, the use of imidazolinone herbicides has increased in recent years [44]. Imazapyr is one of the most abundant herbicide identified in local water sources through a chemical survey of water in agricultural areas [24, 45].It has high solubility in water, it is a non-selective herbicide and kills plants by inhibiting the production of an enzyme required in the biosynthesis of certain amino acids even at concentrations below the detection limits of analytical equipment [32, 46]. Moreover, imazapyr is a persistent herbicide, which has a half-life varying from 21 days to 49 months in field studies, with a high mobility in soils. Therefore, it is likely suspected to contaminate groundwater [47]. It is also well known that imazapyr requires prolonged irradiation time due to its transformation to toxic intermediates compared to others that transform directly to carbon dioxide and water, i.e., complete mineralization [33, 46]. Attempts to eliminate imazapyr present in drinking water by treatment with ozone have been demonstrated to be unsuccessful since half of the initial compound remains in water after the process [47]. Furthermore, in the literatures we could notice several studies on imidazolinone degradations by photolysis [9, 14] and few on photocatalytic degradations [15, 16].

Photocatalysis emerges as a suitable alternative for the management of streams affected by this pollutant, since most of the stable compounds can be completely decomposed [48]. Nevertheless, previous to the real application of this technology, detailed information on the kinetic and mechanistic aspects of the photocatalytic oxidation of imazapyr is required. Up to now, most of the studies already performed have been focused on the direct photolytic decomposition of imazapyr [23, 26]. Very few data have been obtained on the photocatalytic route [11, 23].

Herein, we aim to investigate Ca_xMnO_y-TiO_2 composites, and their application in the photodegradation of methylene blue model pollutant and imazapyr herbicide under UV-visible light irradiation. The photocatalytic properties of the composites of titanium and calcium

manganese oxide mixtures have been investigated in this work for the first time. Moreover, parameters as manganese oxides types, manganese content in the composite (1–50 wt. %), and calcium incorporation have been also studied for the first time to analyze their effect on the morphology and photoactivity of the obtained composite.

Consequently, aiming at further enhancing the photocatalytic activity of manganese and titanium oxides through synergistic effect, herein, we prepared Ca_xMnO_y-TiO_2 composites through a facile precipitation reaction. The results proved that Ca_xMnO_y-TiO_2 composites with different textural properties exhibited high photoactivity for the decomposition of imazapyr herbicide and methylene blue under UV-vis illumination. Moreover, a possible catalytic mechanism for pollutant degradation was investigated and could be proposed as a new sustainable, and practical system to decompose water contaminants under solar radiation.

2.2. Material and methods

2.2.1. Chemicals

TiO_2 hombikat UV100, (99%), purchased from Sachtleben Chemie was used as titanium source for composite synthesis. Manganese (II), (III), (IV) Oxides (99 %) were provided by Sigma Aldrich, other chemical like hydrochloric acid, potassium permanganate, sodium hydroxide, manganese chloride tetra-hydrate (99 %), Potassium chloride, calcium sulphate and various solvents used during the synthesis were purchased from Sigma Aldrich. Imazapyr herbicide (95%), provided from American Cyanamid Company. Double distilled water was supplied from Millipore waters Milli Q distillation unit.

Chemical composition, origin of the chemicals and production method of materials and the elemental analysis as obtained by the ICP-OES (Inductively Coupled Plasma (ICP), with optical emission spectrometer (OES)) are summarized in Table 2.1.

Table 2.1. Composite name, Chemical composition, origin of the chemicals and the elemental analysis as obtained by the ICP technique

Composite name	*Chemical composition*	*Origin of the Chemicals*	***Ca*** */wt.%*	***Mn*** */wt.%*	***Ti*** */wt.%*	***O*** */wt.%*	***Ca+Mn : Ti***
Ti	100 wt.-%TiO_2	TiO_2Hombikat - UV 100 #19; (99 %) Sachtleben Chemie	0.00	0.00	58.0	42.00	**0.000**
Ti-500	100 wt.-%TiO_2	TiO_2Hombikat - UV Annealed at 500°C	0.00	0.00	58.0	42.00	**0.000**
Ti-1MnO	1 wt.-% MnO/ 99 wt.-% TiO_2	Mn (II)Oxide(99 %); Sigma Aldrich	0	0.58	64.2	35.22	**0.00903**
Ti-5MnO	5 wt.-% MnO / 95 wt.-% /TiO_2	Mn(II)Oxide(99 %); Sigma Aldrich	0	2.93	58.72	38.13	**0.0499**
Ti-5MnO_2	5 wt.-% MnO_2/ 95 wt.-% TiO_2	Mn(IV)Oxide(99 %); Sigma Aldrich	0	2.96	59.16	37.8	**0.05003**
Ti-5Mn_2O_3	5 wt.-% Mn_2O_3/ 95 wt.-% TiO_2	Mn(III)Oxide(99 %); Sigma Aldrich	0	2.89	58.83	38.21	**0.04912**
Ti-1Ca0.1Mn	1 wt.-% $Ca_{0.1}MnO_y$/ 99 wt.-% TiO_2	Precipitation reaction	0.17	0.30	57.5	42.05	**0.008064**
Ti-5Ca0.1Mn	5 wt.-% $Ca_{0.1}MnO_y$/ 95wt.-% TiO_2	Precipitation reaction	0.99	1.90	59.3	37.86	**0.048822**
Ti-10Ca0.1Mn	10 wt.-% $Ca_{0.1}MnO_y$ / 90 wt.-%TiO_2	Precipitation reaction	1.81	3.80	55.1	39.34	**0.101806**
Ti-75Ca0.1Mn	75 wt.-% $Ca_{0.1}MnO_y$ / 25 wt.-%TiO_2	Precipitation reaction	10.1	22.3	42.9	24.73	**0.756377**
Ti-5Ca0.3Mn	5 wt.-% $Ca_{0.3}MnO_y$/ 95wt.-% TiO_2	Precipitation reaction	1.02	1.87	58.7	38.4	**0.04912**

2.2.2. Preparation of Calcium-Manganese oxide

2.2.2.1. Preparation of the manganese series

The catalysts were prepared via a previously reported precipitation routes [31]. Three solutions were prepared: solution A: 24 g of Potassium hydroxide KOH added to 50 ml of

water ;Solution B: 5,28 g Manganese II MnO was added to calcium chloride $CaCl_2$ and to 50 ml of water; Solution C: 1,58g of potassium permanganate $KMnO_4$.

The three solutions were slowly combined as follows: A solution of manganese chloride tetra-hydrate $Mn(Cl)_2 \cdot 4H_2O$ (B) was added slowly to a KOH solution (A) under vigorous magnetic stirring. A white $Mn(OH)_2$suspension was then formed. A $KMnO_4$ solution (MnO_4^-/Mn^{2+} = 0.335) was added slowly to the gel under continuous stirring. Subsequently, a brownish black suspension was generated. The mixtures were kept stirred for 15min. After being filtered for 3 times, washed and air-dried at 60 °C, a brownish-black product denoted as Ca_xMnO_y was finally obtained. [31]

2.2.2.2. Preparation of the calcium series

For this series, the amount x of $CaCl_2 \cdot H_2O$ used for the preparation of solution B was varied. $Ca_{0.1}MnO_y$ and $Ca_{0.3}MnO_y$ were synthesized by a precipitation reaction, synthetic route for the preparation of calcium birnessites developed by Suib et al. [31]

2.2.2.3. Preparation of the composite Ca_xMnO_y /TiO_2

The commercial titanium dioxide TiO_2 (Hombikat, UV-100) was mixed with different amounts of manganese oxide Ca_xMnO_y (1-wt % to 50-wt %) prepared by precipitation and co-precipitation with calcium chloride dihydrate to find out the best efficiency and stability.

All the composites were annealed at 500°C during 24 h to ensure the formation of a uniform and stable powder and to make sure that the physical contact between both materials is reached.

For comparison, the pure TiO_2 was also annealed at 500°C during 24h, so that further processes affecting the other composites such as sintering or any phase transformations could be compared to TiO_2. In addition, the standard error varies from one composite to another, which means that the reaction rate constants k changed as a function of iteration error. The pure titanium has the lowest fault tolerance of 0.19%, however Ti-5Ca0.3Mn has the highest one equal to 2.5%.

2.2.3. Catalyst characterization

Powder X-ray diffraction (XRD) patterns of the prepared samples were obtained using an X-ray diffractometer (Rigaku-Dmax 2500) with monochromatized Cu Ka radiation (= 0.15405 nm, 40 kV, 100 mA). The samples were scanned in the range 2θ = 10–100◦. Additionally, Surface morphology was carried out using scanning electron microscopy (SEM, CamSacn CS44, E-O-GmbH). Elemental analysis and chemical composition of the catalyst was examined using energy dispersive X-ray spectroscopy (EDX, CamSacn CS44, E-O-GmbH). Absorption spectra were recorded from 250 nm to 800 nm range with Lambda 650 UV-VIS spectrophotometer at normal incidence. Photoluminescence (PL) spectra were conducted using a Renishaw1000 Raman

system using a 387 nm laser at room temperature. Nitrogen sorption was performed with micrometrics ASAP 2010 system at77 K and the surface area, porosity, and pore size distribution were derived by differentiating them according to BET method. Elemental analysis via optical emission spectrometry with inductively coupled plasma (ICP-OES, after dissolution of the sample in an aqueous HNO_3/HF solution) is summarized in Tab. 1.

2.2.4. Photocatalytic performance

2.2.4.1. Reaction procedure

The photocatalytic degradation of methylene blue and imazapyr herbicide was investigated in aqueous suspension in the presence of Ti-5Mn and pure titanium used as a photocatalysts. In a typical reaction, 100 mg of the photocatalyst previously annealed at 500°C during 24 h were added to 500 ml of a 5 mg L^{-1} of methylene blue or 5 µM of imazapyr solution in a reactor as shown in schema 1, the irradiation experiments were carried out under light generated by a medium pressure mercury lamp at 150W in a Duran cell ($\lambda > 300$ nm), placed inside the reactor. In addition, a cooling water system was set up to prevent overheating of the lamp and the solution. Furthermore, the solution was exposed to ultrasonic treatment for 1 minute in order to suspend the catalyst. Immediately afterwards, the stirring was started and maintained 30min in dark to ensure the adsorption equilibrium between the solution and the catalyst particles. Samples were taken every 5 minutes using a syringe of 2 mL and then filtered for 2 times in order to remove all the catalyst.

2.2.4.2. Analytical methods

The evolution of methylene blue concentration with time was monitored by UV-vis spectrophotometery (Varian Carry 50). The detection wavelength of methylene blue solution was set at 665 nm.

Imazapyr concentration and intermediates products of imazapyr photodegradation were determined by MS-ESI Bruker Esquire 3000 plus instrument supplied by Bruker Daltonics Esquire used for direct mass determination. ESI was carried out with the vaporizer at 220 °C and nitrogen as sheath (551 kPa) and auxiliary (138 kPa) gas to assist with the preliminary nebulization and to initiate the ionization process. A discharge current of 4.5 µA and spray voltage set of 5 KV were applied.

2.3. Results and discussion

2.3.1. Characterization of Ca_xMnO_y /TiO_2 composite

The effect of calcination temperature of Ti-5Ca0.1Mn composite on methylene blue degradation was investigated in this study. The highest activity was achieved for the catalyst annealed at 500°C (Figure 2.1).

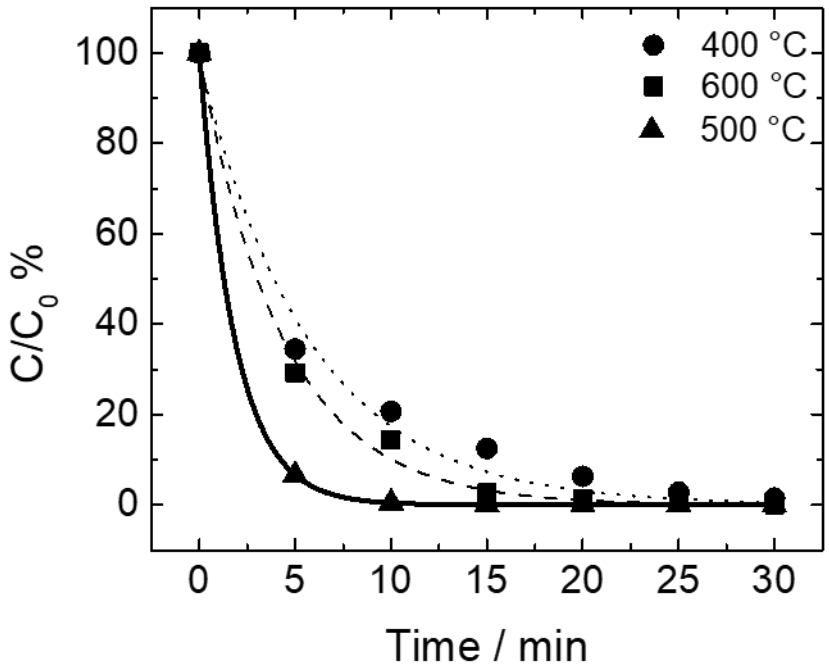

Figure 2.1.Concentration of methylene blue during photocatalytic degradation as a function of time over Ti-5Ca0.1Mn annealed at different temperatures ($C_{(Methylene\ blue)}$= 5 mg L^{-1}); stirring speed = 1000 min^{-1}, $m_{catalyst}$= 100 mg).

Yung-Fang Chen et al.[29-32] have reported in their previous work the effect of calcination temperature on the crystallinity of TiO_2 and have concluded that TiO_2 peaks become sharper and rutile phase peaks appear as the calcination temperature is increased[31-54].
Kim et al.[5] have also demonstrated that above the calcination temperature of 550°C rutile phase peaks appear which suggests that there is a phase transition from anatase to rutile at about 550°C[5-46].

In the present study, with increasing calcinations temperature, the photocatalytic activity of the Ti-5Ca0.1Mngradually increased, this may be due to a more pronounced crystallization of the anatase phase [45]. The decrease in photocatalytic activity when the calcination temperature

is above 500 °C, could be explained either by the formation of rutile peaks, or the sintering and growth of TiO_2 crystallites, which agrees with previous studies [32, 33].

Figure 2.2 shows XRD diffraction patterns for five selected oxides.Ti,Ti-500, Ti-5Ca0.1Mn samples are present in the anatase phase; XRD patterns exhibit strong diffraction peaks at 25° from the (101) plane and 48° from the (200) plane indicating the presence of TiO_2 in the anatase phase. All reflection positions are in good agreement with the reference spectrum and are indexed in the spectrum itself (JCPDS no.: 88-1175 and 84-1286) [47].

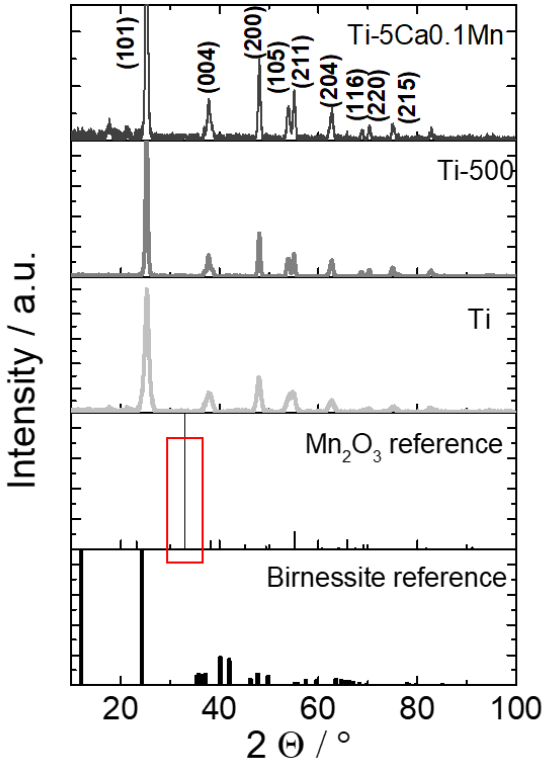

Figure 2.2.XRD-patterns of birnessite, Manganese (III) oxide Mn_2O_3, commercial titanium dioxide Hombikat UV100 (Ti), Ti-500, and Ti-5Ca0.1Mn. All the composites were annealed at 500 °C during 24 h.

The characteristic reflections indicating the presence of the pure birnessite phase which should appear at about 12 ° and 25°are absent for all the composites samples(Appendix B).This might be due to the proportion of amorphous to crystalline material and the amount of birnessite/MnO_2.This result was expected, since the anatase phase presents 95 wt.-% of the composite.

The characteristic reflections indicating TiO_2 in the rutile phase 27°, 36°and 55°are absent, proving that samples retained their original phase during calcinations [7, 23]. Moreover, the crystallinity of the pure titanium was improved by the effect of thermal treatment and/or surface modification as evidenced by the sharper reflexes.

However Ti-5MnO_2 and Ti-5Mn_2O_3 samples present some additional phases and strong diffraction reflexes at 33° indicating Manganese oxide phase, Ti-5Mn_2O_3shows a strong signal of Mn_2O_3. This was expected since $Mn_2O_3$was used for the synthesis of the composite. However, the emergence of attenuated reflexes of Mn_2O_3 in the diffraction pattern of Ti-5MnO_2 composite with tetravalent manganese oxide is not explained, due to the different oxidation states of the manganese.

SEM images of Ti and Ti-5Ca0.1Mncomposite (Appendix C) did not reveal any noticeable change in the morphology and particle size of the synthesized composite as expected due to the low manganese oxide content in the materials. These results were in good agreement with XRD results which did not show any clear manganese oxide peaks in the composite.

To confirm the Ca_xMnO_y concentration in the synthesized materials, a full elemental analysis was carried out after the synthesis.

Table 2.1shows the calculated amount of Ca_xMnO_y added to TiO_2 samples during the preparation compared with the actual amounts as obtained from ICP analysis in the final products. The difference between the theoretical and the actual Ca_xMnO_y weight percentage in each of the samples can be attributed to partial loss of sample during the sieving procedure. The results show that Ca_xMnO_y was incorporated in the final solid product with a Ca_xMnO_y/TiO_2ratio comparable to the aimed ratio determined at the Section 2.1.

To explore the relationship between the absorbance and the photocatalytic efficiencies of Ca_xMnO_y/TiO_2composites, DR-UV-vis spectra at different manganese oxides and Ca_xMnO_y contents are depicted in Figure 2.3. It is clearly seen that all prepared samples show a characteristic spectrum with a sharp absorption edge at 387 nm which is consistent with the band gap of anatase TiO_2 (ca. 3.1-3.2 eV) (Figure 2.3a) [36].

A significant red shift in the absorbance of Ti-5Ca0.1Mn was observed, which was attributed to band gap shifting. The tangent drawn shows an absorbance maxima of 387 nm and 421 nm for the pure TiO_2 and Ti-5Ca0.1Mn composite, respectively, which corresponds to a band gap of 3.18 and 2.89 eV, respectively. Indicating that e^-/h^+ pairs can be generated, even when the particle is irradiated with long wavelength-visible light.

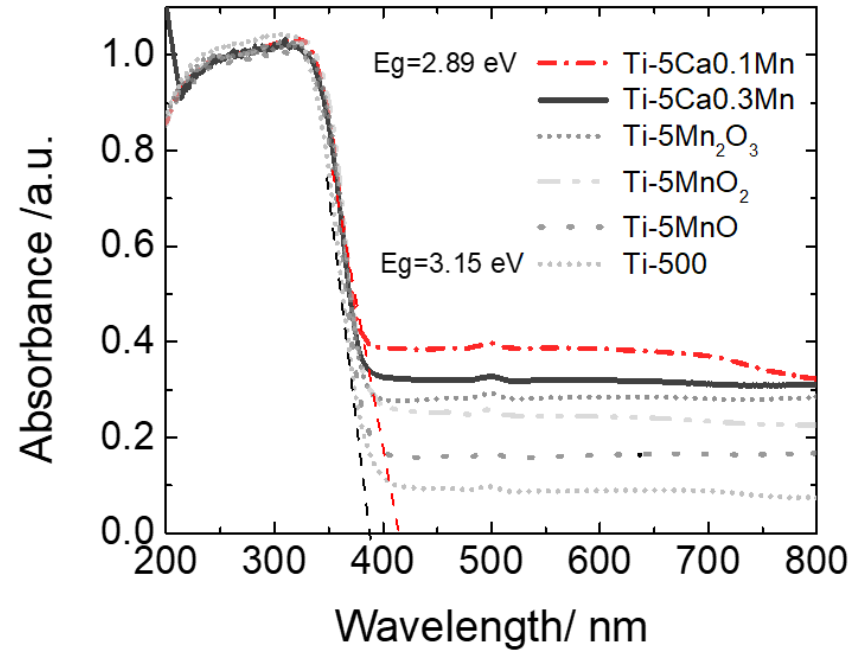

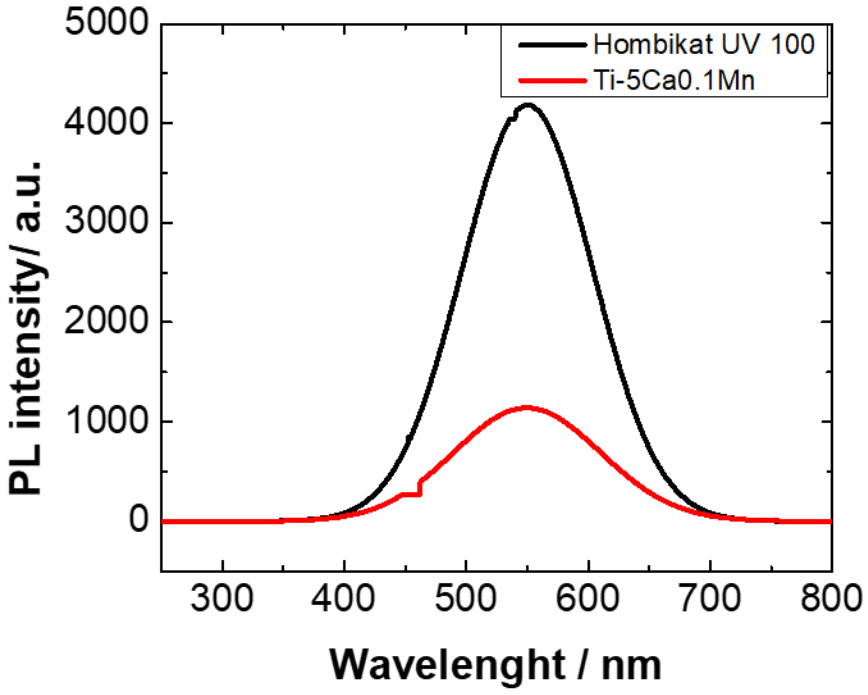

Figure 2.3.**(a)**UV-vis absorption spectra of aTi-500, Ti-5MnO, Ti-5MnO_2, Ti-5Mn_2O_3,Ti-5Ca0.1Mn, Ti-5Ca0.3Mn.**(b)** Photoluminescence spectra for Hombikat UV 100 TiO_2 and Ti-5Ca0.1Mn samples in ethanol. The excitation wavelength (λex) was 325 nm.

Mansoob Khan et al.[10,12] have observed same behavior for modified titanium dioxide film and suggested that band gap decreases can be due to the localized gap states induced by Ti^{3+} but could also be attributed to oxygen vacancies, which is responsible for the enhanced photocatalytic activity in the visible range.

Furthermore, since the amount of manganese oxides is maximum 5 wt.-% on the composite and it's increasing the absorption for the visible light, which is assumed that the particles of manganese oxides have been deposited during the synthesis mainly on the surface of TiO_2, to effect this significant increase in the absorption.

Thus, the difference of absorbance between the composites and pure titanium could be explained by the decrease of charge-carrier traps leading to an increase of the efficiency of the electron-hole separation and formation of the Schottky barrier by the electron transfer from the conduction band of TiO_2 to the conduction band of manganese oxide [37, 38].

Thus, more MnOx covers the surface of TiO_2, higher is the absorbance of photons and better is the photo generation of charge carriers (e^-/h^+) and higher is the photoactivity.

Therefore, in order to investigate charge carrier transfer as well as to understand the fate of the electron-hole pairs between TiO_2 and Ca_xMnO_y, we carried out photoluminescence (PL) measurements (Figure 2.3b).

Strong emission from UV 100 $TiO_2$was observed under 387 nm excitation compared to the synthesized Ti-5Ca0.1Mn resulted in near 70% reduction in the emission intensity. Similar trends were also observed by A. Ansari et al. [14, 15] who examined the Ag–TiO_2 powder. As the PL emission is the result of the recombination of excited electrons and holes, the lower PL intensity of Ti-5Ca0.1Mn composite may indicate a decrease in the recombination rate, i.e. [7, 15],this can be attributed to the decreased recombination of charge-carriers, which are trapped in the energy level below the conduction band in the Ti-5Ca0.1Mn composite.

Therefore, the Ca_xMnO_y particles deposed on the surface of TiO_2 accept the photo induced electrons and increase rapidly the efficiency of charge separation in the TiO_2 near the surface, [7, and 12] resulting in the decrease of the recombination of the photo induced electron/hole pairs in TiO_2, which result in a lower PL intensity. On the other hand, an excess of Ca_xMnO_y loading, leading to a low quantum efficiency and lower photocatalytic activity could be a result of rapid recombination for electron/ holes, caused by a surplus of Ca_xMnO_y which act as a recombination center for electrons and holes [12, 14].

The differences in the textural properties of synthesized composites become clear from the N_2 sorption isotherms shown in Appendix D and summarized in Table 2.2. All analyzed materials exhibit pores in the size range between 10 to 80 nm, mostly distributed in the size range of 10

nm to 20 nm, while the pores having a size from 20 nm to about 25 nm are limited, though, Ti-5Mn_2O_3 shows significantly fewer pores with a diameter>20 nm than the other composites. It has also the lowest surface area and pore volume. This might be due to the micropore filling with Mn_2O_3 since it was used for the synthesis of the composite. These results were in good agreement with XRD results which show clear manganese oxide peaks in Ti-5Mn_2O_3 composite. Furthermore, micropores observed in the presence of pure TiO_2 decreased with increasing manganese calcium oxide content in the material, the hysteresis loop shifts to higher relative pressures.

Table 2.2. Specific surface area and total pore volume of prepared TiO_2 composites

Composites	**S_{BET} (m^2/g)**	**V_{Total} (cm^3/g)**
Ti	330.93	0.360
Ti-500	113.53	0.388
Ti-5MnO	87.4	0.290
Ti-5MnO_2	89 .4	0.307
Ti-5Mn_2O_3	84.6	0.298
Ti-5Ca0.1Mn	97.3	0.347
Ti-5Ca0.3Mn	89.7	0.305

Viewed overall, the distribution of pore sizes is very similar in all the composites, there are mainly mesopores. Correspondingly larger mesopores with diameters of 10-20 nm are formed with increasing mass fraction of manganese calcium oxide in the composites. Moreover, the surface area and pore volume of Ti-5Ca0.1Mn composite are so far considered higher than all other composites.

In the light of the above discussion, it can be concluded that band gap decreases from 3.18 and 2.89 eV leading to the high absorbance of Ti-5Ca0.1Mn in the visible range, and low PL intensity could be considered as a strong indication of the efficiency of charge separation, and good inhibition of electron-holes recombination rates. These approaches ultimately reveal that the photoelectron transfer is from TiO_2 to Ca_xMnO_y, which favors O_2 reduction considered as the rate-determining step in photocatalytic environmental purification.

2.3.2. Photocatalytic performance

2.3.2.1. Photocatalytic degradation of methylene blue

Originally, methylene blue was chosen as target pollutant to measure the photocatalytic activity of various catalysts. Results are depicted in Table2.3 and Figures 2.4 to 2.6.

Based on the exponential decay of concentration (Appendix A), the photoactivity profile of samples loaded with a small content of manganese oxide was fitted assuming a first order reaction.

$$\boldsymbol{C = C_0 exp(-k \cdot t)} \qquad \textbf{(1)}$$

In which C is the concentration of methylene blue at time t, C_o is the initial concentration, and k is the observed rate constant.

Many authors have reported that the kinetic behavior of photocatalytic reaction can be described by a modified Langmuir–Hinshelwood model [39, 40]. At low concentration, the number of catalytic sites is not limiting factor and the rate of degradation is proportional to the substrate concentration, in accordance with apparent first-order kinetics. Thus, the apparent first-order model gives a better fit with dye pollutant at low concentration.

Figure A.1 (Appendix A) shows the comparison between the degradation of methylene blue when catalyzed by the purchased titanium dioxide (Ti), and different Ca_xMnO_y-TiO_2 composites. It is clear that all the Ca_xMnO_y-TiO_2composites exhibit much higher photocatalytic activities than pure TiO_2 or Ca_xMnO_y, and the highest photo degradation efficiencies of methylene blue was achieved with two synthetic birnessite samples with varying calcium content Ti-5Ca0.1Mn and Ti-5Ca0.3Mn, providing evidence that incorporation of calcium was important in order to increase the catalytic activity of the oxides. This effect could be attributed to the enhancement of the adsorption of the anionic species such as Cl^- present in the methylene blue solution by the increase of positive charging of the composite surface. Furthermore, the adsorption activity of the catalyst is an important influencing factor in degradation process [7, 25]. The adsorption capabilities against specific surface of the samples and degradation rate constant for methylene blue were investigated and shown in Figure 2.4.

The adsorption X of methylene blue on composite was determined at the end of the adsorption phase and was investigate as a function of their specific surface (Figure 2.4).

A trend to a linear dependence between adsorption and specific surface area was observed. The higher the specific surface area is, the higher is the methylene blue adsorption on the material and higher is the reaction rate constant of the methylene blue degradation (Figure 2.4a).

The generally higher reaction rate for Ti-5Ca0.1Mn (0.266 min^{-1}) and Ti-5Ca0.3Mn (0.206 min^{-1}) as compared to Ti-5Mn_2O_3(0.128min^{-1}) and Ti-5MnO_2 (0.144 min^{-1}) can be correlated to the specific surface and adsorption which are respectively (0.42 10^{-2} $mg.mg^{-1}$; 84.5 $m^2.g^{-1}$) forTi-5Mn_2O_3 ,(0.62 10^{-2} $mg.mg^{-1}$;89.38$m^2.g^{-1}$) for Ti-5MnO_2, (0.93 10^{-2} $mg.mg^{-1}$,89.7$m^2.g^{-1}$)for Ti-

5Ca0.3Mn, (0.97 10^{-2} mg.mg^{-1};97.26m^2.g^{-1}) for Ti-5Ca0.1Mn but also for their manganese oxide state.

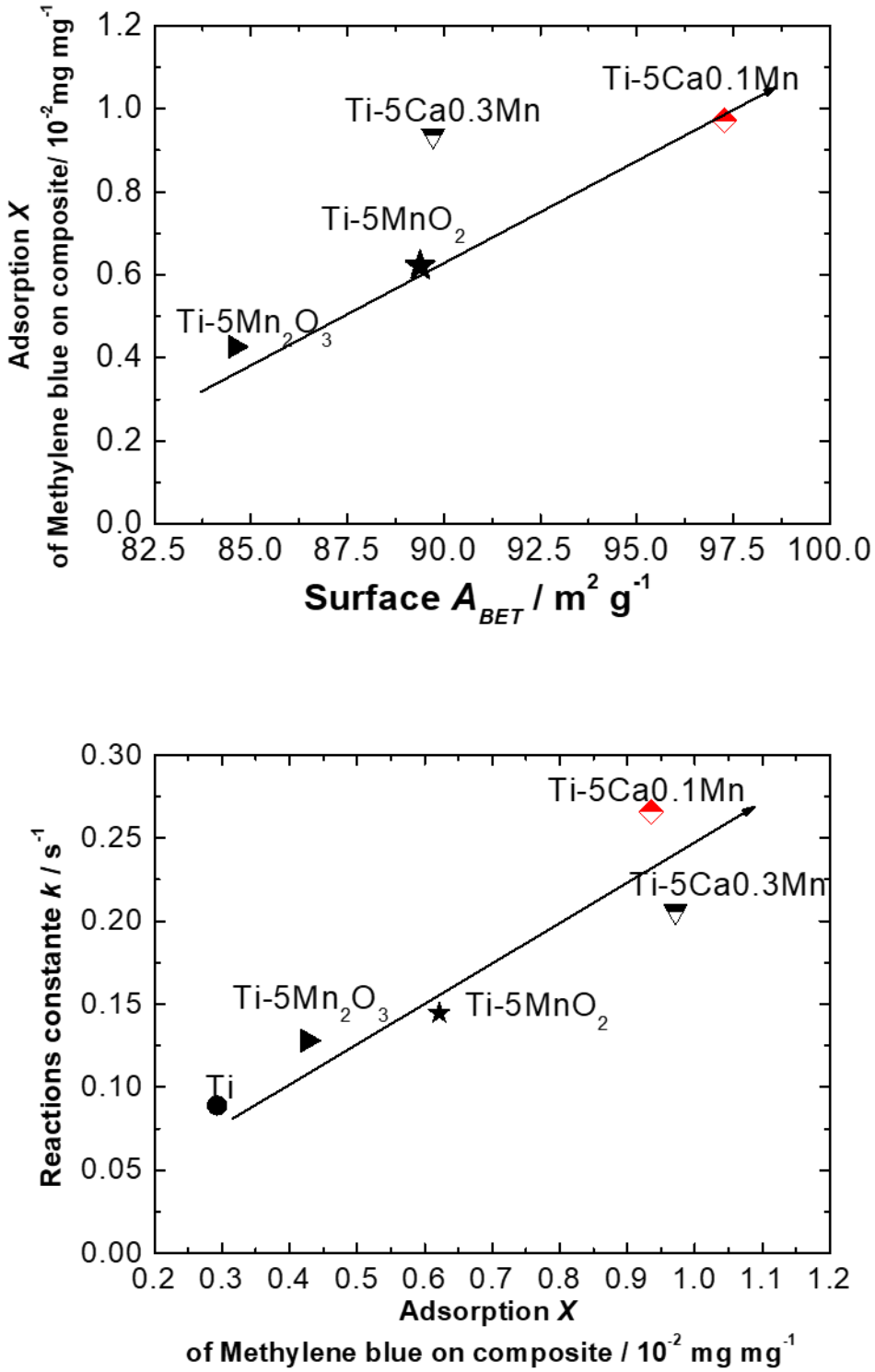

Figure 2.4. **(a)**Adsorption of methylene blue on composite as a function of specific surfaces area.**(b)** Reaction constant k as a function of Adsorption X of Methylene blue on the composites ;($C_{(Methylene\ blue)}$= 5 mg L^{-1}); stirring speed = 1000 min-1, m catalyst= 100 mg).

Overall, the composite Ti-5Ca0.1Mn was chosen because of its high methylene blue adsorption capacity, high surface area and high reaction constant compared to Ti-5Ca0.3Mn, these results indicate that Ti-5Ca0.1Mn composite can efficiently decompose methylene blue dye suggesting its potential wide application in herbicides degradation.

Table 2.3. Degradation rate constants of various composites for the degradation of methylene blue;($C_{(Methylene\ blue)}$ = 5 mg L^{-1}); stirring speed = 1000 min^{-1}, mcatalyst= 100 mg).

Composites	**k/min^{-1}**	**Standard error**
Ti	0.089	0.0019
Ti-5MnO	0.136	0.0050
Ti-5MnO_2	0.144	0.0151
Ti-5Mn_2O_3	0.128	0.0164
Ti-1Ca0.1Mn	0.164	0.0114
Ti-5Ca0.3Mn	0.206	0.0225
Ti-5Ca0.1Mn	0.266	0.0253

In order to evaluate the efficiency of Ca_xMnO_y loading in the composite. The residual concentration of methylene blue after different exposure intervals and different manganese oxide loadings is presented in (Figure 2.5). It is evident that the reaction rate constant of the methylene blue degradation increases until 5 % of $Ca_{0.1}$MnOy. Further increase in the manganese oxide concentration leads to different behavior.

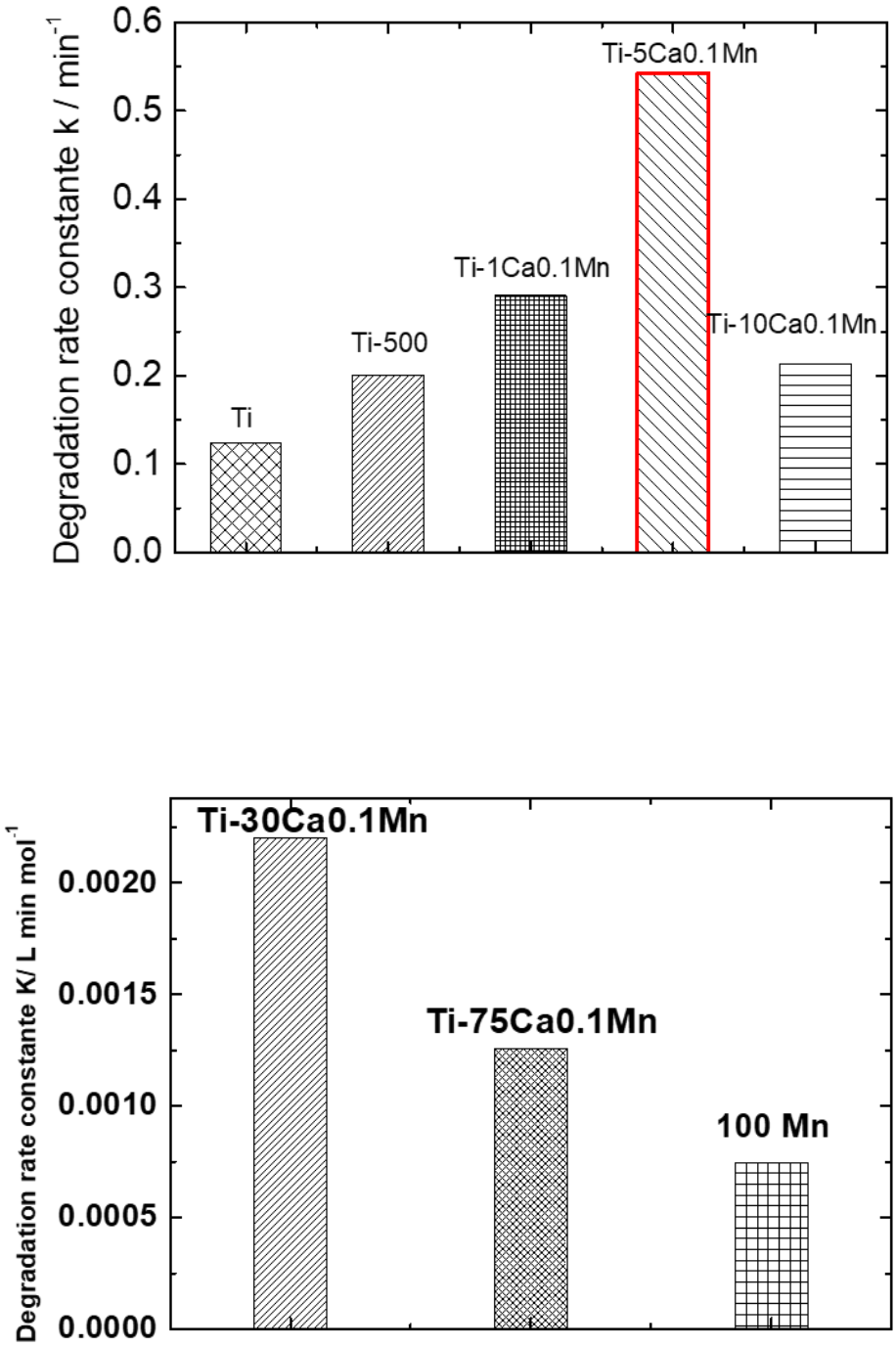

Figure 2.5. Degradation rate constant for different catalyst (a) Ca_xMnO_y loading < 10%;(b) Ca_xMnO_y loading>10%, ($C_{(Methylene\ blue)}$= 5 mg L^{-1}); stirring speed = 1000 min^{-1}, m catalyst= 100 mg).

As the concentration of manganese oxide ions increases, the surface barrier becomes higher, and the space charge region becomes narrower, the electron–hole pairs within the region are efficiently separated by the large electric field before recombination [19-25].

On the other hand, when the concentration of manganese oxide is more than 5 wt.-%, TiO_2 samples become dark in color. Thus, the changed optical properties of the samples could lead to the screening of the light towards the $TiO_2$and may prevent the excitation of electrons from the valence to conduction band [7-22].

This might be explained by the space charge layer, this region becomes very narrow and the penetration depth of light into TiO_2 greatly exceeds the space charge layer; therefore the recombination of the photo generated electron–hole pairs in semiconductor become easier. Ola et al [40] have reported same results in their review about semiconductor coupling. Indeed, there is an optimum concentration of Ca_xMnO_y in the surface of TiO_2 particles to make the thickness of space charge layer substantially equal to the light penetration depth and for more efficient separation of photo induced electron–hole pairs [24].

Furthermore, the photodegradation profile of samples loaded with a small content of manganese oxide fit well with the pseudo first order kinetics model. However, as present in figure 2.6, when the concentration was above 10 wt.-% of Ca_xMnO_y, the data were not further fitted by the pseudo first order kinetic model.

The photoactivity profile of Ti-30Ca0.1Mn,Ti-75Ca0.1Mn and 100wt.-%of Ca0.1MnOx was fitted assuming second order reaction[30, 14].

$$\mathbf{1/C = k.t + 1/C_0} \qquad \textbf{(2)}$$

It follows by substituting $t=t_{1/2}$ and $C=1/2[C]_0$ that the half-life of a methylene blue species [30, 15]that is consumed in a second order reaction is:

$$\boldsymbol{t_{1/2}=1/(1/K.[C]_0)} \qquad \textbf{(3)}$$

Therefore, unlike a first order reaction, the half-life of a substance in a second order reaction varies with the initial concentration.

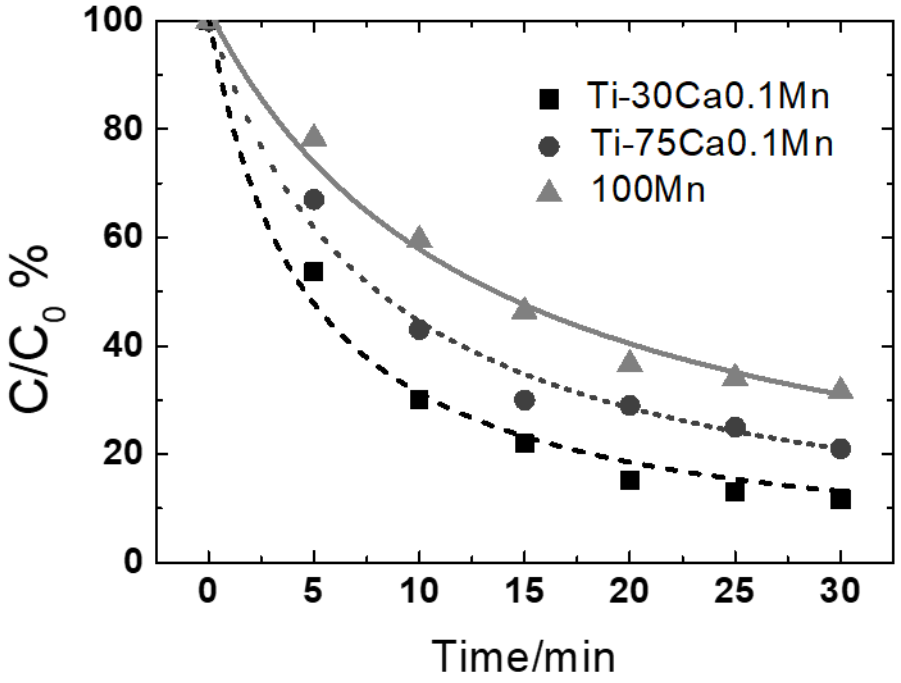

Figure 2.6. Concentrations of Methylene blue as a function of time for different catalyst ;($C_{(Methylene\ blue)}$= 5 mg L^{-1}); stirring speed = 1000 min^{-1}, m catalyst= 100 mg).

A consequence of this dependence is, that species that decay by second order reaction (which includes some environmentally harmful substances) may persist in low concentrations for long periods because their half-lives are long when their concentrations are low. In general, for an n^{th} order reaction the half-life is related on the rate constant and the initial concentration of A by:

$$t_{1/2}=(1/K.[A]^{n-1}) \quad (4)$$

Consistence of photocatalytic degradation reactions with second order model is not expected but this unusual case was reported in the photocatalytic degradation of Auramine O aqueous solutions over ZnO catalyst owing to constraints in fitting the kinetic data to other than the second order kinetics (Kumar et al. 2007).The recombination kinetics of charge carriers has been widely proven to be consistent with type I second order model (Serpone et al. 1995; Colombo and Bowman 1996; Bauer et al. 2004).

Similar behavior of second-order-kinetics was also reported in the case of Safranin Orange photodegradation with ZnS and CdS nanoparticles and was explained on the basis of dimerization of the dye under investigation (Zhang et al.2005).

This change in kinetics could be explained by a possible blocking of active sites on the surface of the composites when the amount of the MnOx exceeds 10 wt.-%. Conversely, the photo catalysis performance was deteriorated at high Ca_xMnO_y concentration. As depicted in figure 2.6, the photocatalytic activity in terms of rate constant for the methylene blue degradation are 0.000747 min L mol^{-1}, 0.00126 min L mol^{-1} and 0.0022 min L mol^{-1} for 100Mn, Ti-75Ca0.1Mn and Ti-30Ca0.1Mn respectively.

Based on the obtained results, the as-prepared Ti-5Ca0.1Mn composite with unique properties and characteristics compared to the other composites was tested for imazapyr herbicide degradation.

2.3.2.2. Photocatalytic degradation of imazapyr

Whereas academic studies have to be done in single constituent model solutions, real wastewater contains a lot of compounds. Therefore, we chose another kind of organic pollutant, imazapyr herbicide.

The photocatalytic degradation of imazapyr was performed with the same protocol of methylene blue degradation in order to compare the performance of Ti-5Ca0.1Mn composite.

Figure 2.7 reveals the changes in the kinetics of imazapyr disappearance using pure TiO_2 and Ti-5Ca0.1Mn composite as catalyst, after 10 min of irradiation, the characteristic peaks of imazapyr were found to decline to 59% for pure TiO_2 and 91% for Ti-5Ca0.1Mn composite (Appendix E).

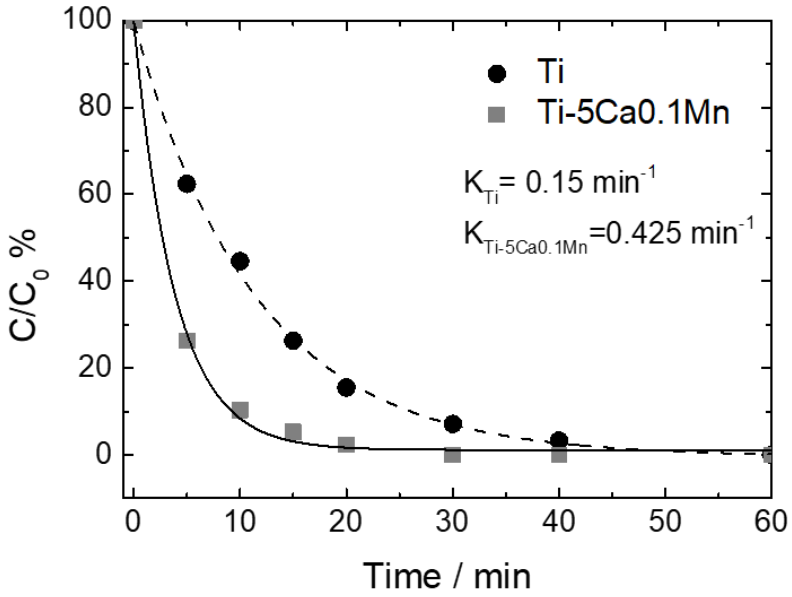

Figure 2.7. Concentrations of imazapyr as a function of time for Ti and Ti-5Ca0.1Mn composite ;($C_{(Imazapyr)}$=5 µM); stirring speed = 1000 min^{-1}, m catalyst= 100 mg).Aqueous suspension 1: 3 acetone/Milli-Q water

Additionally, the photocatalytic activity, in terms of rate constant was found to increase from k= 0.15 min^{-1} to k=0.425 min^{-1} for pure TiO_2 and Ti-5Ca0.1Mn composite respectively following the pseudo first order kinetic. The results indicate correspondingly that degradation of methylene blue occurs at a faster rate under UV-vis irradiation in comparison with imazapyr herbicide. In case of methylene blue, more than 98 % degradation efficiency was observed in 10 min irradiation time using Ti-5Ca0.1Mn composite, whereas 96% of imazapyr degradation was achieved after 20 min of irradiation. The prolonged irradiation time required for the degradation of imazapyr herbicide compared to the degradation of methylene blue could be attributed to the heavy molecular weight, complex structure and stable intermediates products of imazapyr compared to intermediate products generated during the photodegradation of methylene blue[49-50].The results are in good agreement with the earlier findings [24, 63] that suggested that an increase in molecular weight and complexity of pollutant can lead to the generation of intermediates, which may adsorb on the surface of the catalyst. Slow diffusion of the generated intermediates from the catalyst surface can result in the deactivation of active sites on the photocatalyst and result in a reduction in the degradation rate.

2.4. Conclusions

In summary, an eco-friendly and low-cost Ca_xMnO_y-TiO_2 composite materials were successfully prepared using a facile and straightforward route based on precipitation reaction for birnessite and mechanically mixed with commercial titanium dioxide with different weight fractions (1-wt % to 50-wt %) .

Significant differences in the photocatalytic activities for the prepared composites were observed, with maximum photocatalytic activity achieved with two synthetic birnessite samples Ti-5Ca0.1Mn andTi-5Ca0.3Mn with varying calcium content, attributed to the high adsorption capacity and specific surface area compared to other manganese oxides composite. Imazapyr herbicide and methylene blue dye were effectively decomposed with the Ti-5Ca0.1Mn composite, degradation process coincided well with the pseudo-first-order kinetic model and complete disappearance was observed in less than 20 min. The photocatalytic activity, in terms of rate constant was found to increase from 0.124 $min^{-1}$to 0.542 min^{-1} and from 0.15min^{-1} to 0.425 min^{-1} for methylene blue dye and imazapyr herbicide, respectively in presence of commercial titanium dioxide TiO_2 and Ti-5Ca0.1Mn composite respectively. Based on the optical and electrical properties of materials analysis, it can be speculated that the improvement

of photocatalytic activity is a result of a reduction of band gap from 3.18 eV to 2.89 eV for pure TiO_2 and Ti-5Ca0.1Mn composite respectively, additionally to an efficient inhibition of electron-holes recombination rates due to the deposition of manganese oxide mainly on the surface of titanium dioxide leading to an effective charge separation, and transfer between the materials. Therefore, it is expected that in future Ca_xMnO_y-TiO_2 composites with unique properties and characteristics will be synthesized and may solve various wastewater treatment, energy and environment problems.

Acknowledgements

The authors are very grateful to the German Academic Exchange Service (DAAD) and Institute of Technical Chemistry of Leipzig for funding the research that underpins this article, as well as the many actors Leipzig University for Help in mass spectrometry analysis.

Supplementary data

Supplementary data to this article can be found online.

References

[1]I. K. Konstantinou, T.A. Albanis, TiO_2-assisted photocatalytic degradation of azo dyes in aqueous solution: kinetic and mechanistic investigations: A review Appl. Catal. B.49 (2004) 1–14

[2]J. Du, C. Chen, F.Cheng, J. Chen, Rapid Synthesis and Efficient Electrocatalytic Oxygen Reduction/ Evolution Reaction of $CoMn_2O_4$ Nanodots Supported on Graphene, Inorg. Chem. 54 (2015) 5467−5474

[3]I. Konstantinou, V. Sakkas, and T. Albanis, Photocatalytic degradation of the herbicides propanil and molinate over aqueous TiO_2 suspensions: identification of intermediates and the reaction pathway, Appl. Catal. B, 34 (2001) 227–239.

[4]H. Li, W. Li, S. Gu, F. Wang, X. Liu, C. Ren, Forming oxygen vacancies inside in lutetium-doped Bi2MoO6 nanosheets for enhanced visible-light photocatalytic activity, Molecular Catalysis 433 (2017) 301–312

[5]Y.F. Chena, C-Y. Leec, M-Y. Yenga, H-T. Chiua. The effect of calcination temperature on the crystallinity of TiO2 nanopowders, J. Cryst. Growth.247 (2003) 363–370

[6] M.R. Eskandarian, M. Fazli, M.H. Rasoulifard, H. Choi, Decomposition of organic chemicals by zeolite-TiO2 nanocomposite supported onto low density polyethylene film under UV-LED powered by solar radiation. Appl. Catal. B 183 (2016) 407–416

[7] M.H. Rasoulifard, M.Fazli , M. R.Eskandarian, Performance of the light-emitting-diodes in a continuous photoreactor for degradation of Direct Red 23 using UV-LED/S2O82 process. J. Ind. Eng. Chem., 24 (2015) 121-126.

[8] M.H. Rasoulifard, M. Akrami, M. R.Eskandarian, Degradation of organophosphorus pesticide diazinon using activated persulfate: Optimization of operational parameters and comparative study by Taguchi's method. J. Taiwan. Inst. Chem. Eng. 57(2015) 77–90

[9] M.H. Rasoulifard, M. Fazli, M. R.Eskandarian, Kinetic study for photocatalytic degradation of Direct Red 23 in UV–LED/nano-TiO2/S2O82_ process: Dependence of degradation kinetic on operational parameters. J. Ind. Eng. Chem, 20 (2014), 3695-3702

[10] M. Mansoob Khan, S.A. Ansari, D. Pradhan, M. Omaish Ansari, D.H. Han, J. Lee, M.H.Cho. Band gap engineered TiO2 nanoparticles for visible light induced photo electrochemical and photocatalytic studies. J. Mater. Chem. A, 2 (2014), 637-644

[11] S.A. Ansari, M. Mansoob Khan, M. Omaish Ansaric, M. H. Cho. Nitrogen-doped titanium dioxide (N-doped TiO2) for visible light photo catalysis, New J. Chem., 40 (2016)3000-3009.

[12] M. O. Ansari, M. M. Khan, S. A. Ansari and M. H. Cho, Electrically conductive polyaniline sensitized defective- TiO2 for improved visible light photocatalytic and photo electrochemical performance: A synergistic effect. New J. Chem., 39 (2015) 8381-8388.

[13] S. Kalathil, M. M. Khan, S. A. Ansari, J. Lee, M. H. Cho. Band gap narrowing of titanium dioxide (TiO2) nanocrystals by electrochemically active biofilms and their visible light activity. Nanoscale, 5 (2013) 6323-6326.

[14] M. O.Ansari, M.M. Khan, S. A. Ansari, K. Raju, J. Lee, M. H. Cho. Enhanced Thermal Stability under DC Electrical Conductivity Retention and Visible Light Activity of Ag/TiO2@Polyaniline Nanocomposite Film. ACS Appl. Mater. Interfaces, 6 (11) (2014) 8124-8133.

[15] M. M. Khan, S.A. Ansari, M. I. Amal, J. Lee, M. H. Cho. Highly Visible Light Active Ag@TiO2 Nanocomposites Synthesized by Electrochemically Active Biofilm: A Novel Biogenic Approach, Nanoscale, 5 (2013) 4427-4435;

[16] J. Dong, J. Han, Y. Liu, A. Nakajima, S. Matsushita, S. Wei, W. Gao. Defective Black TiO2 Synthesized via Anodization for Visible-Light Photocatalysis.ACS Appl. Mater. Interfaces. 6 (2014) 1385−1388

[17] S. A. Ansari, M. M. Khan, M. O. Ansari, M. H. Cho. Silver nanoparticles and defect-induced visible light photocatalytic and photo electrochemical performanceofAg@m-TiO2 nanocomposite. Solar Energy Materials & Solar Cells 141 (2015)162-170.

[18] B. Sharma, P.K. Boruah, A.Yadav, M.R. Da.TiO2–Fe2O3 nanocompositeheterojunction for superior charge separation and the photocatalytic inactivation of pathogenic bacteria in water under direct sunlight irradiation. J. of Environ .Chem .Eng. 6 (2018) 134–145

[19]X. Wen, C. Niu, L.Zhang and G. Zeng, Novel p-n heterojunction BiOI/CeO2 photocatalyst for wider spectrum 2 visible-light photocatalytic degradation of refractory pollutant. Dalton Trans.15(2017).

[20]J. Du, C. Chen, F. Cheng, J. Chen, Rapid Synthesis and Efficient Electrocatalytic Oxygen Reduction/ Evolution Reaction of CoMn2O4 Nanodots Supported on Graphene. Inorg. Chem. 54 (2015) 5467−5474

[21]A.Tawari, W-D. Einicke, R. Gläser, photocatalytic Oxidation of NO over Composites of Titanium Dioxide and Zeolite ZSM-5. Catalysts. (2016) 6-31

[22]B. Liu,X. Zhao,C. Terashima, A. Fujishima, K. Nakata. Thermodynamic and kinetic analysis of heterogeneous photo catalysis for semiconductor systems. Phys. Chem. Chem. Phys. 19 (2014)

[23] K. Sridharan, E. Jang, T. J. Park, Novel visible light active graphitic C_3N_4–TiO_2 composite photocatalyst: Synergistic synthesis, growth and photocatalytic treatment of hazardous pollutants, Appl. Catal. B.143 (2013) 718– 728

[24] T.He, J. Yao. Photochromism in composite and hybrid materials based on transition-metal oxides and polyoxometalates, Prog. Mater.Sci, 51 (2006) 810–879

[25] R. Marschall, Semiconductor Composites: Strategies for Enhancing Charge Carrier Separation to Improve photocatalytic Activity. Adv. Funct. Mater. 24 (2014) 2421–2440

[26]C.Lopano,P. Heaney, J.Post ; J.Hanson, S. Komarneni, Time-resolved Structural Analysis of K- and Ba-exchange Reactions with Synthetic Na-birnessite Using Synchrotron X-ray Diraction. Am. Miner. 92 (2007) 380-387.

[27]K. P. Lucht, J. L.Mendoza-Cortes. Birnessite: A Layered Manganese Oxide to Capture Sunlight for Water-Splitting Catalysis, Phys. Chem. *C*, 40 (2015) 22838–22846

[28] H. Chen, L. Wang, Nanostructure sensitization of transition metal oxides for visible-light photo catalysis, Beilstein J. Nanotechnol. 5(2014) 696–710.

[29]S. J. A. Moniz, S.A. Shevlin, Xiaoqiang An, Z-X. Guo, J. Tang, Fe_2O_3–TiO_2 Nanocomposites for Enhanced Charge Separation and Photocatalytic Activity. Chem. Eur. J. 20 (2014) 1 – 10

[30]M. Ibáñez, J. V Sancho, O. J. Pozo, and F. Hernández, Use of quadrupole time-of-flight mass spectrometry in environmental analysis: elucidation of transformation products of triazine herbicides in water after UV exposure. Anal. Chem.76 (2004)1328–35.

[31] C. E. Frey, M. Wiechen, P. Kurz, Water-oxidation catalysis by synthetic manganese oxides systematic variations of the calcium birnessite theme, Dalton Trans. 43(2014) 4370

[32]B.A. Pinaud, Z. Chen, D. N. Abram, T.F. Jaramillo. Thin Films of Sodium Birnessite-Type MnO_2: Optical Properties, Electronic Band Structure, and Solar Photo electrochemistry J. Phys. Chem. C.23 (2011)11830–11838

[33]S.D.Sharma, K.K. Saini, C. Kant, C.P. Sharma, S.C. Jain. Photo degradation of dye pollutant under UV light by nano-catalyst doped titania thin films. Appl. Catal. B. 84 (2008) 233–240

[34]L. G. Devi, N. Kottam, N. Murthy, S. G. Kumar, Enhanced photocatalytic activity of transition metal ions Mn^2+, Ni^2+ and Zn^2+ doped polycrystalline titania for the degradation of Aniline Blue under UV/solar light. J. Mol. Catal. 328 (2010) 44–52

[35]S. Erdemoglu , S. Karaaslan , F. Sayılkan , B. Izgi , M. Asilturk , H. Sayılkan , F. Frimmel , S. Gucer, photocatalytic degradation of Congo Red by hydrothermally synthesized nanocrystalline TiO2 and identification of degradation products by LC–MS, J. Hazard. Mater. 155 (2008) 469–476

[36] U.I.Gaya, A.H. Abdullah, Heterogeneous photocatalytic Degradation of Organic, Contaminants over Titanium Dioxide: A Review of Fundamentals, Progress and Problems. J. Photochem. Photobiol. C: Photochem. Rev. 9(2008) 1-12.

[37] M. S. Hamdy, P. Nickels, I. H. Abd-Elmaksood, H. Zhou, E. H. El-Mossalamy, A. O. Alyoubi, Lynch, A. Nathan, and G. Thornton, Parameters controlling the photocatalytic performance of ZnO/Hombikat TiO2 composites, J. Photochem. Photobiol. A Chem.228 (2012) 1–7.

[38]O. Ola, M.M. Maroto-Valer, Review of material design and reactor engineering on TiO_2 photocatalysis for CO2 reduction, J. Photochem. Photobiol. C: Photochem. Rev. 24 (2015) 16–42

[39]L. Zhang, Y. Nie, C. Hu, and X. Hu, "Decolorization of methylene blue in layered manganese oxide suspension with H2O2," J. Hazard. Mater.190 (2011) 780–785.

[40]G. H. Safari, M. Hoseini, M. Seyedsalehi, H. Kamani, J. Jaafari , A. H. Mahv, Photocatalytic degradation of tetracycline using nanosized titanium dioxide in aqueous solution, Int. J. Environ. Sci. Technol. 12 (2015) 603–616

[41]G. Colon, M. Maicu, M.C. Hidalgo, J.A. Navıo, Cu-doped TiO2 systems with improved photocatalytic activity, Appl. Catal. B.67 (2006) 41–51

[42]U. G. Akpan and B. H. Hameed, Parameters affecting the photocatalytic degradation of dyes using TiO2-based photocatalysts: A review, J. Hazard. Mater.170 (2009) 520–529.

[43]X. Bai, R. Zong, C. Li, D. Liu, Y. Liu, and Y. Zhu, Environmental Enhancement of visible photocatalytic activity via Ag @ C 3 N 4 core – shell plasmonic composite, Appl. Catal. B. 147 (2014) 82–91.

[44] S. Chiron, S. Papilloud, W. Haerdi, and D. Barcelo, Automated on-line liquid-solid extraction followed by liquid chromatography-high-flow pneumatically assisted electrospray mass spectrometry for the determination of acidic herbicides in environmental waters, Anal. Chem. 67 (1995)1637–1643

[45] A. Di Corcia, C. Crescenzi, E. Guerriero, and R. Samperi, Ultratrace determination of atrazine and its six major degradation products in water by solid-phase extraction and liquid chromatography- electrospray/mass spectrometry,Environ. Sci. Technol.31 (1997)1658–1663,.

[46] A. Houas, H. Lachheb, M. Ksibi, E. Elalouui, C. Guillard, and J.-M. Herrmann, Photocatalytic degradation pathway of methylene blue in water, Appl. Catal. B. 31 (2001)145–157.

[47]A. O. Ibhadon and P. Fitzpatrick, Heterogeneous Photocatalysis: Recent Advances and Applications, Catalysts, 3 (2013)189–218

[48]K. Aston, N. Rath, A. Naik, U. Slomczynska, O. F. Schall, D. P. Computer-Aided Design (CAD) of Mn(II) Complexes: Superoxide Dismutase Mimetics with Catalytic Activity Exceeding the Native Enzyme Riley , Inorg. Chem. 40(2001) 1779-1789

[49]Q. Jin, H. Arimoto, M. Fujishima, and H. Tada, Manganese Oxide-Surface Modified Titanium(IV) Dioxide as Environmental Catalyst, Catalysts,3 (2013) 444–454.

[50]R. Jothiramalingam and M. K. Wang, Synthesis, characterization and photocatalytic activity of porous manganese oxide doped titanium dioxide for toluene decomposition, J. Hazard. Mater. 147 (2007) 562–569.

[51]A.A. Ismail, I. Abdelfattah, M. F. Atitar , L. Robben, H.Bouzid , S.A. Al-Sayari, D.W. Bahnemann, Photocatalytic degradation of imazapyr using mesoporous Al_2O_3–TiO_2nanocomposites, Sep. Purif. Technol. 145 (2015) 147–153

[52]I. K. Konstantinou, T. a. Albanis, Photocatalytic transformation of pesticides in aqueous titanium dioxide suspensions using artificial and solar light: Intermediates and degradation pathways, Appl. Catal. B. 42 (2003) 319–335

[53]B. Li, G. Gao, D. Zhai, C. Wei, Y. He, H. Du, and F. Kang, Synthesis, characterization and electrochemical performance of manganese dioxide in a quaternary microemulsion: The role of the co-surfactant and water, Int. J. Electrochem. 8(2013) 8740–8751

[54]H. Li, D. Wang, H. Fan, T. Jiang, X. Li, and T. Xie, Synthesis of ordered multivalent Mn-TiO_2 nanospheres with tunable size: A high performance visible-light photocatalyst, Nano Res. 4 (2011) 460–469

[55]G. H. Safari, M. Hoseini, M. Seyedsalehi, H. Kamani, J. Jaafari , A. H. Mahv, Photocatalytic degradation of tetracycline using nanosized titanium dioxide in aqueous solution, Int. J. Environ. Sci. Technol. 12 (2015) 603–616

[56]Y. Bessekhouad , N. Chaoui , M. Trzpit , N. Ghazzal , D. Robert , J.V. Weber . UV–vis versus visible degradation of Acid Orange II in a coupled CdS/TiO2 semiconductors suspension. J. Photochem. Photobiol. A 183 (2006) 218–224

[57]B. K. Vijayan, N. M. Dimitrijevic, J. Wu, and K. A. Gray, The effects of Pt doping on the structure and visible light photoactivit of titanium dioxide nanotubes, J. Phys. Chem. C. 114 (2010) 21262–21269

[58]E. M. Saggioro, A. S. Oliveira, T. Pavesi, C. G. Maia, L. F. V. Ferreira, and J. C. Moreira, Use of titanium dioxide photocatalysis on the remediation of model textile wastewaters containing azo dyes, Molecules, 16 (2011) 10370–10386,.

[59]S. D. Sharma, K. K. Saini, C. Kant, C. P. Sharma, and S. C. Jain, Photodegradation of dye pollutant under UV light by nano-catalyst doped titanium dioxide thin films, Appl. Catal. B. 84 (2008) 233–240

[60]R. Rahimi, E. Fard , S.Saadati, M.Rabbani, Degradation of methylene blue via Co–TiO2 nano powders modified by meso-tetra (carboxyphenyl)porphyrin. J. Sol-Gel Sci. Technol. 62 (2012) 351–357

[61]L. G. Devi , B. N. Murthy, S. G. Kumar, Photocatalytic activity of V5+, Mo6+ and Th4+ doped polycrystalline TiO_2 for the degradation of chlorpyrifos under UV/solar light, J. Mol. Catal. A: Chem. 308 (2009) 174–181

[62]I. Zaharieva, M. M. Najafpour, M. Wiechen, M. Haumann, P. Kurz, and H. Dau, Synthetic manganese–calcium oxides mimic the water-oxidizing complex of photosynthesis functionally and structurally, Energy Environ. Sci.4 (2011) 2400–2408

[63]M. Saif and M. S. A. Abdel-Mottaleb, Titanium dioxide nanomaterial doped with trivalent lanthanide ions of Tb, Eu and Sm: Preparation, characterization and potential applications, Inorganica Chim. Acta, 360 (2007) 2863–2874

Chapter 3: Photocatalytic degradation of imazapyr using Ca_xMnO_y-TiO_2 heterostructures under UV and visible irradiation

Salma Bougarrani[a,*], Preetam K. Sharma[b], Jeremy W. J. Hamilton[b], Anukriti Singh[b], M. Canle[c], Mohammed El Azzouzi[a], J. Anthony Byrne[b]

[a]Laboratory of Spectroscopy, Molecular Modelling, Materials, Nanomaterials, Water and Environment, University Med V, Avenue Ibn Battouta, BP 1014, Agdal, Rabat, Morocco

[b]NIBEC, Ulster University, Newtownabbey, BT37 0QB, United Kingdom

[c]Chemical Reactivity and Photoreactivity Group, Department of Chemistry, Faculty of Sciences & CICA, University of A Coruña, E-15071 A Coruña, Spain

*corresponding author: salma.bougarrani@gmail.com

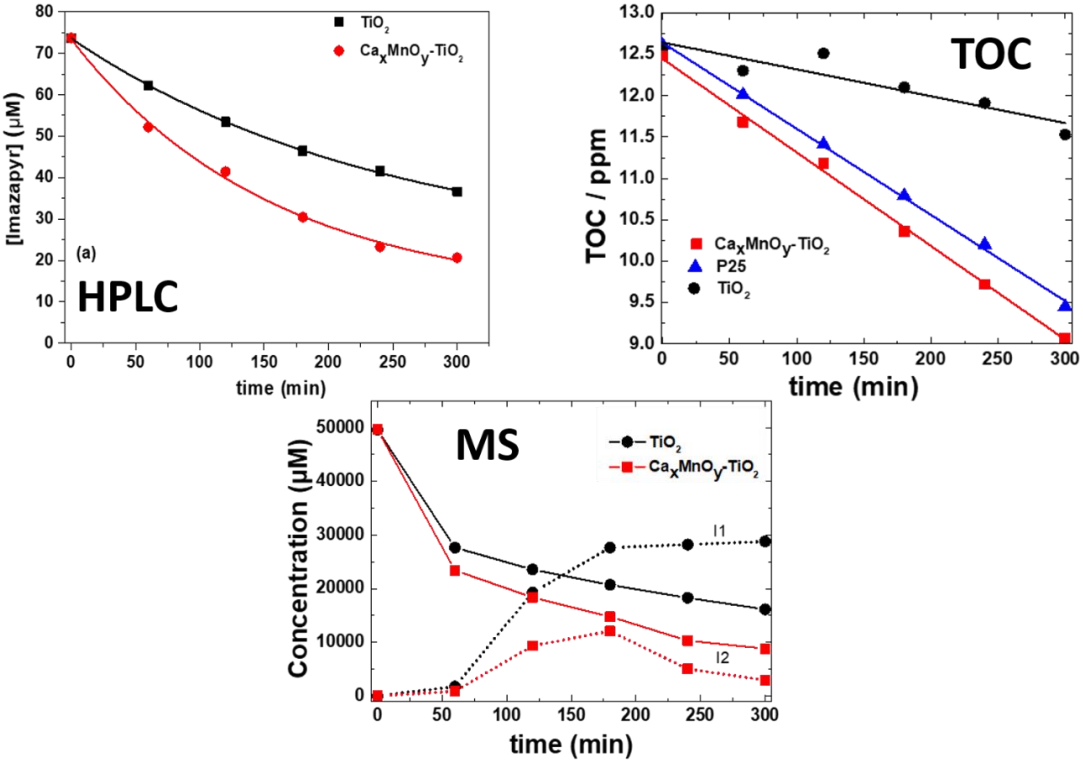
HPLC
(a)
[Imazapyr] (μM)
time (min)
TiO2
CaxMnOy-TiO2
TOC
TOC / ppm
time (min)
CaxMnOy-TiO2
P25
TiO2
MS
Concentration (μM)
time (min)
TiO2
CaxMnOy-TiO2
I1
I2

Abstract:

The formation of heterostructures of TiO_2 (Hombikat UV100) with layered manganese dioxide (birnessite) was investigated to improve the photocatalytic efficiency under UV-Vis irradiation. Ca_xMnO_y was prepared by a precipitation method and then mixed with TiO_2 by mechanical grinding following by annealing at 500°C to obtain Ca_xMnO_y-TiO_2. The photocatalytic activity was determined using phenol and imazapyr herbicide as model pollutants in a stirred tank reactor under UV-Vis and visible only irradiation. Ca_xMnO_y-TiO_2 showed a higher degradation rate (10.6 $\mu M \cdot h^{-1}$) than the unmodified TiO_2 (7.4 $\mu M \cdot h^{-1}$) for imazapyr under UV-Vis irradiation. The mineralization rate, was 4.07 $\mu M \cdot h^{-1}$ for Ca_xMnO_y-TiO_2 and 1.21 $\mu M \cdot h^{-1}$ for TiO_2. Apart from the degradation under UV-Vis, some photocatalytic degradation was obtained in the Vis region for Ca_xMnO_y-TiO_2. In the Ca_xMnO_y-TiO_2 system, the concentration of intermediate products reached a maximum at 180 min of irradiation before decreasing again to half the maximum in 120 min. For unmodified TiO_2, the intermediates continuously increased with irradiation time but there was no decrease in the concentration of intermediate products observed. The enhanced efficiency of the Ca_xMnO_y-TiO_2 for the complete degradation of the imazapyr and intermediates is probably due to the greater adsorption of polar species on the surface of the Ca_xMnO_y. Based on the experimental results, a photocatalytic degradation mechanism has been proposed.

Keywords: persistent organic pollutants, photocatalysis, TiO_2, birnessite, surface modification, degradation pathway, mass spectrometry.

3.1. Introduction

Persistent organic pollutants such as pesticides have attracted global environmental concern due to their adverse impacts on the environment and public health [1,2]. Many persistent organic pollutants (POPs), such as pesticides can be highly toxic due to their long half-life, their stability and their ability of long-range transportation [3]. POPs can also produce hazardous by-products during chemical reactions classified as oxidation, esterification, hydrolysis, or other degradation processes in water[4,5].

The new approaches are needed for the treatment of polluted water to expand the range of water sources that can be recycled. To promote long-term water resources preservation, the on-site reuse of treated wastewater for agricultural and industrial activities may be the most appropriate technology to ensure availability and sustainable water management in water-deprived regions. Different treatment processes have been explored to reduce or eliminate water POPs and to limit the health effects of the exposures to these toxic chemicals by consuming contaminated water[1,5] .

Most traditional water treatment methods, including physicochemical treatment and biological degradation, transfer the pollutant from hydrosphere to other environmental compartments [7]. Advanced oxidation processes (AOPs) have the potential to actual degrade persistent organic POPs, and may lead to complete mineralization (if given long enough) [8].

Among AOPs, heterogeneous photocatalysis using TiO_2 has been widely investigated for the degradation of POPs in water [8,9]. The key advantage of AOPs is the complete mineralization of organic carbon into CO_2 and, whilst photocatalytic AOPs systems offer further advantages of low cost due to the use of catalytic materials, no consumable chemicals and the potential use of sunlight. Although TiO_2 photocatalysis shows a great potential for degradation of POPs, its solar absorption is poor. With typical photocatalysts such as TiO_2, the band gap (3.2 eV for anatase) is limited to the UV domain, which accounts for less than 4% of the entire solar spectra thus limiting their efficiency [11]. Poor selectivity of TiO_2 photocatalysis to eliminate low-level of POPs in contaminated waters with the presence of other highly concentrate POPs is another disadvantage of heterogeneous photocatalysis [11,12].

In order to design highly active photocatalyst systems, researchers have attempted to improve solar efficiency of photocatalyst materials through modification with other photocatalytic or electrocatalytic materials such as RuO_2, Fe_2O_3, ZnO and V_2O_5[14]. Surface modification of TiO_2 can also increase activity through modification of surface adsorption properties leading to differing selectivity, or changes in recombination due to the development of semiconductor

hetero-junctions [14,15]. Ca_xMnO_y has attracted a lot of attention due its potential as an oxidation catalyst, with different adsorption properties to TiO_2 and an narrow band gap of 2.20–2.63 eV, [16,17]. It is reported to have excellent electron transport properties, and it may serve as a sensitizer and electron-accepting co-catalyst in an MnO_y/TiO_2 heterostructured material [19].
Devi et al. reported that Mn-TiO_2 demonstrated enhanced absorption in the visible light region and therefore higher photocatalytic activity under solar irradiation [20]. They attributed in the improvement in activity to the synergistic effect of mixed anatase-rutile phase, smaller crystallite size and partially filled electronic configuration of Mn^{2+}, which could *serve* as electron and hole shallow traps.
Although it has been shown previously that MnO_y based semiconductors exhibited enhanced photocatalytic performance with respect to the pure photocatalyst alone, some problems still hinder further application of these nanocomposites [21]. To improve on this, different metal ions intercalated into birnessite has been investigate for use as a surface modification with TiO_2. Recently, Cortes et al. have demonstrated that birnessite structures containing Sr, Al, B and Ca have good light harvesting ability, and Ca-birnessite type is predicted to be the most suitable candidate for water splitting due its suitable direct band gap for light capturing [22]. Additionally, birnessite readily participates in cation-exchange and oxidation-reduction reactions [23] .
In this work, Ca_xMnO_y-TiO_2 photocatalysts were fabricated and characterised for various physicochemical properties. The materials were tested for the photocatalytic degradation of imazapyr in aqueous suspension and intermediate products were investigated by high-performance liquid chromatography, mass spectrometry and total organic carbon analysis. Also, the influence of Ca_xMnO_y on the photocatalytic activity for imazapyr degradation has been systematically elucidated. The photocatalytic activity and intermediate products for imazapyr degradation may provide new insight for the utilisation of birnessite materials for the photocatalytic wastewater treatment.

3.2. Materials and methods

3.2.1. Reagents

TiO_2 Hombikat UV100 nanoparticles were obtained from Sachtleben Chemie and TiO_2 P25 was obtained from Evonik Aeroxide. Imazapyr herbicide (99%), hydrochloric acid, calcium sulphate, sodium hydroxide, potassium permanganate, manganese chloride tetrahydrate, potassium

chloride, phenol and various solvents were purchased from Sigma Aldrich and used without further purification. Deionized water was obtained from an ELGA Purelab DI water unit.

3.2.2. Preparation of the photocatalyst

Calcium birnessite (Ca_xMnO_y) was synthesized trough a precipitation method described by Frey et al. [24] . In brief, $MnCl_2 \cdot 4H_2O$ was added to KOH under vigorous stirring. $KMnO_4$ solution was then added to the reaction mixture. After 3 h of reaction, the solution was filtered through a Whatman glass fibre filter, followed by drying in oven at 60°C. Ca_xMnO_y with a variety of Mn to Ca ratios were prepared and the ratio of 1.6 was used for the further investigation due previous investigations towards imazapyr degradation [25]. Ca_xMnO_y powder (5 wt.%) was mixed with TiO_2 by mechanical grinding followed by annealing under vacuum at 500°C (ramp $2^{\circ}C \cdot min^{-1}$ up rate and $1^{\circ}C \cdot min^{-1}$ down rate) for 24 h to obtain Ca_xMnO_y-TiO_2[25].

3.2.3. Catalyst characterization

Powder X-ray diffraction (XRD) patterns recorded using an Rigaku-Dmax 2500 instrument with monochromatized Cu K_α radiation (0.15405 nm, 40 kV, 100 mA) in the range 10°–100°. Absorption spectra were recorded between 250 nm and 800 nm with a Lambda 650 UV-Vis spectrophotometer. The zeta potentials of the synthesized catalysts were determined in aqueous solution at different pH values, using Malvern Zetasizer Nano ZS model. X-ray photoelectron spectra (XPS) of the catalysts were recorded using a Kratos Axis Ultra system. Wide-energy survey scans and high-resolution scans were performed at pass energies of *160* eV and 20 eV respectively. The obtained XPS spectra were analysed using CasaXPS software. The calibration of the energy positions was done following normalization of the shifting C 1s peak to 284.8 eV. The XPS peaks were fitted using mixed Gaussian-Lorentzian (GL30) function on a Shirley background. Transmission electron microscopy (TEM) analysis was performed with a JEOL JEM-2100F instrument at 200 kV electron acceleration voltage. Samples for TEM analysis were prepared by the sonication of catalysts in ethanol followed by dip coating or drop-casting on the TEM grids**.**

3.2.4. Photocatalytic reactor

The photocatalytic degradation of pollutants was performed in the stirred tank photocatalytic reactor (STR) previously reported [26]. The reactor contained a reservoir for the pollutant-photocatalyst solution (water-jacketed walled vessel) and a stainless-steel propeller used to ensure good mass transfer as turbulent flow within the reactor transports the organic pollutant towards the dispersed photocatalyst. A xenon source (125 W) was used as UV-Vis irradiation

source. A 410 nm UV cut-off filter was used for determining the visible only photocatalytic activity of the materials. The light intensity entering the reactor was measured at different areas across the sample window using a calibrated radiometer (Jobin Yvon Gemini 180). The average UV intensity (280-400 nm) was determined to be 12.3 $W \cdot m^{-2}$. Water circulation was kept on throughout the photocatalytic experiments to maintain a constant reaction temperature of 25°C.

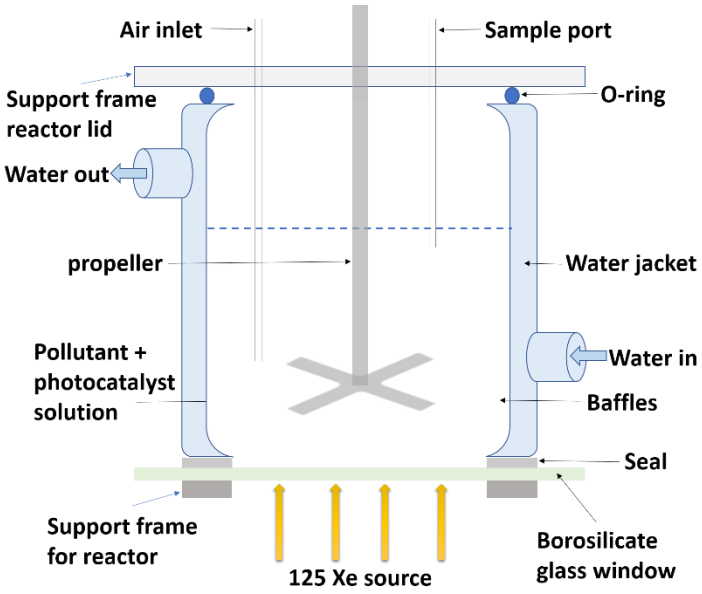

Figure 3.1. Schematic representation of a stirred rank reactor.

3.2.5. Photocatalytic experiments

In a typical experiment, an aqueous solution (200 cm^3) of test pollutant with photocatalyst was added in the dark for 60 min with air sparging to establish the adsorption equilibrium.

Before irradiation in the sun test, mixture of catalyst and of AMX was soaked in the dark for 60 min at room temperature, immediately afterwards

Phenol (1 mM) and imazapyr (75 µM) were the test pollutants for the photocatalytic degradation experiment. The optimal loading of Ca_xMnO_y -TiO_2 was determined to be 30.6 $mg \cdot L^{-1}$ (details are given in supplementary information (SI) S1). The Xe lamp was switched on and allowed to stabilize for 1 h before irradiating the reactor. The propeller rotation speed was adjusted to 2000 rpm. Air-sparging (900 $cm^3 \cdot min^{-1}$) was kept on throughout the experiment. After a 1 h dark period, the photocatalytic experiment was carried out for a period of 5 h. Batch samples (1.5

cm^3) for analysis were taken from the reactor every hour and tested further using the analytical techniques described below.

3.2.6. Analytical methods

3.2.6.1. *High performance liquid chromatography (HPLC)*

Imazapyr and phenol concentrations were determined using reverse phase HPLC system equipped with a UV detector (Agilent 1200 series) with Supelco IL (250.0 mm x 4.6mm, 5 µm separation column) and Supelco guard column (supelguard C18 (22.0 mm x 4.0mm, 5µm). The mobile phase was a mixture of 40% methanol and 60% water adjusted to pH 3.2 by adding formic acid, isocratic elution at a flow rate 1 $ml \cdot min^{-1}$. The injection volume of 20 µL and 250 nm UV detection wavelength were used for imazapyr. For phenol, 30 µL injection volume and UV detection wavelength of 270 nm was used.

Six different imazapyr concentrations were used to perform the analyses of calibration curves (R^2 value of 0.999). Limit of detection (LoD), and limit of quantitation (LoQ) describing the smallest concentration of a measured that can be reliably measured by an analytical procedure were calculated. For phenol, the values of LOD was 9.82 ppb and LOQ was 29.47 ppb. The values of LOD and LOQ were 6.53 ppb and 18.62 ppb, respectively for imazapyr.

3.2.6.2. *Mass spectrometry-Electrospray Ionisation (MS-ESI)*

By-products generated during the photodegradation of imazapyr were determined by mass spectrometry-electrospray ionization (MS-ESI) recorded on Bruker Esquire 3000 plus instrument. The working parameters of ESI were determined in previous work by Bougarrani et al. [25]

3.2.6.3. *Total organic carbon (TOC) analysis*

TOC analysis was carried out using a Shimadzu 5000A analyser. The TOC analyser measures total carbon (TC) and inorganic carbon (IC) and determines TOC by subtracting the IC contribution from TC. The TC is determined by oxidizing the carbon in a furnace at 680˚C using Pt catalysts. The IC is determined by the acidification of the sample to convert IC to CO_2. The CO_2 liberated by both TC and IC analysis was quantitatively determined by the IR analysis.

3.3. Results and discussion

3.3.1. Materials investigations

Fig. S2 (SI) shows the XRD patterns of Ca_xMnO_y-TiO_2 and TiO_2. X-ray diffraction peaks of pure TiO_2 can be assigned to the anatase phase, rutile phase was not detected indicating that samples retained their original phase during calcination and no peaks associated with separated birnessite phases which should appear at about 12 ° and 25° were detected [27,28].

This could be either explained by the fact that the amount of birnessite/MnO_2 which did not exceed 5% in the total composition of Ca_xMnO_y-TiO_2, or due to the total concentration of amorphous to crystalline material [29]. However, the peaks of Ca_xMnO_y-TiO_2 ccomposite are much sharper than TiO_2, which indicate bigger particle size. The Scherrer equation was used to determine the particle size and it was confirmed that crystalline sizes of TiO_2 and Ca_xMnO_y-TiO_2 (annealed at 500˚C) are 8.4 and 19.9 nm, respectively.

Fig. S3(SI) shows the absorption spectra of pure TiO_2 and Ca_xMnO_y-TiO_2. It was confirmed from the spectrum of pure TiO_2 shows its characteristic sharp absorption edge at 387 nm, which is consistent with the band gap of anatase TiO_2 (ca. 3.2 eV) [30]. Ca_xMnO_y-TiO_2 by contrast shows a broad adsorption across the visible range due to surface modification.

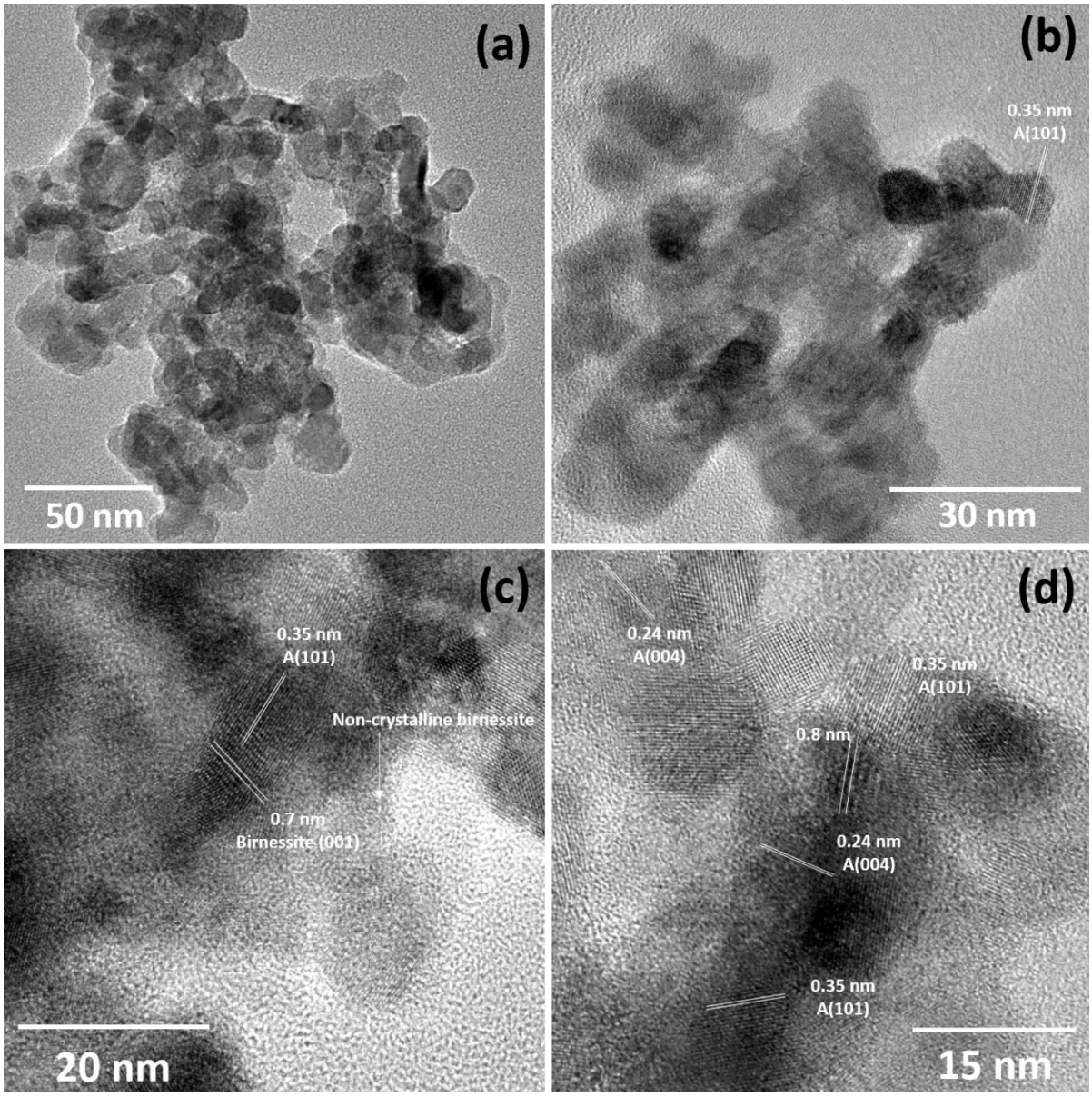

Figure 3.2. (a-d) TEM images of Ca_xMnO_y-TiO_2 at different magnifications.

The observed TEM images of Ca_xMnO_y-TiO_2 are shown in Fig. 3.2. The different TiO_2 particles neck together to form bigger clusters resulting in bigger particle sizes. This can be clearly observed in Fig. 3.2(a). The lattice spacing from the aggregates at higher magnification can be observed: spacings of 0.35 nm correspond to A(101) and 0.24 nm correspond to A(004). Birnessite is a manganese oxide mineral with layered structure[23]. Birnessite crystals have hexagonal unit cells with interlayer spacing of 0.7 nm [32, 33]. Birnessite layers corresponding to the interlayer spacing of 0.7 nm can be visualised in Fig. 3.2(c). In Fig. 3.2(d), the interlayer spacing of 0.8 nm is believed to be due to the enhanced layer separation of birnessite material due to sonication. The lattice edges are due to the birnessite layers, less birnessite lattices being observed as compared to TiO_2 lattices. This is due to the poor crystalline properties of the

birnessite materials and various non-crystalline regions have been observed [31]. The non-crystalline regions are located around TiO_2 particles. Overall, Ca_xMnO_y layers are encapsulating TiO_2 particles but no information about the overall surface coverage could be obtained.

The chemical composition of the Ca_xMnO_y-TiO_2 was further characterized by X-ray photoelectron spectroscopy (XPS). As Ca_xMnO_y is only 5% of TiO_2 (by weight) XPS analysis of Ca_xMnO_y alone was carried out to determine the elemental composition (Fig. 3.3). The survey scan (Fig. 3.3(a)) indicates that the material has Ca, Mn and O along with traces of carbon. The ratio of Mn to Ca is 1.67 which is slightly different from the precursors' ratio of 1.6. The high-resolution scans for Ca 2p, Mn 2p and O 1s are shown in Fig. 3.3(b-d). The binding energy position of Ca $2p_{3/2}$ is 347.2 and Mn $2p_{3/2}$ is 642.5 eV which are corresponding to the oxides[34,35]. As shown in Fig. 3.3(c), Mn is mainly in the Mn^{4+} state with some (13.7%) Mn^{3+}. The XPS analysis of Ca_xMnO_y-TiO_2 is shown in Fig. S4 (SI). The wide-energy survey scan in Fig S4 (a, SI) shows the peaks corresponding to C (adventitious), Ti, Ca, Mn and O. The Ca_xMnO_y to TiO_2 ratio is 3.3 from the survey spectra. The high-resolution scans for Ti 2p, O 1s, Ca 2p and Mn 2p regions are shown in Fig. S4(b-e, SI). The binding energy position of Ca, Mn and Ti are consistent with the oxides position in the literature[16].

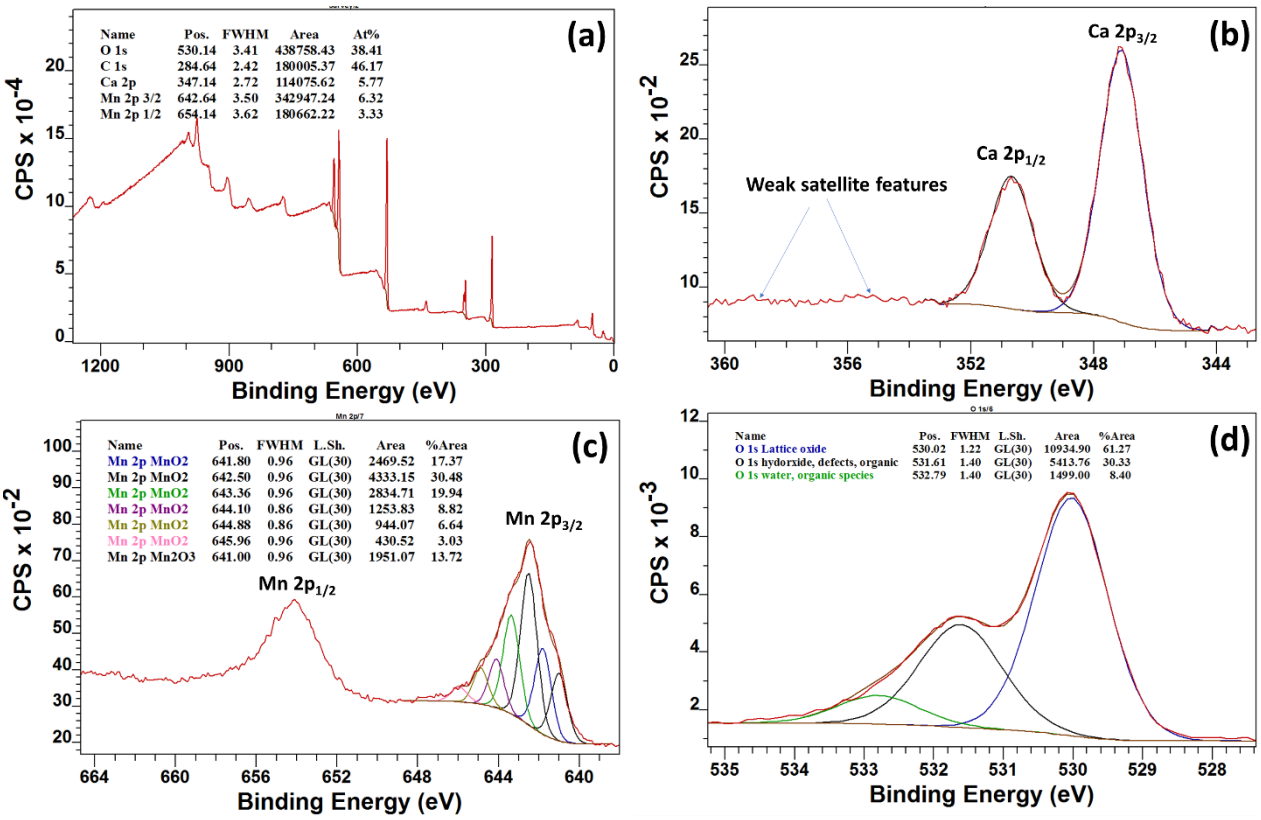

Fig. 3.3. (a) Survey, (b) Ca 2p, (c) Mn 2p and (d) O 1s of Ca_xMnO_y samples.

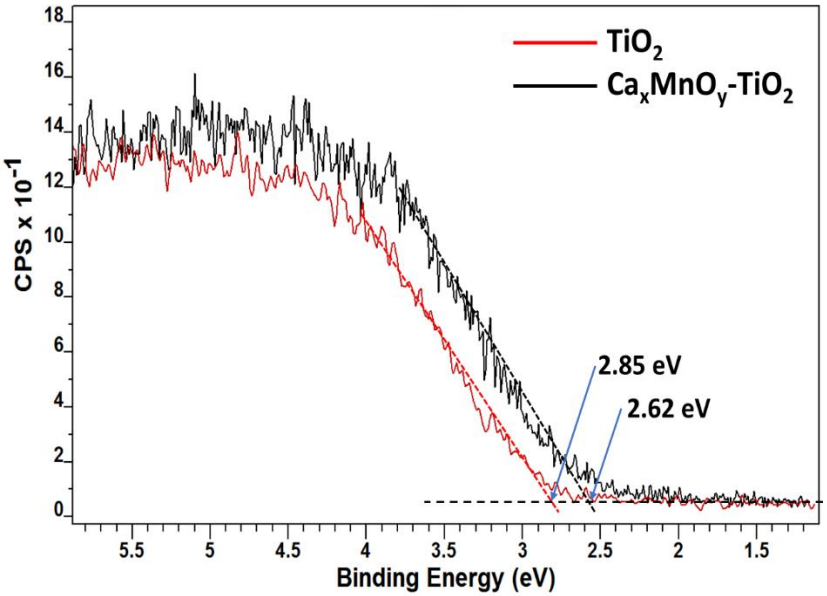

Figure 3.4. Valence Band XPS of TiO_2 and Ca_xMnO_y-TiO_2.

The valence band (VB) XPS was utilised to determine the VB edge for the materials as shown in Fig. 3.4. The valence band edge position vs Fermi level for Ca_xMnO_y-TiO_2 and TiO_2 were 2.62 and 2.85 eV, respectively. The shift of the VB edge to a lower value, by around 0.2 eV, is indicative of the possible band-gap narrowing which is consistent with the UV-Vis absorption spectra. Modification of TiO_2 with Ca_xMnO_y, reduces the band-gap of TiO_2, and improve the photocatalytic activity under visible light irradiation.

The combination of semiconducting oxides can produce differences in the internal electric field within photocatalysts altering charge transfer and recombination within the photocatalyst [35]**.** To investigate charge carrier recombination in the photocatalysts, photoluminescence measurements were performed. Photoluminescence is often used to investigate recombination in photocatalyst and photocatalytic composite systems [36]. With reduction in luminescence intensity correlating with improved catalytic activity. Ansari et al. have reported similar activity and photoluminescence properties of unmodified TiO_2 and modified TiO_2 with Ag [38,30]. Photoluminescence (PL) measurements are illustrated in Fig. S5 (SI).

Broad emission peaks, centred ~550 nm, associated with electron-hole recombination were observed from all photocatalysts under 387 nm excitation. Emission intensity decreases more than 70% was observed when comparing Ca_xMnO_y-TiO_2 to TiO_2. The lower PL intensity of Ca_xMnO_y-TiO_2, indicative of reduced recombination rate [36], suggests the modified material will be more capable than the parent photocatalyst for degradation applications, investigated with phenol and imazapyr as model pollutants.

Therefore, it has been assumed that Ca_xMnO_y layers are encapsulating TiO_2 particle resulting in an effective separation of charge-carrier traps and leading to an efficient electron-hole separation, which result in *a* lower photoluminescence intensity as compared to unmodified TiO_2 [39,40]. On the other hand, lower degradation efficiency was observed when higher concentration of Ca_xMnO_y was used in the synthesis of the composite, this could hypothetically be explained by more rapid recombination caused by a surplus of Ca_xMnO_y which can act as a recombination center for electrons and holes, or due to the shielding effects [41].

To better understand the pollutant photocatalyst surface interactions related to photodegradation of imazapyr, the surface electrostatic charges of the suspended catalysts were investigated. Zeta potential values and isoelectric point of TiO_2 and Ca_xMnO_y-TiO_2 were measured in aqueous solution with different pH values. Obtained results are presented in Fig. 3.5 and Table 3.1.

Due to the limited migration of reactive oxygen species from the surface of photocatalysts the extent of surface adsorption of pollutants during will significantly affect the photocatalytic activity [42]. The surface charge affects the adsorption of charged pollutants and this electrostatic interaction is strongly affected by pH [3, 43].

Comparing TiO_2 and Ca_xMnO_y- TiO_2 the acid–base equilibrium governing the surface of metal oxides in water, was performed via zeta potential measurement (Fig. 3.5). Fitting the observed curves to the expected sigmoidal behaviour, a small shift is observed in the point of zero charge between materials, pH_{ps}=6.1 for TiO_2 and pH_{pzc}=6.7 for Ca_xMnO_y-TiO_2. Attari et al. (2016) have reported that imazapyr shows 5 pKa's, corresponding to the formation of five different ionic species.

The adsorption of imazapyr on the surface of catalyst is accelerated with decreasing the pH of the solution, resulting in stronger and more stable electrostatic interactions, which is expected to enhance the photocatalytic degradation rate of imazapyr [43]. Carrier et al. have reported similar results for photocatalytic degradation of imazapyr [44].

Comparing unmodified TiO_2 and Ca_xMnO_y-TiO_2 composite, the improvement of the photocatalytic activity in the presence of Ca_xMnO_y for pH 4.1± 0.1 could be explained by the stronger electrostatic attraction between negative charge of imazapyr and more positively charged (37.73 mV) Ca_xMnO_y-TiO_2 compared to TiO_2 (26.3 mV).

Table 3.1. The pH value, isoelectric point and zeta potential of pure TiO_2 and Ca_xMnO_y-TiO_2.

Catalyst	Zeta potential (mV)	pH	Isoelectric point
TiO_2	26.3 ± 0.4	4.14	6.1±0.2
Ca_xMnO_y-TiO_2	37.7 ± 0.5	4.09	6.7±0.2

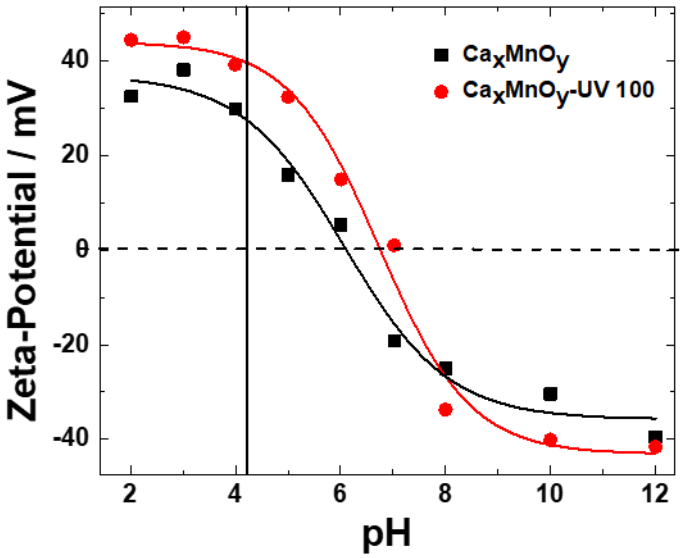

Figure 3.5. Zeta potentials at different pH in 1 mM KCI.

3.3.2. Photocatalytic activity of Ca_xMnO_y-TiO_2

The photocatalytic activity of TiO_2 and Ca_xMnO_y-TiO_2 in aqueous medium, under UV-Vis and visible only irradiation, was assessed using phenol and imazapyr as model compounds. As the pollutant degradation rate was decreasing with the change in the pollutant concentration, the photocatalytic activity was fitting assuming pseudo first-order kinetics

$$C = C_0 \, exp(-k \cdot t) \qquad (1)$$

Where, C is the pollutant concentration at time t, C_o is the concentration at the start of the experiment, and k is the degradation rate constant.

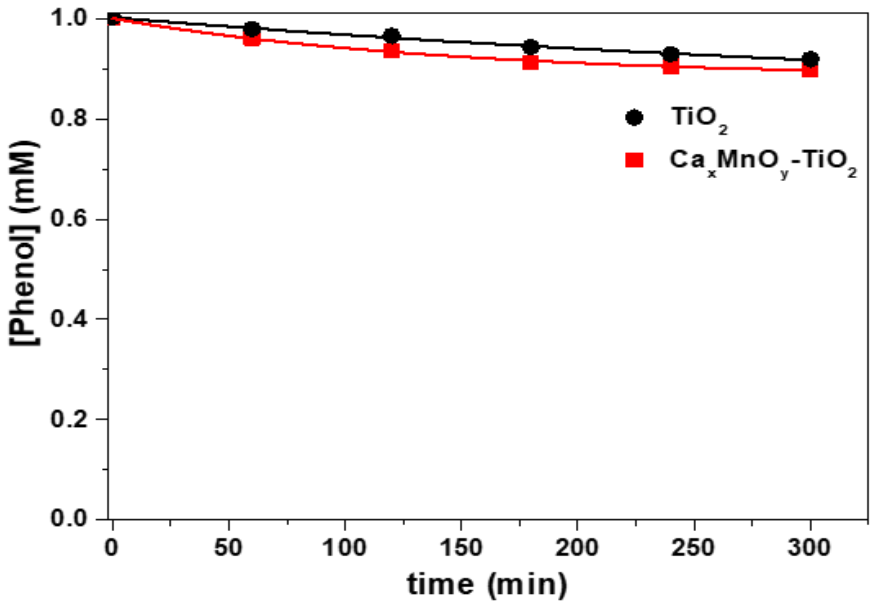

Figure 3.6. Change in phenol concentration over time for TiO_2 and Ca_xMnO_y-TiO_2 under UV-Vis irradiation.

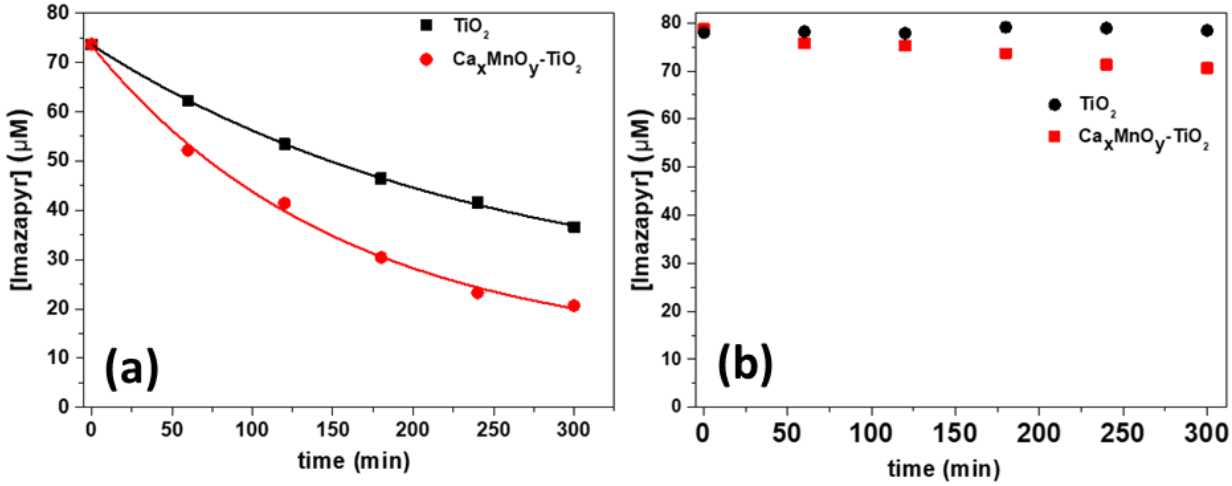

Figure 3.7. Change in imazapyr concentration over time for TiO_2 and Ca_xMnO_y-TiO_2 under (a) UV-Vis irradiation and (b) visible only irradiation determined by HPLC monitoring.

As shown in Fig. 3.6 and 3.7 (a), Ca_xMnO_y-TiO_2 shows a photocatalytic activity under UV-Vis irradiation that is higher towards both phenol ($k=(6.9\pm0.8)\cdot10^{-3}$ min^{-1}) and Imazapyr ($k_{Imazapyr}=(6.4\pm0.8)\cdot10^{-3}$ min^{-1}) degradation than that of commercial TiO_2 alone, for which $k_{phenol}=(2.1\pm0.9)\cdot10^{-3}$ min^{-1} and $k_{Imazapyr}=(4.0\pm0.3)\cdot10^{-3}$ min^{-1}. Modification of TiO_2 with Ca_xMnO_y leads to a ca. 3-fold rate enhancement for phenol degradation and 1.5-fold for imazapyr degradation.

Ca_xMnO_y-TiO_2 was also tested as catalysts of the photo-degradation of imazapyr under visible only irradiation (λ>410 nm). The results showed a lower degradation rate (, $k=1.4\cdot10^{-3}$ min^{-1}). However, for comparison, no degradation of imazapyr was observed in the same period when using TiO_2 (Fig. 3.7(b)).

The mineralization rate of aqueous imazapyr was evaluated by monitoring the changes in TOC as function of time in the reaction systems (Fig. 3.8). Upon comparison, the observed mineralization rates are 4.07 $\mu M\cdot h^{-1}$ and 1.21 $\mu M\cdot h^{-1}$ (0.679 $ppm\cdot h^{-1}$ and 0.195 $ppm\cdot h^{-1}$) for Ca_xMnO_y- TiO_2 and TiO_2 respectively.

The mineralization rates of imazapyr is 2.6 and 6.12 times slower than its photodegradation rates in the presence of CaxMnOy-TiO_2 and TiO_2, respectively. The results suggest that some intermediates products are more readily degraded by the composite than the TiO_2 alone under UV-Vis irradiation. The rate of mineralisation was also compared to P25 and was found to be similar for the CaxMnOy-TiO_2.

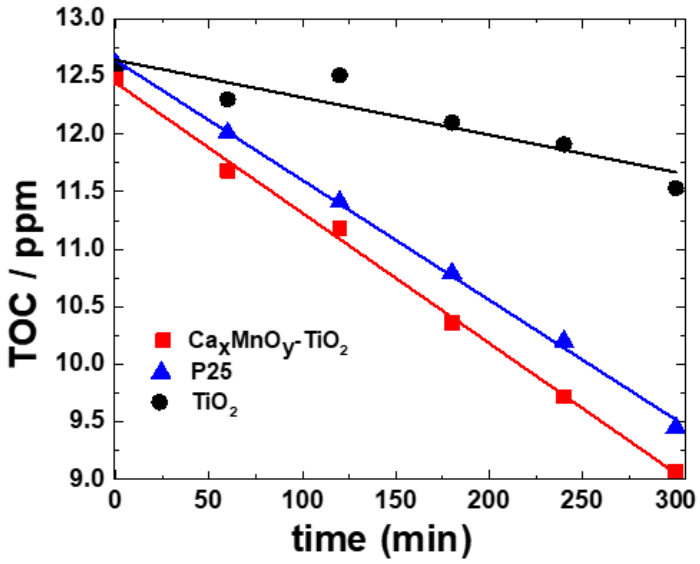

Figure 3.8. TOC versus time for the degradation of imazapyr under UV-vis light.

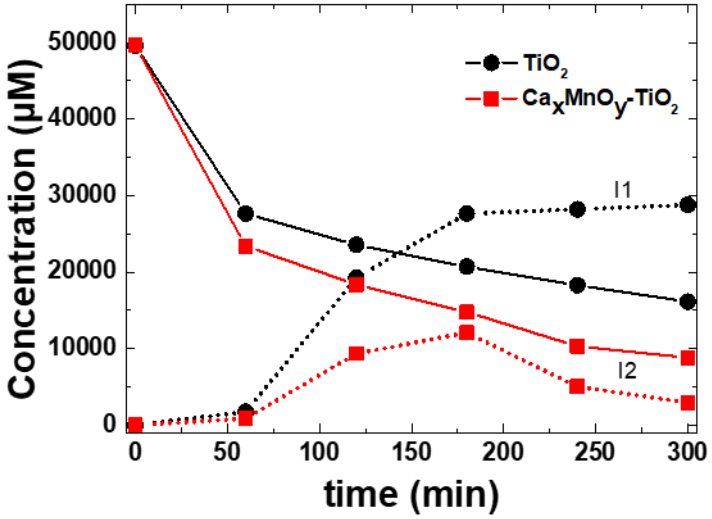

Figure 3.9. Intensity changes of Imazapyr (solid line) and intermediates sum (dots) over the catalysts Ca_xMnO_y-TiO_2 (I2) and TiO_2 (I1), determined by MS-ESI.

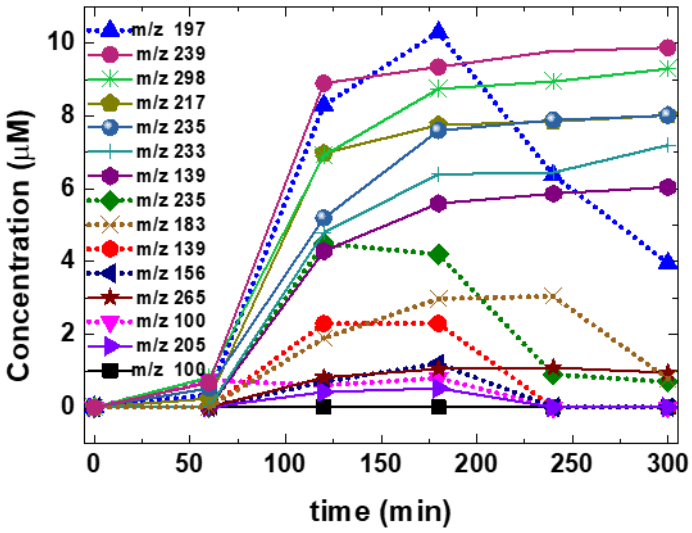

Figure 3.10. The change in concentrations for various intermediates (represented by their corresponding m/z) of the photocatalytic imazapyr degradation, determined by the MS-ESI. The

To investigate the degradation profiles of intermediates produced on catalysts Ca_xMnO_y-TiO_2 (dots) and TiO_2 (solid line) as shown in Fig. 3.9 and 3.10, mass spectroscopy electrospray ionisation (MS-ESI) was utilised. ESI was used for the detection of both positively and negatively charged intermediates of the photocatalytic degradation by coupling a quadrupole ion trap mass spectrometer with continuous polarity switching. By the mass spectrometric

fragmentation of the most intense ions, unknown intermediates were identified. The major final products in the presence of TiO_2 and Ca_xMnO_y-TiO_2 detected are compared to the corresponding peak areas, as monitored by HPLC, and listed in Table 3.2 and Fig. 3.9 and 3.10. Fig. 3.11 to 3.13 shows the positive and negative mode mass spectra for imazapyr photocatalysis using TiO_2 and Ca_xMnO_y-TiO_2.

The results summarized in Table 3.2 show that nine intermediates, including one detected in the negative mode, were generated in by TiO_2, but only six intermediates, including four detected in the negative mode, were generated in the presence of Ca_xMnO_y-TiO_2.

As shown in Fig. 3.9, the total concentration of intermediate products generated after 180 min photocatalytic degradation of imazapyr, using Ca_xMnO_y-TiO_2 (42.2 mM) are clearly much less abundant compared to TiO_2 (75.92 mM), which confirms HPLC analysis. In the presence of Ca_xMnO_y-TiO_2 the concentration of intermediate products achieved a maximum following 180 min of irradiation before a subsequent decrease of the intermediate concentration. By contrast, with TiO_2, different intermediate products were observed which continuously increased with irradiation time and no decrease in their concentration was observed. The differences in TiO_2 product removal profiles between photocatalysts under study suggest Ca_xMnO_y-TiO_2 to be a better system not only due to the higher degradation rate of the herbicide imazapyr pollutant, but due to the more efficient degradation of the intermediate products.

Table 3.2. Photoproducts of Imazapyr degradation and their intensities identified by the positive and negative modes of MS-ESI

Product number	Formula	Molar Mass	MS-ESI		Intensity in the presence of (TiO_2) au.	Intensity in the presence of (Ca_xMnO_y-TiO_2) a.u.
			Positive mode $(M+H)^+$	Negative mode $(M-H)^-$		
1 (Imazapyr)	**$C_{13}H_{15}N_3O_3$**	**261.281**	262.14	260.45	20696	14760
2	**$C_{12}H_{15}N_3O$**	**217.272**	218.7	216.2	3081	Nd.
3	**$C_{12}H_{15}N_3O_2$**	**233.271**	234.5	232.4	2096	Nd.
4	**$C_{12}H_{15}N_3O_4$**	**265.269**	266.42	264.13	1230	Nd.
5	**$C_{11}H_{17}N_3O_3$**	**239.275**	240.3	238	6051	Nd.
6	**$C_8H_{11}N_3O_3$**	**197.194**	198.2	196.5	5690	9340
7	**$C_{10}H_9N_3O_4$**	**235.199**	236.2	234.9	3120	948
8	**$C_9H_7N_3O_3$**	**205.173**	206.18	204.3	980	Nd.
9	**$C_7H_5NO_5$**	**183.119**	Nf.	182.5	Nd.	586
10	**$C_7H_5NO_4$**	**167.120**	Nf.	166.7	Nd.	Nd.
11	**$C_6H_5NO_3$**	**139.110**	Nf.	138.48	1986	523
12	**$C_7H_{12}N_2O_2$**	**156.185**	Nf.	155.2	Nd.	396
13	**$C_3H_4N_2O_2$**	**100.077**	Nf.	99.8	428	291

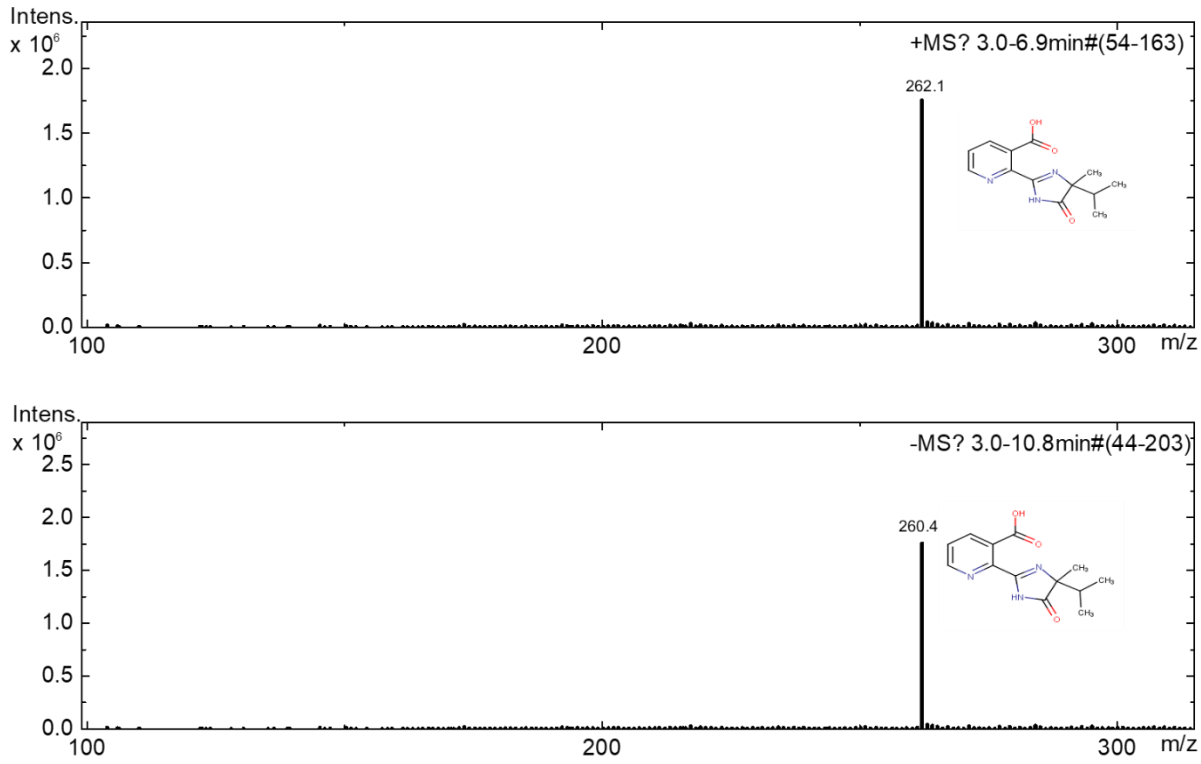

Figure 3.11. MS (positive and negative) mode of imazapyr before irradiation

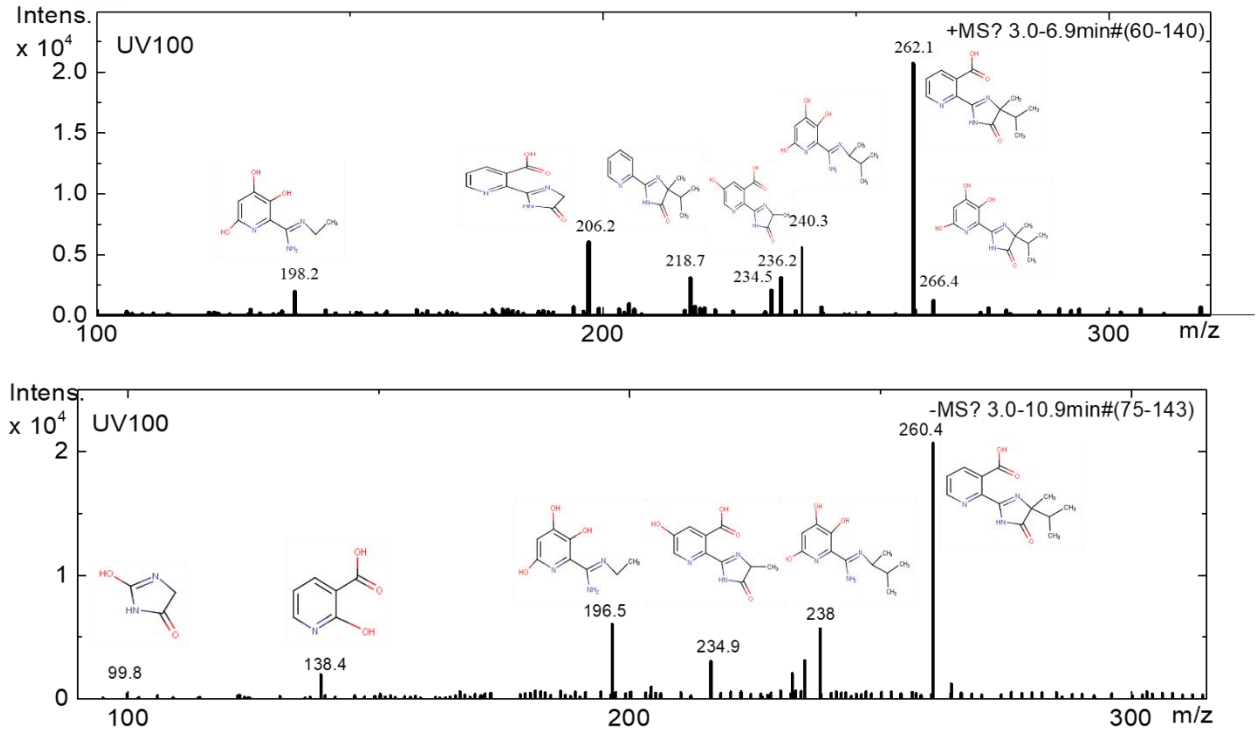

Figure 3.12. MS (positive and negative) mode of products generated after 300 min of irradiation using TiO_2 photocatalyst.

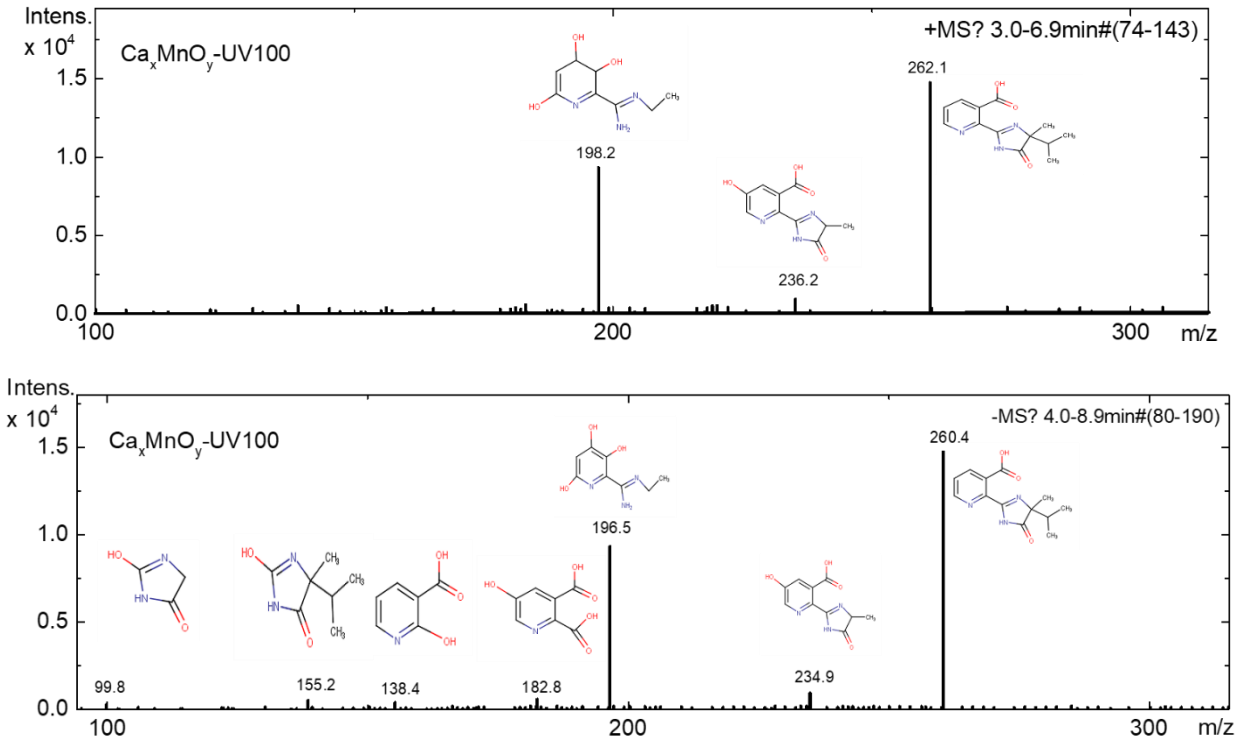

Figure 3.13. MS (positive and negative) mode of products generated after 300 min of irradiation using Ca_xMnO_y- TiO_2.

The structures of intermediates were identified by MS-ESI after 300 min of degradation in the positive and negative mode. The identified intermediates were utilised for the construction of various competing degradation pathways for aqueous solution of imazapyr (Fig. 3.14).

In pathway (I), the product with m/z of 233 was formed by decarbonylisation of the carboxyl group on the pyridine ring initiated by the attack of hydroxyl radical. The product of m/z 239 may be attributed to the consecutive hydroxylation of the aromatic ring followed by a proton movement by the breakage of the imidazole ring via CO loss. Afterwards, the aliphatic chain of the above molecule is oxidized, leading to a successive loss of methyl groups that provides the product of m/z 197.

The compound of m/z 217 (Pathway IV) is attributed to decarboxylation of pyridinic cycle, confirmed oxidation with holes h^+ that in addition to $HO^{\bullet}$. The initial imazapyr degradation products indicate that imazapyr adsorbs on the surface of photocatalyst by the carboxylic group binding [44].

In the second pathway (II), the product of m/z 235 and m/z 205 could be attributed to the oxidation of methyl groups on imidazole ring. The products of m/z 139 and m/z 100 are formed by the bond scission between imidazole and pyridine cycles. Another possible $HO^{\bullet}$ attack should lead to bonding break between both cycles (Pathway III) followed by hydroxylation of the

product m/z=167, m/z= 156 and m/z=183 detected in ESI(-). Such pathway is predominant in the anionic form of imazapyr that should be dominant in acid solution and could explain imazapyr degradation pathway in the presence of Ca_xMnO_y-TiO_2.

As most of the by-product formed after 300 min of irradiation using Ca_xMnO_y-TiO_2 catalyst were negatively charged and mainly with small molecular weight, their binding to the catalyst surface would be enhanced and this could increase the degradation process. Hongbin Fu et al.[1] reported that photodegradation of RhB with two photocatalyst systems occurred via two competitive pathways and have discussed different intermediate products identified in both systems, the enhanced photocatalytic activity of the parent sample for intermediate products was ascribed to the surface modification and the enhancements in the adsorption of the polarised organic reactants.

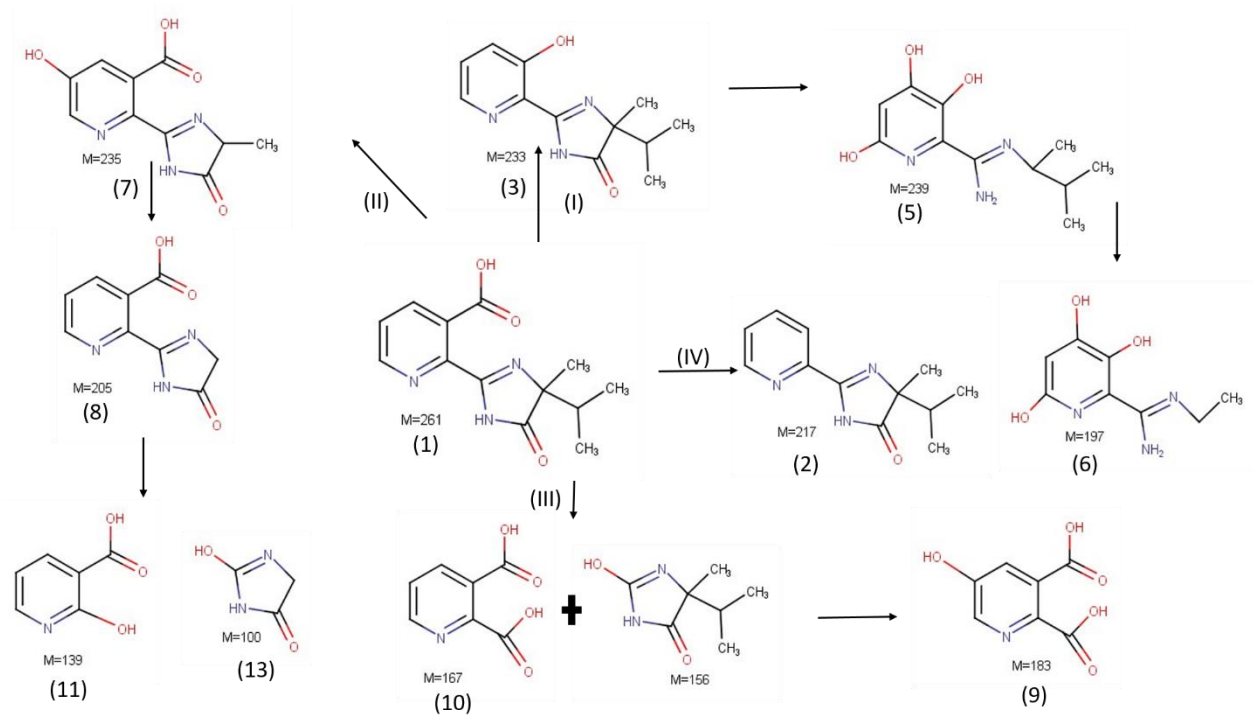

Figure 3.14. Degradation pathways for Imazapyr.

From these results, it seems clear that Ca_xMnO_y plays an important role in the enhancement of photocatalytic activity of TiO_2. The formation of Ca_xMnO_y-TiO_2 extends the spectral photocatalytic response into the visible region, indicating the possibility of the band-gap narrowing.

Ca_xMnO_y is present only on the surface of TiO_2 since usually Mn-doped TiO_2 are synthesized at higher temperatures (>600˚C) [20,30]. The reduction in the band-gap is proposed to be due to

the surface modification of TiO_2 via Ca_xMnO_y. The surface modification occurs via the formation of Ti-O-Mn bonds at the interface. XPS and TEM measurements support this hypothesis. The optical absorption of Ca_xMnO_y-TiO_2 and TiO_2 were measured from the valence band XPS and UV-Vis spectra. Ca_xMnO_y- TiO_2 showed a band energy of 2.9 eV, to be compared to 2.6 eV for pure TiO_2. The slight extension of the optical absorption may be attributed to the reduction in the effective band-gap.

Sayilgan et al. reported that manganese oxide facilitates the excited electron transfer to the surface and therefore reduces the chances of the recombination of photogenerated electron-hole [45]. Ca_xMnO_y enhances the photocatalytic efficiency by acting as an electron acceptor to capture the electrons from TiO_2 conduction band. This reduces the recombination efficiency of the photogenerated change carriers. The photogenerated change carriers reach to the surface for the generation of more reactive oxygen species which in turn can enhance the photocatalytic degradation of the pollutants. When photons of energy greater than the band-gap irradiate on semiconductor material, electron/hole pairs are generated. In this investigation, the surface modification of TiO_2 by Ca_xMnO_y results in enhanced photocatalytic activity due to two reasons. First, the separation of the photogenerated charges at the heterojunction. As shown in Fig. 3.15, the photogenerated electrons in titania conduction band transfers to the conduction band of Ca_xMnO_y, as it is at lower potential which makes the process thermodynamically favourable. Under these circumstances, the holes in the valence band of TiO_2 will generate $HO^{\bullet}$ by oxidation of water and the e^- in the conduction band of Ca_xMnO_y will generate $O_2^{\bullet-}$ by reduction of O_2. Two pathways will be open, one, based on $HO^{\bullet}$, faster, leading to highly hydroxylated compounds, and the other one, slower, based on $O_2^{\bullet-}$ and leading first less hydroxylated compounds. This agrees with the observed products. The second reason is the reduction in the effective band-gap. As Ca_xMnO_y has band gap in the visible region (2.4 eV, which corresponds to 516 nm), it generates electron hole pairs, giving the visible activity which is a fraction of the UV photocatalytic activity.

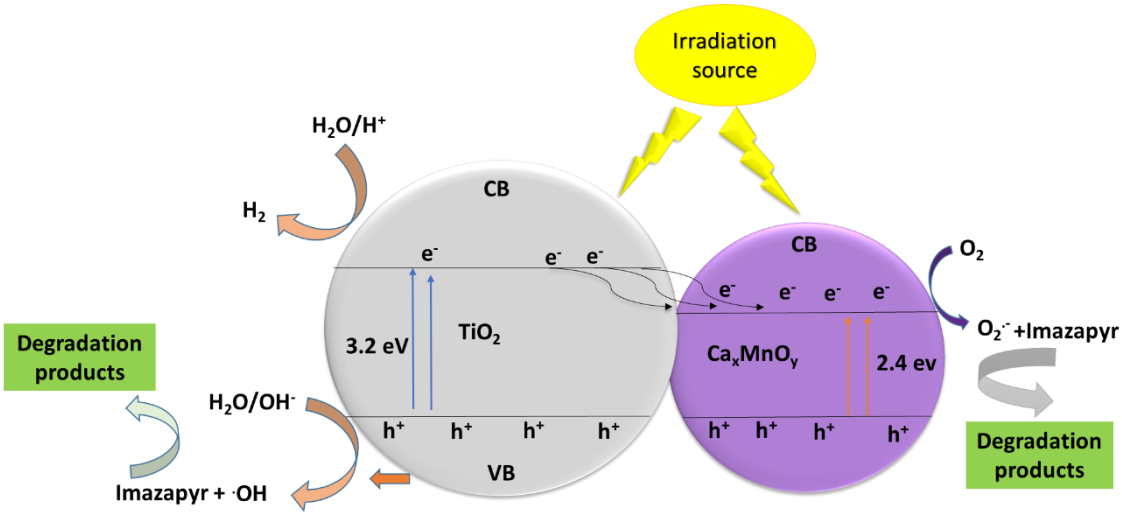

Figure 3.15. Possible mechanism for the enhancement in the photocatalytic activity of TiO_2 by Ca_xMnO_y modification.

3.4. Conclusion

Ca_xMnO_y-TiO_2 heterostructures were prepared by the synthesis of birnessite by chemical co-precipitation method and subsequent mixing with commercial titanium dioxide by grinding, followed by annealing. As a result, Ca_xMnO_y layers are proposed to be encapsulating the TiO_2 particles. Ca_xMnO_y contributed towards the enhancement of the photocatalytic activity of Ca_xMnO_y-TiO_2 by three ways: extending the photon absorption into the visible range by band-gap narrowing (only slightly), possibly improving charge transfer and lowering recombination of charge carriers, and by altering intermediate adsorption and degradation. The main intermediate products of photodegradation process of imazapyr were examined. In the Ca_xMnO_y-TiO_2 system, the concentration of intermediates continuously increased with irradiation time, to achieve a maximum at 180 min of irradiation, and decreased by more than half in the following hours, whereas intermediates did not decompose in the case of the TiO_2 system. The enhanced photocatalytic activity was ascribed to the Ca_xMnO_y surface modification which adsorbs pollutant/intermediates with higher efficiency which improve their photocatalytic decomposition rate.

Acknowledgements.

JAB, PS, MEA and SB would like to acknowledge financial support from British Council under STREAM-MINA Institutional Links Scheme (Grant number 278072873). MC acknowledges support from *Ministerio de Economía y Competitividad* (Spain) through project CTQ2015-71238-R (MINECO/FEDER).

References

[1] H. Fu, S. Zhang, T. Xu, Y. Zhu, J. Chen, Photocatalytic Degradation of RhB by Fluorinated Bi $_2$ WO $_6$ and Distributions of the Intermediate Products, Environ. Sci. Technol. 42 (2008) 2085–2091. doi:10.1021/es702495w.

[2] A. Di Corcia, C. Crescenzi, E. Guerriero, R. Samperi, Ultratrace determination of atrazine and its six major degradation products in water by solid-phase extraction and liquid chromatography- electrospray/mass spectrometry, Environ. Sci. Technol. 31 (1997) 1658–1663. doi:10.1021/es960494t.

[3] P. Pizarro, C. Guillard, N. Perol, J.M. Herrmann, Photocatalytic degradation of imazapyr in water: Comparison of activities of different supported and unsupported TiO2-based catalysts, Catal. Today. 101 (2005) 211–218. doi:10.1016/j.cattod.2005.03.008.

[4] C. Martínez, S. Vilariño, M.I. Fernández, J. Faria, M.L. Canle, J.A. Santaballa, Mechanism of degradation of ketoprofen by heterogeneous photocatalysis in aqueous solution, Appl. Catal. B Environ. 142–143 (2013) 633–646. doi:10.1016/j.apcatb.2013.05.018.

[5] M. Maicu, M.C. Hidalgo, J.A. Navı, Cu-doped TiO 2 systems with improved photocatalytic activity, 67 (2006) 41–51. doi:10.1016/j.apcatb.2006.03.019.

[6] J. Xue, S. Ma, Y. Zhou, Z. Zhang, M. He, Facile photochemical synthesis of Au / Pt / g-C3N4 with plasmon- enhanced photocatalytic activity for antibiotic degradation Facile Photochemical Synthesis of Au / Pt / g-C 3 N 4 with Plasmon-Enhanced Photocatalytic Activity for Antibiotic Degradation, (2015). doi:10.1021/acsami.5b01212.

[7] E. Quivet, R. Faure, J. Georges, J.O. Païssé, B. Herbreteau, Kinetic studies of imazapyr photolysis and characterization of the main photoproducts, Toxicol. Environ. Chem. 86 (2004) 195–204. doi:10.1080/02772240400007054.

[8] H. Liu, W. Guo, Y. Li, S. He, C. He, Photocatalytic degradation of sixteen organic dyes by TiO2/WO3-coated magnetic nanoparticles under simulated visible light and solar light, J. Environ. Chem. Eng. 6 (2018) 59–67. doi:10.1016/j.jece.2017.11.063.

[9] M.M. Haque, D. Bahnemann, M. Muneer, Photocatalytic Degradation of Organic Pollutants : Mechanisms and Kinetics, Photocatalytic Degrad. Org. Pollut. Mech. Kinet. 3 (2012) 294–326. doi:10.5772/1381.

[10] C. Anderson, A.J. Bard, Improved Photocatalytic Activity and Characterization of Mixed TiO2/SiO2 and TiO2/Al2O3 Materials, J. Phys. Chem. B. 101 (1997) 2611–2616. doi:10.1021/jp9626982.

[11] I. Konstantinou, V. Sakkas, T. Albanis, Photocatalytic degradation of the herbicides propanil and molinate over aqueous TiO2 suspensions: identification of intermediates and the reaction pathway, Appl. Catal. B. 34 (2001) 227–239. http://linkinghub.elsevier.com/retrieve/pii/S0926337301002181.

[12] D.A. Links, C. E. Frey, M. Wiechen, P. Kurz, Water-oxidation catalysis by synthetic manganese oxides systematic variations of the calcium birnessite theme, 43(2014) 4370, Catal. Sci. Technol. (2012) 2–5. doi:10.1039/c2cy20399e.

[13] N.C.T. Martins, J. Ângelo, A.V. Girão, T. Trindade, L. Andrade, A. Mendes, N-doped carbon quantum dots/TiO2composite with improved photocatalytic activity, Appl. Catal. B Environ. 193 (2016) 67–74. doi:10.1016/j.apcatb.2016.04.016.

[14] H. Dong, G. Zeng, L. Tang, C. Fan, C. Zhang, X. He, Y. He, An overview on limitations of TiO2-based particles for photocatalytic degradation of organic pollutants and the corresponding countermeasures, Water Res. 79 (2015) 128–146. doi:10.1016/j.watres.2015.04.038.

[15] X. Shen, L. Zhu, G. Liu, H. Yu, H. Tang, Enhanced photocatalytic degradation and selective removal of nitrophenols by using surface molecular imprinted Titania, Environ. Sci. Technol. 42 (2008) 1687–1692. doi:10.1021/es071788p.

[16] B.A. Pinaud, Z. Chen, D.N. Abram, T.F. Jaramillo, Thin films of sodium birnessite-type MnO2: Optical properties, electronic band structure, and solar photoelectrochemistry, J. Phys. Chem. C. 115 (2011) 11830–11838. doi:10.1021/jp200015p.

[17] S. Kalathil, M.M. Khan, S.A. Ansari, J. Lee, M.H. Cho, Band gap narrowing of titanium dioxide (TiO2) nanocrystals by electrochemically active biofilms and their visible light activity, Nanoscale. 5 (2013) 6323. doi:10.1039/c3nr01280h.

[18] S. Bougarrani, K. Skadell, R. Arndt, M. El Azzouzi, R. Gläser, Novel Ca x MnO y /TiO 2 Composites for Efficient Photocatalytic Degradation of Methylene Blue and the Herbicide Imazapyr in Aqueous Solution under Visible Light Irradiation, J. Environ. Chem. Eng. (2018). doi:10.1016/j.jece.2018.02.026.

[19] P. Paudel, A. Negusse, D.P. Jaisi, Birnessite-Catalyzed Degradation of Glyphosate:A Mechanistic Study Aided by Kinetics Batch Studies and NMR Spectroscopy, Soil Sci. Soc. Am. J. 79 (2015) 815. doi:10.2136/sssaj2014.10.0394.

[20] L.G. Devi, N. Kottam, S.G. Kumar, Preparation and characterization of Mn-doped titanates with a bicrystalline framework: Correlation of the crystallite size with the synergistic effect on the photocatalytic activity, J. Phys. Chem. C. 113 (2009) 15593–15601. doi:10.1021/jp903711a.

[21] R. Munter, Advanced Oxidation Processes - Current Status and Prospect, Proc. Est. Acad. Sci. Chem. 50 (2001) 59–80. doi:10.1002/9780470561331.ch18.

[22] K.P. Lucht, J.L. Mendoza-Cortes, Birnessite: A Layered Manganese Oxide to Capture Sunlight for Water-Splitting Catalysis, J. Phys. Chem. C. 119 (2015) 22838–22846. doi:10.1021/acs.jpcc.5b07860.

[23] J.E. Post, Manganese oxide minerals: Crystal structures and economic and environmental significance, Proc. Natl. Acad. Sci. 96 (1999) 3447–3454. doi:10.1073/pnas.96.7.3447.

[24] C.E. Frey, M. Wiechen, P. Kurz, Water-oxidation catalysis by synthetic manganese oxides – systematic variations of the calcium birnessite theme, Dalt. Trans. 43 (2014) 4370–4379. doi:10.1039/C3DT52604F.

[25] S. Bougarrani, K. Skadell, R. Arndt, M. El Azzouzi, R. Gläser, Novel CaxMnOy/TiO2composites for efficient photocatalytic degradation of methylene blue and the herbicide imazapyr in aqueous solution under visible light irradiation, J. Environ. Chem. Eng. 6 (2018) 1934–1942. doi:10.1016/j.jece.2018.02.026.

[26] P.S.M. Dunlop, A. Galdi, T.A. McMurray, J.W.J. Hamilton, L. Rizzo, J.A. Byrne, Comparison of photocatalytic activities of commercial titanium dioxide powders immobilised on glass substratMuaes, J. Adv. Oxid. Technol. 13 (2010) 99–106. doi:10.1515/jaots-2010-0113.

[27] X. Xu, X. Zhou, X. Li, F. Yang, B. Jin, T. Xu, G. Li, M. Li, Electrodeposition synthesis of MnO2/TiO2nanotube arrays nanocomposites and their visible light photocatalytic activity, Mater. Res. Bull. 59 (2014) 32–36. doi:10.1016/j.materresbull.2014.06.025.

[28] K. Thamaphat, P. Limsuwan, B. Ngotawornchai, Phase Characterization of TiO2 Powder by XRD and TEM\n, Nat. Sci. 42 (2008) 357–361.

[29] B. Li, G. Gao, D. Zhai, C. Wei, Y. He, H. Du, F. Kang, Synthesis, characterization and electrochemical performance of manganese dioxide in a quaternary microemulsion: The role of the co-surfactant and water, Int. J. Electrochem. Sci. 8 (2013) 8740–8751.

[30] C. Byrne, G. Subramanian, S.C. Pillai, Recent advances in photocatalysis for environmental applications, J. Environ. Chem. Eng. (2017). doi:10.1016/j.jece.2017.07.080.

[31] J.E.P. David R. Veblen, Crystal structure determinations of synthetic sodium, magnesium, and potassium birnessite using TEM and the Rietveld method, Am. Mineral. 75 (1990) 477–489.

[32] F. V. Chukhrov, B.A. Sakharov, A.I. Gorshkov, V.A. Drits, Y.P. Dikov, Crystal Structure of Birnessite from the Pacific Ocean, Int. Geol. Rev. 27 (1985) 1082–1088.

doi:10.1080/00206818509466485.

[33] Q. Jin, H. Arimoto, M. Fujishima, H. Tada, Manganese Oxide-Surface Modified Titanium(IV) Dioxide as Environmental Catalyst, Catalysts. 3 (2013) 444–454. doi:10.3390/catal3020444.

[34] Y.-K. Hsu, Y.-C. Chen, Y.-G. Lin, L.-C. Chen, K.-H. Chen, Birnessite-type manganese oxides nanosheets with hole acceptor assisted photoelectrochemical activity in response to visible light, J. Mater. Chem. 22 (2012) 2733–2739. doi:10.1039/C1JM14355G.

[35] P. V Kamat, Manipulation of Charge Transfer Across Semiconductor Interface.pdf, J. Phys. Chem. Lett. 3 (2012) 663–672.

[36] X.-J. Wen, C.-G. Niu, L. Zhang, G.-M. Zeng, Novel p–n heterojunction BiOI/CeO $_2$ photocatalyst for wider spectrum visible-light photocatalytic degradation of refractory pollutants, Dalt. Trans. 46 (2017) 4982–4993. doi:10.1039/C7DT00106A.

[37] M.M. Khan, S.A. Ansari, D. Pradhan, M.O. Ansari, D.H. Han, J. Lee, M.H. Cho, Band gap engineered TiO $_2$ nanoparticles for visible light induced photoelectrochemical and photocatalytic studies, J. Mater. Chem. A. 2 (2014) 637–644. doi:10.1039/C3TA14052K.

[38] Khan; M.M.; Ansari; S.A.; Amal; M.I.; Lee; J. and Cho; M.H., Highly visible light active Ag@ TiO 2 nanocomposites synthesized using an electrochemically active biofilm: a novel biogenic approach, Nanoscale. 10 (2013) 4427–4435.

[39] E. Mugunthan, M.B. Saidutta, P.E. Jagadeeshbabu, Photocatalytic degradation of diclofenac using TiO<inf>2</inf>–SnO<inf>2</inf>mixed oxide catalysts, Environ. Technol. (United Kingdom). 3330 (2017). doi:10.1080/09593330.2017.1411398.

[40] D.L. Liao, C.A. Badour, B.Q. Liao, Preparation of nanosized TiO2/ZnO composite catalyst and its photocatalytic activity for degradation of methyl orange, J. Photochem. Photobiol. A Chem. 194 (2008) 11–19. doi:10.1016/j.jphotochem.2007.07.008.

[41] H. Li, D. Wang, H. Fan, T. Jiang, X. Li, T. Xie, Synthesis of ordered multivalent Mn-TiO2 nanospheres with tunable size: A high performance visible-light photocatalyst, Nano Res. 4 (2011) 460–469. doi:10.1007/s12274-011-0102-4.

[42] M. Pelaez, N.T. Nolan, S.C. Pillai, M.K. Seery, P. Falaras, A.G. Kontos, P.S.M. Dunlop, J.W.J. Hamilton, J.A. Byrne, K. O'Shea, M.H. Entezari, D.D. Dionysiou, A review on the visible light active titanium dioxide photocatalysts for environmental applications, Appl. Catal. B Environ. 125 (2012) 331–349. doi:10.1016/j.apcatb.2012.05.036.

[43] M.F. Atitar, R. Dillert, D.W. Bahnemann, Surface Interactions between Imazapyr and the TiO2Surface: An in Situ ATR-FTIR Study, J. Phys. Chem. C. 121 (2017) 4293–4303. doi:10.1021/acs.jpcc.6b11673.

[44] M. Carrier, N. Perol, J.M. Herrmann, C. Bordes, S. Horikoshi, J.O. Paisse, R. Baudot, C. Guillard, Kinetics and reactional pathway of Imazapyr photocatalytic degradation Influence of pH and metallic ions, Appl. Catal. B Environ. 65 (2006) 11–20. doi:10.1016/j.apcatb.2005.11.014.

[45] E. Sayilgan, T. Kukrer, N.O. Yigit, G. Civelekoglu, M. Kitis, Acidic leaching and precipitation of zinc and manganese from spent battery powders using various reductants, J. Hazard. Mater. 173 (2010) 137–143. doi:10.1016/j.jhazmat.2009.08.063.

Chapter 4: Aqueous Imazapyr Degradation by Ozonation, Photocatalysis, and Photocatalyzed ozonation by Ca_xMnO_y-TiO_2 Composite

Salma Bougarrani[a,*], Lahbib Latrach[b], Laila El Azzouzi[a], Asmae Bouziani [a],

Salma Chhaiba[c], Abdul J. Chaudhary[d], Mohammed El Azzouzi[a]

[a] Laboratory of Spectroscopy, Molecular Modeling, Materials, Nanomaterials, Water and Environment (LS3MN2E), Faculty of Sciences, University Med V , Avenue Ibn Battouta, BP 1014, Agdal, Rabat, Morocco

[b] Faculty of Sciences Semlalia, Cadi Ayyad University, PO Box: 2390, Marrakech, Morocco.

[C] Laboratory of Applied Solid Chemistry, Faculty of Science, Mohammed V University, Rabat, Morocco

[d] Institute Institute of the Environment, Health and Societies, College of Healtth and Life Science Brunel University ,London

Corresponding author:

Salma Bougarrani, Laboratory of Spectroscopy, Molecular Modeling, Materials,

Nanomaterials, Water and Environment, Med V University, BP 1014, Agdal, Rabat, Morocco

Tel: +212660425050; Fax: +212 537 774 261

ORCID: 0000-0003-3085-9556

E-mail:salma.bougarrani@gmail.com

Graphical abstract

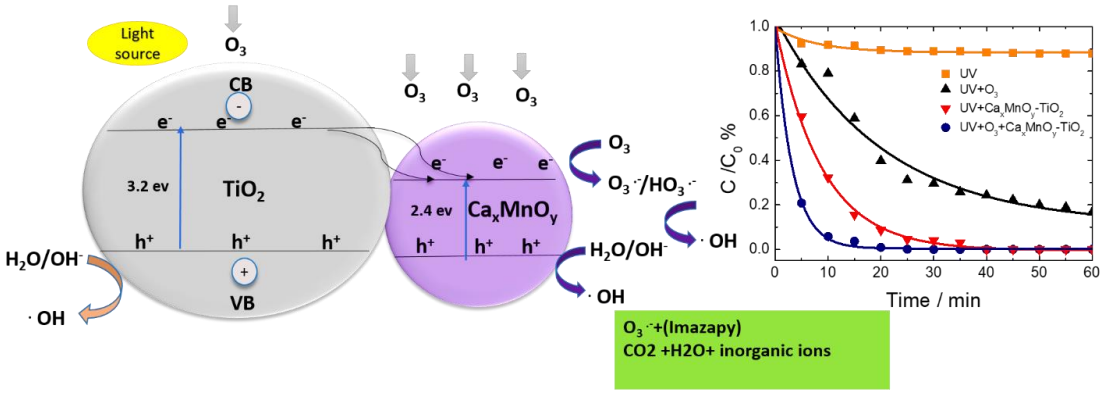

Organics oxidation mechanism of Imazapyr and the generation pathways of hydroxyl radicals in Photocatalyzed ozonation by Ca_xMnO_y-TiO_2 Composite

Abstract

Aqueous imazapyr degradation by ozonation, photocatalysis, and photocatalyzed ozonation by Ca_xMnO_y-TiO_2 composite has been investigated in this paper. The kinetics of the photocatalytic degradation of imazapyr were analysed taking into account the effect of the pH, the Ca_xMnO_y-TiO_2 mass concentration as well as imazapyr concentration. The results of this study show that imazapyr removal followed a first-order kinetic model with a rate constant of 0.547 min^{-1} and 0.425 min^{-1} for photocatalytic ozonation and heterogeneous photocatalysis respectively, while second-order kinetic for ozonation process with a rate constant of 0.053 $mol.L^{-1}.min^{-1}$ at pH 7.Complete degradation of imazapyr was achieved within 10 min using photocatalytic ozonation for 5µM of imazapyr in the presence of 100 $mg.L^{-1}$ of Ca_xMnO_y-TiO_2 composite at pH 7. The high constant rate exhibited by Ca_xMnO_y-TiO_2 in the presence of ozone may be explained considering the high hydroxyl surface population of this sample supported by the fact that the deposition of the porous manganese oxide mainly on the surface of titanium dioxide that can easily accommodate the hydroxyl groups. Furthermore, it was also considered that the dissolved ozone was easy to accept electrons generated on the surface of Ca_xMnO_y-TiO_2 so that the recombination of the positive hole and negative electron pairs was hindered, ultimately a large number of radicals formed. The results obtained also confirmed that more than 95% degradation of photoproducts of imazapyr, in the presence of Ca_xMnO_y-TiO_2, was also achieved, indicating the complete mineralization of imazapyr photoproducts.

Keywords: Ca_xMnO_y-TiO_2 composite; Degradation; Imazapyr herbicide; Ozonation; Photocatalytic ozonation; Wastewater

4.1. Introduction

Pesticides constitute one of the most widespread types of contaminants found in stream water and soils.[1] Imazapyr, 2-(4-methyl-5-oxo-4-propan-2-yl-1H-imidazol-2-yl) pyridine-3-carboxylic acid, being a hetero aromatic molecule, is a non-selective herbicide which belongs to the imadazolinone family.[2] Imazapyr a non-biodegradable pesticide widely used both in agriculture and horticulture farming is a persistent herbicide, with a half-life varying from 21 days to 49 months, and a high mobility in soils. [3]Therefore, it is likely suspected to contaminate soil and groundwater. [4]

Regarding the potential health risks associated with exposure to these chemicals by consumption of contaminated water, different management and treatment methods must be applied to reduce the concentration of these emerging contaminants.[5] Traditional physical techniques such as adsorption, coagulation, flocculation, sedimentation, bio-filtration and gas stripping, [6] have been considered to be among the available technologies for wastewater treatment, but there are many pollutants that are persistent to these processes. Thus, many efforts are currently focused on developing new technologies for not only wastewater treatment but also production of drinking water.(Bai *et al.*, 2014 ;Aba-Guevara *et al.*, 2017)

Advanced oxidation processes (AOPs) have been considered as promising technologies to remove pesticides from water, including Fenton-like oxidation and ozonation. A propitious way to achieve mineralization of organic pesticides is by the combination of different advanced oxidation processes (AOPs), such as photo-catalyzed ozonation.

Many researchers have proved that O_3 is a powerful oxidizing with an extreme reduction potential, which therefore reacts with various organic pollutants, however, ozone has a relatively low solubility, stability, and selectively in water.[9] Ozone reacts with organic compounds at acidic pH, and in many cases does not completely mineralize certain organic substances.[10] These disadvantages make the application of ozone alone to treat polluted water economically and technically undesirable.

In the ozonation approach, the catalyst activity depends on the absorbance of ozone on the surface.[11] Ozone adsorption on the surface of the catalyst is important, as it can be converted to •OH, which is ascribed to decomposition of the O_3 molecules. O_3 decomposition occurs in various types of active centers. Hence, the acidic and basic nature of the surface plays a crucial role in the process.[12]

Recently, alternative ozonation processes catalyzed by transition metals have been investigated for degradation of organics. Numerous metals (Fe, Mn, Ni, Co, Zn, Ag, Cr) under various forms

(salt of reduced metal, solid oxide, deposited metal on support) were reported to enhance the efficiency of ozone towards the removal,[13] or the conversion of different organic compounds in aqueous solution.(Contreras *et al.*, 2002;Wang and Osterloh, 2014)

Furthermore, many researchers proved that the application of ozone combined by MnO_2 was a promising technique for the treatment of wastewater at natural values of pH.[16] The Mn(II) has been used as catalyst in the ozonation of same pollutants as atrazine, simazine and oxalic acid.[17] The role of Mn(II) in the oxalic acid at pH 4 is to interact with ozone to generate Mn(III) or Mn(IV) simultaneously with $^{\bullet}OH^{-}$ radicals which can also act as oxidant agents.[18] The authors proposed an interaction between oxalic acid and the surface of Mn(III) species leading to Mn(II) and CO_2.

Recently [19], have investigated the degradation of imazapyr onto the novel Ca_xMnO_y/TiO_2 composite. The authors have concluded that 5 % Ca_xMnO_y-TiO_2 composite possesses excellent photocatalytic performance due to the enhanced visible light absorption and efficient charge separation of TiO_2 by Ca_xMnO_y surface modification. In spite of the promising results using manganese dioxide as a catalyst, only few studies have been published, and therefore, more detailed studies are required.

The aim of this work is to study for the first time the performance of the combination of ozone and Ca_xMnO_y/TiO_2 composite on the photodegradation of imazapyr, to compare this technology with several different AOPs: photolysis, heterogeneous photocatalysis and ozonation processes and to analyse the degradation products as function of time under varied conditions. The kinetics of the photocatalytic degradation of imazapyr were analysed taking into account the effect of the pH, the amount of catalyst, irradiation time and initial imazapyr concentration.

4.2. Material and Methods

4.2.1. Material

Ca_xMnO_y-TiO_2 composite were synthesized by using a method developed by Bougarrani et al., [19]. The method is based on the precipitation of birnessite and co-precipitation with calcium chloride dehydrate, then mixed with 95% of commercial titanium dioxide TiO_2 by mechanical grinding. Imazapyr herbicide, (95%) was purchased from American Cyanamid Company and used without further purification; chemical structure of imazapyr herbicide is shown in (Figure 4.1).The other chemicals used in the experiments were purchased from Riedel-de Hahn AG. They were all of analytical grade and used without further purification. All solutions were prepared using Milli-Q water at room temperature collected from Milli-Q apparatus, (Millipore,

Bedford).Analytical grade organic solvents were used for high performance liquid chromatography (HPLC).

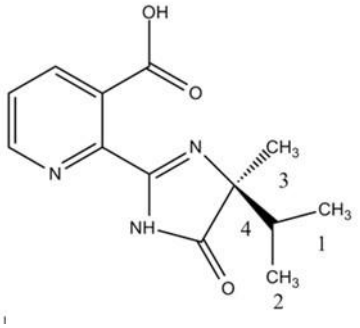

Figure 4.1. Chemical structure of imazapyr herbicide

4.2.2. Methods

The degradation of imazapyr was followed using Hitachi HPLC system equipped with a UV detector. The flow rate was 0.5 mL/min and the injection volume was fixed at 50 µL. The eluent was a mixture of 40% acetonitrile (ACN) and 60% Milli-Q water at pH=3.4 (pH adjusted by adding formic acid), isocratic elution at a flow rate 1 ml/min. Samples from reaction solutions were injected without any further dilution. The concentration of aqueous ozone was determined by Spectrometric method indigo trisulfonate. The change in the absorption value of the indigo was monitored by using Shimadzu UV-160A UV-Vis Spectrophotometer at 600 nm.

4.2.3. Catalyst characterization

Surface morphology and chemical composition was carried out using scanning electron microscopy (SEM-EDX, CamSacn CS44, E-O-GmbH). Powder X-ray diffraction (XRD) patterns of the sample were obtained using an X-ray diffractometer (Rigaku- Dmax 2500) with monochromatized Cu Ka radiation (= 0.15405 nm, 40 kV, 100 mA). Absorption spectra were recorded from 250 nm to 800 nm range with Lambda 650 UV-VIS spectrophotometer at normal incidence. By-products analysis was carried out using a mass spectrometry coupled to electrospray ionization system (ESI) for a qualitative and quantitative analysis. MS analysis was performed on Bruker Esquire 3000 plus mass spectrometer equipped with an ESI interface and an ion trap (Bruker- Daltonics Analytik GmbH Bremen, Germany). The ESI probe tip and capillary potentials were set at 2.5 kV and 25 V, respectively.

4.2.4. Photocatalytic experiments

In a typical reaction, 100 mg.L^{-1} of Ca_xMnO_y-TiO_2 composite were added to 500 mL of 5 µM of imazapyr solution in a double walled cylindrical photo-reactor (shown in Figure 4.2). Then the solution was exposed to ultrasonic treatment for 2 minutes in order to suspend the catalyst. Immediately afterwards, the stirring was started and maintained over 1h in the dark to ensure the adsorption equilibrium between the solution and the catalyst particles.

The irradiation experiments were carried out under light generated by a medium pressure mercury lamp at 150W in a Duran cell ($\lambda > 300$ nm), placed inside the reactor. Additionally, a cooling water system was set up to prevent overheating of the lamp and of the solution. Every 5 minutes, samples were taken using a syringe of 2 mL, and filtered for 2 times in order to remove all the catalyst.

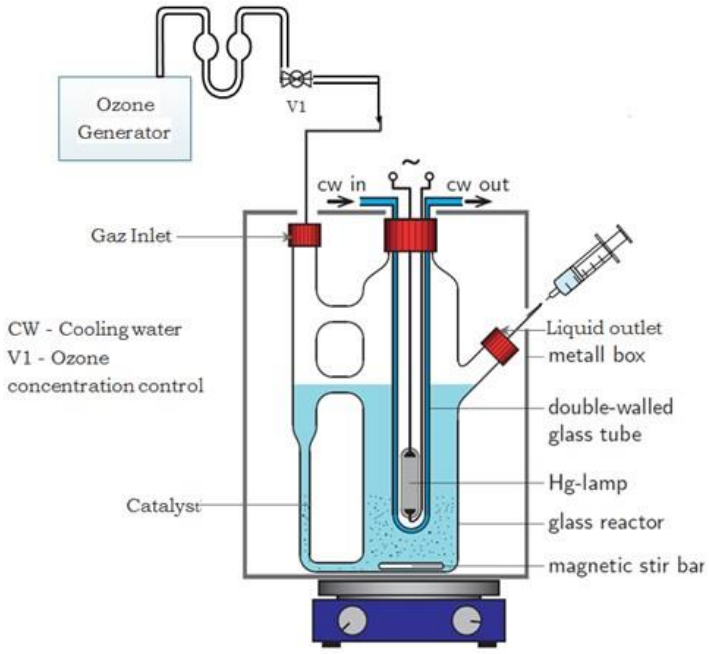

Figure 4.2. Scheme of photocatalytic ozonation reactor used for imazapyr degradation.

4.2.4.1. Photolysis experiment

The same experimental set up was used as in the previous section but without the addition of Ca_xMnO_y-TiO_2 composite suspension.

4.2.4.2. Ozonation experiment

The ozone treatment was carried out by using a generator with a production capacity of about 200 mg/h of ozone gas produced from air and injected into the sample. The input power was AC220V/50Hz and the pump output was 2-3 L/min. The ozone concentration of about 10 $mg.L^{-1}$ was used for the experiment by regulating the gas flow rate. The concentration of ozone was analysed using an ozone analyzer (The amount of ozone was estimated by volumetric method trapping it in KI solution and titrating the liberated iodine using standard thiosulfate solution with starch as indicator). Flow rates and ozone concentrations were calibrated and highly reproducible. All the experiments were conducted in a semi-batch reactor with continuous flow of ozone. Thus, steady-state concentration of ozone is maintained. Parameters were checked in duplicate runs, prior to and after each of the experiments. The same procedure was adopted in dark for experiment control.

4.2.4.3. Photocatalytic ozonation experiment

The imazapyr degradation experiments were carried out in a simple photocatalyzed ozonation reactor as presented in Figure 4.2 with same procedures reported below but with ozonation.

4.3. Results and discussion

4.3.1. Characterisation of Ca_xMnO_y-TiO_2

Figure 4.3 shows XRD diffraction patterns for birnessite, manganese (III) oxide (Mn_2O_3), and Ca_xMnO_y-TiO_2 composite. XRD patterns of Ca_xMnO_y-TiO_2 composite exhibit strong diffraction peaks at 25° from the (101) plane and 48° from the (200) plane indicating the presence of TiO_2 in the anatase phase.[20] The characteristic reflections of pure birnessite phase which should appear at about 12° and 25°are absent,[21] which might be due to the proportion of amorphous to crystalline material and the amount of birnessite/MnO_2.This result was expected, since the anatase phase presents 95 wt.-% of the composite. To confirm the Ca_xMnO_y concentration in the synthesized materials, a full elemental analysis was carried out after the synthesis. It was confirmed from the ICP analysis that the experimental ratio of Ca_xMnO_y-TiO_2 was comparable with the final products as obtained from ICP analysis Table 4.1, which suggest that the particles of manganese oxides have been deposited during the synthesis mainly on the surface of TiO_2. The SEM images of Ca_xMnO_y-TiO_2 composite and pure titanium dioxide (Figure 4.4) did not

reveal any noticeable change in the morphology and particle size of the synthesized composite as expected due to the low manganese oxide content in the materials.

Table 4.1. Chemical composition, specific surface area and total pore volume of Ca_xMnO_y-TiO_2 composite

Composite name	Chemical composition	Origin of the Chemicals	Ca /wt.%	Mn /wt.%	Ti /wt. %	O /wt.%	Ca+Mn : Ti	S_{BET} (m^2/ g)	V_{Total} (cm^3/g)
Ca_xMnO_y-TiO_2	5wt.-% Ca_xMnO_y/ 95wt.-% TiO_2	Precipitation reaction	0.99	1.90	59.3	37.86	0.04882	97.3	0.347

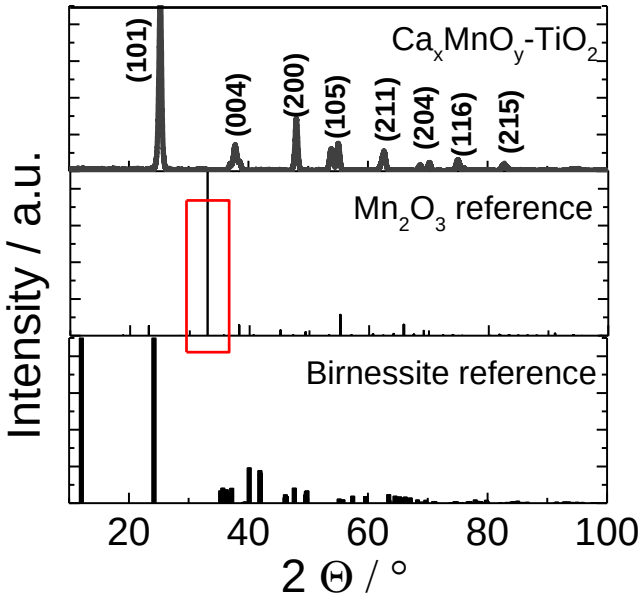

Figure 4.3. XRD-patterns of birnessite, Manganese (III) oxide Mn_2O_3, commercial titanium dioxide Hombikat UV100 (Ti), Ti-500, and Ti-5Ca0.1Mn. All the composites were annealed at 500 °C during 24 h.

To compare the band gap of the synthesized composite Ca_xMnO_y-TiO_2 and pure titanium dioxide, DR-UV-vis spectra of both materials is depicted in Figure 4.5. It is clearly seen that pure titanium dioxide shows a characteristic spectrum with a sharp absorption edge at 387 nm which is consistent with the band gap of anatase phase,[22] a band gap shifting was observed in the case of Ca_xMnO_y-TiO_2. The tangent drawn shows an absorbance maxima of 387 nm and 421 nm for the pure TiO_2 and Ca_xMnO_y-TiO_2 composite, which corresponds to a band gap of 3.18 and 2.89 eV, respectively. Indicating that e^-/h^+ pairs can be generated, even when the particle is irradiated with long wavelength-visible light.

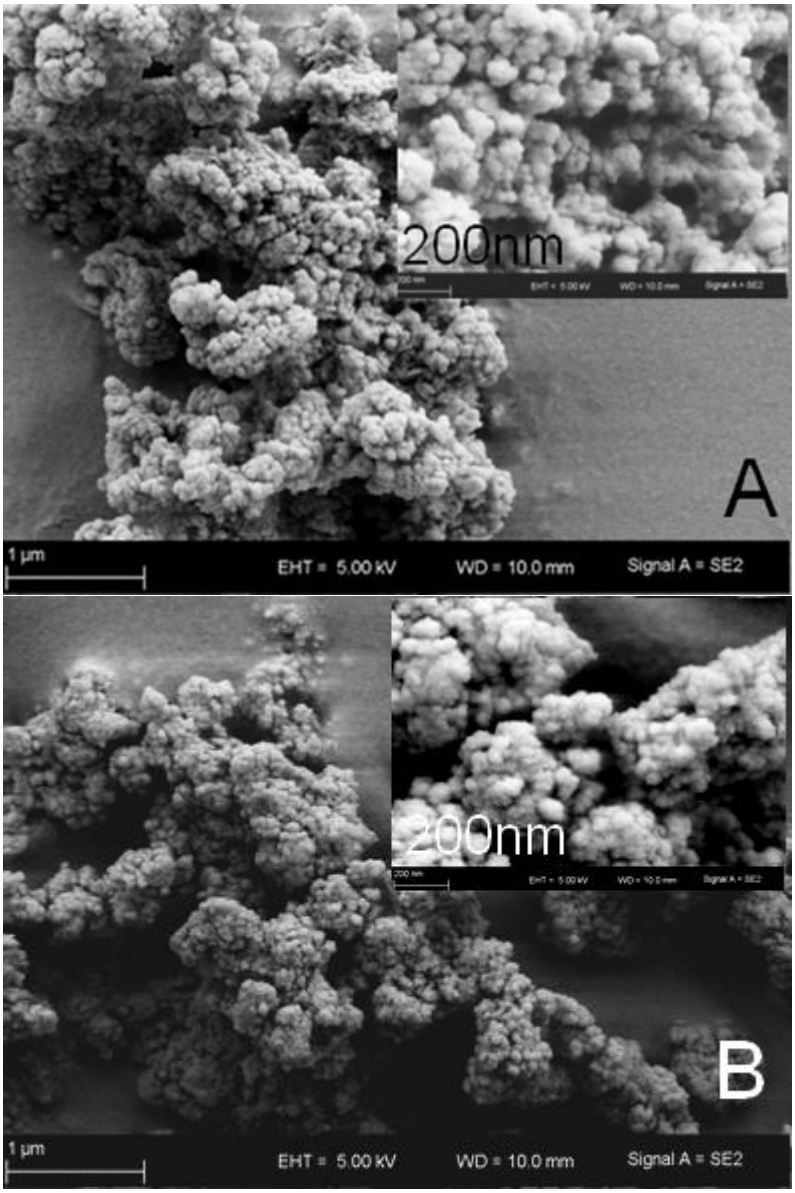

Figure 4.4. Representative SEM images of catalysts (A) TiO_2 (B) Ca_xMnO_y-TiO_2

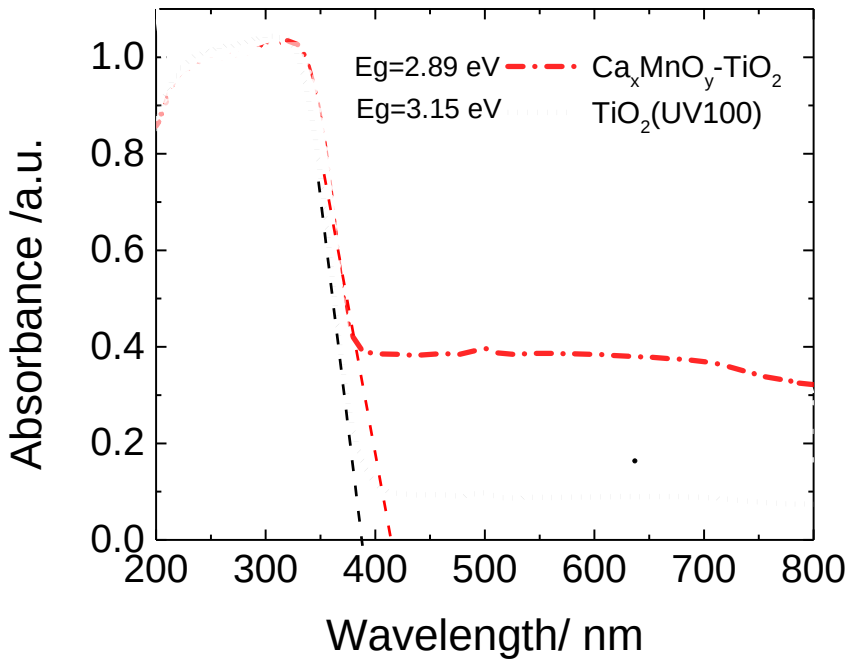

Figure 4.5. UV-vis absorption spectra of pure TiO_2 and Ca_xMnO_y-TiO_2 composite

4.3.2. Degradation of imazapyr by different AOPs

In order to compare the efficiency of photolysis (UV),dark adsorption, heterogeneous photocatalysis (Ca_xMnO_y-TiO_2/UV), Ca_xMnO_y-TiO_2/O_3, ozonation (O_3/UV), the sum of (UV+Ca_xMnO_y-TiO_2 and UV+O_3)and photocatalytic ozonation (O_3/ Ca_xMnO_y-TiO_2/UV), experiments were carried out using the same initial concentration of imazapyr, and the same amount of Ca_xMnO_y-TiO_2, at pH 7,(Figure 6a). Imazapyr was the only organic compound initially present in the aqueous solutions used in this study. The HPLC chromatograms representing imazapyr degradation after 10 min of irradiation with different oxidative chemical processes is presented in Figure 6b.

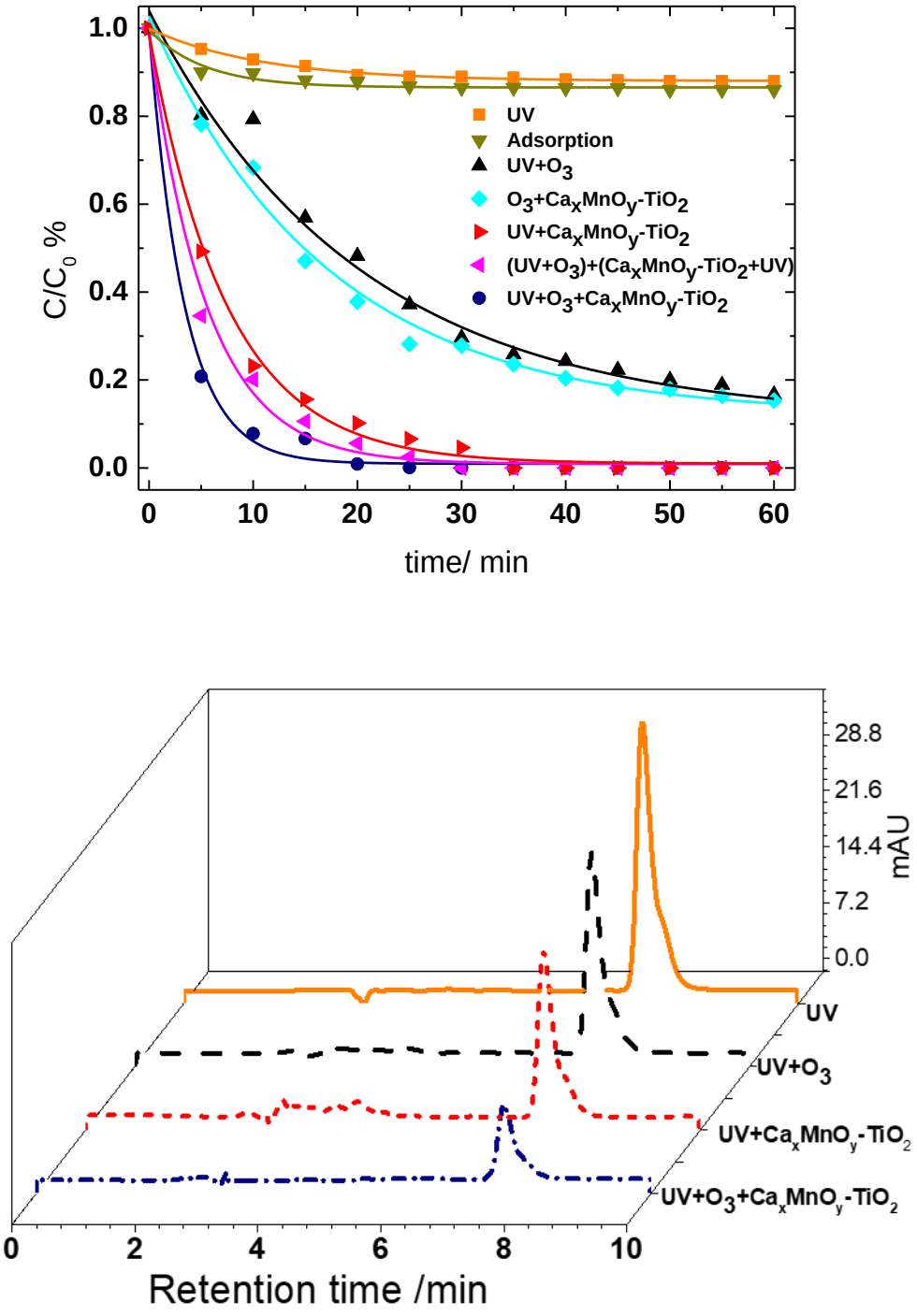

Figure 4.6. (a) Imazapyr degradation as a function of time with different oxidation methods (b) HPLC chromatograms of imazapyr degradation after 10 min of irradiation by photolysis (UV), ozonation (O_3/UV), photocatalysis (Ca_xMnO_y-TiO_2 /UV), and photocatalytic ozonation (O_3/ Ca_xMnO_y-TiO_2 /UV). C (Imazapyr)= 5 µM ; stirring speed = 1000 min-1, m TiO_2= 50 mg.

Before irradiation in the reactor, mixture of catalyst and of imazapyr was soaked in the dark for 60 min at room temperature to reach adsorption equilibrium on surface catalyst, no important adsorption effects were observed. The photolysis experiments for imazapyr were performed in reactor by a medium pressure mercury lamp at 150W. The samples were collected every hour and were analysed in HPLC. Over the 60 min irradiation, only 5% of imazapyr was degraded. The literature reports that direct photolysis is usually not an option due to the low quantum efficiency for most pesticides.[5] Imazapyr adsorption into Ca_xMnO_y-TiO_2 composite has also been investigated in this study, kinetics analysis reveals that no more than 8% of imazapyr has been adsorbed into the composite.

As expected, photocatalytic ozonation showed the highest degradation efficiency for imazapyr herbicide compared to the sum of (UV+Ca_xMnO_y-TiO_2 and UV+O_3).This behaviour could be explained by an apparent synergism between heterogeneous photocatalysis and ozonation as demonstrated in many literatures, which gives rise to an improvement of degradation efficiency. The enhanced oxidation rate mainly results from a large amount of hydroxyl radicals generated from a synergistically induced decomposition of dissolved ozone, besides superoxide ion radicals and the photo-induced holes which react more rapidly with imazapyr herbicide.

Sanchez et al.[23] combined these two methods for the removal of aniline from water and found that the decomposition rate of aniline is larger than when individually treated by either of the two methods.

The photogenerated electrons can react with the molecules of ozone generating ozonide radicals, while decreasing the possible recombination of electron hole pairs. [24]; Ajmal et al. [25] also reported similar results for the mineralisation of dibutyl phthalate, chlortetracycline and carbaryl, when photocatalytic ozonation was compared with other advanced oxidation techniques. Furthermore photocatalysis in the presence of Ca_xMnO_y-TiO_2 composite shows higher degradation of imazapyr compared to the ozonation process, and complete degradation was achieved within 40 min of irradiation. On the other hand, under ozone flow and UV irradiation, low activities were displayed, showing different fitting for experimental curves, similar activity was observed in the presence of ozone and Ca_xMnO_y-TiO_2 composite. It has been confirmed that low degradation is observed under direct ozonation, the combination of ozone and the photocatalyst improved slightly the reaction rate, resulting in more than 70% of imazapyr degradation after 40 min of irradiation.

The data shown in all presented Figures are the average values of three experiments. Standard deviations of three replicate experiments is * $p < 0.0043$.

4.3.3. Effects of parameters on the degradation of Imazapyr

4.3.3.1. Effect of Ca_xMnO_y-TiO_2 composite dose on imazapyr degradation

The effect of catalyst amount on imazapyr degradation was studied in the range 50 to 400 mg.L^{-1} under pH 7 and the results are shown in Figure 4.7. Imazapyr degradation increases to 96.0% by increasing catalyst concentration to 100 mg.L^{-1} beyond which the effect is less pronounced. Thus, 100 mg.L^{-1} of Ca_xMnO_y-TiO_2could be considered as the optimal concentration and this amount agrees well with reported results by other authors.(Carrier *et al.*, 2006; Klauson *et al.*, 2010) This improvement can be attributed to the increasing of active sites by providing more Ca_xMnO_y-TiO_2 particles, which plays the semiconductor role in the photocatalysis process. Consequently, the formation of electron-hole pairs and reactive hydroxyl radicals on the surface of semiconductor increased, which improved the oxidation of imazapyr into other intermediates. Moreover, it should be noticed that the reduction in the degradation efficiency at higher catalyst loading (more than 100 mg.L^{-1}) may be also related to increased scattering and turbidity effects, which does not allow the penetration of light into all available surface of particles. On the other hand, the agglomeration of particles results in the decrease of activated reaction sites.

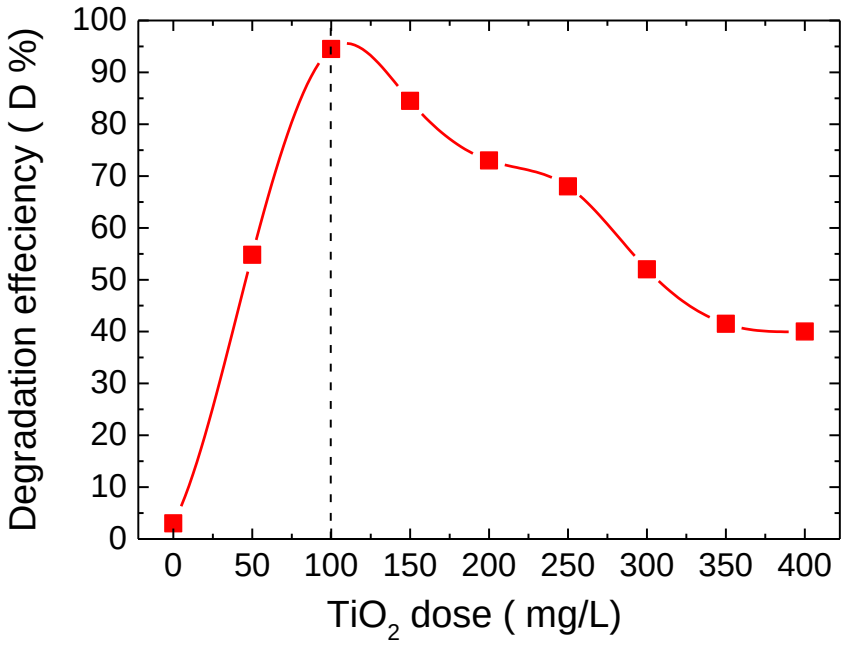

Figure 4.7. Degradation rate of imazapyr under variation of Ca_xMnO_y-TiO_2 concentration. $C_{(Imazapyr)}$= 5 µM ; stirring speed = 1000 min^{-1}, aqueous suspension Milli-Q water.

4.3.3.2. Effect of initial herbicide concentration

The pollutant concentration in water is an important factor to determinate the oxidation efficiency. The effect of the initial herbicide concentration was studied for six concentrations of imazapyr by photocatalysis, ozonation and photocatalytic ozonation. The initial herbicide concentrations were 1µM, 3 µM, 5 µM, 7 µM, 9 µM and 15 µM (0.26 $mg.L^{-1}$, 0.79 $mg.L^{-1}$, 1.31 $mg.L^{-1}$, 1.83 $mg.L^{-1}$, 2.36 $mg.L^{-1}$, 3.9 $mg.L^{-1}$ respectively).For this series of experiments, the catalyst and the ozone doses were kept constant at 100 $mg.L^{-1}$ and 10 $mg.L^{-1}$ respectively. The irradiation time was fixed at 10 min for all samples after the adsorption step under dark conditions.

Obtained results showed that removal efficiency representing the disappearance of imazapyr decreases after a certain limit, with increasing the initial concentration of imazapyr. As shown in Figure 4.8, the removal efficiency declines considerably when imazapyr concentration was up to 3 µM for ozone treatment, however, high removal efficiency was maintained until 7 µM of imazapyr concentration for photocatalytic ozonation and photocatalysis respectively, but gradually decreases with raising imazapyr concentration. A possible explanation resides in the fact that as imazapyr concentration increases, it is possible that more organic substances are deposed on the surface of Ca_xMnO_y-TiO_2, whereas less number of photons are available to reach the catalyst surface and the probability of reaction between imazapyr molecules and oxidizing species also decreases, thus resulting in less degradation percentage, the quantity of oxidation species such as ozone, hydroxyl radicals, or other species could also be considered as a limiting factor for imazapyr degradation under higher concentration of target pollutants.

However, other authors have stated that raising the initial concentration of pollutant in water led to an increased degradation percentage which was due to increased availability of pollutants for oxidative reactions with active oxidizing species,[28] either adsorbed on the photocatalyst or in the bulk solution.[29] This behavior was observed once imazapyr concentration rises from 1 to 3 µM, thus, removal efficiency increased with approximately 5% for all treatment processes.

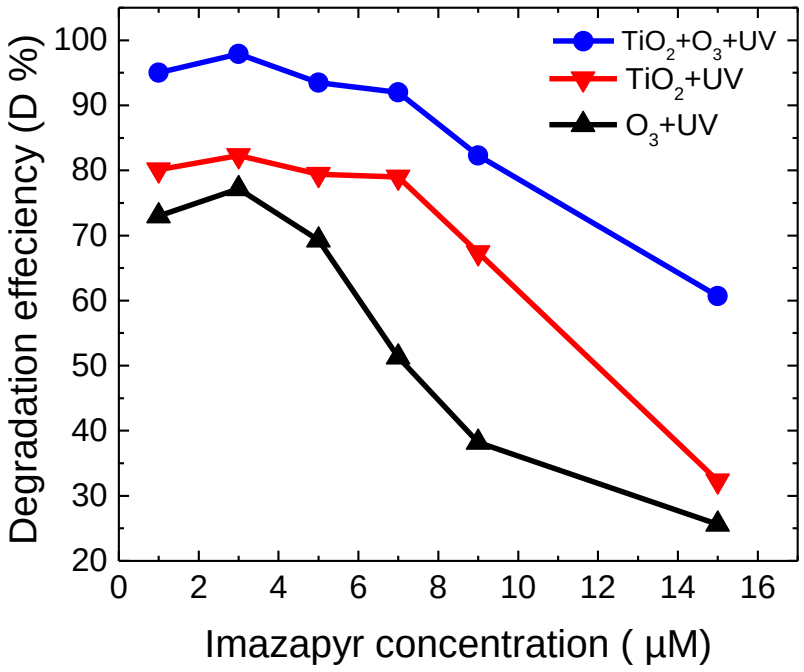

Figure 4.8. Degradation efficiency of imazapyr as a function of imazapyr concentration, mTiO_2=50 mg; stirring speed = 1000 min^{-1}, aqueous suspension Milli-Q water

4.3.3.3. Effect of pH

Taking into account that the probe molecule imazapyr exhibits five distinct species with three pK_a values (1.88, 3.60 and 10.80) (Figure 4.9) and Ca_xMnO_y-TiO_2 has a pH dependent surface charge, any interaction between the probe molecule and the photocatalyst surface can be explained assuming attractive and repulsive forces between these species. To evaluate the influence of pH on imazapyr degradation by ozonation, photocatalysis and photocatalytic ozonation, experiments were carried out at acidic pH 3, neutral pH 7 and basic pH 10.

Many authors have reported that the kinetic behavior of photocatalytic reaction can be described by a modified Langmuir–Hinshelwood model.[30] Based on the exponential decay of concentration of imazapyr, the photoactivity profile was fitted assuming a first order reaction.

$$\boldsymbol{C = C_0 exp(-k \cdot t)} \qquad (1)$$

In which *C* is the concentration of imazapyr at time *t*, C_0 is the initial concentration, and *k* is the observed rate constant.

The kinetics of imazapyr degradation onto Ca_xMnO_y-TiO_2 were studied at three different pH values. The respective concentration vs. time plots are presented in (Figure 4.10). Photodegradation of

imazapyr in the presence of Ca_xMnO_y-$TiO_2$is presented in (Figure 4.10a), the highest degradation is obtained at pH 3 with a first order rate constant of 0.425 min^{-1}, while this rate decreases with the increase of the pH from pH 3 to pH 7 and pH 10, the rates constant achieved 0.228 min^{-1}, 0.195 min^{-1} respectively.

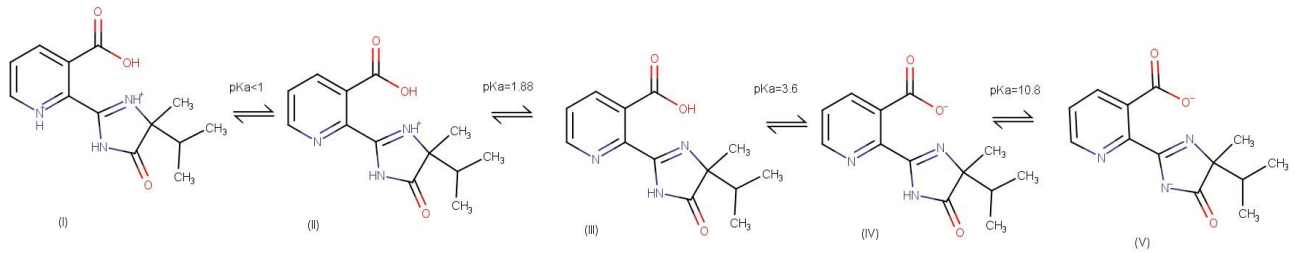

Figure 4.9. Different forms of the herbicide imazapyr and the associated acid–base dissociation constants.

The effect of pH on imazapyr degradation assisted by the Ca_xMnO_y-$TiO_2$is influenced by the acid–base equilibrium governing the surface of metal oxides in water.[19] have demonstrated in their previous work that the surface of Ca_xMnO_y-TiO_2 is positively charged at pH values below the point of zero charge (pHpzc) of the Ca_xMnO_y-TiO_2 sample, neutral at the pHpzc, and negatively charged at pH values above the pHpzc, Furthermore, the pHpzc of the used Ca_xMnO_y-$TiO_2$is reported to be in the range of 7-7.2. Imazapyr has 5 pKa's, corresponding to the formation of five different ionic species, depending on the pH of the solution different types of interactions between the probe molecule and the charged Ca_xMnO_y-TiO_2 surface are expected. (Figure 4.10),

At 1.9 < pH < 3.6 the neutral form of imazapyr (III) in (Figure 4.9), and at 3.6 < pH <pHpzc (Ca_xMnO_y-TiO_2) the negatively charged imazapyr (IV) will be the main species interacting with the positively charged Ca_xMnO_y-TiO_2 surface. The high rate constant for imazapyr degradation for pH below 7 could be explained by the strong electrostatic attraction between negative charge of imazapyr and positive charge of Ca_xMnO_y-TiO_2. On the contrary, at pHpzc (Ca_xMnO_y-TiO_2) < pH < 10.8 the negatively charged imazapyr molecule (IV) is interacting with Ca_xMnO_y-TiO_2surface which is also negatively charged, which could slow down the interactions between imazapyr and Ca_xMnO_y-TiO_2 catalyst and therefore decrease the reaction rate of imazapyr degradation.

The influence of pH on imazapyr degradation by ozonation was also investigated in this study, the decomposition of imazapyr by ozone is found to be second-order for pH 3 and pH 7 and first order for pH 10 (Figure 4.10B). In acidic pH 3 and neutral pH 7 solutions, the overall

reaction of ozone with organic compounds is second order, first order with respect to each reactant respectively (R^2=0.972 & R^2= 0.974). Therefore, the imazapyr disappearance rate equation can be expressed as follow:

$$\frac{d[imazapyr]}{dt} = k[O_3][imazapyr]$$

The overall rate constant increases significantly from 0,036 mol.L^{-1}.min^{-1} to 0.053 mol.L^{-1}.min^{-1} for pH 3 and pH 7 respectively. The results suggest that the reactions are predominated by direct oxidation of imazapyr with ozone molecules. [31] Under acidic pH, ozone molecule is main reactive species and its reactivity is very low relative to hydroxyl radical,[32] so the degradation of imazapyr is very low. As the solution becomes more basic, the rate of photocatalyzed decomposition of ozone to secondary oxidants, such as hydroxyl radicals increases. While the increase in pH facilitates the hydroxyl radical concentration, the effect of pH on the substrate reactivity is also equally vital for efficient conversion. For alkaline solutions with pH10, the hydroxyl radical reactions seem predominated over ozonation of imazapyr. Therefore, the imazapyr disappearance rate equation can be expressed as follow:

$$\frac{d[imazapyr]}{dt} = k[imazapyr]$$

The obtained results indicate that the process effectiveness increases significantly and highest conversion was recorded at pH10 with a first order rate constant of 0.140 min^{-1} (R^2=0,993).

In a review of literature on the kinetics of the reaction of ozone with organic compounds, the most common observation is the reported disagreement among different researchers as the order of the decomposition,[33] furthermore, although it's generally agreed that pesticide degradation may be described by a first-order reaction for alkaline solution and second order for acidic ones.[11]

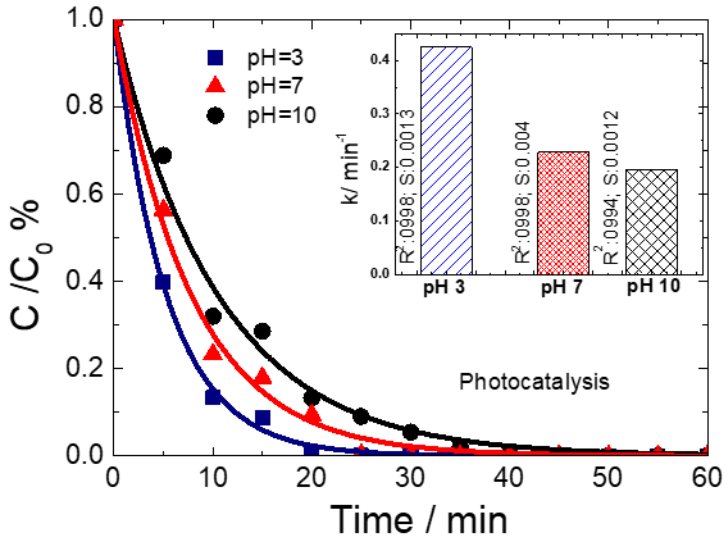
pH=3
pH=7
pH=10
C /C0 %
Time / min
Photocatalysis
k/ min-1
R2:0998; S:0.0013
R2:0998; S:0.004
R2:0994; S:0.0012
pH 3
pH 7
pH 10

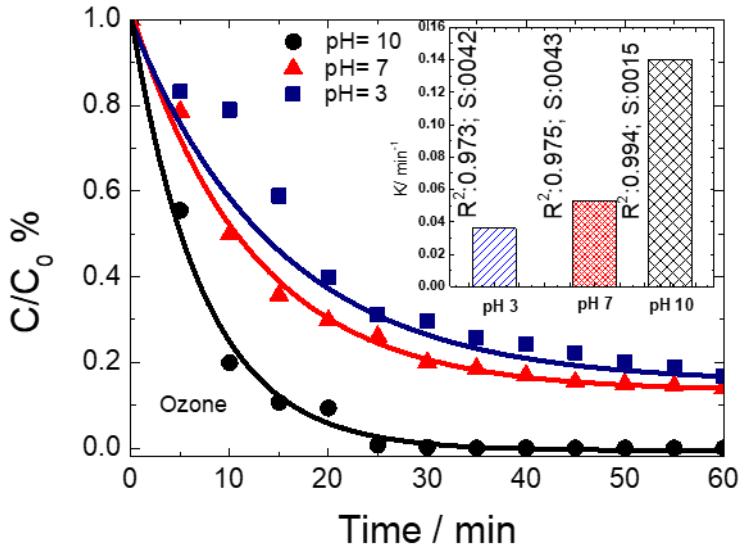
pH= 10
pH= 7
pH= 3
C/C0 %
Time / min
Ozone
K/ min-1
R2:0.973; S:0042
R2:0.975; S:0043
R2:0.994; S:0015
pH 3
pH 7
pH 10

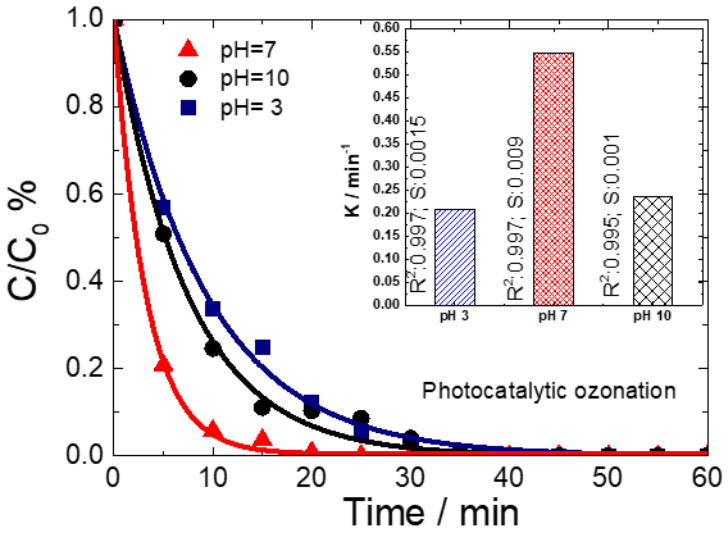

Figure 4.10. Imazapyr degradation as a function of time for different pH by photocatalysis (Ca_xMnO_y-TiO_2 /UV) (A), ozonation (O_3/UV) (B), Photocatalytic ozonation (O_3/Ca_xMnO_y-TiO_2 /UV) (C) $C_{(Imazapyr)}$= 5 µM); stirring speed = 1000 min^{-1}, m TiO_2= 50 mg). V=500 mL. Aqueous suspension Milli-Q water.

The study of pH influence on the photocatalytic ozonation process would be helpful to understand the degradation mechanism and would help reaching a higher degree of removal. Based on the exponential decay of imazapyr concentration, the degradation by photocatalytic ozonation profile was also fitted assuming a first order reaction model (Figure 4.10 C). Similar results have been reported by Khan et al.[34] First order reaction kinetics have been reported for the degradation and mineralization of chlorinated pesticides and insecticides and other various water pollutants by photocatalytic ozonation.[35]

The data given in this Figure 4.10 C clearly showed that the highest degradation of imazapyr is obtained at pH 7 with a first order rate constant of 0.547 min^{-1}, while this amount decreases considerably at pH 3 and pH 10, the rates constant achieved 0.207 min^{-1}, 0.234 min^{-1} respectively. The fitting parameters, rate constant K derived from Figure 4.7 are summarized in Table 4.2.

Table 4.2. Rate constant of imazapyr degradation for photocatalytic ozonation, photocatalysis (Ca_xMnO_y-TiO_2) and ozone.

Experiments N°	pH	Photocatalytic ozonation (UV/ Ca_xMnO_y-TiO_2/O_3)			Photocatalysis (UV/ Ca_xMnO_y-TiO_2)			Ozone (UV/ O_3)		
		Rate constant K	R^2	Standard Deviation	Rate constant K	R^2	Standard Deviation	Rate constant K	R^2	Standard Deviation
N°1	*3*	0.205	0.998	0.00018	0.425	0.999	0.001	0.037	0.974	0.0043
N°2	*3*	0.210	0.997	0.00012	0.427	0.997	0.0016	0.0396	0.973	0.0041
N°3	*3*	0.206	0.996	0.00016	0.423	0.998	0.0013	0.036	0.972	0.0042
Mean	3	0.207 (min^{-1})	0.997	0.00015	0.425 (min^{-1})	0.998	0.0013	0.036 ($mol.L^{-1}.min^{-1}$)	0.973	0.0042
N°1	*7*	0.547	0.997	0.009	0.230	0.988	0.004	0.054	0.975	0.0043
N°2	*7*	0.549	0.996	0.009	0.228	0.988	0.0038	0.052	0.975	0.0043
N°3	*7*	0.545	0.998	0.009	0.226	0.989	0.0042	0.053	0.975	0.0043
Mean	*7*	0.547 (min^{-1})	0.997	0.009	0.228 (min^{-1})	0.989	0.004	0.053 ($mol.L^{-1}.min^{-1}$)	0.975	0.0043
N°1	*10*	0.237	0.993	0.0009	0.193	0.994	0.0014	0.140	0.993	0.0015
N°1	*10*	0.235	0.997	0.0011	0.194	0.995	0.001	0.137	0.995	0.0016
N°1	*10*	0.23	0.995	0.0095	0.188	0.996	0.0012	0.143	0.994	0.0013
Mean	*10*	0.234 (min^{-1})	0.995	0.001	0.191 (min^{-1})	0.994	0.0012	0.140 (min^{-1})	0.994	0.0015

4.3.4. By-products degradation

From an environmental point of view, it is necessary to analyze the reaction of intermediates to exclude the formation of compounds more toxic than imazapyr herbicide. Reaction intermediates and final products at specific time interval of photocatalytic ozonation degradation reactions

were identified by MS-ESI. Imazapyr shows important fragment molecular ion peak at m/z = 262. However, there are several separation peaks appearing during the degradation experiment, which can be ascribed to the intermediates of imazapyr degradation.

MS-ESI data of reaction samples before and after the photoreaction of imazapyr in the presence of Ca_xMnO_y-TiO_2 was analysed and compared to the photodegradation reaction of imazapyr in the presence of commercial TiO_2 (Hombikat UV100).

It is clear from (figure 4.11) that 1h of irradiation time was enough to remove imazapyr, and the kinetics of Imazapyr disappearance follows the first-order reaction for both Ca_xMnO_y-TiO_2 composite and TiO_2 systems.

After 10 min irradiation, the intensity of the main peak fragment of imazapyr representing the concentration, was found to decrease to 39% and 58% for Ca_xMnO_y-TiO_2 composite and TiO_2 respectively.

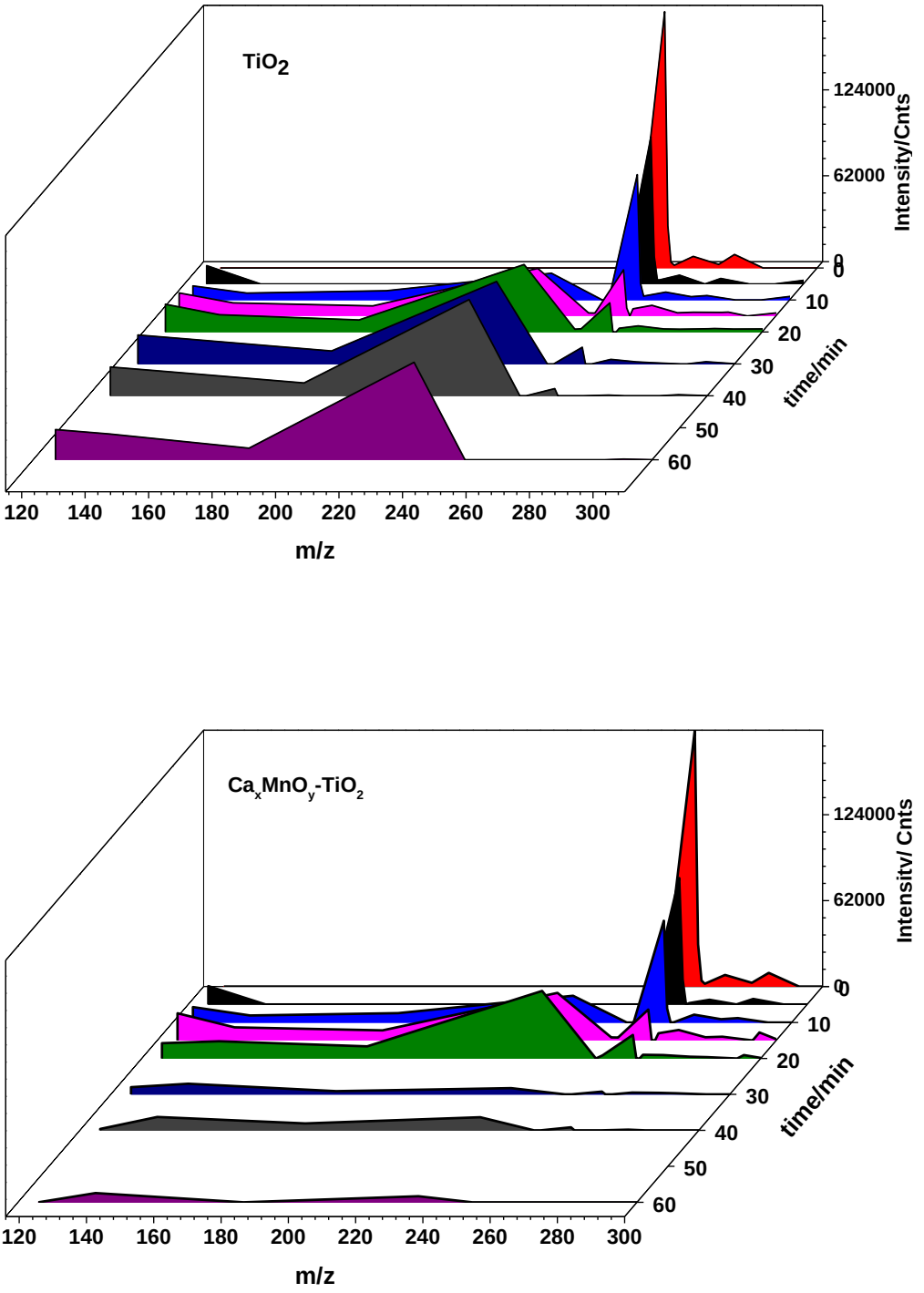

Figure 4.11. Three-dimensional plot of MS-ESI analysis of Photocatalytic ozonation degradation of imazapyr in the presence of pure TiO_2 and Ca_xMnO_y-TiO_2 composite. $C_{(Imazapyr)}$= 5 µM ; stirring speed = 1000 min^{-1}, m TiO_2= 50 mg. V=500 mL. Aqueous suspension Milli-Q water.

Following the identification of different photoproducts and their corresponding intensities that represent the concentration of photoproducts generated as a function of time. It has been confirmed that the total concentration of imazapyr photoproducts in the presence of Ca_xMnO_y-TiO_2 underwent a fast drop to achieve more than 95% of degradation, indicating the mineralization of imazapyr photoproducts.

When comparing the degradation of imazapyr in the presence of TiO_2, it was clear that different intermediate products appears with different m/z fragments and were continuously increasing with prolonging irradiation time and are maintain not decomposed, which indicated that the structure and property of intermediate products in both systems are different.(Quivet *et al.*, 2004; Atitar, Dillert and Bahnemann, 2017) Further investigations of end products of imazapyr degradation are underway in this laboratory. Hence, we can suggest that the high constant rate exhibited by Ca_xMnO_y-TiO_2 in the presence of O_3+UV may be explained considering the high hydroxyl surface population of this sample. This high surface concentration, confirmed in recent study, is supported by the fact that the deposition of the porous manganese oxide mainly on the surface of titanium dioxide that can easily accommodate the hydroxyl groups, additionally to an efficient charge separation, and transfer between the materials. Furthermore, it was also considered that the dissolved ozone was easy to accept conduction band electrons generated on the surface of Ca_xMnO_y-TiO_2, So that the recombination of the positive hole and negative electron pairs was hindered, ultimately a large number of radicals formed. Besides, electron transfer from Ca_xMnO_y-TiO_2 to the ozone molecule generate hydroxyl radicals through the formation of an ozonide radical, thereby accelerating the oxidation process. The enhanced photoactivity of Ca_xMnO_y-TiO_2 sample for intermediate products compared to the commercial TiO_2 was ascribed to the surface modification which could easily adsorb polarized organic reactants and thus promote photocatalytic decomposition of intermediate products.

4.3.5. Effect of water matrix

Wastewater may contain various pollutants; organic solvents and inorganic substances are in general present in wastewater streams. In order to determine the effect of organic matrix, [38] have discussed in a previous study the effect of interactions between imazapyr/ Humic (HA) and Imazapyr /fulvic acids(FA).

The effect of the presence of HA on photodegradation of imazapyr herbicide in water was studied by irradiation of different mixtures of HA/herbicide (0.5:1 and 1:1 by volume). The kinetic rate

constant k of imazapyr decreases from 0.242 h^{-1} to 0.014 h^{-1} in 0.5/1 HA/herb and 1/1 HA/herb respectively.

The obtained results clearly demonstrate that low concentration of HA substances did not affect the degradation kinetics, however at high concentration, HA exhibit a screening effect on the photochemical degradation of imazapyr, but also acts as hydroxyl radical scavengers, and a competition for free radicals between imazapyr and organic matrix could be responsible for decreased efficiency of catalyst directly affecting photocatalytic efficiency.

4.4. Conclusion

In this investigation, ozonation, photocatalysis, and photocatalyzed ozonation by Ca_xMnO_y-TiO_2 composite have been employed to degrade imazapyr herbicide in water. The kinetics of the photocatalytic degradation of imazapyr were analysed taking into account the effect of the pH, the initial imazapyr concentration as well as Ca_xMnO_y-TiO_2 mass concentration. However, special attention was focused on the influence of the pH on the reaction rate. The results of this study showed that imazapyr removal followed a first-order kinetic model with a rate constant of 0.547 min^{-1} and 0.425 min^{-1} for photocatalytic ozonation and heterogeneous photocatalysis respectively, while second order kinetic for ozonation process with a rate constant of 0.053 $mol.L^{-1}.min^{-1}$ at pH 7.This study concluded that imazapyr degradation is strongly influenced by the operating parameters such as TiO_2 concentration, initial imazapyr concentration and pH. The results suggest that a concentration of 5 µM of imazapyr, 100 mgL^{-1} of Ca_xMnO_y-TiO_2 composite and 10 mgL^{-1} of ozone under pH 7 are able to initiate hydroxyl radicals from the decomposition of ozone and degrade imazapyr in less than 10 min. The effect of pH on imazapyr degradation is mainly influenced by the acid–base equilibrium governing the surface of titanium oxides in water. The high constant rate exhibited by Ca_xMnO_y-TiO_2 in the presence of ozone may be explained considering the high hydroxyl surface population of this sample supported by the fact that the deposition of the porous manganese oxide mainly on the surface of titanium dioxide that can easily accommodate the hydroxyl groups. Furthermore, it was also considered that the dissolved ozone was easy to accept electrons generated on the surface of Ca_xMnO_y-TiO_2, so that the recombination of the positive hole and negative electron pairs was hindered, ultimately a large number of radicals formed. It has been confirmed that the total concentration of imazapyr photoproducts in the presence of Ca_xMnO_y-TiO_2 underwent a fast drop to achieve more than 95% of degradation, indicating the mineralization of imazapyr photoproducts. Consequently, it can be concluded that the combination of ozonation and photocatalysis, catalysts with high activity

under visible light and systematic optimization of operational parameters are completely necessary to achieve this goal.

Acknowledgements

The authors would like to thank the National Center of Scientific and Technical Research (CNRST) for technical support to this work.

Conflicts of interest

The authors declare no conflicts of interest

References

[1] J. Louch, “Measurement of Glyphosate, Imazapyr, Sulfometuron Methyl, and Metsulfuron Methyl in Needle Branch Streamwater,” no. 13, p. 130, 2013.

[2] M. Tu, C. Hurd, and J. M. Randall, *Weed Control Methods Handbook : Tools & Techniques for Use in Natural Areas*, no. April. 2001.

[3] S. Maddila, E. O. Oseghe, and S. B. Jonnalagadda, “Photocatalyzed ozonation by Ce doped TiO2catalyst degradation of pesticide Dicamba in water,” *J. Chem. Technol. Biotechnol.*, vol. 91, no. 2, pp. 385–393, 2016.

[4] G. Yang, Z. Jiang, H. Shi, T. Xiao, and Z. Yan, “Preparation of highly visible-light active N-doped TiO2 photocatalyst,” *J. Mater. Chem.*, vol. 20, no. 25, p. 5301, 2010.

[5] U. Ibrahim and A. Halim, “Heterogeneous photocatalytic degradation of organic contaminants over titanium dioxide : A review of fundamentals , progress and problems,” *J. Photochem. Photobiol. C Photochem. Rev.*, vol. 9, pp. 1–12, 2008.

[6] M. Rasoulifard, M. Fazli, and M. Eskandarian, “Kinetic study for photocatalytic degradation of Direct Red 23 in UV-LED/nano-TiO2/S2O82-process: Dependence of degradation kinetic on operational parameters,” *J. Ind. Eng. Chem.*, vol. 20, no. 5, pp. 3695–3702, 2014.

[7] X. Bai, R. Zong, C. Li, D. Liu, Y. Liu, and Y. Zhu, “Enhancement of visible photocatalytic activity via Ag@C3N4core-shell plasmonic composite,” *Appl. Catal. B Environ.*, vol. 147, pp. 82–91, 2014.

[8] C. G. Aba-Guevara, I. E. Medina-Ramírez, A. Hernández-Ramírez, J. Jáuregui-Rincón, J. A. Lozano-Álvarez, and J. L. Rodríguez-López, “Comparison of two synthesis methods on the preparation of Fe, N-Co-doped TiO2materials for degradation of pharmaceutical compounds under visible light,” *Ceram. Int.*, vol. 43, no. 6, pp. 5068–5079, 2017.

[9] T. E. Agustina, H. M. Ang, and V. K. Vareek, “A review of synergistic effect of photocatalysis and ozonation on wastewater treatment,” *J. Photochem. Photobiol. C Photochem. Rev.*, vol. 6, no. 4, pp. 264–273, 2005.

[10] J. Wang *et al.*, “USE OF SELECTED ADVANCED OXIDATION PROCESSES (AOPs) FOR WASTEWATER TREATMENT – A MINI REVIEW,” vol. 1, no. 3, pp. 1034–1042, 2015.

[11] S. Maddila *et al.*, “Effective degradation of acid orange 10 by catalytic ozonation in the presence of Au-Bi2O3 nanoparticles,” *Catal. Today*, vol. 227–228, no. 3, pp. 1227–1233, 2002.

[12] G. H. Safari, M. Hoseini, M. Seyedsalehi, H. Kamani, J. Jaafari, and A. H. Mahvi, “Photocatalytic degradation of tetracycline using nanosized titanium dioxide in aqueous solution,” pp. 603–616, 2015.

[13] M. A. Fox and M. T. Dulay, “Heterogeneous Photocatalysis,” *Chem. Rev.*, vol. 93, no. 1, pp. 341–357, 1993.

[14] S. Contreras, E. Pascual, S. Esplugas, J. Gim, and M. Rodrı, “Comparison of different advanced oxidation processes for phenol degradation,” *Water Res.*, vol. 36, pp. 1034–1042, 2002.

[15] J. Wang and F. E. Osterloh, “Limiting factors for photochemical charge separation in BiVO4/Co3O4, a highly active photocatalyst for water oxidation in sunlight,” *J. Mater. Chem. A*, vol. 2, pp. 9405–9411, 2014.

[16] T. O. Anode, H. Layered, D. Hydroxide, and M. C. Cathode, “Thèse – Tesi di Dottorato – PhD thesis Soliu Oladejo GANIYU Electrochemical Advanced Oxidation Processes for Removal of Organic pollutants from Water : Performance Studies for Sub-stoichiometric Titanium Oxide Anode and Hierarchical Layered Double Hydroxi,” 2016.

[17] C. Anderson and A. J. Bard, “Improved Photocatalytic Activity and Characterization of Mixed TiO2/SiO2 and TiO2/Al2O3 Materials,” *J. Phys. Chem. B*, vol. 101, no. 14, pp. 2611–2616, 1997.

[18] R. L. Narayana, M. Matheswaran, A. Abd, and P. Saravanan, “Photocatalytic decolourization of basic green dye by pure and Fe , Co doped TiO 2 under daylight illumination,” *DES*, vol. 269, no. 1–3, pp. 249–253, 2011.

[19] S. Bougarrani, K. Skadell, R. Arndt, M. El Azzouzi, and R. Gläser, “Novel Cax MnOy /TiO2 Composites for Efficient Photocatalytic Degradation of Methylene Blue and the Herbicide Imazapyr in Aqueous Solution under Visible Light Irradiation,” *J. Environ. Chem. Eng.*, 2018.

[20] L. G. Devi, N. Kottam, B. N. Murthy, and S. G. Kumar, “Enhanced photocatalytic activity of transition metal ions Mn2+, Ni2+and Zn2+doped polycrystalline titania for the degradation of Aniline Blue under UV/solar light,” *J. Mol. Catal. A Chem.*, vol. 328, no.

1–2, pp. 44–52, 2010.

[21] C. E. Frey, M. Wiechen, and P. Kurz, “Water-oxidation catalysis by synthetic manganese oxides – systematic variations of the calcium birnessite theme,” *Dalt. Trans.*, vol. 43, no. 11, pp. 4370–4379, 2014.

[22] Y. F. Chen, C. Y. Lee, M. Y. Yeng, and H. T. Chiu, “The effect of calcination temperature on the crystallinity of TiO2 nanopowders,” *J. Cryst. Growth*, vol. 247, no. 3–4, pp. 363–370, 2003.

[23] L. Sánchez, J. Peral, and X. Domènech, “Aniline degradation by combined photocatalysis and ozonation,” *Appl. Catal. B Environ.*, vol. 19, no. 1, pp. 59–65, 1998.

[24] X. . Li, F. . Li, C. . Yang, and W. . Ge, “Photocatalytic activity of WOx-TiO2 under visible light irradiation,” *J. Photochem. Photobiol. A Chem.*, vol. 141, no. 2–3, pp. 209–217, 2001.

[25] A. Ajmal, I. Majeed, and N. Malik, “Principles and mechanisms of photocatalytic dye degradation on TiO2 based photocatalysts : a,” *R. Soc. Chem. Adv.*, vol. 4, pp. 37003–37026, 2014.

[26] M. Carrier *et al.*, “Kinetics and reactional pathway of Imazapyr photocatalytic degradation Influence of pH and metallic ions,” *Appl. Catal. B Environ.*, vol. 65, no. 1–2, pp. 11–20, 2006.

[27] D. Klauson, J. Babkina, K. Stepanova, M. Krichevskaya, and S. Preis, “Aqueous photocatalytic oxidation of amoxicillin,” vol. 151, pp. 39–45, 2010.

[28] H. Chen, X. Y. Liu, X. D. Hao, and Y. X. Zhang, “Facile biphasic synthesis of TiO2–MnO2nanocomposites for photocatalysis,” *Ceram. Int.*, vol. 42, no. 16, pp. 19425–19428, 2016.

[29] S. Bougarrani, L. El Azzouzi, S. Akel, L. Latrach, A. Bouziani, and M. El Azzouzi, “Factors influencing Imazapyr herbicide removal from wastewater using photocatalytic ozonation,” *Acta Chim.Slov.*, vol. 65, 2018.

[30] M. Pirilä, *Adsorption and Photocatalysis in Water Treatment*. 2015.

[31] M. S. Hamdy, W. H. Saputera, E. J. Groenen, and G. Mul, “A novel TiO2composite for photocatalytic wastewater treatment,” *J. Catal.*, vol. 310, pp. 75–83, 2014.

[32] M. Sui, S. Xing, L. Sheng, S. Huang, and H. Guo, “Heterogeneous catalytic ozonation of ciprofloxacin in water with carbon nanotube supported manganese oxides as catalyst,” *J.*

Hazard. Mater., vol. 227–228, pp. 227–236, 2012.

[33] S. S. Al-shamali *et al.*, "The photocatalytic degradation of atrazine on nanoparticulate TiO2films," *Appl. Catal. B Environ.*, vol. 42, no. 1, pp. 11–20, 2014.

[34] Khan; M.M.; Ansari; S.A.; Amal; M.I.; Lee; J. and Cho; M.H., "Highly visible light active Ag@ TiO 2 nanocomposites synthesized using an electrochemically active biofilm: a novel biogenic approach," *Nanoscale*, vol. 10, no. 5, pp. 4427–4435, 2013.

[35] P. Paudel, A. Negusse, and D. P. Jaisi, "Birnessite-Catalyzed Degradation of Glyphosate:A Mechanistic Study Aided by Kinetics Batch Studies and NMR Spectroscopy," *Soil Sci. Soc. Am. J.*, vol. 79, p. 815, 2015.

[36] E. Quivet, R. Faure, J. Georges, J. O. Païssé, and B. Herbreteau, "Kinetic studies of imazapyr photolysis and characterization of the main photoproducts," *Toxicol. Environ. Chem.*, vol. 86, no. 1–4, pp. 195–204, 2004.

[37] M. F. Atitar, R. Dillert, and D. W. Bahnemann, "Surface Interactions between Imazapyr and the TiO2Surface: An in Situ ATR-FTIR Study," *J. Phys. Chem. C*, vol. 121, no. 8, pp. 4293–4303, 2017.

[38] S. Bougarrani *et al.*, "The influence of humic acids extracted from Chaouia soil on the behavior of transition metal ions and pesticides," *Moroccan J. Chem.*, vol. 3, pp. 446–452, 2017.

Chapter 5: Factors influencing Imazapyr herbicide removal from wastewater using photocatalytic ozonation

S. Bougarrani [1,*], L. El Azzouzi [1], L. Latrach [2], A. Bouziani [1], M. El Azzouzi [1]

[1] Laboratory of Spectroscopy, Molecular Modeling, Materials, Nanomaterials, Water and Environment, (LS3MN2E) Faculty of Sciences, University Mohammed V. BP 1014, Rabat, Morocco.

[2] Faculty of Sciences Semlalia, Cadi Ayyad University, PO Box: 2390, Marrakech, Morocco.

Corresponding author:

Salma Bougarrani, Laboratory of Spectroscopy, Molecular Modeling, Materials, Nanomaterials, Water and Environment, Med V University, BP 1014, Agdal, Rabat, Morocco

Tel: +212660425050; Fax: +212 537 774 261

ORCID: 0000-0003-3085-9556

E-mail:salma.bougarrani@gmail.com

Abstract

This study investigates the degradation of imazapyr herbicide from wastewater by photocatalytic ozonation using TiO_2 as a semiconductor. Effects of operational parameters on imazapyr removal efficiency including TiO_2 dosing, initial herbicide concentration and pH were also studied. Obtained results showed that more than 90% of removal efficiency representing the disappearance of Imazapyr was maintained until 7 µM, further increase of Imazapyr concentration leads to decrease in removal efficiency, the optimal TiO_2 loading where Imazapyr degradation reached the maximum removal rate of 93.0 % is (200 mg/L). Otherwise, the degradation of Imazapyr followed the first-order kinetics and complete degradation was achieved within 20 min using photocatalytic ozonation for 5µM of Imazapyr at pH 7. Photocatalytic rate constant of maximum removal of Imazapyr by photocatalytic ozonation process was 0.247 min^{-1}.

Keywords

✓ Degradation, Imazapyr herbicide, Ozonation, Photocatalytic Ozonation, Wastewater treatment

6.1. Introduction

Persistent organic pollutants such as pesticides have attracted global environmental concerns in recent decades due to its adverse impacts on the environment and public health. Among the various pesticides, imazapyr is one of the widely used herbicide. Imazapyr is a non-selective herbicide that belongs to the imidazolinone family [1]. Imazapyr is a persistent herbicide, which has a half-life varying from 21 days to 49 months in field studies, with a high mobility in soils. Therefore, it is suspected to contaminate groundwater [2]. This pollutant is often found in the municipal sewage effluents and soil with varying trace concentrations in different parts of the world [3].

In recent years, various technologies have been developed and tested in laboratory scales or pilot plants to remove various recalcitrant organic pollutants from wastewater in order to minimize the potential health risks associated with exposure to these chemical pollutants [4]. One of the alternatives to gain greater mineralization efficiency is the use of ozone in the presence of catalyst in order to enhance the free hydroxyl radicals production [4-5]. The photocatalytic ozonation have been studied by many studies worldwide and the high efficiency of this treatment has been explained by a synergistic effect between ozonation and photocatalysis. The photogenerated electrons can react with ozone molecules generating ozonide radicals while decreasing the possible recombination of electronehole pairs. Mehrjouei et al. [5] and Ye et al. [6] reported that among six different advanced oxidation processes, photocatalytic ozonation was the most efficient for completing mineralisation of 4- chloronitrobenzene. These promising techniques are used for the treatment of contaminated water and wastewater to evaluate their capability in the decomposition of pollutants such as pesticides and to assess the treatment efficiencies of these combinations [7].

The advanced oxidation processes (AOPs) have been developed as one of the most promising options in the removal of various persistent organic pollutants by the generation of hydroxyl radicals (·OH) [8-9]. Due to its low-cost and chemical stability, semi-conductor material like TiO_2 has been successfully used in recent years [10-12]. However, the photocatalytic ozonation degradation of pesticides is largely dependent on operating parameters such as TiO_2 dosage, initial herbicide concentration and solution pH. Understanding the effects of these factors on the photocatalytic degradation efficiency have an importance when designing a sustainable and efficient technique for wastewater treatment.

Based on this background informations, the present study aaimed at performing a comprehensibe evaluation of the capacity of photocatalytic ozonation to treat imazapyr from wastewater.

The laboratory studies reported in this paper investigates the capacity and the applicability of TiO_2-photocatalytic ozonation in removing imazapyr herbicide from wastewater. Operational parameters such as TiO_2 initial concentration, initial herbicide concentration and pH were also investigated.

6.2. Material and Methods

6.2.1. Material

Imazapyr herbicide, (95%) was purchased from American Cyanamid Company. TiO_2 Hombikat UV100 (99%) was purchased from Sachtleben Chemie in powdered form. The chemical structure of imazapyr herbicide is shown in figure 5.1. Potassium indigo trisulfonate was purchased from Riedel-de Hahn AG. The other chemicals used in the experiments were purchased from Riedel-de Hahn AG. They were all of analytical grade and used without further purification. All solutions were prepared using Milli-Q water at room temperature collected from Milli-Q apparatus (Millipore, Bedford).

Sample analysis from the study of the photocatalytic degradation of imazapyr was carried out using a mass spectrometry coupled to electrospray ionization system (ESI) for a qualitative and quantitative analysis. MS analysis was performed on Bruker Esquire 3000 plus mass spectrometer equipped with an ESI interface and an ion trap (Bruker-Daltonics Analytik GmbH Bremen, Germany). The ESI probe tip and capillary potentials were set at 2.5 kV and 25 V, respectively. The concentration of aqueous ozone was determined by Spectrometric method indigo trisulfonate according to Bader and Hoigne, (1982) [13]. The absorption analysis of the indigo was monitored by Shimadzu UV-160A UV-Vis Spectrophotometer at 600 nm.

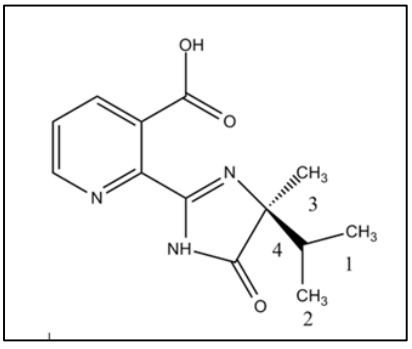

Figure 5.1.Chemical structure of imazapyr herbicide.

6.2.2. Photocatalytic ozonation experiment

Titanium dioxide (100 % anatase, average particle size of 10 nm and BET Method–Brunauer, Emmett and Teller [BET] surface of > 250 m^2 g^{-1}) was used without any pre-treatment.

In a typical reaction, 200 mg/L of TiO_2 were added to 500 mL of 5 µM of imazapyr solution in a double walled cylindrical photoreactor (figure 5.2). Then, the solution was exposed to ultrasonic treatment for 2 minute in order to suspend the catalyst. Immediately afterwards, the stirring was started and maintained over 1h in the dark to ensure the adsorption equilibrium between the solution and the catalyst particles. The imazapyr degradation experiments were carried out in a simple photocatalyzed ozonation reactor, as presented in figure 5.2, with combining photocatalysis and ozonation.

The irradiation experiments were carried out under light generated by a medium pressure mercury lamp at 150W in a Duran cell (λ > 300 nm), placed inside the reactor. A cooling water system was set up to prevent overheating of the lamp and of the solution. Samples were taken every 10 min and filtered two times in order to remove all the catalyst. The photocatalytic ozonation degradation of Imazapyr herbicide was investigated in an aqueous suspension 1: 3 acetone/water mixture in the presence of pure titanium used as a catalyst. Imazapyr showed important fragments molecular ion peak at m/z = 262 and m/z = 284, The MS-ESI detects the Imazapyr under two forms (combinated to H^+ wich gives m/z= 262 and combinated to Na^+ with m/z 284) and their degradation was followed as a function of time.

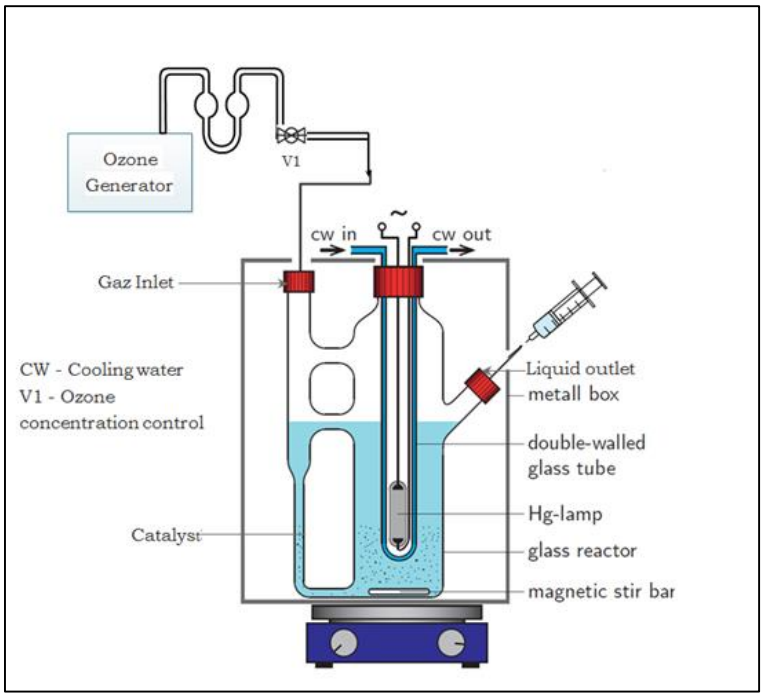

Figure 5.2.Scheme of photocatalytic ozonation reactor used for imazapyr degradation.

6.3. Results and discussion

6.3.1. Effect of TiO_2 dose on imazapyr degradation

Variations of Imazapyr removal rate under different TiO_2 dose are presented in figure 5.3. Imazapyr degradation increased slowly and reached the maximum removal rate of 93.0 % in the concentration of 200 mg/L. Thus, this TiO_2 dose (200 mg/L) could be considered as the optimal concentration of hombikat UV 100. The optimal amount of Hombikat UV 100 agrees well with reported results by other authors [14-26]. This improvement can be attributed to the increasing of active sites by providing more TiO_2 particles, which plays the semiconductor role in the photocatalysis process. Consequently, the formation of electron-hole pairs and reactive hydroxyl radicals on the surface of semiconductor increased, which improved the oxidation of imazapyr into other intermediates.

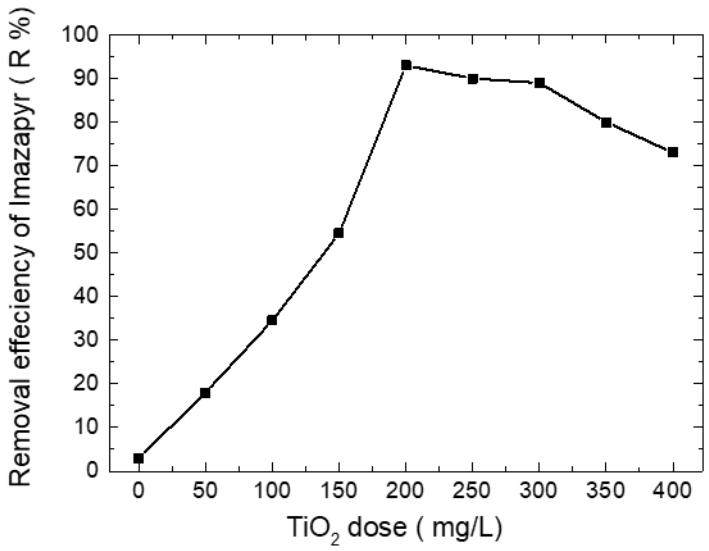

Figure 5.3. Removal rate of imazapyr under variation of TiO_2 concentration. $C_{(Imazapyr)}$= 5 µM ; stirring speed = 1000 min^{-1}, aqueous suspension 1: 3 acetone/ Milli-Q water.

6.3.2. Effect of initial herbicide concentration

The pollutant concentration in water is an important factor to determine the oxidation efficiency and the synergistic effects of photocatalytic ozonation processes [12-15]. The effect of the initial herbicide concentration was studied for six concentrations of imazapyr by photocatalytic ozonation. The initial herbicide concentrations were 1µM, 3 µM, 5 µM, 7 µM, 9 µM and 15 µM (0.26 mg/L, 0.79 mg/L, 1.31 mg/L, 1.83 mg/L, 2.36 mg/L, 3.9 mg/L respectively).

For this series of experiments the catalyst and the ozone doses were kept constant at 200 mg/L and 10 mg/L respectively. The irradiation time was fixed at 10 min for all samples after the adsorption step under dark conditions.

Obtained results showed that more than 90% of removal efficiency representing the disappearance of imazapyr was maintained until 7 µM, further increase of imazapyr concentration leads to decrease in removal efficiency (figure 5.4). A possible explanation resides in the fact that as imazapyr concentration rises, it is possible that more organic substances are deposed on the surface of TiO_2, whereas less number of photons are available to reach the catalyst surface and the probability of reaction between imazapyr molecules and oxidizing species also decreases, thus resulting in less degradation percentage [13].

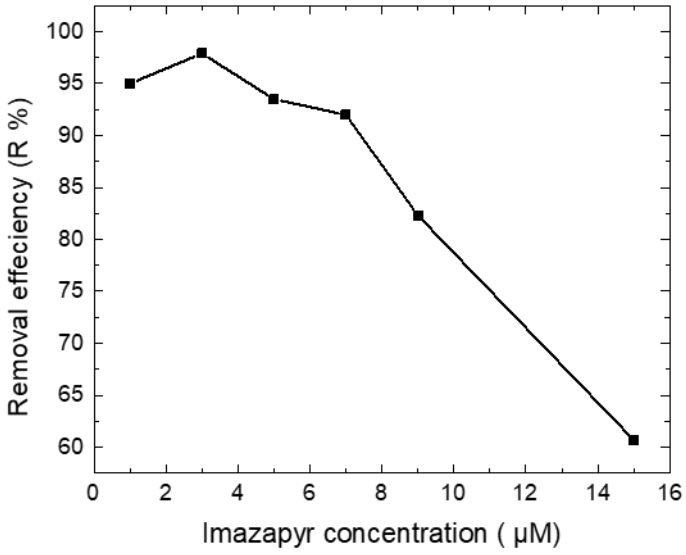

Figure 5.4: Removal efficiency of imazapyr as a function of imazapyr concentration, $m_{catalyst}$=100 mg; stirring speed = 1000 min^{-1}, aqueous suspension 1: 3 acetone/ Milli-Q water.

6.3.3. Effect of pH influence on Imazapyr degradation

Knowledge of the kinetics required to assess the efficiency of systems engineered for the oxidation of a variety of pollutants. Reliable kinetic studies require obvious substrate decay measurements. Thus, for comparison of the efficiency of these treatment processes, kinetic studies of imazapyr decomposition were carried out.

In all experimental runs, imazapyr concentration was found to decrease with irradiation time. A first order kinetics fitting of the thus obtained concentration vs. time plots allows to

calculate the respective first order rate constants. Based on the exponential decay of concentration of imazapyr, the photoactivity profile was fitted assuming a first order reaction.

$$\boldsymbol{C = C_0\, exp(-k \cdot t)} \quad (1)$$

In which C is the concentration of imazapyr at time t, C_o is the initial concentration, and k is the observed rate constant.

Many aurhors have reported that the kinetic behavior of photocatalytic reaction can be described by a modified Langmuir-Hinshelwood model.[19]

The influence of pH on the effectiveness of imazapyr degradation by photocatalytic ozonation is shown in figure 5.5. The degradation experiments were carried out at pH values of 3, 7, and 10. Imazapyr removal rate reached a maximum at pH 7 with a first order rate constant of 0.247 min^{-1}. However, for pH 3 and 10, the photocatalytic activity decreased appreciably. The rates constant at pH 3 and pH 10 are 0.107 min^{-1}, 0.134 min^{-1} respectively (Table5.1). The study of pH influence on the photocatalytic ozonation process would be helpful to understand its underlying mechanism and would help obtaining a higher degree of removal. Based on the exponential decay of imazapyr concentration, the degradation by photocatalytic ozonation profile was fitted assuming a first order reaction model. Similar finding have been reported by Beduk et al. [14] and by Balcioglu et al [15]. These authors have reported first order reaction kinetics for the degradation and mineralization of chlorinated pesticides and insecticides and other various water pollutants by photocatalytic ozonation [14-16].

The results, shown in figure 5.5, demonstrates that the optimal conditions for imazapyr degradation with photocatalytic ozonation is neutral pH. On the other hand, the combination of two oxidation systems, ozonation and photocatalysis, for water treatment under optimal conditions are reported to have increased oxidation efficiencies (synergy) compared to the sum oxidation efficiencies of these two oxidation systems separately [16-19]. Several studies have discussed the synergistic effects of photocatalytic ozonation on degradation and removal of different substances from aqueous solutions and the effects are reported in terms of the degradation and/or mineralization efficiencies or oxidation rate constants of model water pollutants [17-21]. The efficiency of photocatalytic ozonation is mainly attributed to the formation of more reactive and non-selective hydroxyl radicals in the oxidation medium, which react with almost all organic molecules at a rate of 10^6- 109 $M^{-1}s^{-1}$ [18-25]. In addition to the synergistic effects which occur during photocatalytic ozonation compared to simple photocatalysis in presence of oxygen. Sanchez et al. [13-23], Li et al. [14-24], also reported similar results for the mineralization of aniline, dibutyl phthalate, respectively.

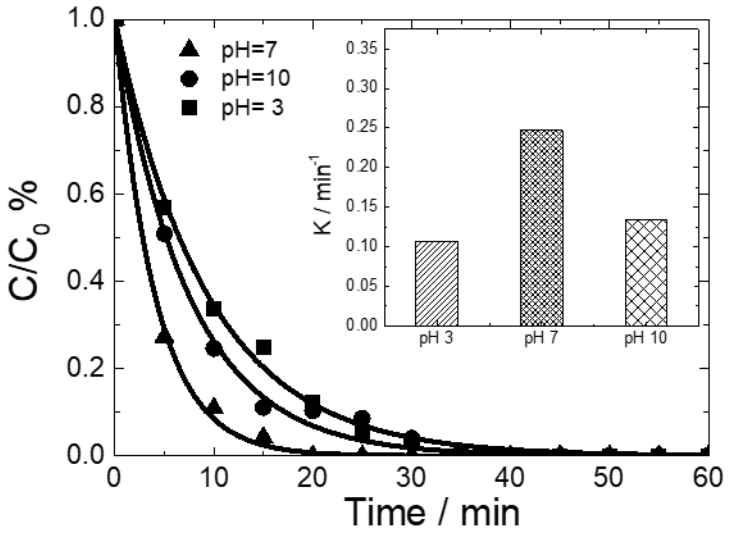

Figure 5.5: Concentration of imazapyr as a function of time for different pH, $C_{(Imazapyr)}$= 5 μM); stirring speed = 1000 min^{-1}, m TiO_2= 100 mg).aqueous suspension 1: 3 acetone/ Milli-Q water.

Table 5.1: Rate constant of imazapyr degradation with photocatalytic ozonation for different pH.

pH	Photocatalytic ozonation		
	Rate constant K	**R^2**	**Standard Deviation**
3	0.107 (min^{-1})	0.997	0.0012
7	0.247 (min^{-1})	0.997	0.0009
10	0.134 (min^{-1})	0.995	0.0015

6.4. Conclusion

This study demonstrated the ability of photocatalytic ozonation using TiO2 as semiconductors for the degradation of imazapyr herbicide as organic pollutants. Imazapyr degradation is strongly influenced by the operating parameters such as TiO2 concentration, initial imazapyr concentration and pH. Under optimized conditions (TiO2 dose of 200 mg/L, 5µM of initial imazapyr concentration and pH 7), up to 95 % of imazapyr removal was achieved within 20min with removal rate constant of 0.247 min−1. Results of the present investigation suggest that photocatalytic ozonation using TiO2 is efficient for the removal of imazapyr form wastewater. The high efficiency of photo catalytic ozonation could be explained by a synergistic effect between ozonation and photocatalysis. The photogenerated electrons can react with ozone molecules generating ozonize radicals while decreasing the possible recombination of electron hole pair, so better electron- whole separation.

Therefore, the application of photocatalytic ozonation under the optimal conditions is recommended for organic pollutants treatment such as imazapyr herbicides in order to promote environmental and human health protection.

References

[1] M.R. Assalin , S.G. De Moraes , C. N. Queiroz , V.L. Ferracini & N. Duran, *J Environ Sci Health B* , 45:1, (2009) , 89-94

[2] G. Kaichouh, N. Oturan, M. A. Oturan, A. El Hourch & K. El Kacemi, *Environ Technol*, 29:5, (2008) 489-496

[3] K. Ikehata & M. G El-Din, *Ozone-Sci Eng*, 27:3, (2005) 173-202

[4] I. Oller a, W. Gernjak a, M.I. Maldonado a, L.A. Perez-Estrada a, J.A. Sanchez-Perez b, S. Malato, *J Hazard Mater B*, 138 (2006) 507–517

[5] P. Pizarro, C. Guillard, N. Perol, J.-M. Herrmann, *Catal. Today* 101 (2005) 211–218

[6] H.Ebrahimi, F.Ghorbani Shahna, *ARCH ENVIRON PROT* Vol. 43 no.1 (2017) 65–72

[7] D.Bamba, P.Atheba, D.Robert, A.Trokourey, B. Dongui, *Environ. Chem. Lett.* (2008), 6, 163–167.

[8] O.K. Boggard,A.L Gimsing, *Pest Manag* Sci. (2008), 64, 441–456.

[9] C. Shifu, L,Yunzhang. S, *Chemosphere* (2007), 67, 1010– 1017.

[10] K. Okehata, M.G.EI-Din, *Ozone Sci. Eng.*, **27**, (2005)83.

[11] S. Maddila, S. Rana, R. Pagadala & S. B. Jonnalagadda, *DESALIN* WATER TREAT, (2015)1–12

[12] S.Maddila, V.O. Ndabankulu and S.B Jonnalagadda *Global NEST J.* (2016), 18(2), 269-278.

[13] L. Sanchez, J. Peral, & X.Domenech, *Appl Catal B*, (1998), 19, 1, pp. 59–65.

[14] K. Usharani, M.Muthukumar, and K. Kadirvelu, *Int. J. Environ. Res*., 6(2): (2012) 557-564.

[15] M. Gar Alalma, A. Tawfika, S. Ookawara, *J. wat Proc Eng* 8 (2015) 55–63.

[16] B.H. Hameed, U.G. Akpan, , *J Hazard Mater* 170 (2009) 520–529.

[17] G. Zhang, Q. Wang, W. Zhang, T. Yuan and P. Wang. *Photochem Photobiol Sci*, (2017)98-103.

[18] M. Faycal Atitar, and Detlef W. Bahnemann, *J. Phys. Chem. C* (2017) 1-36.

[19] I.Djerdj ,D. Arcon, Z. Jagliid, M. Niederberger . *J. Solid State Chem.* 181 (2008) 1571–1581

[20] Lissemore, L.,C.Y. Hao, P. Yang, P.K. Sibley, S. Mabury, and K.R. Solomon. *J. Chemosphere* 64 (2006) 717–729

[21] G. H. Safari, M. Hoseini, M. Seyedsalehi, H. Kamani, J. Jaafari , A. H. Mahv *Int. J. Environ. Sci. Technol.* 12 (2015) 603–616

[22] Kümmerer, K. *J. Environ. Manage.* 90 (2009) 2354-2366.

[23] T. Li, S.G. Yang, L.S. Huang, B.X. Gu, Y.W. Du, *Nanotechnology* 15 (2004) 1479–1482.

[24] R.M. Wang, C.M. Liu, H.Z. Zhang, C.P. Chen, L. Guo, H.B. Xu,S.H. Yang. *Appl. Phys. Lett.* 85 (2004) 2080-2082

[25] E.K. Putra, R. Pranowo, J. Sunarso, N. Indraswati, S. Ismadji. *Water Res.* 43 (2009) 2419-2430

[26]. Klavarioti, M., Mantzavinos, D., Kassinos, D. *Environ. Int.* 35, (2009) 402-417.

Chapter 6: The influence of humic acids extracted from Chaouia soil on the behavior of transition metal ions and pesticides

S.Bougarrani [(a)]* , L.El azzouzi[(a)], A.Bouziani[(a)] , S.Akel[(a)], L.Latrach[(b)] , Z.Baicha[(c)], M.El azzouzi[(a)]

[(a)] Laboratory of Materials, Nanomaterials and Environment, Faculty of Sciences, University Mohammed V. BP 1014, Rabat, Morocco.

[(b)] Cadi Ayyad University, PO Box: 511, 40000, Marrakech, Morocco.

[(c)] Laboratory of Mechanics and Industrial Processes, Chemical Sciences Research Team, ENSET Mohammed V University, E-10100, Rabat, Morocco.

Corresponding author:

Salma Bougarrani, Laboratory of Spectroscopy, Molecular Modeling, Materials,

Nanomaterials, Water and Environment, Med V University, BP 1014, Agdal, Rabat, Morocco

Tel: +212660425050; Fax: +212 537 774 261

ORCID: 0000-0003-3085-9556

E-mail:salma.bougarrani@gmail.com

Abstract

Humic acids (HAs) exist ubiquitously in environments and have a variety of functional groups, which allow them to complex with metal ions and pesticides. Furthermore, these interactions can not only alter the environmental behavior, but also influence the removal and transportation of those pollutants. The study of the interaction between Cu (II), VO (II) and Mn (II) with HAs provides environmental information on the oxidation states of paramagnetic metals and their mechanisms of binding to humic acids. Electron spin resonance (ESR) study demonstrates that VO (II) and Cu (II) ions are bound with oxygen ligands to HAs, while the Mn (II) complex occurs as $[Mn(H_2O)_6]^{2+}$. Additionally, Cu (II) ions are more strongly bound to soil HAs than Mn (II) ions. The effect of the presence of HA on photolysis of Tribenuron-methyl (TRB) and Imazapyr (IMAZ) herbicides in water was studied by irradiation of different mixtures of HA/herbicide (0.5:1 and 1:1 by volume). The kinetic rate constant k of TRB and IMAZ decreases from 0.0029 h^{-1} to 0.0012 h^{-1} and from 0.242 h^{-1} to 0.014 h^{-1} in 0.5/1 HA/herb and 1/1 HA/herb respectively. The obtained results clearly demonstrate that HA substances exhibit a screening effect on the photochemical degradation of the two herbicides. The protective effect of HAs on the TRB and IMAZ degradation could be explained with an inclusion and/or adsorption of the herbicide molecules in the humic matrix.

***Key words**: Complex, Humic acids, pesticides, photolysis, transition metals.*

6.1. Introduction

Water pollution has become a critical issue worldwide. The presence of various contaminants such as trace metals ions and organic compounds into the environment and their fate are matters of increasing concern in recent years [1, 2].

The fate of these contaminants in soil and surface water depends upon the physico-chemical behavior of these pollutants. Humic acid (HA) and fulvic acid (FA) exist ubiquitously in the environment and have a variety of functional groups, which allow them to complex with metal ions and pesticides [3], which would provide much needed information on the mobility, transport and immobilization of these elements in terrestrial and aquatic environments. Moreover, these interactions can not only alter the environmental behavior, but also influence the removal and transportation of heavy metals. Thus, this complexation by humic substances can enhance or retard uptake and toxicity of these compounds by organisms [4]. Additionally, transition metals such as VO, Cu, and Mn are biologically essential at trace levels, but can be toxic when present in excess amounts. These elements are found in soil to be incorporated into the structure of humic acids [4, 5]. The humic substances are subject of increasing attention because of their reactivity as sunlight absorbers. They have a significant ability to absorb light and transfer this energy to other substrates and in some cases strongly affect photolysis of xenobiotics [1,5]. Ge and Chen, [6] have reported that humic substances may have some impact as a photosensitizer when irradiated at wavelength longer than 290 nm. They have also been reported to produce oxygen species upon irradiation [7], and be able to photo induce the transformation of pesticides [5, 8]. They could behave as quenchers or as light scatters on the photodegradation kinetics of vetenary drugs and herbicide as well because of their known reactivity under sunlight on the surface of water [9].Previous research has demonstrated that the presence of herbicide in environmental matrices is affected by different parameters. Additionally, it has been demonstrated that those herbicides are sensitive to UV visible light [10]. However, several factors and experimental conditions such as pH, temperature, oxidative species, irradiation wavelength and water matrix components can affect the photo chemical pathways of certain pollutants in aquatics system. Tribenuron-methyl benzoate (TRB) and Imazapyr (IMAZ) are two widely used herbicides to control a wide range of weeds in cereal crops and sugar beet [11, 12]. However, in long or short term use, these pollutants have a direct relationship with adverse effects in ecosystems and human health [13, 14].

The Food & Agriculture Organization (FAO) carried out in 2015 a survey about the effect of pesticides on human health and environment in Morocco [15].

The results of survey determined that Chaouia plain is an important agricultural area with a big cereals, fodder crops and industrial crops plantations. This plain is characterized by the excessive use of pesticides and groundwater for the agriculture leading to the contamination of the unconfined aquifer by drift, vertical drainage and leaching, the soil of Chaouia plain is also characterized by the high concentration of dissolved organic matter (DOM), which is mostly composed of humic substances (HSs) and can be viewed as a natural constituent in aquatic systems [16].

This work highlights the influence of humic acids extracted from Chaouia soil on the behavior of VO, Cu, and Mn transition metals. The phenomena, factors and potential mechanisms involved in the process are also discussed thoroughly. we tried to assess contributions of photolysis to the degradation of Tribenuron-methyl (TRB) and Imazapyr (IMAZ) herbicide in aqueous solutions by partial simulation of natural conditions with addition of HA and exposure to light.

6.2. Materials and methods

6.2.1. Humic acids (HAs) extraction

The HA used in this investigation are from surface horizon (0–20 cm) of soil originated from Chaouia, which is agricultural and semiarid area in Morocco. Main physicochemical properties of the soil from which HA were extracted are (C_{total} = 1.56; N_{total} = 0.16; pH (H_2O) = 7.7). HA were extracted by 0.1 M NaOH and 0.1 M $Na_4P_2O_7$ (v/v) mixture under nitrogen [17]. The sample was suspended in 2N HCl to remove carbonates and the above mixture was added with stirring for 16 h. The solution was centrifuged to eliminate suspended clay and acidified at pH lower than 2 with 6N HCl. The HA precipitate was separated by centrifugation and purified by HCl/HF 0.5% (v/v) treatment. Dissolution into alkaline solution and precipitation by acid was repeated three times. The final alkaline solution was passed through an Amberlite IRN 77 cation exchange resin column to obtain an acid form of HA, which dialyzed against distilled water and freeze dried. Characterization of HA was achieved by elemental analysis and determination of acidities [18] with ESR spectroscopy technique. ESR spectroscopy is an adequate technique for the study and for obtaining structural information about transition metal ions in soil organic matter. It can also provide unique information on the oxidation states of paramagnetic metals and their mechanisms of binding to HAs 19. Therefore, an ESR study of the interaction between VO (II), Cu (II) and Mn (II) with HAs can provide environmental information.

50 mL of HA at concentration (30 mg/L, were exposed for photodegradation at various illumination time. Experiments were carried out at pH = 7.0 (pH of environmental interest), buffered with a mixture of K_2HPO_4 3.9×10^{-4} mol/L and KH_2PO_4 6.1×10^{-4} mol/L (1/1; v/v).

6.2.2. Metal ions/ HA complexes

Solutions of VO (II), Cu (II) and Mn (II) were prepared by dissolving sulphates in distilled water to produce concentrations of 1, 3, and 5 % (wt-metal ion/wt-HA). Samples containing 100 mg of HA were dissolved in 0.1 M NaOH and precipitated by 6 N HCI at pH values below 2. After centrifugation the fresh coagulates were separately mixed with solutions of VO (II), Cu (II) and Mn (ll) ions. The pH value was adjusted in the range of 4-5 by addition of HCl or NaOH. This range of pH corresponds to the dissociation of carboxylic acid groups of HAs [11]. In aqueous systems, HAs are normally insoluble at pH values lower than 6.5. These insoluble HAs are able to react with trace metal ions more efficiently than solubilized ones [11]. Exceptionally for Mn (II)-HA, in order to study the simultaneous competition of Mn (II) and Cu (II) and to identify which is more strongly bound to HA, amounts (<1 mg) of Cu (II) ions were added to Mn(II)-HA solutions. The mixtures were shaken for 24 h at room temperature and each mixture was centrifuged. The precipitates were separated from the supernatant solutions and washed alternatively with distilled water and 1 N HCl in order to remove the non-complexed ions.

6.2.3. Analytical procedure

6.2.3.1. Electron Spin Resonance (ESR) Analysis

ESR spectra were recorded at -170 °C, on powder, by a VARIAN spectrometer operating at X band frequency. The spin Hamiltonian parameters of ESR spectra (e.g. g-values and hyperfine coupling constants A) were calculated. For g determination, DPPH (2.2-Di-(4-tert-octaphenyl)-1 -picryhydrazyl) was used as reference substance.

6.2.3.2. UV-Vis absorption

UV-Vis absorption spectra were recorded using Uvikon 930 spectrophotometer. Total Organic Carbon (TOC) contents were determined with a calibrated Carmograph8 apparatus [19].

6.2.3. Photo-reactor

Photo-degradation processes were carried out using a cylindrical photo-reactor placed in suntest Heraeus apparatus. The irradiation source was xenon lamp (T = 20 °C), which provides a good simulation of solar light. The lamp was placed above the surface of the solution. The solution was homogenized by continuous stirring with a magnetic stirrer.

6.3. Results and discussions

6.3.1. Humic acids properties

The main characteristics of HA are shown in table 6.1. The characteristics of HA are close to those reported in the literature data [20] with some differences in the determined chemical properties such as total acidity and acid group. The spin Hamiltonian parameters (A and g) were calculated from spectra according to the literature data [21]. From all formed complexes, the A and g parameters are listed in table 6.2. The values of these parameters provide no significant difference from each complex at different percentages. This result indicates that incorporated metal ions occupied the same site in the HAs.

The results from the ESR data (A and g parameters) for the investigated complexes are summarized in table 6.2. For the VO (II)-HA complex, vanadyl ions are strongly immobilized in inner-sphere complexes by HA, with four oxygen donor atoms in equatorial plane of the VO (II) group [18, 20]. For Cu (II)-HA complexes, Cu (II) ions are also associated with four oxygen donor atoms. In the case of Mn (II) complexes, A_{iso} and g_{iso}, suggested that Mn (II) ions are incorporated as $[Mn(H_2O)_6]^{2+}$ by electrostatic bounding only [18, 20].

Oxygen functional groups involved in the complexation of VO (II) and Cu (II) ions can originate from two carboxylates or two hydroxy-phenol for neutralizing the charge of the ions, two other oxygen groups can provide carbonyls or methoxyls [18]. Consequently, VO (II) and Cu (II) ions are bound with oxygen ligands to HAs, while the Mn (II) complex occurs as $[Mn(H_2O)_6]^{2+}$. Also, Cu (II) ions are more strongly bound to soil HAs than Mn(II) ions. These results are in correlation with literature data [18 and 20].

Table 6.1. Analytical characteristics of extracted HA.

Parameters	Unit	Values
C	%	41.70
H	%	2.51
N	%	2.47
O	% (by difference)	53.32
Total acidity	meq / g	6.04
Phenolic acidity	meq / g	0.77
Carboxylic acidity	meq / g	3.93
Mineral acidity	meq / g	1.34

Table 6.2. ESR data for VO (II)-HA Cu (II)-HA Mn (II)-HA complexes.

ESR data M(II)-HA	A//(G)	A (G)	A_{iso}(G)	g//	g⊥	g_{iso}
VO (II)-HA						
1%	197.8	75.8	116.5	1.9354	1.9878	1.9703
3%	193.5	75.7	115.0	1.9193	1.9863	1.9640
5%	194.8	73.2	113.8	1.9340	1.9855	1.9684
Cu (II)-HA		Not	Not			
1%	135.8	detected	detected	2.3292	2.0759	2.1603
3%	135.2			2.3324	2.0759	2.1614
5%	136.7			2.3364	2.0759	2.1627
Mn (II)-HA	Not	Not		Not	Not	
1%	detected	detected	96.0	detected	detected	2.0036
3%			96.4			2.0036
5%			96.4			2.0036

6.3.2. Photolysis of HA

HA extracted from Chaouia soil, were evaluated for their individuality and properties through elemental analysis E4/E6 ratio and total acidity. HA fraction was composed of El-C and El-N (41.7 % and 2.47 % respectively). However, the E4/E6 value, which is the ratio

of absorption intensities at 465 and 665 nm, is widely used to characterize HA. The E4/E6 ratio is supposed to decrease with increasing condensation of aromatic humic constituent's [12]. The E4/E6 ratio is governed by the molecular size [22]. Figure 6.1 represents the values of (TOC) and E4/E6 ratio as a function of time. The results show that the E4/E6 ratio as well as the TOC value are both constant with increasing time of irradiation, reflecting photo-stability of HA molecules after 24 h of continuous irradiation. Higher degree of aromaticity of HA's was evidenced by lower E4/E6 ratio value of 1.91.

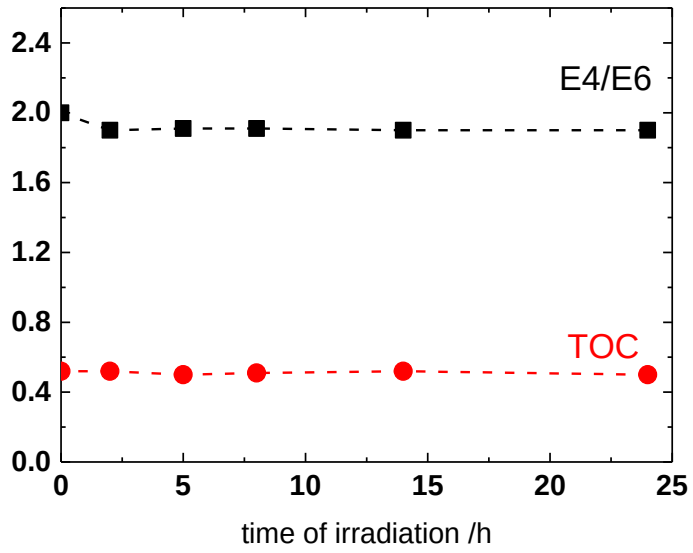

Figure 6.1. E4/E6 and TOC at different irradiation times.

6.3.2.1. Photolysis of HA in the presence of herbicide (TRB and IMAZ) molecules

In order to assess the contributions of photolysis to the degradation of herbicides in aqueous solutions by partial simulation of natural conditions with addition of HA and exposure to sunlight, different mixtures of HA/herbicide (0.5/1 and 1/1 by volume) were prepared and irradiated by solar light. According to the results dissipated in figure 6.2 & 6.3, the addition of the HA to the solution of TRB or IMAZ herbicides results in a decrease in kinetic rate constant (k) and a significant increase in the half-life ($t_{1/2}$). The kinetic rate constant k of TRB decreases from 0.0029 h^{-1} to 0.0012 h^{-1}, however the half-life time ($t_{1/2}$) increases from 267.8 h to 552.2 h in 0/1 HA/herb and 1/1 HA/herb respectively. The kinetic rate constant k of IMAZ decreases from 0.242 h^{-1} to 0.014 h^{-1}, however the half-life time ($t_{1/2}$) increases from 2.9 h to 49 h in 0/1 HA/herb and 1/1 HA/herb respectively. The overall kinetic rate constant was decreasing with increasing HA concentration. This screening effect can be explained by prevailing HA-

photosensitized reactions over the shielding effect. The second possibility is less probable, as an inclusion and/or adsorption of the herbicide molecules in the humic matrix.

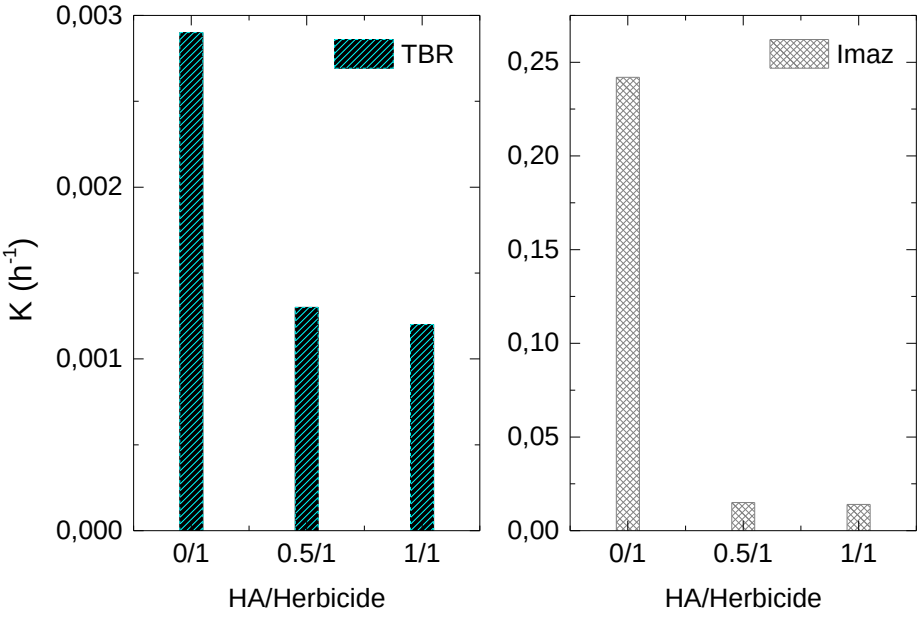

Figure 6.2. Kinetic rate constant (k) of photolysis of TRB and IMAZ in the presence of HA.

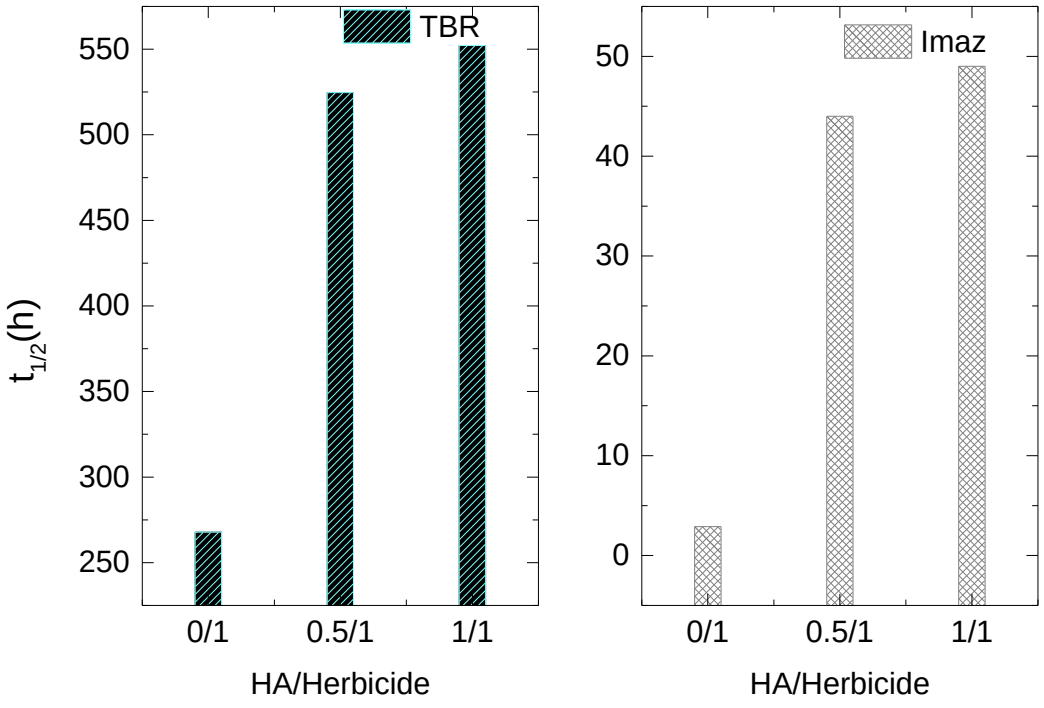

Figure 6.3. The half-life time ($t_{1/2}$) of photolysis of TRB and IMAZ in the presence of HA.

6.4. Conclusion

The present study indicated that HAs have complex effects on the removal and environmental behavior of transition metal ions and pesticides. Furthermore, this work demonstrated that the presence of HAs could significantly modify the mechanisms controlling metal ions removal and transportation in aquatic environments. These mechanisms involved complexation, the functional groups involved in complexation can originate from carboxylates and carbonyl groups also the competition between Cu (II) and Mn (II) shows that Cu (II) is more strongly bound to HA, adsorption, electrostatic force, catalysis and so on.

The photochemical behaviour of HAs isolated from agricultural soil has been found photostable in buffered solution upon 24 h of irradiation. HAs substances exhibit a screening effect on the photochemical degradation of herbicides. This protective effect induced a decrease of photolysis rate and favors herbicides activity of TRB and IMAZ.

References

[1] J. Porras, C. Bedoya , J-S. Agredo , A. Santamaría ,J. Fernandez, R.Torres-Palma. Water Research 94 (2016) 1-9

[2] B. Petriea, R. Bardenb, B. Kasprzyk-Horderna. Water Research 72 (2015) 3–27

[3] W. Tang, G. Zeng , J. Gong , J. Liang, P. Xu, C. Zhang, B. Huang. Science of the Total Environment 468–469 (2014); 1014–1027

[4] R. Al-Rasheed, D. Cardin. Chemosphere 51 (2003); 925–933

[5] P. Chellan , P. Sadler. Philos Trans A Math Phys Eng Sci (2015); 373(2037)

[6] M. Gmurek, M. Olak-Kucharczyk, S. Ledakowicz. J Environ Health Sci Eng. (2015); 13-2

[7] Toshiyuki Katagi Rev Environ Contam Toxicol (2004); 182:1–195

[8] H. Kerndorff, M. Schmitzer. Geochim. Cosmochim, 44 (1980); 1701-1708.

[9] E. SELLI, D. BAGLIO, L. MONTANARELLA, G. BIDOGLIO. Wat. Res. Vol. 33, No. 8, (1999). 1827-1836

[10] H. Prosen, L. Zupancic-Kralj .Environmental Pollution 133 (2005) 517–529

[11] M. Mekkaoui , M. El Azzouzi , M. Ferhat , J. M. Chovelon, P. Meallier.Toxicological & Environmental Chemistry 80:1-2(2001) , 31-39

[12]M.MEKKAOUI,M.EL.AZZOUZI ,A.BOUHAOUSS,M.FERHAT,A.DAHCHOU ,S.GUIT TONNEAU P.MEALLIER ; Fresenius Envir BULL 9; (2000) 789-790

[13] M. Elazzouzi , M. Mekkaoui , S. Zaza , M. El Madani , A. Zrineh & J. M. Chovelon , Journal of Environmental Science and Health, Part B: Pesticides,Food Contaminants, and Agricultural Wastes, 37:5(2002), 445-451

[14]E. Korzeniewska, M. Harnisz. J. Environ. Manage. 123, (2013). 1–7.

[15] FAO, ONSSA, Etude sur le suivi de l'effet des pesticides sur la santé humaine et l'environnement Rapport final (2015)

[16] H. FEKKOUL; Groundwater contamination by nitrates, salinity and pesticides (2012)

[17] M. Mekkaoui, M. Elazzouzi, A. Bouhaouss, M. Ferhat, J. M. Chovelon,P. Meallier ; Vol. 2 INTERNATIONAL JOURNAL OF PHOTOENERGY (2000)

[18] Fatai A. Taiwo, Spectroscopy 17 (2003) 53–63 53 IOS Press

[19] N.Senesi, G. Sposito, J. Martin P . Sci. Tot. Environ. 55 (1986); 351-362.

[20] P. M. Huang,J. Berthelin,Jean-Marc Bollag,William B. McGill; Environmental Impacts of Soil Component Interactions: Land Quality Volume 1 (2002); 4-6

[21] N.Senesi, G. Sposito Sci. Soc. Am. J. 48.(1984); 1247-1253

[22] Marc Pansu, Jacques Gautheyrou Handbook of Soil Analysis: Mineralogical, Organic and Inorganic Methods; (2014); 412-416

Chapter 7: Conclusions and Recommendation for Future Research

7.1. Summary and major achievement

The environmental and health challenges posed by the wide spread of persistent organic pollutants such as pesticides and their active metabolites in aquatic environments has considerably increased the interest of researcher in developing effective, efficient, economical and environmental compatible technologies for their complete destruction to avoid their release to the environment.

Advanced Oxidation Processes constitute a response to such requirements due to the high efficiency they have shown for the mineralization of persistent organic pollutants and their degradation by-products.

The goal of the present thesis was to design highly active photocatalyst systems and to assess the potential of different AOPs for the removal of organic pollutants from wastewater.
In this work, new heterostructures of TiO_2 (Hombikat UV100) with layered manganese dioxide (birnessite) was investigated to improve the photocatalytic efficiency under UV-Vis irradiation. During this research, the synthesis methods and conditions were explored, structures and physicochemical properties of the composites were well studied, and photocatalytic degradation activities were completely evaluated. Finally, the mechanism and the relationship between structure, physicochemical properties, and photodegradation performance were also tried to be explained. The main outcomes of this work are presented below:

Paper (I and II)

- ⇨ New visible light driven Ca_xMnO_y modified UV100 was successfully synthesized based on the preparation of birnessite by chemical co-precipitation and mixing with commercial titanium dioxide with different weight fractions (1-wt % to 50-wt %) by mechanical grinding, followed by annealing. As a result, Ca_xMnO_y layers are encapsulating TiO_2 particles.

- ⇨ Significant differences in the photocatalytic activities for the prepared composites were observed, with maximum photocatalytic activity achieved with two synthetic birnessite samples Ti-5Ca0.1Mn and Ti-5Ca0.3Mn with varying calcium content, attributed to the high adsorption capacity and specific surface area compared to other manganese oxides composite.

- ⇨ The photocatalytic activity was determined using methylene blue, and imazapyr herbicide as model pollutants under UV-Vis irradiation and Vis only. Various conditions of composite synthesis were investigated, and the results suggested that a correlation exists between the calcium manganese oxide content, oxidation state and the changes in the UV–vis absorption properties

- ⇨ The photocatalytic activity, in terms of rate constant was found to increase from 0.124 min^{-1} to 0.542 min^{-1} and from 0.15min^{-1} to 0.425 min^{-1} for methylene blue dye and imazapyr herbicide, respectively in presence of commercial titanium dioxide TiO_2 and Ca_xMnO_y- TiO_2 composite respectively.

- ⇨ Based on the optical and electrical properties of materials analysis, it can be speculated that Ca_xMnO_y contribute to the enhanced photocatalytic activity of Ca_xMnO_y- TiO_2 in three ways:

    - Extending the light absorption into the visible range: the improvement of photocatalytic activity is a result of a reduction of band gap from 3.18 eV to 2.89 eV for pure TiO_2 and Ca_xMnO_y- TiO_2 composite respectively,

- An efficient inhibition of electron-holes recombination rates due to the deposition of manganese oxide mainly on the surface of titanium dioxide
- Improving the charge separation, and transfer between the materials.

⇨ The main intermediate products of photodegradation process of imazapyr were examined. In the Ca_xMnO_y-UV100 system, the concentration of intermediates continuously increased with irradiation time, to achieve a maximum at 180 min of irradiation, and decreased by more than half in the following hours, whereas intermediates did not decompose in the case of the UV100 system.

⇨ The enhanced photocatalytic activity of the photocatalyst was ascribed to the surface modification, so that the catalyst could easily adsorb polarized organic reactants and thus promote their photocatalytic decomposition.

⇨ We also provide a mechanistic explanation of higher performance of Ca_xMnO_y-UV100 in comparison to parent compound based on the band edge positions and band gaps of both components.

Paper (III and IV)

⇨ A comparative study on the degradation of imazapyr in aqueous solution by ozonation, photocatalysis and photocatalytic ozonation in the presence of Ca_xMnO_y-TiO_2 composite have been investigated in this research.

⇨ Effects of operational parameters on imazapyr removal efficiency including Ca_xMnO_y-TiO_2 dosing, initial herbicide concentration and pH were also studied and optimized.

⇨ Special attention was focused on the influence of the pH on the reaction rate. It was concluded that imazapyr degradation is mainly influenced by the acid–base equilibrium governing the surface of titanium oxides in water.

- The results of this study showed that imazapyr removal followed a first-order kinetic model with a rate constant of 0.547 min^{-1} and 0.425 min^{-1} for photocatalytic ozonation and heterogeneous photocatalysis respectively, while second order kinetic for ozonation process with a rate constant of 0.053 $mol.L^{-1}.min^{-1}$ at pH 7.

- The results suggest that a concentration of 5 µM of imazapyr, 100 mgL^{-1} of Ca_xMnO_y-TiO_2 composite and 10 mgL^{-1} of ozone under pH 7 are able to initiate hydroxyl radicals from the decomposition of ozone and degrade imazapyr in less than 10 min.

- High constant rate exhibited by Ca_xMnO_y-TiO_2 in the presence of ozone may be explained considering the high hydroxyl surface population of this sample supported by the fact that the deposition of the porous manganese oxide mainly on the surface of titanium dioxide that can easily accommodate the hydroxyl groups.

- it was also considered that the dissolved ozone was easy to accept electrons generated on the surface of Ca_xMnO_y-TiO_2, so that the recombination of the positive hole and negative electron pairs was hindered, ultimately a large number of radicals formed.

- It has been confirmed that the total concentration of imazapyr photoproducts in the presence of Ca_xMnO_y-TiO_2 underwent a fast drop to achieve more than 95% of degradation, indicating the mineralization of imazapyr photoproducts.

- The main operating parameters were examined both in Ca_xMnO_y-TiO_2 and TiO_2 (UV100) systems and was concluded that optimal photocatalyst dosing for Ca_xMnO_y-TiO_2 is 100 mgL^{-1}, while 200 mgL^{-1} for commercial TiO_2.

- Photocatalytic ozonation process in the presence Ca_xMnO_y-TiO_2 leads to a ca. 2-fold rate enhancement for imazapyr and a ca.4.3-fold for intermediate products , while compared to photocatalytic ozonation in the presence of commercial TiO_2 (Hombikat UV100).

- ⇨ The high efficiency of photocatalytic ozonation could be explained by a synergistic effect between ozonation and photocatalysis. The photogenerated electrons can react with ozone molecules generating ozonize radicals while decreasing the possible recombination of electron hole pair, so better electron- whole separation

- ⇨ Consequently, it can be concluded that the combination of ozonation and photocatalysis, catalysts with high activity under visible light and systematic optimization of operational parameters are completely necessary for organic pollutants treatment such as imazapyr herbicide in order to promote environmental and human health protection.

Paper (V)

In the last part of this research, the effect of the interaction between imazapyr and humic substances has been investigated.

- ⇨ The present study indicated that HAs have complex effects on the removal and environmental behavior of transition metal ions and pesticides.

- ⇨ At low concentration, HA substances did not affect the degradation kinetics, however at high concentration, HA exhibit a screening effect on the photochemical degradation of imazapyr, but also acts as hydroxyl radical scavengers, and a competition for free radicals between imazapyr and organic matrix could be responsible for decreased efficiency of catalyst directly affecting photocatalytic efficiency.

7.2. Research Contributions

This study has attempted to make a contribution to the field of degradation of persistent organic pollutants and especially imazapyr herbicide, with the use of new synthesised composites. This thesis has shown that it is possible to consider abundant materials such as birnessite for the synthesis of novel materials for water treatment. In addition, this research also aimed at utilizing the prepared novel materials as more sustainable water treatment materials. The sustainability concept consists of three aspects: environmental, social and economic. By utilizing more abundant materials, by employing photocatalysts able to absorb natural sunlight and moving towards visible wavelengths can significantly reduce cost, and therefore the sustainability of the process is increased. Photocatalysis can be performed in ambient conditions and thus energy needed for heating and pressurizing water treatment systems is minimized, which as well enhances the sustainability. In addition, as far as the oxidation and mineralisation of imazapyr herbicide in wastewater are concerned, the combination of ozone, appropriate photocatalyst, optimum design and optimized conditions, an effective reactor design that stimulate the synergistic effects and benefits of photocatalytic ozonation systems also contributes positively to the sustainability of a water treatment process, by decreasing the environmental load of the purified water due to mineralization compared to using ozonation and photocatalysis separately. However, this thesis has also shown that there are limitations and challenges to be overcome concerning the applications of the studied techniques. For example, in order to move this treatment method from the lab to commercial utilisation, more attention should be focused on the immobilisation of photocatalyst particles onto inert substrates, as slurry applications of photocatalysis are not economically justifiable, due to the additional high costs of photocatalyst filtration after treatment.

7.3. Recommendations and future direction

In order to promote the feasibility of photocatalytic water technology in the near future, several key photocatalyst issues need to be taken into consideration, including:
(i) Catalyst improvement for a high photo-oxidation efficiency that can utilize wider solar spectrum
(ii) Catalyst immobilization strategy to provide a cost effective solid-liquid separation. Two research studies have been started in that direction:

1st one: porous hybrid microspheres of Ca_xMnO_y-TiO_2 composites have been prepared by gelation of an intercalated commercials clays (clays Montmorillonite Na, Montmorillonite 20A, Montmorillonite 30B), followed by drying with super-critical CO_2.

- ⇨ Material caracterisation and investigation of photocatalytic activity of imazapyr herbicide degradation on the new synthesized microspheres need to be realized.

2nd one: The effect of the nature of substrate (Ge, Si and SnO_2) on the band gap of Ca_xMnO_y-TiO_2 ultra-thin films is under study

(iii) Assessing the toxicity of the solution beside the heterogeneous system should be investigated for other pollutants especially pesticides residues.

(IV) Treatment of real wastewater effluents
The thesis work has been achieved by studying synthetic solutions of the selected pollutants, therefore it is important to test the experiments realized here with real wastewater effluents. The real effluents behave differently when treated by AOPs techniques because of the multicomponent nature of it organic content, varying pH and its significant quantities of inorganic ions.

Supplementary data

Appendix A. Degradation rate constant of methylene blue in the presence of different manganese oxides and different loading

Appendix B.Powder XRD-patterns of pure birnessite, Manganeseoxide (II,III,IV),Ti, Ti-500,Ti-5Mn_2O_3,Ti-5MnO_2, Ti-5Ca0.1Mn and Ti-5Ca0.3Mn.

Appendix C. Representative SEM images of catalysts (A) Ti (B)Ti-5Ca0.1Mn

Appendix D. Pore width distribution for Ti, Ti-500, Ti-5MnO_2, Ti-5Mn_2O_3, Ti-5Ca0.1Mn, Ti-5Ca0.3Mn composite

Appendix E. Three-dimensional plot of MS-ESI analysis of Imazapyr (A) in presence of Ti(B) in presence of Ti-5Ca0.1Mn

Appendix F. (a) UV-Vis spectra and (b) absorbance vs concentration for Ca_xMnO_y-TiO_2

Appendix G. Powder XRD-patterns of TiO_2 and Ca_xMnO_y-TiO_2.

Appendix H. UV-vis absorption spectra of TiO_2 and Ca_xMnO_y-TiO_2. All the samples were annealed at 500°C for 24 h.

Appendix I. XPS spectra of Ca_xMnO_y-TiO_2 showing (a) Survey, (b) Ti 2p, (c) O 1s, (d) Ca 2p and (e) Mn 2p.

Appendix J. Photoluminescence spectra for TiO_2 and Ca_xMnO_y-TiO_2. All the samples were annealed at 500°C during 24 h. The excitation wavelength (λ_{ex}) was 325 nm.

Appendix K. Imazapyr photolysis under 125 W Xe under UV-Vis irradiation.

Table A.1.Degradation rate constant of methylene blue in the presence of Ti-5Mn, Ti-1Mn, Ti-10Mn, Ti-500 and Ti ;($C_{(Methylene\ blue)}$= 5 mg L^{-1}); stirring speed = 1000 min^{-1}, m catalyst= 100 mg)

composite	k/min^{-1}	Standard error
Ti-5Mn	0.54245	0.00102
Ti-1Mn	0.29087	0.02512
Ti-10Mn	0.21328	0.01754
Ti-500	0.20022	0.00508
Ti	0.12422	0.00917

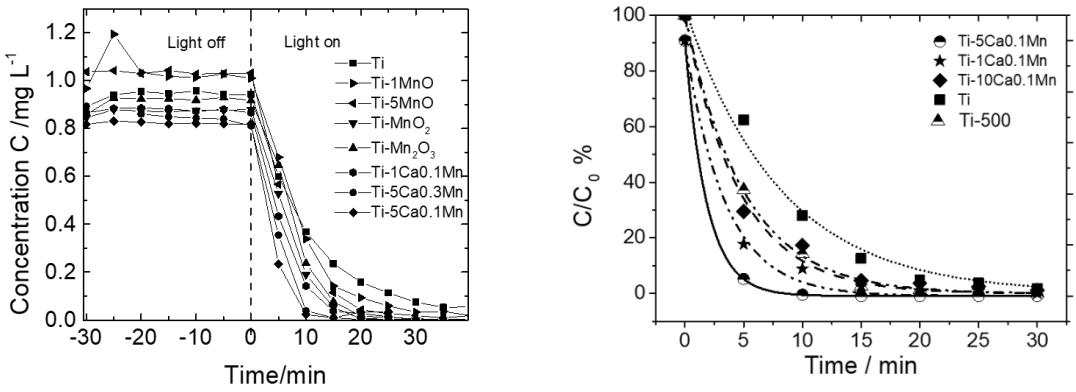

Figure A.1. Concentrations of methylene blue as a function of time for different catalyst (a) different manganese oxides, (b) different manganese oxides loading;($C_{(Methylene\ blue)}$= 1 mg L^{-1}); stirring speed = 1000 min^{-1}, m catalyst= 100 mg).

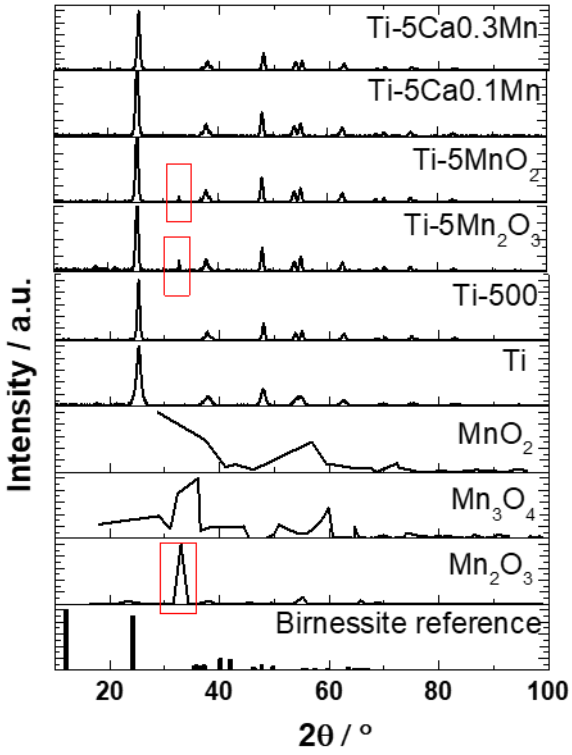

Figure B.1. Powder XRD-patterns of pure birnessite, Manganese(II) oxide Mn_2O_3, Manganese(II,III) oxide Mn_3O_4,Manganese(IV)MnO_2,Ti commercial titanium Hombikat UV100, Ti-500 commercial titanium annealed at 500 °C,Ti-5Mn_2O_3 composed with 5 wt.-% Mn_2O_3 and 95 wt.-% TiO_2 ,Ti-5MnO_2 composed with 5 wt.-% MnO_2 and 95 wt.-% TiO_2, Ti-5Ca0.1Mn composed with 5 wt.-% $Ca_{0.1}MnO_y$ and 95 wt.-% TiO_2 and Ti-5Ca0.3Mncomposed with 5 wt.-% $Ca_{0.3}MnO_y$ and 95 wt.-% TiO_2. All the composites were annealed at 500 °C during 24 h.

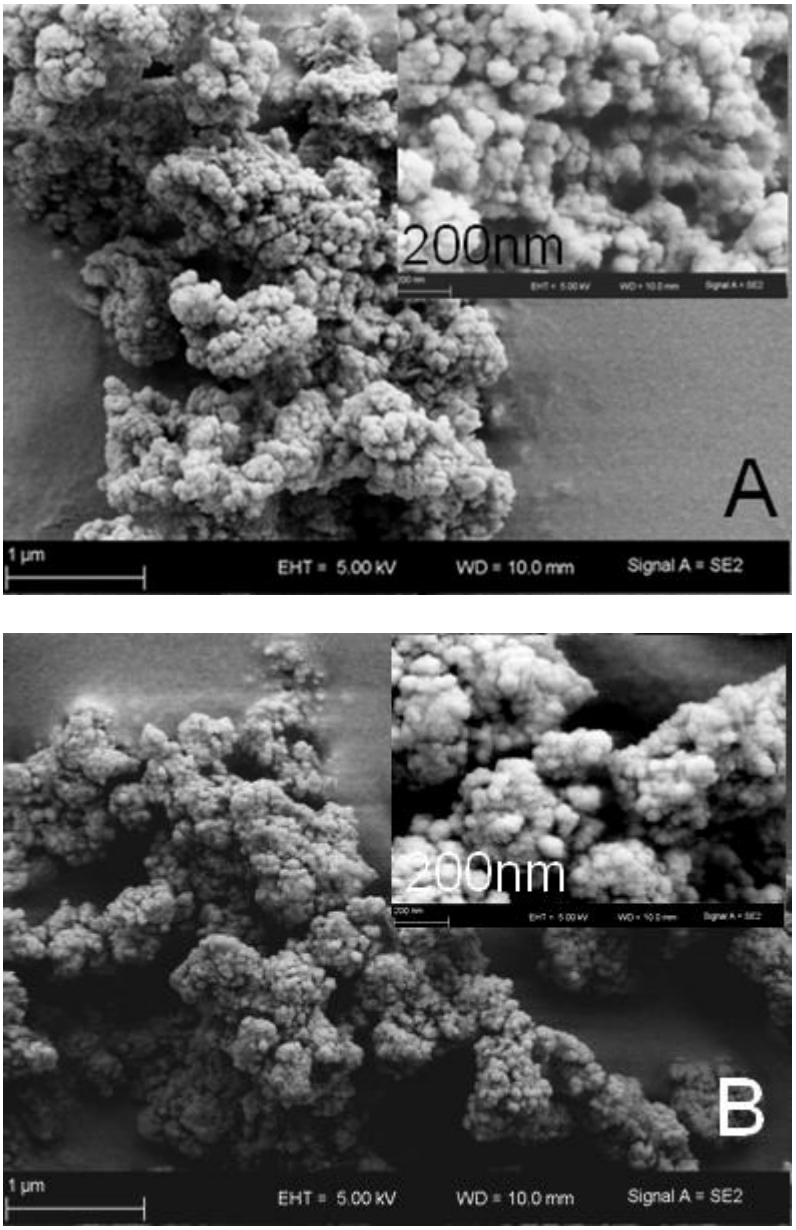

Figure C.1. Representative SEM images of catalysts (A) Ti (B)Ti-5Ca0.1Mn

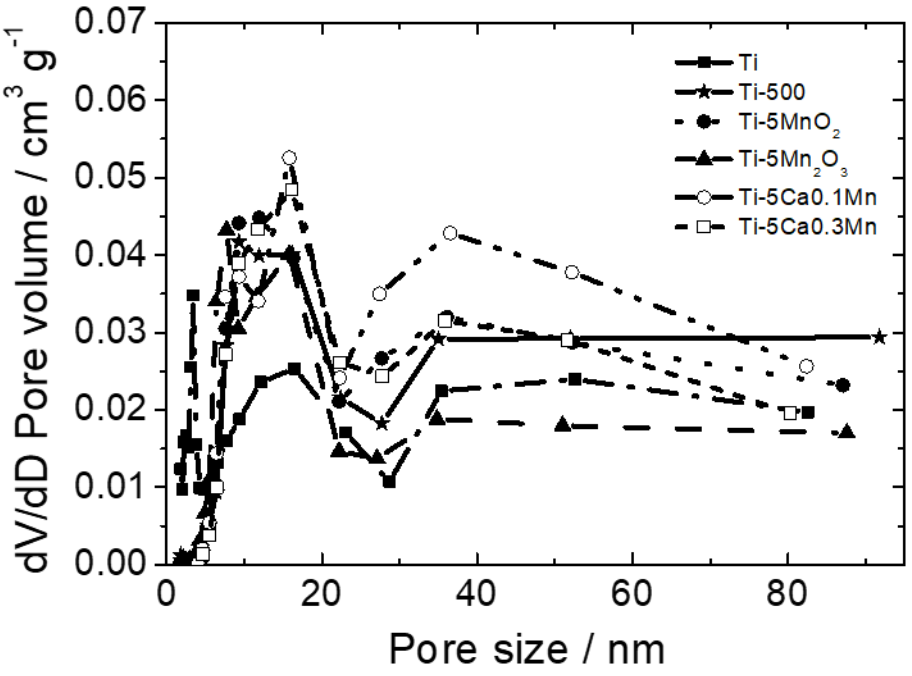

Figure D.1. Pore width distribution determined using the BJH method on the desorption branch of the isotherm for Ti, Ti-500, Ti-5MnO_2, Ti-5Mn_2O_3, Ti-5Ca0.1Mn, Ti-5Ca0.3Mn composite

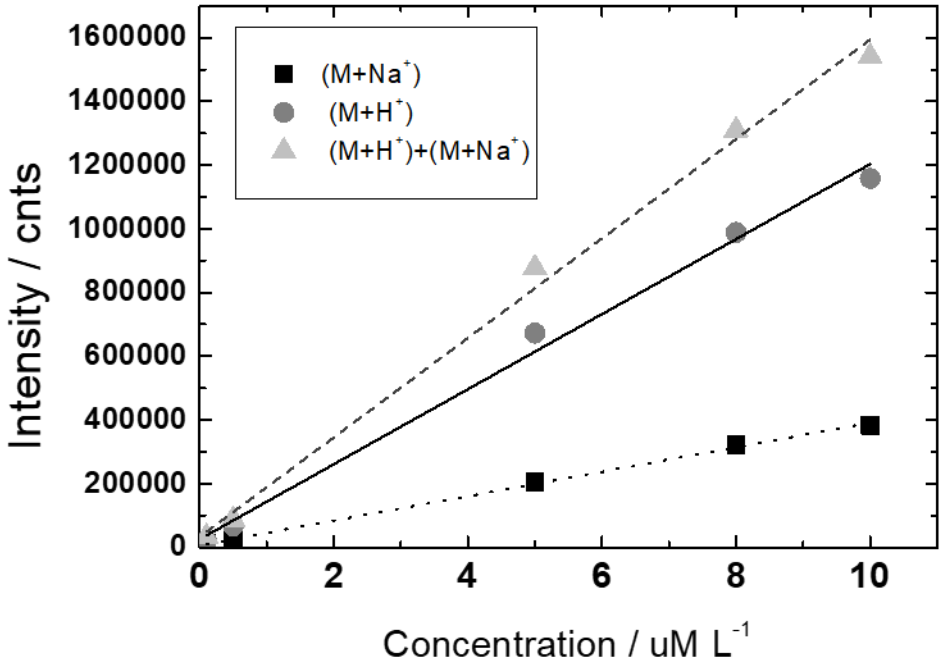

Figure E.1. Intensity of ($M+H^+$) and ($M+Na^+$) as a function of the concentration of Imazapyr solution

Note: Specificity, linearity and recovery studies were conducted by injecting of different known concentrations of linearity solutions 10, 1, 0.1, 0.05 and 0.01 µg/l .they were prepared by serial dilution method.

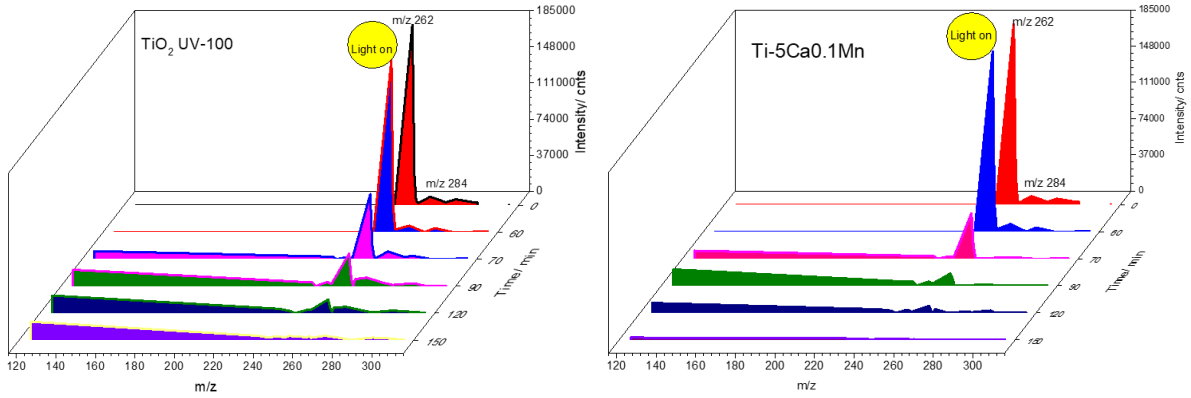

Figure E.2. Three-dimensional plot of MS-ESI analysis of Imazapyr (A) in presence of Ti(B) in presence of Ti-5Ca0.1Mn

S1. Catalyst loading in the STR reactor

The optimal loading of Ca_xMnO_y-TiO_2 in the reactor was determined by measuring the UV-Vis absorbance spectra for various concentrations of Ca_xMnO_y-TiO_2 as shown in figure S1(a). The absorption spectra were superimposed on the AM1.5 spectra in 280-400 nm range ($A_{solar}=\sum A_yS_y/\sum S_y$) to obtain the absorbance with respect to Ca_xMnO_y-TiO_2 concentration (Figure S1(b)). The Beer-Lambert law was used to determine the concentration corresponding to absorption of 99% of the photons (A=2).

$$\mathbf{A=\varepsilon \cdot C \cdot l;\ C= A/(l \cdot \varepsilon) = 30.6\ mg/L}$$

Here, l=6 cm (reactor path length) and ε=0.01077 $M^{-1} \cdot cm^{-1}$, were used to determine the optimal loading, details are provided in the supplementary section.

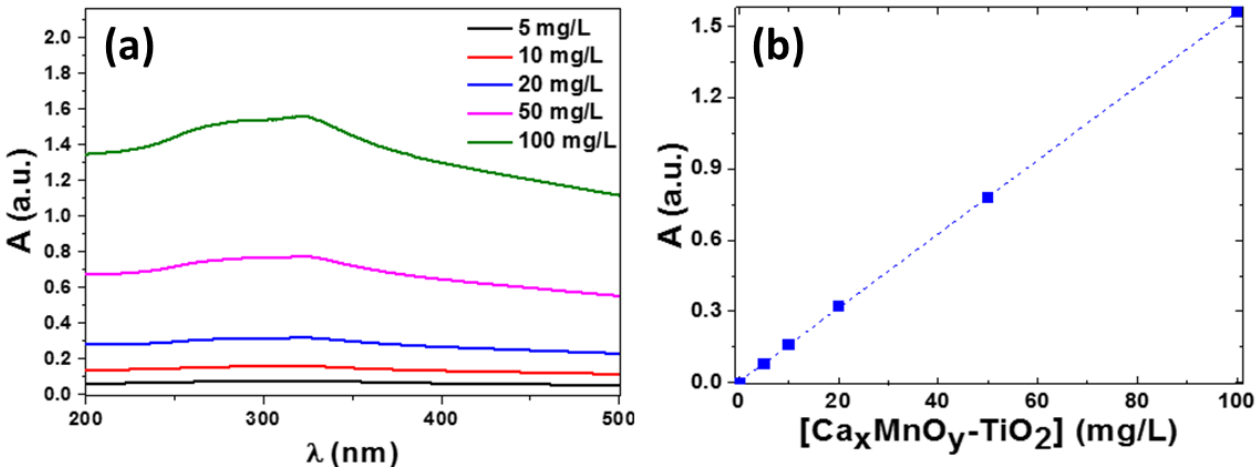

Fig. S1. (a) UV-Vis spectra and (b) absorbance vs concentration for Ca_xMnO_y-TiO_2

S2. Characterization of TiO_2 and Ca_xMnO_y-TiO_2 materials

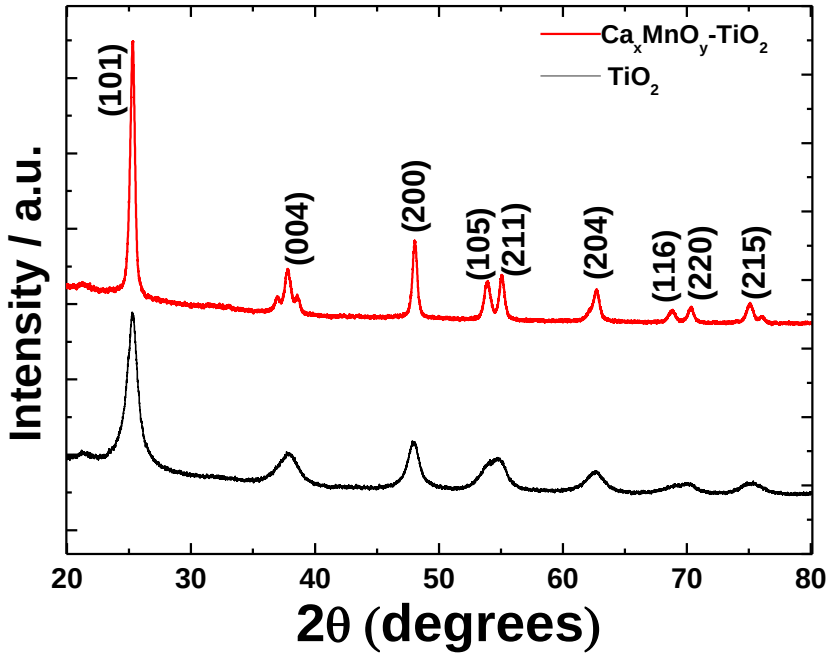

Fig. S2. Powder XRD-patterns of TiO_2 and Ca_xMnO_y-TiO_2.

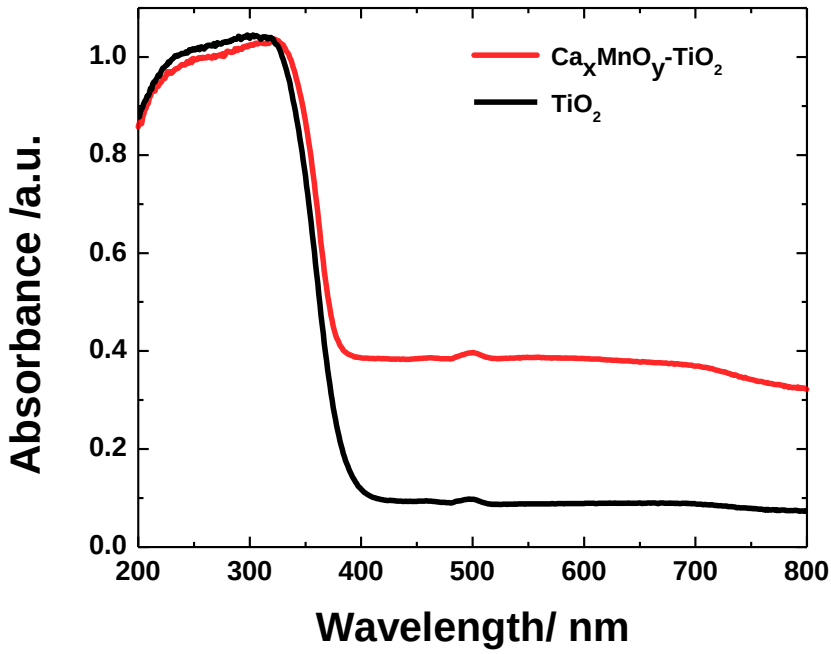

Fig. S3. UV-vis absorption spectra of TiO_2 and Ca_xMnO_y-TiO_2. All the samples were annealed at 500°C for 24 h.

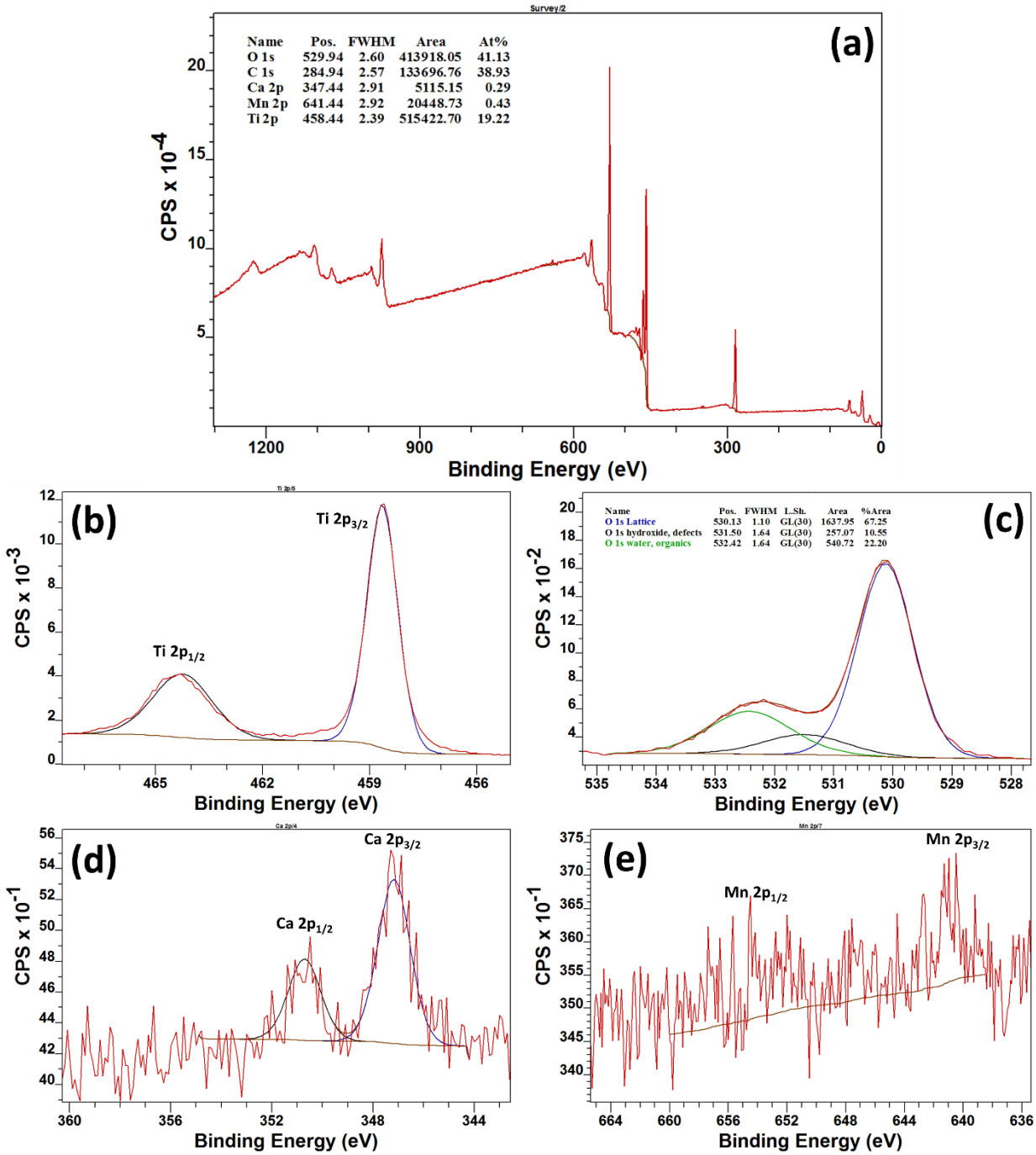

Fig. S4. XPS spectra of Ca_xMnO_y-TiO_2 showing (a) Survey, (b) Ti 2p, (c) O 1s, (d) Ca 2p and (e) Mn 2p.

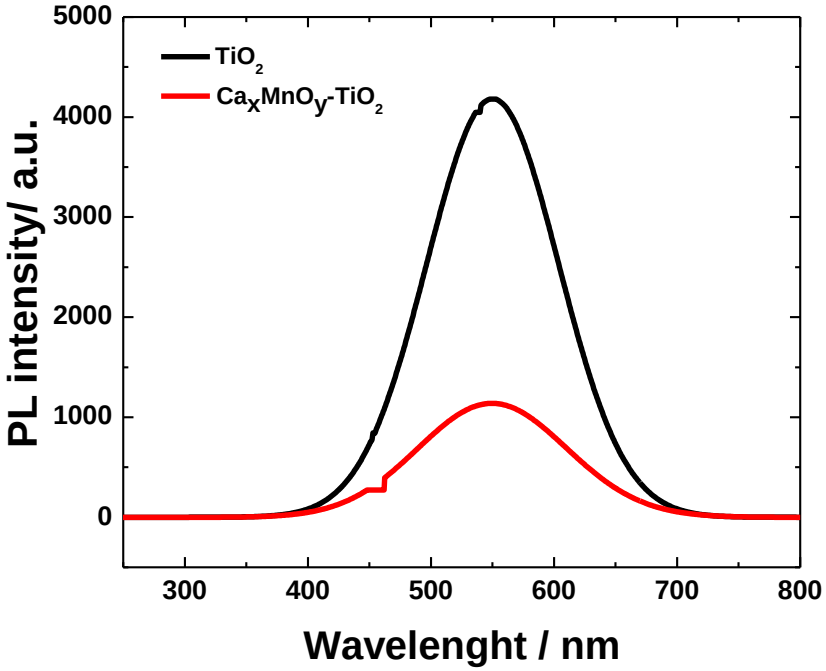

Fig. S5. Photoluminescence spectra for TiO_2 and Ca_xMnO_y-TiO_2. All the samples were annealed at 500°C during 24 h. The excitation wavelength (λ_{ex}) was 325 nm.

S3. Controls for the photocatalytic degradation experiments

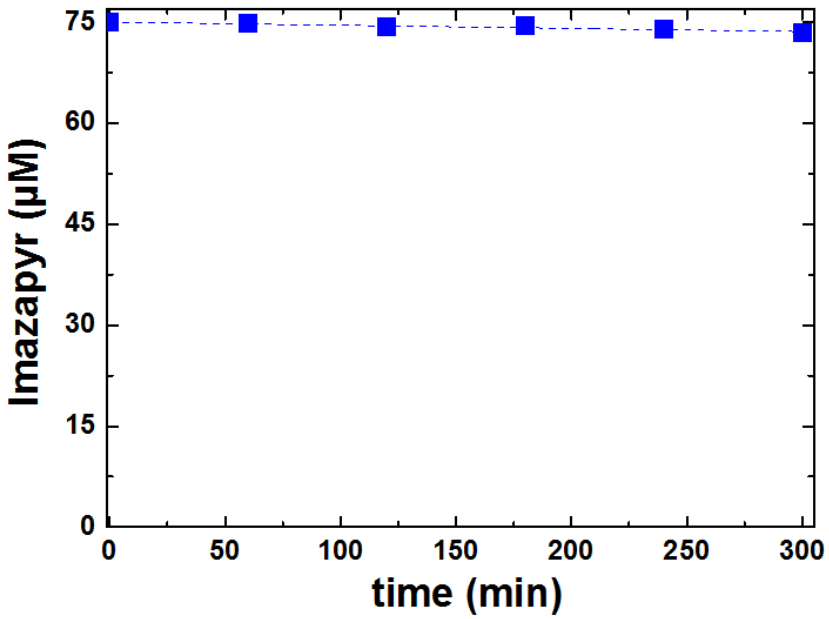

Fig. S6. Imazapyr photolysis under 125 W Xe under UV-Vis irradiation.

The photolysis experiments for imazapyr were performed in the stirred tank reactor under Xe UV-Vis irradiation (125 W). The samples were collected every hour and were analysed in HPLC. Over the 5 h irradiation, the imazapyr concentration reduces by 2% as shown in figure S5. The photolysis rate is much lower than the photocatalysis rate.

The dark adsorption measurements on TiO_2 and Ca_xMnO_y-TiO_2 were performed at the start of corresponding experiment for 1 h and the adsorbed amount of imazapyr and phenol were within the noise range.

Résumé

Le présent travail retrace principalement les résultats de synthèse des nouveaux composites à base d'oxyde de manganèse et d'oxyde de titanium. Le composite 5% Ca_xMnO_y / TiO_2 possède une efficacité photocatalytique dans la région du visible sur la dégradation ainsi que la minéralisation du colorant bleu de méthylène, du phénol ainsi que sur l'herbicide Imazapyr, supérieure à celle obtenue en utilisant le TiO_2 commercial (Hombikat UV 100, Degussa P25). Le dépôt d'oxyde de manganèse principalement à la surface du dioxyde de titane a permis de modifier les propriétés optiques du TiO_2. L'amélioration de l'activité photo-catalytique a été attribuée principalement au rétrécissement de la bande interdite ainsi qu'à la réduction de la recombinaison électron-trou, produisant ainsi une séparation de charge efficace et un transfert entre les matériaux. Finalement, la structure et les propriétés des produis intermédiaires ont été examinés et un mécanisme photo-catalytique a été discuté en détail. De plus, une étude comparative sur la dégradation de l'imazapyr en solution aqueuse par l'ozonation, la photocatalyse et par l'ozonation photocatalytique en présence du composite Ca_xMnO_y-TiO_2 a pu mettre en évidence que la combinaison de l'ozone et de la photoctalyse s'avère efficace pour le traitement des polluants persistants tout en maitrisant les paramètres influençant.

Abstract

Within this thesis, new heterostructures based on layered manganese oxide and titanium dioxide were investigated. Ca_xMnO_y was prepared by a precipitation method and then mixed with TiO_2 by mechanical grinding following by annealing at 500°C to obtain Ca_xMnO_y-TiO_2. Ca_xMnO_y-TiO_2 composite exhibits high photocatalytic efficiency in the visible region toward the degradation and mineralization of methylene blue dye, phenol and Imazapyr herbicide, as compared to TiO_2 system (UV100 and Degussa P25), plausible mineralization pathways for imazapyr was proposed based on the identified intermediates. Ca_xMnO_y contributed to the enhanced photocatalytic activity of Ca_xMnO_y-TiO_2 in three ways: extending the light absorbance into the visible range due the reduction of the band gap from 3.18 eV to 2.89 eV for pure TiO_2 and Ca_xMnO_y-TiO_2 composite respectively, possibly improving charge transfer and lowering recombination of charge carriers, and finally by altering intermediate adsorption and degradation due to the greater adsorption of polar species on the surface of the Ca_xMnO_y, and thus promote their photocatalytic decomposition. Upon comparison of different AOPs, Photocatalytic ozonation process in the presence Ca_xMnO_y-TiO_2 leads to a ca. 2-fold rate enhancement for imazapyr and a ca.4.3-fold for intermediate products, while compared to photocatalytic ozonation in the presence of commercial TiO_2. Particular emphasis was also given to the effect of humic acids extracted from Chaouia soil in Morocco, on the reaction kinetics and mechanisms of imazapyr degradation.